

**INVESTIGATION ON ELECTRIC MOTOR
BRAKING CONTROL SYSTEM FOR
ELECTRIC POWERED WHEELCHAIR**



MUHAMMAD ASYRAF BIN SHAHROM

MASTER OF SCIENCE

UNIVERSITI MALAYSIA PAHANG

UNIVERSITI MALAYSIA PAHANG

DECLARATION OF THESIS AND COPYRIGHT

Author's Full Name : MUHAMMAD ASYRAF BIN SHAHROM

Date of Birth : 6 OCTOBER 1993

Title : INVESTIGATION ON ELECTRIC MOTOR BRAKING
CONTROL SYSTEM FOR ELECTRIC POWERED
WHEELCHAIR

Academic Session : SEM 1 2019/2020

I declare that this thesis is classified as:

- CONFIDENTIAL (Contains confidential information under the Official Secret Act 1997)*
- RESTRICTED (Contains restricted information as specified by the organization where research was done)*
- OPEN ACCESS I agree that my thesis to be published as online open access (Full Text)

I acknowledge that Universiti Malaysia Pahang reserves the following rights:

1. The Thesis is the Property of Universiti Malaysia Pahang
2. The Library of Universiti Malaysia Pahang has the right to make copies of the thesis for the purpose of research only.
3. The Library has the right to make copies of the thesis for academic exchange.

Certified by:

(Student's Signature)

931006045265

IC Number:

Date:

(Supervisor's Signature)

Dr. Mohamad Heerwan Bin Peeie

Supervisor's Name:

Date:

NOTE : * If the thesis is CONFIDENTIAL or RESTRICTED, please attach a thesis declaration letter.

SUPERVISOR'S DECLARATION

We hereby declare that we have checked this thesis and in our opinion, this thesis is adequate in terms of scope and quality for the award of the Master of Science.

(Supervisor's Signature)

Full Name : Dr. MOHAMAD HEERWAN BIN PEEIE

Position : SENIOR LECTURER

Date :

(Co-supervisor's Signature)

Full Name : Dr. MUHAMMAD IZHAR BIN ISHAK

Position : SENIOR LECTURER

Date :

STUDENT'S DECLARATION

I hereby declare that the work in this thesis is based on my original work except for quotations and citations which have been duly acknowledged. I also declare that it has not been previously or concurrently submitted for any other degree at Universiti Malaysia Pahang or any other institutions.

(Student's Signature)

Full Name : MUHAMMAD ASYRAF BIN SHAHROM

ID Number : MMM17015

Date :



UMP

INVESTIGATION ON ELECTRIC MOTOR BRAKING CONTROL SYSTEM
FOR ELECTRIC POWERED WHEELCHAIR



MUHAMMAD ASYRAF BIN SHAHROM

Thesis submitted in fulfillment of the requirements
for the award of the
Master of Science

UMP

Faculty of Mechanical and Automotive Engineering Technology

UNIVERSITI MALAYSIA PAHANG

JANUARY 2020

ACKNOWLEDGEMENTS

In the name of Allah, the most Gracious the most Merciful.

In preparing this thesis, I have engaged with many people in helping me complete this project. First, I wish to express my sincere appreciation to my main thesis supervisor Dr. Mohamad Heerwan bin Peeie and Co-Supervisor Dr. Muhamad Izhar bin Ishak, for their valuable guidance, germinal ideas, advice, motivation and continuous encouragement to give an understanding in this study. Without continued support and interest from them, this thesis would not have been the same as presented here.

My sincere thanks go to all the staff and friends of the Mechanical Engineering Department as well as from the Electric and Electronics Engineering Department, who helped me in many ways directly and indirectly which made my stay in UMP pleasant and unforgettable.

Lastly and most importantly, I would like to thank my father Shahrom bin Md. Shah and my mother Zainab binti Abd Rahman for their love, dream and sacrifice throughout my life, as well as providing motivation all these years for me to achieve greatness in my study. I acknowledge the sincerity of my parents, who consistently encourage me to carry my higher studies in this field. I cannot find the appropriate words that could describe my appreciation for their devotion, support and faith in my ability to attain my goals.

ABSTRAK

Sejak kebelakangan ini, kajian berkenaan Kerusi Roda Elektrik (KRE) telah dikaji secara meluas kerana kepentingannya bagi orang yang kurang upaya untuk bergerak. Semasa meneruni di cerun, sistem brek manual kebiasaannya digunakan untuk mengawal kelajuan dengan menggenggam pada tuil brek. Walau bagaimanapun, tugas ini menjadi sukar jika pengguna adalah warga tua atau lumpuh yang mana terdapat kekurangan pada badan mereka. Oleh itu, kemungkinan terjadinya pelanggaran dan cedera untuk berlaku adalah tinggi. Dalam kajian ini, kawalan automatik brek motor elektrik yang dikenali sebagai Hill Descent Control (HDC) dicadangkan untuk meningkatkan keselamatan KRE semasa menuruni kawasan bercerun. Memandangkan motor elektrik mempunyai kelebihan yang boleh menghasilkan tork semasa brek, “plugging” brek dipasang bersama dengan sistem HDC bagi mengawal kelajuan KRE mengikut kelajuan yang dikehendaki dari pengguna. Analisis kajian ini dibahagikan kepada tiga fasa; penyiasatan prestasi brek menggunakan brek elektrik, pembangunan sistem kawalan brek yang aktif dalam sistem tertanam serta persekitaran simulasi dan analisis sistem kawalan brek yang aktif dalam kerja percubaan dan simulasi. Dari hasil percubaan, “plugging” brek sesuai untuk disatukan dengan sistem kawalan brek aktif berbanding dengan “regenerative” dan “dynamic” brek. Dalam “plugging” brek, dengan menukarkan voltan “plugging” dari 0.5 V hingga 4.5 V, pelbagai kesan tingkah laku dinamik seperti jarak brek, kelajuan tayar dan nisbah gelinciran boleh dicapai. Sementara itu, dari analisis sistem kawalan brek aktif yang disepadukan dengan “plugging” brek, kedua-dua keputusan analisis dari eksperimen dan simulasi menunjukkan kelajuan EPW dapat dikawal pada kelajuan yang dikehendaki $v_d = 0.6$ m/s ketika menuruni lereng bahkan pada kelajuan brek awal yang tinggi 2.5 m/s. Kepentingan kajian ini adalah supaya pembangunan sistem HDC dapat dilaksanakan di EPW untuk mengelakkan roda daripada bergerak secara pantas semasa menuruni di cerun. Dengan mengekalkan kelajuan KRE di lereng, keselamatan pengguna juga boleh ditingkatkan.



UMP

ABSTRACT

In recent years, research on Electric Powered Wheelchair (EPW) has been widely studied due to its high importance of mobility for disabled people. During descent on a slope, the manual braking system is commonly used to control the speed by gripping the brake lever. However, the task becomes difficult if the user is an elderly or paralyzed due to their body's deficiencies. As a result, the possibilities of collision and injuries to occur are high. In this study, the automatic electric motor braking control that is known as Hill Descent Control (HDC) is proposed to increase the safety of EPW during descending on slopes. Since the electric motor has an advantage which can generate the torque during braking, the plugging braking is integrated with the HDC system to control the speed of the EPW according to the desired speed from the user. The analysis of this study is divided into three phases; investigation of braking performance using electrical braking, development of active braking control system in the embedded system as well as the simulation environment and analysis on active braking control system in experimental and simulation work. From the experimental results, the plugging brake is most suitable to integrate with the active brake control system compared to the regenerative and dynamic brake. In the plugging brake, by changing the plugging voltage from 0.5 V to 4.5 V, a variety of dynamic behaviour effects such as braking distance, tire speed and slip ratio can be achieved. Meanwhile, from the analysis of active braking control system that was integrated with plugging braking, both of the experimental and simulation analysis results show the speed of EPW can be maintained at the desired speed of $v_d = 0.6$ m/s during descending on the slope even at a high initial braking speed of 2.5 m/s. The significance of this study is so that the development of the HDC system can be implemented in EPW to prevent the wheels from accelerate during descents on slopes. By maintaining the speed of EPW on slopes, the safety of the user can also be increased.

The logo for UMP (Universiti Malaysia Perlis) is a large, stylized letter 'V' shape. The left side of the 'V' is light blue, the right side is light green, and the bottom point is a darker blue. The letters 'UMP' are written in white, bold, sans-serif font across the center of the 'V'.

TABLE OF CONTENT

DECLARATION	
TITLE PAGE	
ACKNOWLEDGEMENTS	ii
ABSTRAK	iii
ABSTRACT	iv
TABLE OF CONTENT	v
LIST OF FIGURES	x
LIST OF SYMBOLS	xiv
LIST OF ABBREVIATIONS	xv
CHAPTER 1 INTRODUCTION	1
1.1 Introduction	1
1.2 Project Background	1
1.3 Problem Statement	3
1.4 Objective Research	3
1.5 Scopes	4
1.6 Thesis Outlines	4
CHAPTER 2 LITERATURE REVIEW	6
2.1 Development of Electric Powered Wheelchair	6
2.2 Past research: Powered Wheelchair (PW)	6
2.2.1 Commercialization of PW	8
2.3 Present research: Smart Wheelchair	9
2.3.1 Advance user input for Smart Wheelchair	11

2.3.2	Advanced sensors input in Smart Wheelchair	13
2.3.3	The Smart Wheelchair Commercialization	14
2.4	Dynamic control enhancement in EPW	16
2.4.1	Stability control	17
2.4.2	Axial control: Suspension control	20
2.4.3	Longitudinal and lateral control	22
2.5	Braking system in transportation	24
2.5.1	Mechanical braking	24
2.5.2	Electrical Braking	26
2.6	Active control system	42
2.6.1	Hill Descent Control (HDC)	43
2.7	Summary of the review	47
CHAPTER 3 METHODOLOGY		49
3.1	Introduction	49
3.2	Project flow chart	49
3.3	Electric Powered Wheelchair specification and instrumentation	53
3.3.1	Electrical drive system: BLDC motor	55
3.3.2	Motor driver Smart Drive Duo 30	57
3.3.3	Battery	58
3.3.4	2 level speed control Joystick	58
3.3.5	Rotational speed encoder	59
3.3.6	Oscilloscope: Voltage measuring	60
3.3.7	Current sensors	60
3.3.8	Voltage sensors	61
3.3.9	Body speed by using third wheel	63

3.3.10	Myrio Microprocessor Control Unit (MCU)	64
3.4	Data analyse technique	65
3.5	Slope condition setup	66
3.6	Electrical braking analysis procedure	68
3.6.1	Regenerative braking analysis	69
3.6.2	Dynamic braking analysis	70
3.6.3	Plugging braking analysis	72
3.7	Real-time experimental on active braking control system	74
3.7.1	Tuning of PID	75
3.8	EPW mathematical model plant	77
3.8.1	Electrical modelling part	78
3.8.2	Mechanical modelling part	81
3.8.3	EPW Dynamic modelling	83
3.9	Experiment of parameters estimation	86
3.9.1	Estimation of Resistance (R) and Torque Constant (kt)	88
3.9.2	The estimation of bearing (B) and initial torque constant (T_{int})	88
3.9.3	The estimation of moment of inertia, J	89
3.10	Model validation	91
3.10.2	In-wheel BLDC electrical motor model validation	92
3.10.3	Road Surface parameter, k validation	92
3.11	EPW Plant design by using state space method	94
3.12	Simulation of motor braking controller using plugging braking concept	96
CHAPTER 4 RESULTS AND DISCUSSION		98
4.1	Introduction	98
4.2	Analysis of EPW dynamic behaviour using different electrical braking	98

4.2.1	Regenerative braking analysis	98
4.2.2	Dynamic braking analysis	102
4.2.3	Plugging braking analysis	107
4.3	Real time control for EPW during descending on slope using plugging braking technique	119
4.4	The Initial estimation of the Electric motor Parameters	122
4.4.1	Estimation initial parameters of torque constant and resistance	124
4.4.2	Estimation initial of bearing and load torque constant	126
4.4.3	Estimation of moment of inertia	128
4.5	BLDC motor parameters validation	131
4.6	Surface coefficient validation	134
4.7	Simulation of plugging braking controller during descending on slope using plugging braking technique	138
4.7.1	Validation of active braking control	139
4.7.2	Simulation of plugging braking control at high initial braking speed	141
CHAPTER 5 CONCLUSION		146
5.1	Introduction	146
5.2	Conclusions	146
5.3	Recommendations	147
REFERENCES		149
APPENDIX A Gantt chart		161
APPENDIX B SAMPLE APPENDIX 2		162

LIST OF TABLES

Table 2.1	Available specification the commercialized Powered Wheelchair (PW)	9
Table 2.2	Interest research of SW around the globe	10
Table 2.3	Comparison between the mechanical and electrical braking	48
Table 3.1	Specification of Electric Powered Wheelchair (EPW)	54
Table 3.2	Operating condition for SDD-30 motor driver	57
Table 3.3	Table of specification for rotary encoder	59
Table 3.4	Specification of AC712 current sensor	61
Table 3.5	Specification of common voltage sensor for low voltage uses	63
Table 3.6	Slope setting information for experiment base on MS-1184 requirements	68
Table 3.7	Effect of system response by increasing the gain	77
Table 3.8	Responses characteristic	77
Table 3.9	Data sheet to find J parameter	91
Table 3.10	example table for optimum surface coefficient, \underline{k} estimation	93
Table 4.1	The effective of regenerative braking to be occurred	101
Table 4.2	Data distribution of output speed by applied different voltage	123
Table 4.3	Distributed data for torque constant and Resistance estimation	124
Table 4.4	Data distribution for Bearing and Load torque constant estimation	127
Table 4.5	Data distributions by applied different braking torque	128
Table 4.6	Estimated parameter result from the fitting line method	131
Table 4.7	Initial estimate and calibrated parameters	134
Table 4.8	Output response error at different estimated iteration road surface, \underline{k} (plugging voltage, 2.5 V)	136
Table 4.9	Output response error at different estimated iteration road surface, \underline{k} (plugging voltage, 4.5 V)	137

LIST OF FIGURES

Figure 2.1	The Powered Wheelchair invented by George Klein.	7
Figure 2.2	Open loop operation of Powered Wheelchair	7
Figure 2.3	Available type of commercialized Powered Wheelchair.	8
Figure 2.4	Electric Powered wheelchair block diagram operation	10
Figure 2.5	(a) Biometric (b) Brain Computer Interface (BCI)	11
Figure 2.6	Schematic diagram of HBMI	12
Figure 2.7	BCI for EPW navigation	12
Figure 2.8	Laser Range Finder (LRF)	13
Figure 2.9	3D scanners like Microsoft's Kinect	14
Figure 2.10	Commercialized Smart Wheelchair	15
Figure 2.11	Personal Electrical Vehicle (PEV) introduced by Toyota	15
Figure 2.12	Degree of freedom for Electric Powered Wheelchair	16
Figure 2.13	hierarchy of dynamic control for EPW	17
Figure 2.14	Balancing mode of the iBOT 3000	19
Figure 2.15	Active suspension control modelling	21
Figure 2.16	Mechanical disc braking system in light transportation using chord	25
Figure 2.17	Mechanical drum braking system in light transportation using chord	25
Figure 2.18	Four-quadrant operation of electrical motor	26
Figure 2.19	Electrical motor mode (a) Motor (b) Generator	27
Figure 2.20	The dynamic braking operation	29
Figure 2.21	Velocity control using dynamic braking in electric wheelchair	30
Figure 2.22	Close-loop control downhill assist system for electric wheelchair.	31
Figure 2.23	Slip ratio control configuration using dynamic braking	31
Figure 2.24	Block diagram of Permanent Magnet synchronise Motor(PMSM) drive	32
Figure 2.25	Regenerative braking operation	34
Figure 2.26	Implement of Bi-directional Buck-Boost converter electrical drive	35
Figure 2.27	Plugging braking operation	39
Figure 2.28	Hill Descent Control (HDC) in current vehicle	43
Figure 2.29	Type of inclinometer, G sensor for HDC	44
Figure 2.30	Configuration of step-up chopper circuit on the experimental setup	44
Figure 2.31	Experimental result by applying HDC in electrical wheelchair	45
Figure 2.32	Proposed electric drive system in heavy truck	46

Figure 3.1	Flow chart of EPW project for Phase 1	50
Figure 3.2	Flowchart for Phase 2	51
Figure 3.3	Flowchart of Phase 3	52
Figure 3.4	Experimental Electric Powered Wheelchair model	53
Figure 3.5	Parts and sensors used in EPW	55
Figure 3.6	In-Wheel BLDC motor for EPW	55
Figure 3.7	Parts inside in-wheel BLDC motor	56
Figure 3.8	Phase type of BLDC	56
Figure 3.9	Two outputs motor driver provided by Cytron	57
Figure 3.10	12V Lithium GP battery	58
Figure 3.11	Multi-axis Joystick	58
Figure 3.12	B106 Rotary Encoder	59
Figure 3.13	Hand held oscilloscope for voltage measurement	60
Figure 3.14	AC712 current sensor	61
Figure 3.15	Voltage sensor by Arduino	61
Figure 3.16	Circuit schematic of modified voltage sensor for reverse polarity prevention	62
Figure 3.17	Modified voltage sensor with full wave rectifier	62
Figure 3.18	Body speed sensor using third wheel	63
Figure 3.19	Characteristic speed of third tire in different surfaces	64
Figure 3.20	Myrio microprocessor module part	64
Figure 3.21	Real time control panel and data logger	65
Figure 3.22	Illustration of Data acceptable	66
Figure 3.23	Slope condition for wheelchair at UMP	67
Figure 3.24	Tilt meter sensor	67
Figure 3.25	Slope setting for experiment base on MS-1184 requirements	68
Figure 3.26	Wiring schematic for regenerative voltage experiment	70
Figure 3.27	Dynamic braking experiment setup	70
Figure 3.28	Dynamic braking analysis procedure	72
Figure 3.29	Plugging braking experiment setup	72
Figure 3.30	Plugging braking analysis	74
Figure 3.31	Plugging control setup	75
Figure 3.32	PID controller structure	75
Figure 3.33	System response characteristic	76
Figure 3.34	Mathematical model of EPW	78

Figure 3.35	Part of modelling	78
Figure 3.36	Electrical Part of BLDC	79
Figure 3.37	Mechanical part modelling	81
Figure 3.38	Dynamic modelling of EPW	83
Figure 3.39	Myu-Slip curve	85
Figure 3.40	Single model tire simulation analysis flow	86
Figure 3.41	Schematic diagram set up for estimating parameters experiment	87
Figure 3.42	Schematic diagram and experiment equipment setup	87
Figure 3.43	Phases of DC motor operation	89
Figure 3.44	Different of braking speed by applied different braking torque	90
Figure 3.45	Parameters calibration tool in MATLAB Simulink	92
Figure 3.46	Friction coefficient range on mosaic surface	93
Figure 3.47	Block diagram state space of EPW	96
Figure 3.48	Block diagram control of EPW	96
Figure 3.49	Plugging control simulation illustration	97
Figure 4.1	Distance travel for free rolling analysis	99
Figure 4.2	Speed of EPW and tire during free rolling at dry mosaic condition	100
Figure 4.3	Back EMF generation of EPW during descending at slope on dry mosaic surface condition	100
Figure 4.4	Distance travel at different initial braking speed.	102
Figure 4.5	Speed of tire and EPW during dynamic braking at different initial braking speed: (a) 0 m/s (b) 1 m/s (c) 2.5 m/s.	105
Figure 4.6	(a) Slip ratio during dynamic braking at initial different initial braking speed (b) scale up slip ratio	106
Figure 4.7	Distance travel for different plugging braking at initial speed 0 m/s	108
Figure 4.8	Speed of EPW and tire braking at different plugging voltage	108
Figure 4.9	Slip ratio for different applied plugging voltage at initial speed 0 m/s	109
Figure 4.10	Distance travel for different applied plugging voltage at initial speed 1 m/s	111
Figure 4.11	Speed of EPW and tire when different	112
Figure 4.12	Slip ratio for different plugging braking	114
Figure 4.13	Distance travel when different plugging is applied at initial speed 2.5 m/s	115
Figure 4.14	Speed of EPW and tire during plugging voltage is applied at speed 2.5 m/s	117
Figure 4.15	Slip ratio analysis when different plugging braking are applied	118

Figure 4.16	Distance travel by using plugging voltage control at initial speed 0m/s	120
Figure 4.17	Speed of EPW and tire using plugging voltage control at initial speed 0m/s	120
Figure 4.18	Control input of plugging braking during braking at initial speed 0 m/s	121
Figure 4.19	Amplitude response of controlling the speed	122
Figure 4.20	Output speed at different supply voltage	123
Figure 4.21	Fitting curve for torque constant estimation	125
Figure 4.22	Residual estimation of Resistance and Torque constant	126
Figure 4.23	Fitting curve for bearing and load torque constant estimation	127
Figure 4.24	Residuals of Bearing and Load torque estimation	128
Figure 4.25	Deceleration at different applied braking torque	129
Figure 4.26	Fitting curve for moment inertia estimation	130
Figure 4.27	Residuals moment inertia estimation	130
Figure 4.28	Output speed responses between experiment and simulation by using estimated parameters	132
Figure 4.29	Output current responses between experiment and simulation by using estimated parameters	132
Figure 4.30	Output speed responses between experiment and simulation by using calibrated	133
Figure 4.31	Output current responses between experiment and simulation by using calibrated parameters	134
Figure 4.32	Effect of slip ratio by changing the surface coefficient	135
Figure 4.33	Slip ratio response between experiment and simulation	137
Figure 4.34	Validation of distance travel	139
Figure 4.35	validation of speed control	140
Figure 4.36	Validation of plugging voltage input	141
Figure 4.37	(a) Distance travel of EPW (b) Distance travel using plugging voltage at initial speed 2.5m/s	142
Figure 4.38	Speed of EPW and tire	143
Figure 4.39	(a) Input voltage to electric motor (b) Control input of plugging voltage at initial speed 2.5m/s	144
Figure 4.40	Amplitude response of speed	145
Figure 5.1	Hill descent control intergrated with gyro sensor	148

LIST OF SYMBOLS

U	EPW speed (m/s)
ω	Rotational Speed (rad/s)
v_t	Tire Speed (m/s)
T_b	Braking Torque (N.m)
T_f	Friction Torque (N.m)
T_g	Gravitational Torque (N.m)
F_x	Friction Force on x-axis (N)
F_{grip}	Gripping Force (N)
V	Voltage (Volt)
i	Current (Amp)
P	Power (Watt)
B	Bearing Constant
R	Resistance (Ohm)
K_t	Torque Constant
J	Moment of inertia (kg.m^2)
L	inductance
θ	Slope (degree)
σ	Standard Deviation
n	Numbers of Sample
\bar{x}	Mean/Average
K_p	Proportional gain
K_i	Integral gain
K_d	Derivative gain
T_s	Settling Time (s)
T_r	Rise Time (s)
ρ	Slip Ratio
μ	Friction Coefficient

LIST OF ABBREVIATIONS



EPW	Electric Powered Wheelchair
PW	Powered Wheelchair
MW	Manual Wheelchair
SW	Smart wheelchair
EV	Electrical Vehicle
RESNA	Rehabilitation Engineering Society of North America
ADA	American Disability Acts
BLDC	Brushless Direct Current
EMF	Electro Motive Force
DC	Direct Current
PID	Proportional Integral Derivative
SMC	Sliding Mode Control
HDC	Hill Descent Control
HAS	Hill Assist System
PPR	Pulse Per Rotation
PPS	Pulse Per Second
RPM	Revolution Per Minute
SSE	Steady State Error
SOC	State of Charge
RB	Regenerative braking
DB	Dynamic Braking
PB	Plugging Braking
EWB	Electro Wedge Braking

CHAPTER 1

INTRODUCTION

1.1 Introduction

This chapter will discuss the conducted project including the project background, problem statement, objectives, scopes, project planning and the thesis outline in detail. The Gantt chart is also attached to guide the flow of the whole project.

1.2 Project Background

In recent years, Electric Powered Wheelchair (EPW) is widely used due to its mobility. By using the electric motor as the drive system, EPW can be ridden easily. Although the EPW ease the users' mobility, there are some safety aspects that is still lacking such as the difficulty to control the braking speed when descending on slopes. This situation occurs more frequently for those who suffer from physical disabilities. Therefore, the key motivation on this research is to increase the safety for EPW users. The new automated braking system is implemented in EPW which offers safety while maintaining the comfort of EPW users when descending on sloped surfaces.

The Electric Powered Wheelchair (EPW) can be considered as a small-scale electrical transportation. This consideration becomes the second motivation in this research that is to provide the EPW with a suitable safety system for various levels of disabled EPW users by implementing the same safety system that has been used in electric vehicles (EVs). In the last few years, the focus of developing vehicle safety applications has shifted from a passive safety system (PSS) to an active safety system (ASS). The passive safety systems are the systems that react to abnormal events. It means that these systems activate during or after the accident takes place. Thus, the passive safety systems help to reduce or decrease the effect of abnormal events, like an accident, by

implementing safety systems such as air bags and seatbelts. In contrast, the active safety system includes a set of safety features which reduce the chances of an accident or collision to occur in the first place. Some manufacturers call it the 'Primary Safety System'. Manufacturers employ the active safety systems mainly to avoid accidents. These systems activate before the accident takes place so that they could possibly avoid the accident by providing real-time data collecting and processing. The most common example of the active safety system is the Antilock Braking System (ABS) that prevents the tires from being locked during braking (Aksjonov et al., 2018), Traction Control System (TCS) that prevents tires from slipping during accelerating on slippery pavements (Berger et al., 2015) and Hill Descent Control (HDC) that controls the speed of vehicles automatically during descents on a downhill (Y. Luo et al., 2015). These technologies and developments can also be implemented in small-scale transportations such as EPW in order to increase the safety and mobility aspects.

The drive system for EPW is an electrical motor. There are several advantages of electric motors such as fast torque response, small size but powerful output and the ability to generate the electrical braking torque (M. Heerwan et al., 2016). From these advantages, electric motor becomes the role of motivation in accomplishing this project. Without using external braking such as mechanical braking to reduce the speed, this unique machine can produce their own braking mechanism. An electrical motor can change the operation according to the application. This machine can be a motoring operation when the voltage is supplied to the terminal. In another condition, it can be a generator which converts kinetic energy into electrical energy (Gökçe et al. 2015). During the generating operation, the motor will generate the backward voltage known as the back electromotive force (EMF). The current will also flow reversely due to the excessive inertia from the tire. By resisting the current flow, the braking torque will be generated to reduce the speed of motor. This mechanism is known as electrical braking which comprises of regenerative, dynamic and plugging braking. Utilizing the electrical braking, the active safety system such as ABS and HDC can be realized in EPW.

1.3 Problem Statement

The common braking system of EPW is the manual mechanical braking system. In this system, the mechanical braking torque is produced from the friction between the brake pad and wheels. The disadvantage of this braking system is that the braking torque is proportional to the force from the user's hand grip. On a sloped surface, the stopping distance and time are based on the force from the user's hand grip. If the users are elders or paralysed, the EPW will take a longer distance and time to stop due to the low force of hand grip (Massy et al., 2011).

In a critical situation, the EPW will keep accelerating when the angle of slope is too steep. This is caused by the pulling factor from the gravitational force. Although there is a specific regulation of the height of slopes that has been introduced by Malaysia Standard (MS-1184), many buildings do not meet that requirement which stated that sloped surfaces must be lower than 1:12 or 4.8° (Aqmar et al., 2018). For that reason, there are many accidents and injuries reported when descending sloped surfaces (Xiang et al. 2006; Chen et al., 2011; Bertocci et al. 2014; Maeda et al. 2018). Hence, the speed of EPW needs to be controlled properly by applying the active braking control system such as the HDC in EPW. The implementation of this system offers a safety and comfortable ride for EPW users during descents on slopes.

1.4 Objective Research

In this research, the objectives are divided into three that listed as below:

1. To investigate the dynamic behaviour of EPW by using electrical braking during descents on slopes.
2. To develop an active braking control system based on the suitable electrical braking during descents on slopes in experiment and simulation work.
3. To analyse the active braking control system's performance during descents on slopes in experiment and simulation work.

1.5 Scopes

1. The experiment of dynamic behaviours was conducted by using electrical braking which consists of dynamic, regenerative and plugging braking at sloped surfaces.
2. The development of the active braking control system was done in the myRIO embedded system.
3. The performances of the active braking control system has been analyzed in experimental work with the descent on sloped surfaces.
4. The active braking control system was modelled in the MATLAB-Simulink environment.
5. The active braking control system performance was simulated and analyzed in the simulation work.

1.6 Thesis Outlines

The chapter one introduced how project is investigate according to the current issues and potential of development. Besides that, it includes the Introduction, Objectives, Problem statement and Scope of the project. The objective is an aim for the project to be achieved. The problem statement is where the question arises on why need to conduct this project and for what purpose. Furthermore, the scopes are narrowed down to target area so that the whole project will be more focused and precise. In this chapter, the entire project planning is included. In this manner, there will be a timeline to get the project done on time without delay.

Chapter two starts with an introduction to the section. This chapter focuses on journals and paper review on what was done by other researchers on the related project. The journal might not be similar but helpful to give idea, knowledge and guide to the project being conducted. This chapter will also provide basic approaches to use suitable method, tools, equipment and many more. This chapter is crucial as it is the root of how the idea initially sprouted and makes the whole project successful. The content of the section will review on development of Electric Powered Wheelchair (EPW) from past and present. In addition, the electrical braking consist of dynamic, regenerative and plugging and its control strategies are mentioned in this chapter.

Chapter three is about the methodology of the project. Therefore, the project will be divided into the experiment and numerical analysis. The methodology is also a documented process of how the modelling, analysis and experiment of the project are done. In the experiment section, the whole process of the fabrication of EPW and sensors installation will be explained step by step. It also shows the steps to conduct the experiment of braking performances between mechanical and electrical as well as the correct method to estimate the parameter for the EPW mathematical modelling plant. In the numerical simulation, the automatic braking performance of EPW is simulated in Matlab Simulink to analyse the braking control ability and speed respond during descending at slope condition. Chapter three also reveals the project flow chart whenever problems arise during simulation and experiment. This chapter helps to keep track of the simulation analysis and project design period.

Chapter four is the highlighted chapter of the whole thesis. The result and discussion of the entire project will be documented in this chapter. The project will discuss on the braking performance of electrical braking analysis data and also automatic braking control ability of EPW on the slope condition. Justification will be made in this chapter on the result of the project.

Chapter five is the conclusion and recommendation part whereby the whole outcome of the research will be concluded. Several of key findings that found from the investigations are also stated. Recommendations are needed for future improvement and also to enhance the quality of the project in the future.

CHAPTER 2

LITERATURE REVIEW

2.1 Development of Electric Powered Wheelchair

The general keyword of EPW is to indicate the wheelchair whether Powered Wheelchair (PW), Motorized Wheelchair (MW), Electric Wheelchair (EW) or Smart Wheelchair (SW) which are driven by using the electric motor. This chapter will reveal the research and development of EPW from past until present. The reviews are organized as follows: the discussion will start on the past Electric Powered Wheelchair (EPW) development that is known as PW in Section 2.2. Next, the discussion will be appointed on the present research and development that had been made in EPW that is also known as Smart Wheelchair (SW) in Section 2.3. In Section 2.4, the review is focused on dynamic control enhancement in EPW. Followed by that, the review is revealed the types of braking that are being used in nowadays' transportation in Section 2.5 which includes mechanical braking (Sec. 2.5.1) and electrical braking (Sec. 2.5.2). Lastly, Section 2.6 discussed the recent type of system technology that used to control the speed during descending on the slope. This review gave the better understanding and ideas to the researcher about the technologies and system being implemented in EPW. It can also assist the researcher to develop new active control system to enhance the safety system in EPW.

2.2 Past research: Powered Wheelchair (PW)

The first Powered Wheelchair (PW) was invented by George Klein who worked as a mechanical engineer at the National Research Council of Canada. The purpose of PW development is to assist the veterans who suffered quadriplegia or paralysis for certain limb parts during the Second World War II (Ba and Watson, 2016).



Figure 2.1 The Powered Wheelchair invented by George Klein.

Sources: Ba and Watson, (2016)

The operating system of PW is shown in Figure 2.2 which is also known as open loop operation because there are no feedback modules being implemented such as sensors and microcontroller. When the user gives the input from the joystick, the signal will modulate in motor regulator module (motor driver) to form the voltage output which generate the electric input for the electrical motor. In the beginning, the PW's appearance is only equipped with electric motor, battery and joystick controller.

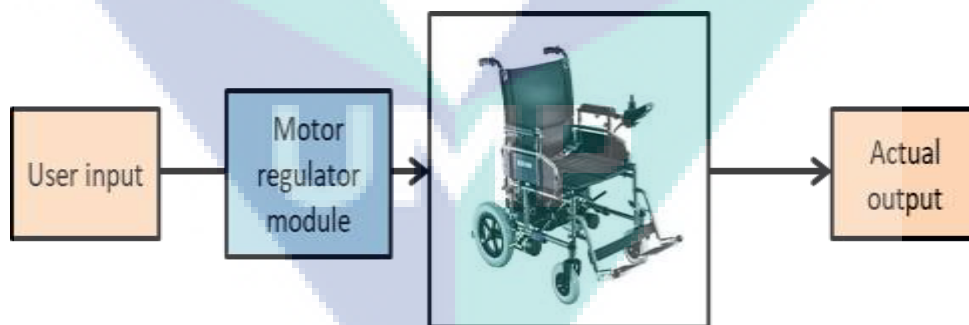


Figure 2.2 Open loop operation of Powered Wheelchair

Then, because some users could not use the traditional joystick for navigation, the head joystick, chin joystick, sip-n-puff and thought control were introduced as alternative for the controller input (Desmond et al., 2013; Millán, 2013; Mazumder et al., 2014; Pasteau et al., 2014; Sinyukov et al., 2014).

2.2.1 Commercialization of PW

The PW development does not stop just as research material. In 1956, the PW became mass sales after the collaboration between Everest & Jennings and the American Wheelchair Company (Fritsch, 2013). Figure 2.3 shows the development of PW invented for disabled people's mobility according to their needs. The recommended PW's specification in shown Table 2.1.

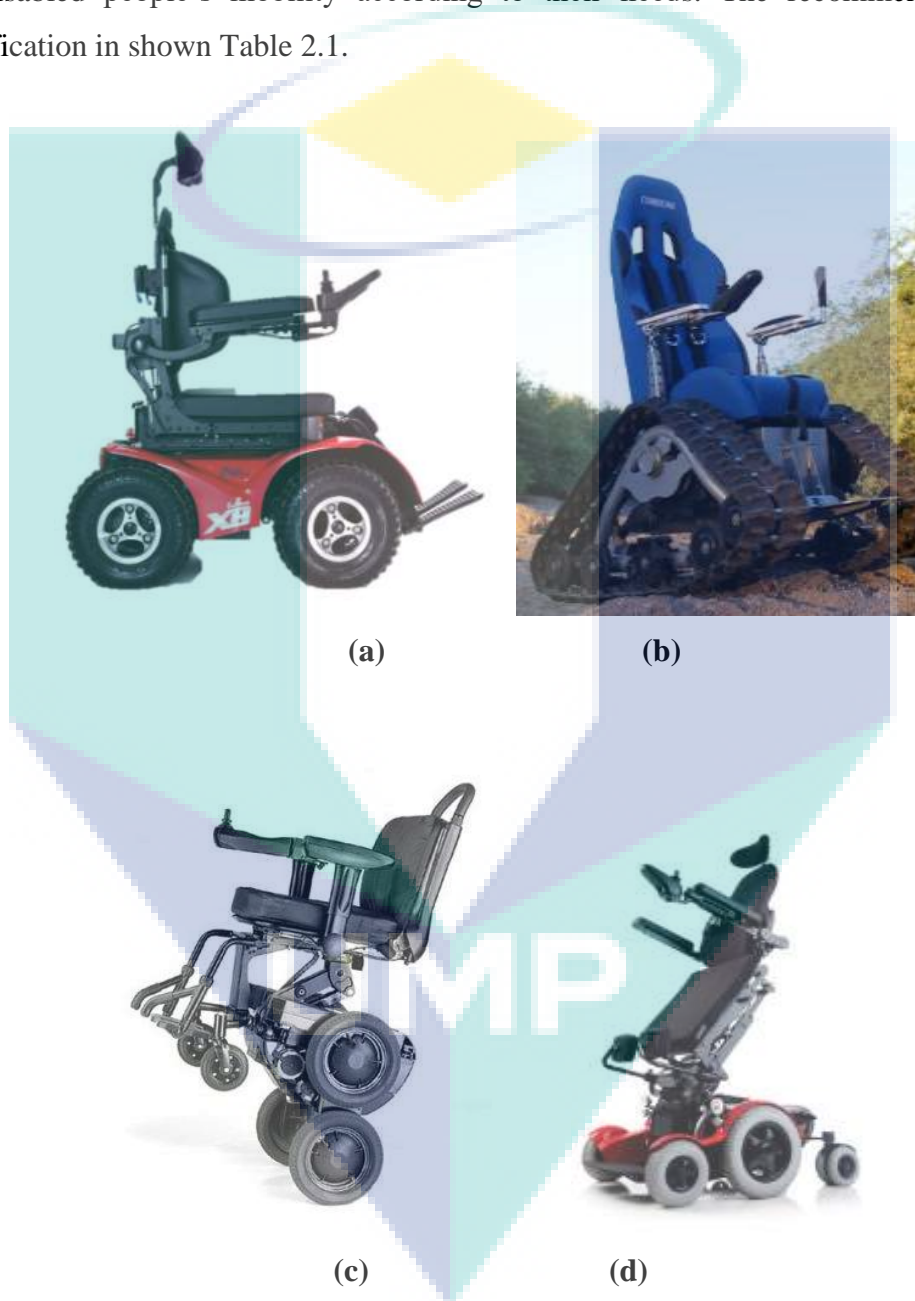


Figure 2.3 Available type of commercialized Powered Wheelchair.
Sources: Fritsch, (2013)

Table 2.1 Available specification the commercialized Powered Wheelchair (PW)

Feature in PW	Details
Drive System	<ol style="list-style-type: none"> 1. front-wheel drive 2. rear-wheel drive 3. all-wheel-drive (Figure 2.3a) 4. All-terrain tank tracks (Figure 2.3b)
Batteries	<ol style="list-style-type: none"> 1. 12 and 24V lithium-ion batteries
User Input (controller)	<ol style="list-style-type: none"> 1. hand joystick 2. sip-n-puff 3. chin joystick 4. head joystick
Seating system	<ol style="list-style-type: none"> 1. Seats are typically upgraded to include cushions that use foam, gel, or air to prevent pressure sores; 2. Backrests are usually padded with foam and can be motorised to tilt and recline; 3. Lateral supports keep the user from tilting side-to-side; and Footrests, are either removable or motorised to accommodate a more comfortable reclining position
Add on feature ability	<ol style="list-style-type: none"> 1. Chassis may be foldable, include stair climbing ability (Figure 2.3c) (Model, 2017) 2. Standing ability (Figure 2.3d)

Overall, past studies have successfully achieved initial technological advancements that aid PW users in their daily activities. By default, the Powered Wheelchair PW is in commercialization phase. Nevertheless, there is little assistive technology included in the wheelchair to make it "smart," which is the goal of research in integrating "intelligent" technology on a PW, called "smart wheelchair" that will be discussed in the next section.

2.3 Present research: Smart Wheelchair

This section presents the current Smart Wheelchair (SW) research achievements around the world revealing a major shift from PW to SW. Different from the PW, the operation of SW became more complex but give better ride performance and mobility. Figure 2.4 shows the closed loop operation where the SW is attached with the sensors as feedback and some computer algorithm.

In general, SW is moved when the user gives inputs to the microprocessor either from the joystick or another type of controller input. The speed sensor is the basic acquisition instrument in EPW which is used to measure the rotational speeds from EPW tires. By comparing with the desired speed, the output is known as error. Next, the microprocessor that works as the brain will calculate the error term in design controller and send the signal to the motor driver based on the predefined algorithms. This system is known as the embedded speed control module that can usually be found in current SW.

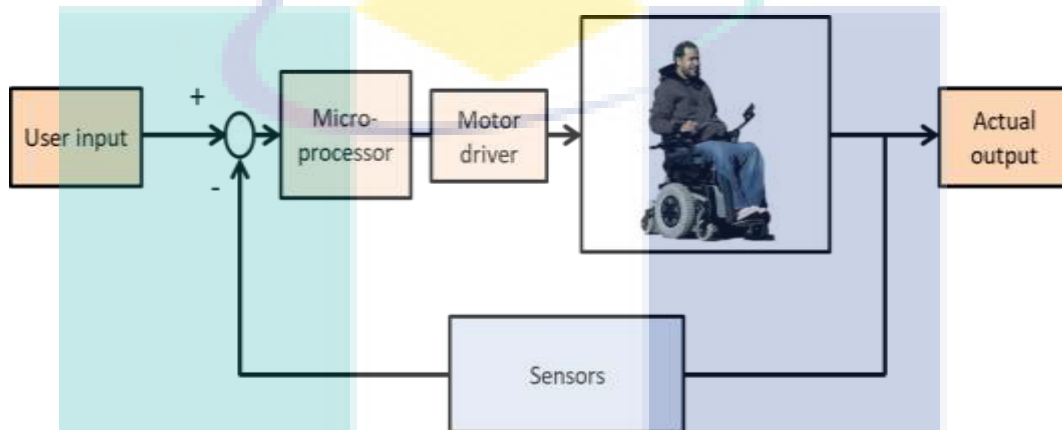


Figure 2.4 Electric Powered wheelchair block diagram operation

Sources: Jain & Argall, (2014)

There is another automatic control feature that is provided in SW such as speed control and traction control. The automatic control feature on this EPW has been reviewed by a group of doctors for patients who use EPW as their primary method of mobility (Steven et al., 2000). Results from the clinical survey show that the feature helped the patients, especially when controlling EPW compared from using the conventional EPW controls. Table 2.2 shows the lists of several institutions around the world that have produced SW prototypes. The list illustrates that interest in the topic of EPW has grown over the years.

Table 2.2 Interest research of SW around the globe

Description	Location	Years
Northwestern University (Jain & Argall, 2014)	Illinois, USA	2014
UMBC (Carrington et al., 2014)	Maryland, USA	2014
University of Nevada, Reno (Leaman & La, 2015)	Nevada, USA	2015
Universiti Malaysia Pahang (Alsibai et al., 2018)	Pahang, Malaysia	2018

2.3.1 Advance user input for Smart Wheelchair

Similar with PW, SW also needs input from user. However, the SW input is more advanced than PW. In this section, this review will discover part of researches regarding advance input that had been implemented in SW operation system. Figure 2.5 shows several of advance input methods that is used in SW which include Biometric and Brain-Computer Interface (BCI) as well as cloud base. The common research of advance input user is biometric motion. The biometric input motion means the user use their body motion as the input for the system to navigate the EPW. Numerous researches show that these types of input help the users with severe cognitive impairment and provide the amount of help needed at each moment to avoid loss of residual abilities.

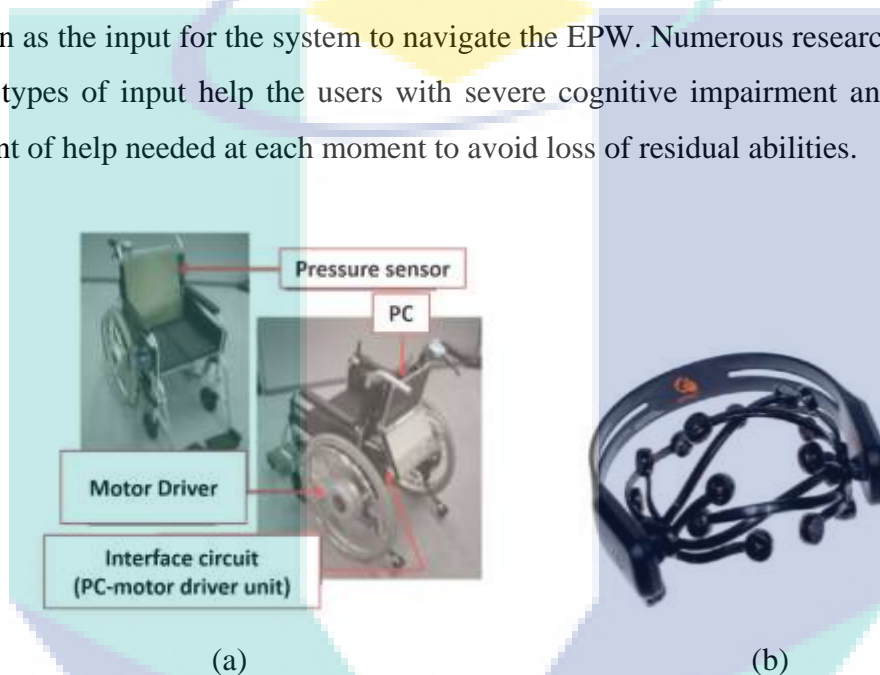


Figure 2.5 (a) Biometric (b) Brain Computer Interface (BCI)

One of the examples of advance input for the electric wheelchair was proposed by Yokota et al., (2011) which is known as Human Body Motion Interface (HBMI). The center of weight on the pressure sensor is attached to the backrest of EPW as shown in Figure 2.5. HBMI uses the body motion which is caused by voluntary action. The velocities of each wheel are determined based on the error between initial and current position of the center of weight. When user tries to stop the wheelchair, the user must rigorously return the center of gravity to the initial position. It has been confirmed by the author that HBMI, which uses the center of weight on the pressure sensor attached on the backrest as the body motion index, has the ability of an interface.

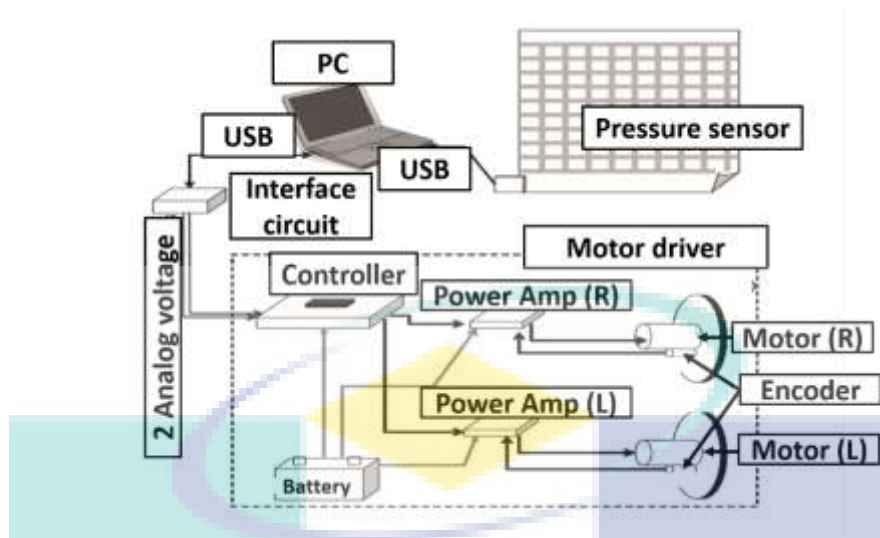


Figure 2.6 Schematic diagram of HBMI

Another type of advance user input is Brain-Computer Interface (BCI). The BCI is a communication between a brain and another device system that allows the signal from the brain which is measured by an electroencephalograph (EEG) directly to some activities such as controlling the prosthetic limb. The interface enables a direct communication pathway between the brain and the object to be controlled. In the case of controlling the EPW, for example, the signal from the brain is transmitted directly to the Electronic Control Unit (ECU) to give the command such as; moving forward, backwards or turn as shown in Figure 2.7.

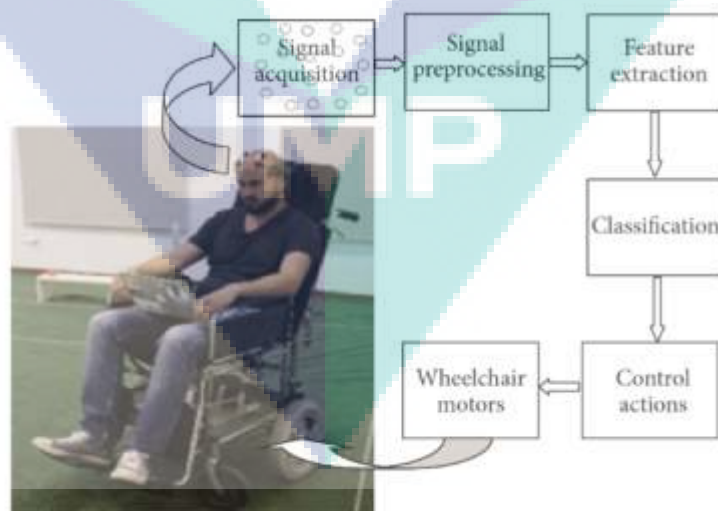


Figure 2.7 BCI for EPW navigation

Source: Abiyev et al., (2016)

The commercially available BCI was evaluated by Urbano et al. (2011), and Fattouh et al., (2013). The BCI can even be used to monitor the user's emotional state, for example, when the user is frustrated, the control unit will stop the wheelchair and wait for a new command from the user. In normal cases, the control unit will continue to execute the previously selected command.

2.3.2 Advanced sensors input in Smart Wheelchair

i. *Laser Range Finder (LRF)*

The frequently used sensor in SW research is the Laser Range Finder (LRF). The LRF can determine accurate obstacle where drop-off detection is possible. It also provides a 180°, two-dimensional scan within the plane of the obstacles in the environment (Rao et al., 2002). Unfortunately, LRFs are expensive, large, and consume lots of power, which make the task of mounting difficult.

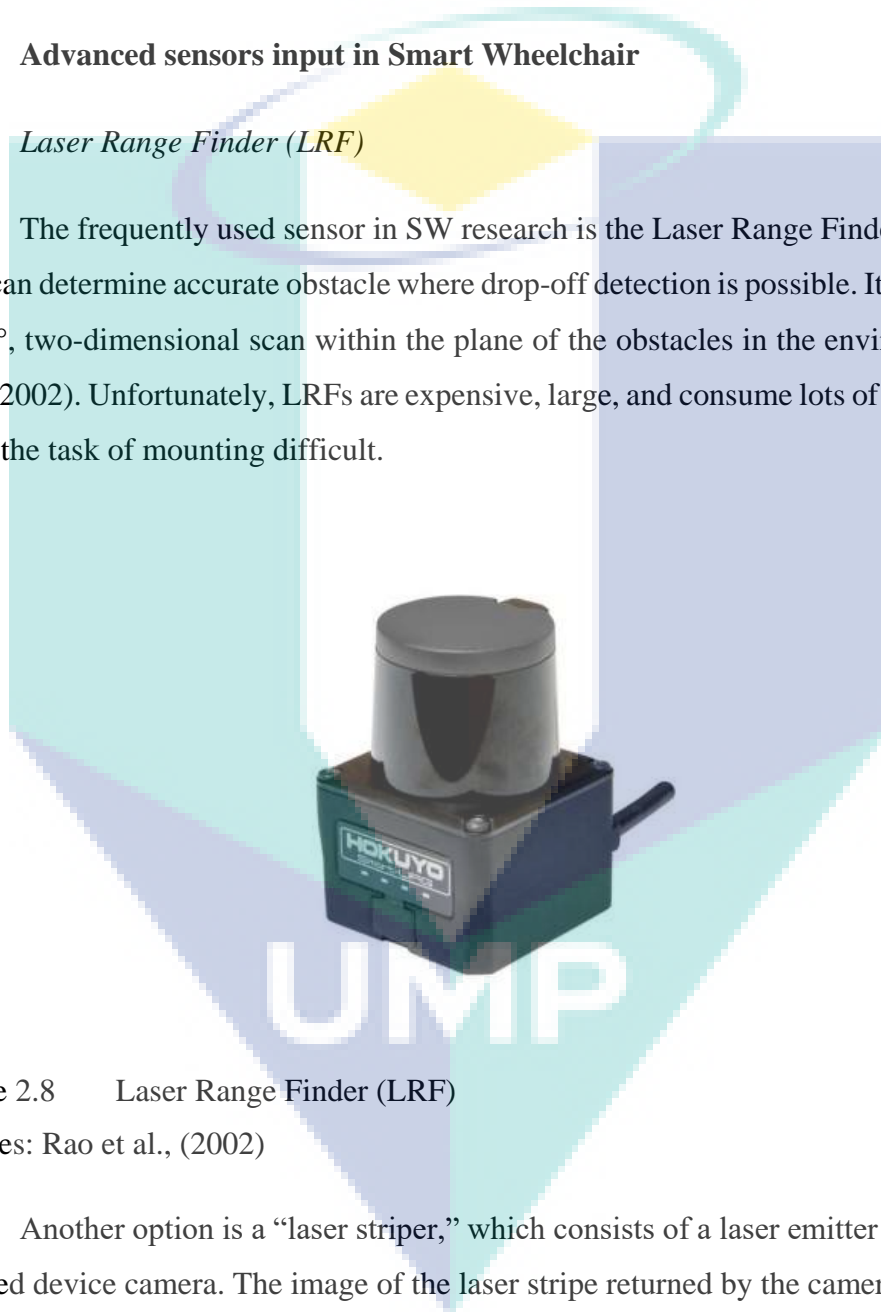


Figure 2.8 Laser Range Finder (LRF)

Sources: Rao et al., (2002)

Another option is a “laser striper,” which consists of a laser emitter and a charge-coupled device camera. The image of the laser stripe returned by the camera can be used to calculate distances to obstacles and drop-offs based on discontinuities in the stripe. A laser striper is less expensive than an LRF but can return false readings when the stripe falls on glass or dark surface.

ii. *Visualize sensor*

By using stereoscopic camera and spherical vision system (Jordan, 2012), 3D scanners like Microsoft's Kinect as shown in Figure 2.9 (Simpson, 2005), and most recently the Structure 3D scanner, it has become possible to use point cloud data to detect hazards like holes, stairs, or obstacles (Cockrell et al., 2013). These sensors have until recently been relatively expensive, were large and would consume a lot of power. The Kinect was found to be a useful tool for target tracking, localization, mapping and navigation (Benavidez and Jamshidi, 2011; Fallon et al., 2012; Kulp et al., 2012).



Figure 2.9 3D scanners like Microsoft's Kinect

Sources: Benavidez and Jamshidi, (2011); Fallon et al., (2012); Kulp et al., (2012)

2.3.3 The Smart Wheelchair Commercialization

Even when the SW is still in the research phase, there are already several types of SW available at the market. Several department and companies already market their SW (Henderson et al., 2014) while providing researchers with embedded system that is fully compatible, and communicates seamlessly with current manufacturer's wheelchair systems. Their system which is available in the market provides number of sensors and runs guidance and navigation algorithms that can modify the human desired joystick trajectory and helped users to avoid obstacles during moving from room to room. SWs should be customized to each consumer, making it difficult to expand a business or lower the cost of a SW (by mass production).

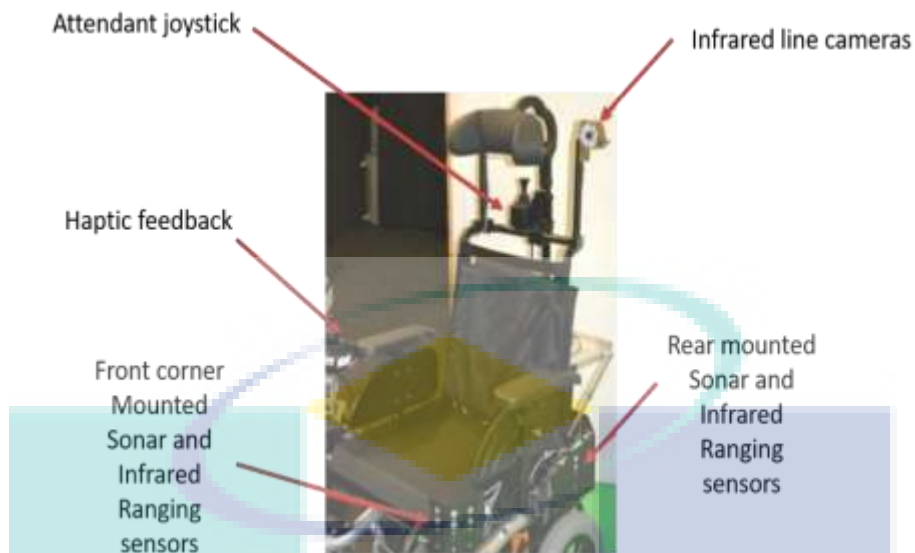


Figure 2.10 Commercialized Smart Wheelchair

Source: Henderson et al., (2014)

Toyota Motor East Japan Inc., a manufacturing subsidiary of Toyota Motor Corporation, has embarked into personal electric vehicle (PEV) business, which demonstrates that there is a market for technology very similar to the SW. PEV is modified for indoor uses by individual with disability. In general, apart from current technological issues, non-technical barriers also hamper the commercialization. Prescribers and insurance providers want to avoid liability and want proof that the SW technology works (Bridge, 2015).



Figure 2.11 Personal Electrical Vehicle (PEV) introduced by Toyota

Source: Bridge, (2015)

2.4 Dynamic control enhancement in EPW

In this section, the discussion will focus on the dynamic control that had been developed for the Electric-Powered Wheelchair (EPW). The improvement or development of dynamics are done through the selected Degree Of Freedom (DOF) (Furukawa and Abe, 1997).

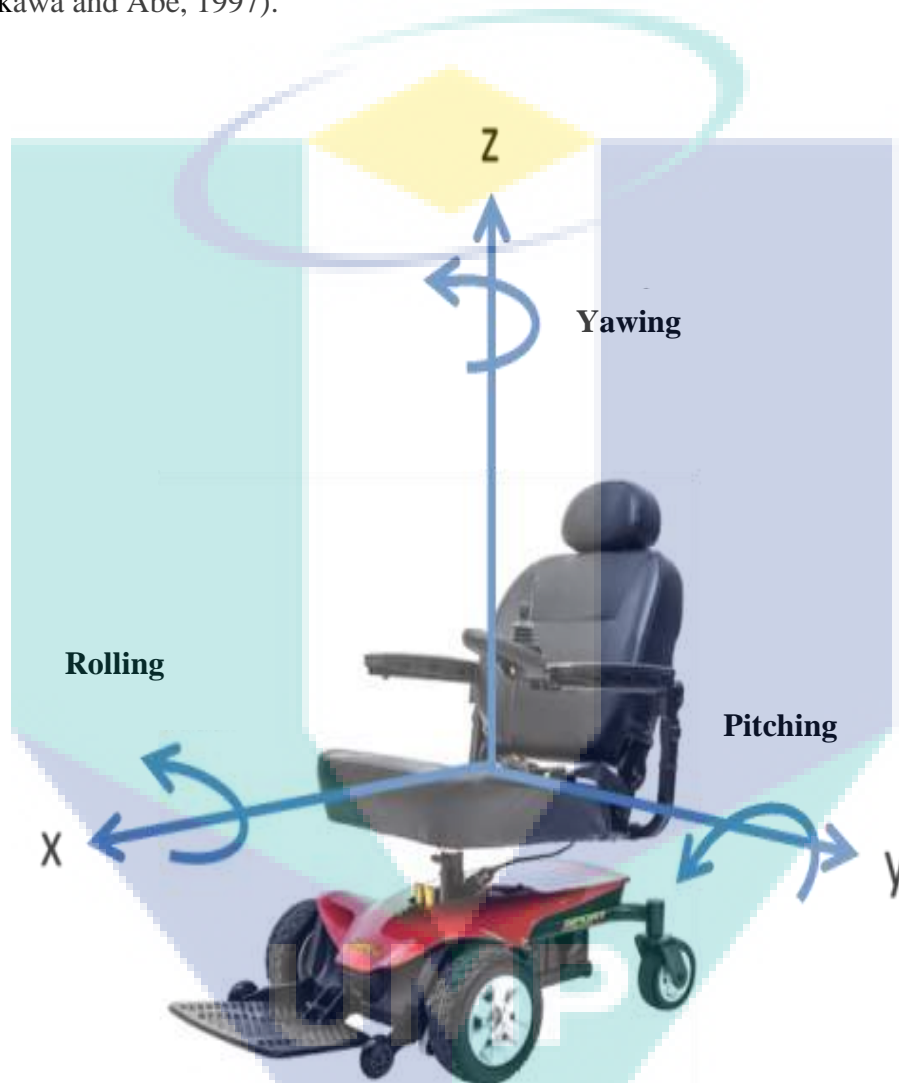


Figure 2.12 Degree of freedom for Electric Powered Wheelchair

Sources: Furukawa and Abe, (1997)

Figure 2.12 shows the 6 DOF of EPW which consist of x, y and z-axis that are known as longitudinal, lateral and axial measured in unit m/s. For each axis, it consists of the rotational angular which is also known as rolling, pitching and yawing measured in unit rad/s that respect to x, y and z-axis. Thus, the dynamic control for the EPW can be divided into three sections which are; longitudinal and lateral, axial and stability control (yawing, pitching and rolling) as shown in Figure 2.13.

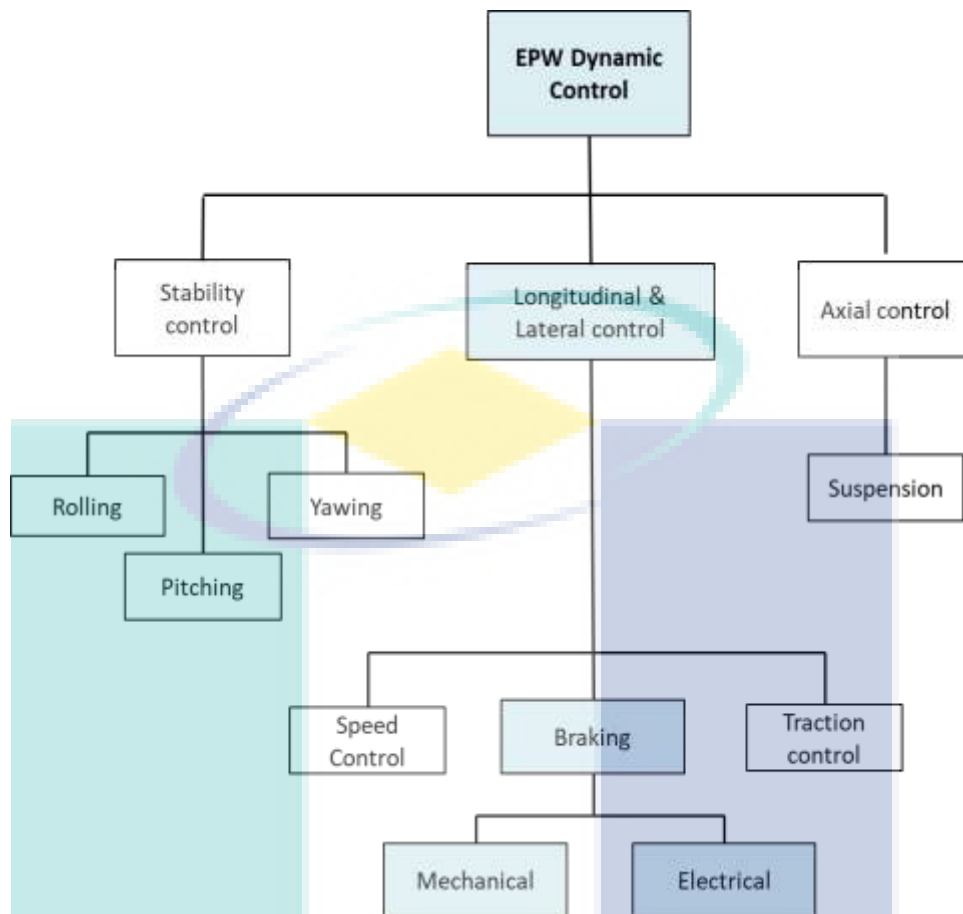


Figure 2.13 Hierarchy of dynamic control for EPW

2.4.1 Stability control

Stability can be described as the ability of object to remain at same position in any condition. There are many factors that cause EPW tips and falls which are; slope height and position of Centre of Gravity (CG) in EPW. When the EPW ascend on the high slope condition, it tends to tilt over. Besides, the tips and fall can occur when the height of CG in EPW is highest from the ground level (Hong et al., 2016). The study accomplished by Kirby and Macleod (2001) stated that the average accident of wheelchair was reported about 85,000 incidents in one year. The number of incidents is estimated to be increased year by year. The United States Consumer Product Safety Commission (USCPSC) also stated that around 770 deaths were reported among the wheelchair users in 14 years, to which large of number percent was contributed by fall and tips problem which is around 77.4% (Ummat & Kirby, 1994). These situations attracted many researches to be conducted to make the wheelchair a safe transportation for the disabled people.

In early research of tips and falls, Kirby et al., (2010). investigated the static stability by using test dummy. The test begins by slightly tilting the wheelchair in different direction at different slope angle. Then, the tilting condition is investigated by changing the load on the wheelchair at certain slope. Based on recorded observation, it can be concluded that at the slope less than 8 percent, the tilt over of wheelchair can be prevented. However, when the slope height is increased, the wheelchair begins to tilt. Another study was conducted by Cooper et al., (2016) to define the stability of a wheelchair by validating between theoretical and data of experiment. The experiment was conducted by using human as the rider. Other than that, Pavec et al., (2011). also developed the kinematic model of wheelchair in order to simulate the stability of wheelchair in different moving condition (lateral and transverse). Ohnabe and Mizuguchi (2011) conducted the experiment to analyse the stability of wheelchair during descending and ascending on tilted over-slope. A study by Cooper et al., (2013) was conducted to observe the stability of wheelchair during braking by comparing the situation when using and without using seat belt and leg rest. The result demonstrated that the stability decreased when the seat belt and leg rest was removed from the wheelchair. The experimental study conducted by Corfman et al., (2014) is also similar to Cooper et al., (2015). However, in Corfman et al., (2014) research, the stability of wheelchair was investigated by the effect of proper seatbelt and leg rest adjustment during avoidance of the obstacles. The result of experiment showed that the dummy with improper adjustment of seatbelt and leg rest fell while avoiding the obstacles. This experiment shows that proper adjustment of seatbelt and leg rest offer better safety for EPW's users.

William and Payandeh (2016) designed a model of an EPW to examine the tipping stability of EPW's user during accelerating. In the research, the length between Centre Gravity (CG) and pivot wheel was changed. The results of improvement showed that the stability can be maintained by changing the mass distribution. In the modern control system, the dynamic control of the wheelchair stability can be enhanced by integrating various sensors and algorithm. The example of EPW that used the sensing device was proposed by Torres (2016). This EPW provides stable seat during movement in uneven terrain by retracting and extending the seat based on proper stability control. Meanwhile in Japan, Ding and Cooper (2016) reported that rehabilitation Centre at Yokohama developed the passive safety system known as air bag cushion. The cushion will be

inflated when the wheelchair is tilted over. Following that, the conducted analysis showed that the implemented system can reduce the shock experienced by user's head.



Figure 2.14 Balancing mode of the iBOT 3000
Sources: Kamen et al., (2017)

More current technology that had been established to solve the stability problems was introduced by Kamen et al. in 2017, known as iBOT 3000 Transporter. Using the inverted pendulum concept, this EPW can balance the body by itself as shown in Figure 2.14. The iBOT Transporter is equipped by advanced sensors such as gyroscope to measure the angular rotational, tilt sensor to measure the EPW's tilt angle and speed encoder to measure distance and speed of tire. The angular rotational that is also known as pitching is set at 0 rad/s. The error between current angular rotational and set angular can be as the input voltage for electric motor to move forward or backward. This situation will lead the position of iBOT 3000 to remain standing and balanced, same as the inverted pendulum concept.

Some researches on iBOT 3000 showed good feedback. A study conducted by Cooper et al., (2017) reported that the iBOT 3000 transporter is very helpful among the EPW users. In that study, the uses of iBOT can be seen around shopping malls as well as researchers' colleagues. Apart from that, iBOT 3000 also offers better transportation especially for people who suffer back bone injuries.

2.4.2 Axial control: Suspension control

The Powered Wheelchair is also commonly used in the outdoor environment. Hence, the EPW often deals with bumpy road, uneven terrain and curb section that causes direct axial force to the EPW's users. Seidel and Heide (2014) stated that direct axial force affects about the users to experience traumatic shock at the back bone especially at spinal cord. Long-term experiences to the shock can cause mental and physical fatigue. In light of this, one of standard regarding whole body vibration had been introduced by American National Standard Institute (ANSI) and International Standard Organization (ISO). There are several important things introduced in this standard including exposure time dealing with vibration (frequency) and amplitude that might cause the physical effects to the EPW's users. Thus, one of improvement to reduce the shock impact to users is by installing the suspension system in EPW. The ideas to install the suspension system is to reduce the axial force that acts directly to the EPW users. In addition, the installation of suspension system can assuage the trauma and offer comfort as well as improve the quality ride to the EPW's users at the same time (Smith and Leggat, 2015).

DiGiovine et al., (2016) investigated the effect of wheelchair mass with the comfort level during traversing the curb, uneven and bumpy road course. Based on ergonomics and comfort level, the survey result showed that users prefer to use ultra-light EPW (less than 13.5 kg) than light-weight EPW (13.5 kg – 16.5 kg) during travelling in different type of terrains. Based on human level vibration transfer, the acceptable natural frequency that human can be exposed to is around 4 Hz to 15 Hz. This value becomes the set point for wheelchair researcher and manufacturer to develop the suspension system. In research field, the use of suspension system in wheelchair becomes trending in lowering the high amplitude and time exposure to vibration. Kwarciak (2016) used the suspension to reduce the vibration transmitted while descending on curb terrain.

In commercialization, Cooper et al., (2016) reported that several manufactures already commercialize powered wheelchair equipped with the passive suspension technology system. Many observations had proven that suspension system can reduce vibration while offering comfort. The example of suspension system in wheelchair that is already invented in the market is known as Omega Trac that was realized from the pattern suspension introduced by Thomas and James in 2015. The features included in Omega Trac such as dual spring in rear and front can be adjusted according to the single

mass of users only. Next, the suspension system in EPW is upgraded by Magic Mobility, Inc in their EPW known as SPECTRE. The additional features in EPW is upgraded from the previous Omega Trac in which the suspension can be adjusted for better axial control in different range weight of users. Many tests had been conducted by using the SPECTRE to investigate the ability to control the axial force and comfortability. Cooper et al., (2016) evaluated the vibration exposure of ten unimpaired users during driving the SPECTRE and manual wheelchair that was equipped with suspension system in six different sidewalks. Power Spectrum Density (PSD) was used to analyse the vibration exposure in different sidewalk. The PSD results showed that the manual wheelchair equipped with suspension system produce high PSD reading than EPW SPECTRE when pass through the block with more than 8mm bevelled edges.

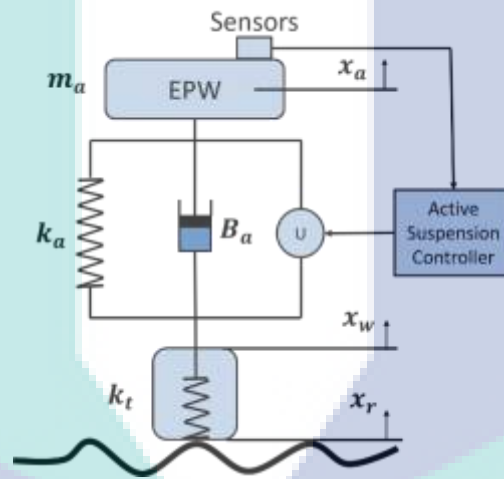


Figure 2.15 Active suspension control modelling

The suspension technology in EPW is shifted from passive to active. The active suspension system that is already used in automotive industry is implemented in EPW to increase the comfort while driving in different terrain condition (Lu and DePoyster, 2015). The combination of advance sensor such as gyroscope and inclinometer can control the axial motion and roll stability automatically as shown in Figure 2.15. The EPW that is equipped with active suspension is already manufactured in Australia, known as Glide Series 8. The advance feature introduced in Glide Series 8 is the height of suspension that can be changed according to terrain height. This automatic system can ensure all tire to stay contact at the ground without rolling and tilting over the EPW (Lendal et al., 2016)

2.4.3 Longitudinal and lateral control

i. Speed control

The most controlled variable in an EPW is speed. During normal operation, the wheelchair driver applies command inputs using a joystick or similar device based on their perception of the wheelchair's speed and direction. An electronic controller then adjusts the voltage to the dc motors to achieve the desired velocity of each motor. A typical speed control algorithm uses tracking, or contour control to follow the speed profile set by the user, regardless of terrain or slope. Therefore, the wheelchair/rider system moves at the same desired speed when going up and down a slope. The same is true when comparing a hard surface to a soft surface.

Speed control research for electric wheelchair was continued by Brown et al. in 1990 when the electric wheelchair had different type load of the driver. Adaptable optimal control developed based on the Proportional-Integral-Derivative (PID) controller had been modified. The variable structure system control is to define several sets of control coefficient applied to the system for a distinct region of the variable load parameter. The result from this research showed that an adaptable optimal control is suitable to control the speed of electric wheelchair based on characteristic load of the driver.

In research of Luo et al., (2014) , they were developed an electric powered wheelchair prototype known as “Luoson III”. By implementing a grey-fuzzy-decision-making (GFD) in Luoson III, the control of this EPW became intelligent. This research was conducted under different friction condition to determine the effectiveness of GFD controller. Through on-board sensors, including an electronic compass and an encoder for each wheel, the controller can estimate the wheelchair motion. The GFD can then determine model parameters to approximate the system dynamics according to the triangular membership function in related equation $y = (\alpha + \beta)/2$. From the result, they achieved their goal to control the velocity of EPW constant at $v = 3$ in/sec when at different condition of surface.

ii. Traction control

Traction control is a technical term used in the automobile industry (Makki & Siy, 2001; Tan & Tomizuka, 1990; Yoshida & Hamano, 2002). When a car accelerates from a dead stop or speeds up while passing another vehicle on a slippery surface, traction control works to ensure maximum friction between the road surface and the tires by stopping the spin of the wheels. Traction control can be applied to EPWs to expand the driving envelope and improve driving safety. Tires are the only part of an EPW that are intended to touch the ground, and any loss of friction can have serious consequences. EPWs are easily stranded in a sprinkling of snow, and wheelchair users often have difficulties on sandy and grassy surfaces (Tadano and Tsukada, 2013).

Currently, several four-wheel-drive EPWs are available that offer enhanced traction under less favourable road conditions. The Extreme 4 × 4 wheelchair produced by Magic Mobility, Inc. is reported to be capable of driving on sand, soft, wet ground, and slippery surfaces with its four drive wheels. This design provides the iBOT 3000 with more degrees of freedom than conventional EPWs and permits the iBOT 3000 to traverse non-uniform surfaces, inclines, climb curbs, and negotiate stairs. Observations are recorded by Algood et al., (2015) using the iBOT 3000 to traverse uneven terrain such as grass, a parking garage curb cut, an uneven sidewalk, and steep driveways. Another all-terrain wheelchair unveiled in 2013 is the OmegaTrac by Teftec Mobility of Spring Branch, Texas. The OmegaTrac's drive system steers through a differential transmission activated by an electric motor and can traverse moderately steep inclined surfaces.

Other than the use of four-wheel drive or improved tires, there has been no research on traction control for two-wheel-drive vehicles under less favourable surface conditions. Work related to traction control is usually found in the automotive literature. In the study of Yoshida and Hamano (2016), a method that constrains the slip ratio of a rover is proposed to limit excessive tire velocity or force so that the planetary rover can successfully traverse sandy obstacles by avoiding spinning wheels stuck in loose soil. Wheelchair traction control schemes can also learn from automotive applications. For example, it is possible to influence traction force by varying the wheel slip, $\lambda = (r\omega - v)/r\omega$ which can be obtained by monitoring the wheel velocity $r\omega$ and the wheelchair velocity v .

2.5 Braking system in transportation

The most important system in the dynamic control of transportation is the braking control system. Research related to the braking for Electric Powered Wheelchair (EPW) is still a slight amount. However, this section will reveal the ideas of braking that had been used in other transportation for the implementation in EPW.

In order to stop a vehicle accurately and properly is depends on the method of braking control that is applied. Another function of the braking system is to control vehicle stability which has been proposed in some researches by Okajima et al., (2015), Lin and Song, (2015), Kim et al., (2016) and Ren et al., (2016). Usually, in electrical-driven vehicles, the mechanical and electrical braking are combined (Ehsani, 2010; Kim et al., 2012; Rouhani et al., 2013; Zijian Zhang, 2010) to improve the braking performance and energy consumption as well (Peeie et al., 2014; Peeie et al., 2017). At high speed, the electric brakes are applied to stop the rotation of tire as fast as possible. Next, when the vehicle is at low speed, the mechanical brakes are applied until the tires stopped. The advantage of this braking combination is that it can reduce the friction and increase the lifespan of brake shoes (Al-sharif, 2016). There are several types of mechanical and electrical brakes that had been employed in electrical transportations that will be discussed in the next section.

2.5.1 Mechanical braking

This braking concept is to reduce the speed of tires by applying friction to the rotating part such as a rotor. There are two common types of mechanical braking for transportation which are disk and drum as discussed below.

i. Disc Brake

This type of brake is commonly used in light and heavyweight vehicles (Atmur & Thomas, 1996; Savary & Soennecken, 1975). There are four main parts of the brake system which are; calliper, rotor, pads and hydraulic/chord line as shown in Figure 2.16. Usually, for light or low-speed transportation, chord line is used as a medium to pull the pads (Tsai et al., 1999). Disk brake works due to the friction between rotor and pad which is produced by calliper grips. This action makes the shaft stops immediately according to the rate of braking power given (Alleyne, 1997).

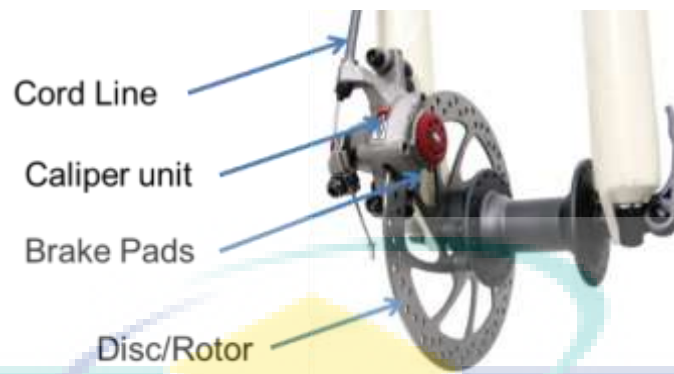


Figure 2.16 Mechanical disc braking system in light transportation using chord

ii. *Drum brake*

The concept of drum brake is still same with disc brake which is to reduce the rotating part by applied friction. The difference of this brake is just only rotating part known as a drum as shown in the Figure 2.17 below. Generally, many of vehicle's rear wheels use this type of brake for normal and parking brake (Mayer & Gallini, 1990). The drum brake works when the brake shoe together with linings attract towards and contact with the drum. Therefore, friction happens, and later cause the speed of the tires to be reduced and finally stopped (Evans, 1976). When brake is not applied, the return spring retracts and it keeps the brake shoe and linings to go back to original position.

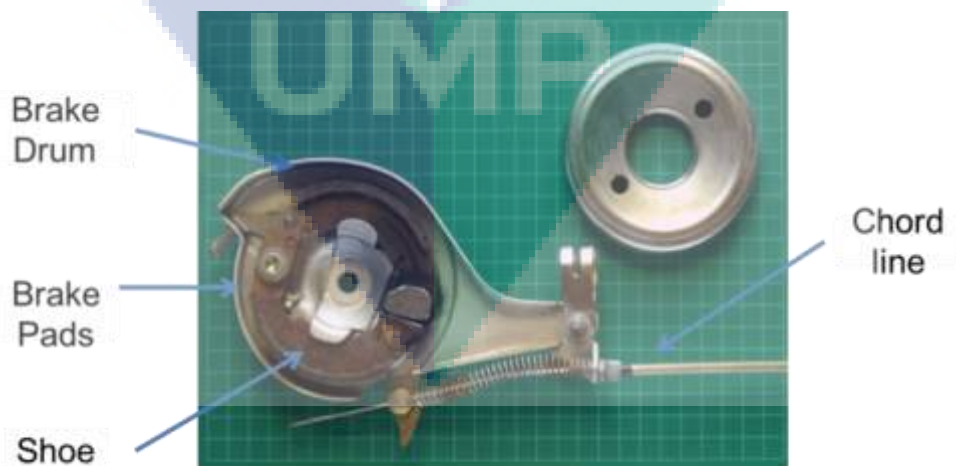


Figure 2.17 Mechanical drum braking system in light transportation using chord

2.5.2 Electrical Braking

Electrical motor is a unique machine which can change its' operation based on the application. Figure 2.18 shows the four-quadrant operation of the electrical motor. Not only for the motoring operation purposed as shown in first and third quadrants, the electric motor also can produce their own braking torque as shown in second and forth quadrants. Thus, rather than using mechanical braking to reduce speed of an electrical transportation, electric braking is also one of the methods that can be used as a braking system for the electrical motor-drive transportation. This braking method also offers the advantages such as high braking efficiency but low maintenance.

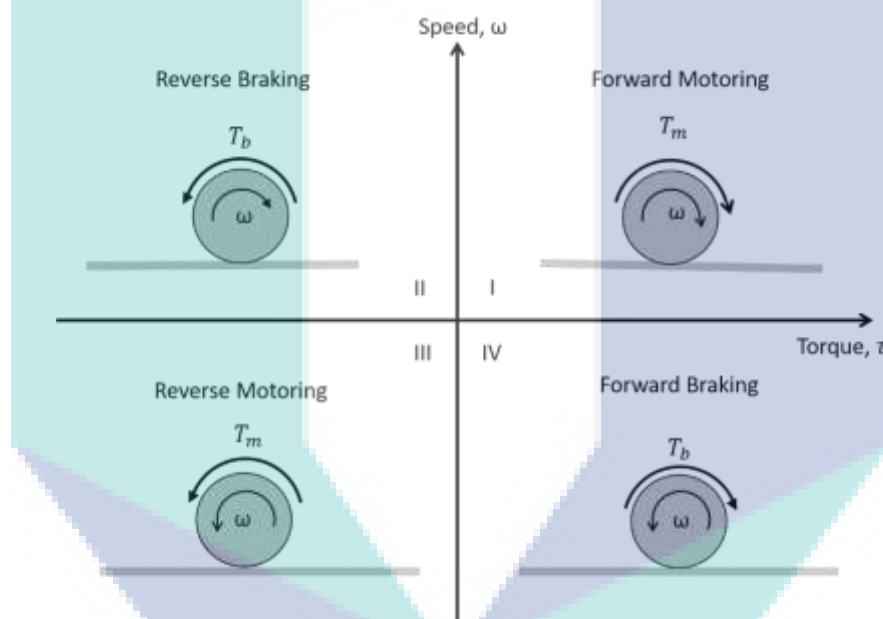


Figure 2.18 Four-quadrant operation of electrical motor

The principal of the electrical braking is come the generator concept where braking effect is generated by the conversion of the kinetic energy into the electric energy. Electrical motor is in motoring mode when the power supply is directly connected as shown in Figure 2.19(a) which also can be derived as equation 2.1 (Gökçe et al., 2016). Meanwhile, when the voltage supply to the motor is cut-off, the kinetic energy still occurs due to the rotation, $\omega(t)$ of the tire which caused by the vehicle inertia (Rakesh & Narasimham, 2012). Thus, the voltage that known as back-EMF will be generated and carries the current, i_{emf} as shown in Figure 2.19 (b). In this condition, the electrical motor is in generator mode that can be derived in mathematical model as equation 2.2.

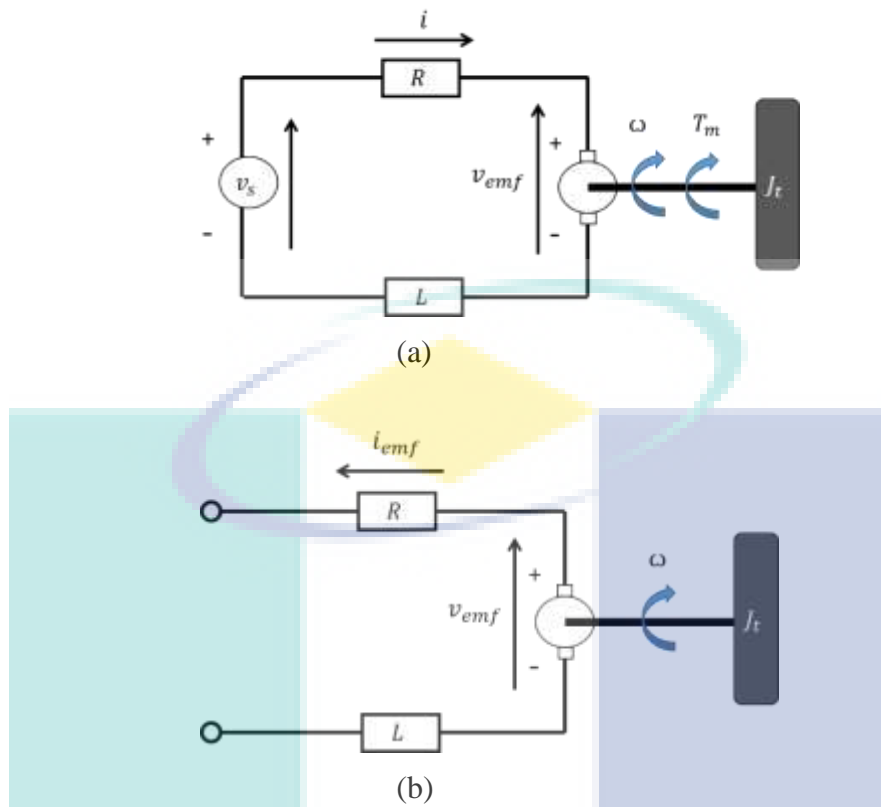


Figure 2.19 Electrical motor mode (a) Motor (b) Generator

$$V_{supply}(t) = L \frac{di(t)}{dt} + R \cdot i(t) + V_{emf}(t) \quad 2.1$$

$$V_{emf}(t) = R \cdot i_{emf}(t) \quad 2.2$$

Where;

V_{supply} = Supply voltage from battery

V_{emf} = Electromotive Force (EMF) voltage

R = Resistance

L = Inductance

i = Current from power supply voltage

i_{emf} = Current from back EMF

The ideas of performing the electrical braking is by applying load to the current flow either by dissipated or resist which caused the braking torque as shown in equation 2.3 (Gadewar & Jain, 2017). This situation leads to the decrease of the rotational speed of the tire. Electric braking can be utilized to the electric transportation by any one of these following methods; dynamic, regenerative or plugging braking.

$$T_b(t) = k_t \cdot i_{emf}(t) \quad 2.3$$

Where;

$T_b = \text{Braking torque (N.m)}$

$k_t = \text{Torque constant}$

i. Dynamic braking

Dynamic braking is known as rheostatic braking. It is the earliest electrical braking that proposed in the electrical transportation or machine (Han et al., 2014). The principle of dynamic braking is the restriction of the current from back EMF by means of electronic resistors. As shown in Figure 2.20, when the switch s_1 is open, the electrical motor will convert into a generator mode and can be derived by mathematical equation as in equation 2.4. The forced rotation from the shaft will produce the back EMF, v_{emf} and carries the current, i_{emf} . The circuit will be shorted when the switch s_2 is closed. Thus, the current, i_{emf} will be restricted and dissipated in the internal resistance, R from the motor coils. The amount of applied resistance to the current flow will significance to the braking effect since its inversely to the braking torque that shown in equation 2.5 (Joseph Godfrey & Sankaranarayanan, 2018).

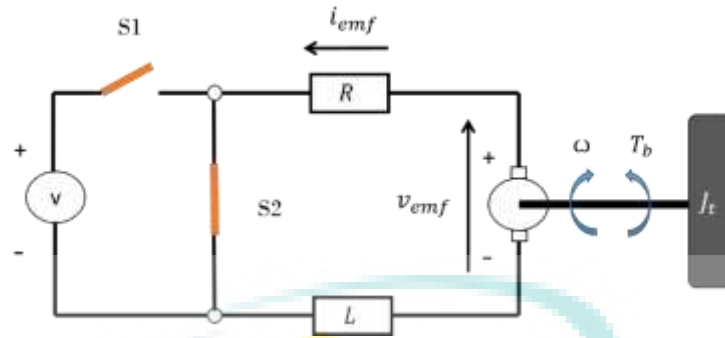


Figure 2.20 The dynamic braking operation

$$V_{emf}(t) = k_t \cdot \omega(t) = i_{emf}(t) \cdot R_{internal} \quad 2.4$$

$$T_b(t) = k_t \cdot i_{emf}(t) = k_t \cdot \frac{V_{emf}(t)}{R_{internal}} \quad 2.5$$

Where;

$R_{internal}$ = internal resistance

ω = rotational speed

T_b = braking torque

Meanwhile in the DC motors, dynamic braking is easily achieved by shorting (short-circuiting) the motor terminals, thus bringing the motor to a fast-abrupt stop. This method, however, dissipates all the energy as heat in the motor itself, and cannot be used in anything other than low-power intermittent applications due to cooling limitations.

Control strategy in the dynamic braking

Although rheostatic braking is obsolete, some of the electrical transportation still used this kind of braking system, such as in locomotive industry (Alturbeh et al., 2018; Ge et al., 2018). In several researches, the dynamic braking is categorized as the simplest and efficient electrical braking. (Yang et al., (2014) mentioned that the advantage of dynamic braking can be found in high-speed transportation. Dynamic braking also can be used as a backup when the primary brake failure occurs. It is obvious that on-board resistors are able only to dissipate energy as heat/waste instead of recycling and reusing for other beneficial purposes.

In the low speed electrical transportation H. Seki et al., (2008) proposed a novel safety driving control scheme for electric power-assisted wheelchairs. The dynamic braking system based on designed minimum jerk velocity was investigated during downhill descending condition. They found out that the braking power can be improved at low-speed range by Short-circuiting the right and left motors in series with a suitable resistor. Experiment result shows that the actual speed followed the designed based model minimum jerk and reference velocity, $v_d = 0.6$ m/s when descending on a downhill road with 6 degrees declined angle.

Then, H. Seki et al., (2009) extended the research by proposing a novel safety and efficient driving control scheme based on the dynamic braking system. In that research, the dynamic braking system with the step-up chopper circuit serially connected to two motors. The velocity feedback control integrated with the variable duty ratio so that it tracks the optimal velocity based on the Minimum Jerk Model. In addition, the proposed dynamic braking system is also applied at the low-speed range in order to suppress the acceleration. Some driving experiments on the practical downhill roads results show the effectiveness of the proposed control system as in Figure 2.21.

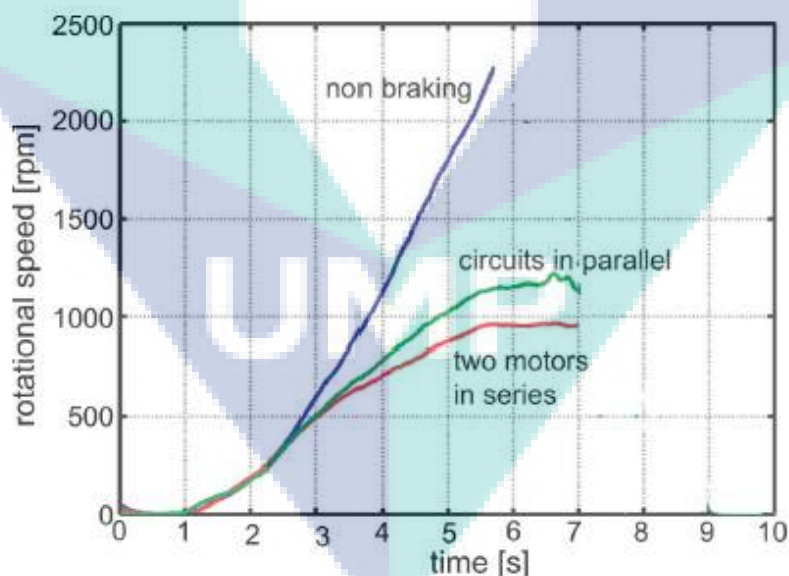


Figure 2.21 Velocity control using dynamic braking in electric wheelchair

H.Seki (2010) also proposed a novel safety and efficient driving control scheme based on the capacitor regenerative braking system. An additional to previous study, the reference velocity is flexibly designed according to the declined angle. Some driving

experiments on the practical downhill roads showed the effectiveness of the proposed close loop control system as in Figure 2.22.

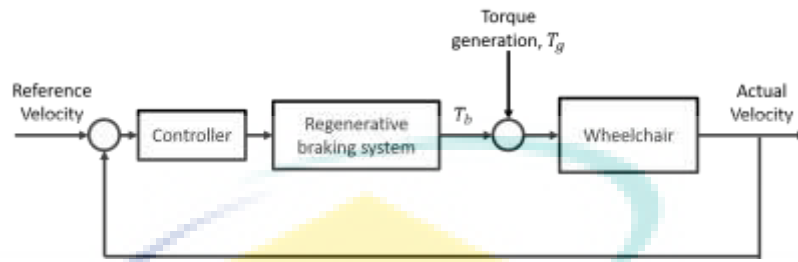


Figure 2.22 Close-loop control downhill assist system for electric wheelchair.

Lin et al., (2014) study a novel method of realizing a non-mechanical antilock braking system (ABS) controller for electric scooters (ESs) based on dynamic braking mechanisms as illustrated in the block diagram in Figure 2.23. In which, a boundary layer speed control is proposed for a guarantee of the optimal slip ratio between tires and road surface. The antilock braking controller, combined with this controller, drives a low-side driving circuit to induce either an open-circuit or a short-circuit loop on the motor stator's coil to a load; it thus produces braking actions analogous to those in the conventional ABS control. The proposed ABS controller is practically realized.

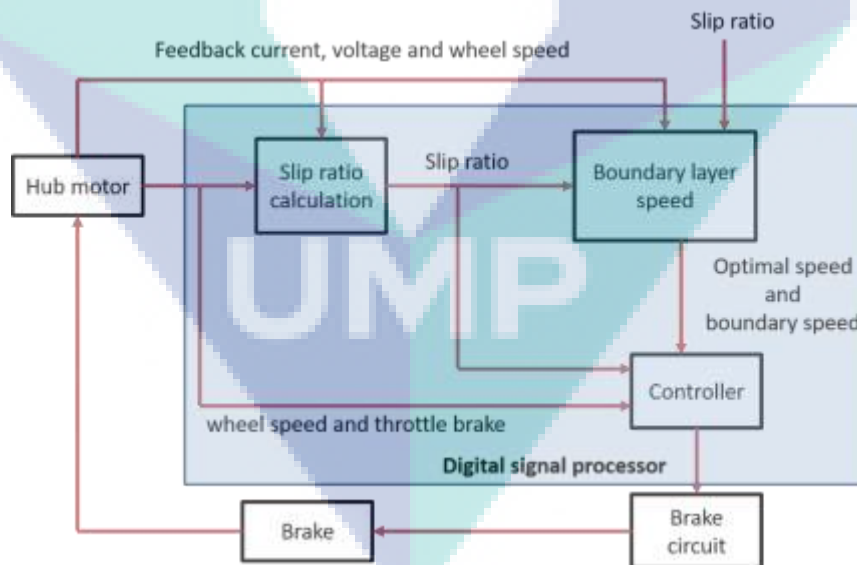


Figure 2.23 Slip ratio control configuration using dynamic braking

Zhu and Dan, (2014) constructed a simulation of motor model in MATLAB Simulink environment. By adjusting the resistance, the effect of motor speed during braking time is different. They found out that when resistance is small, the motor decelerates smooth but when resistance is too large, the motor decelerates fast and

fluctuated. Thus, curve fitting between braking time and resistor value was plotted from 1Ω until 50Ω to know the optimum load resistance. Based on curve fit time-resistance, the result of experiment shows the $R= 9.1\Omega$ is suited on this type of induction motor for dynamic braking purpose without any fluctuations undulating and give faster brake.

In braking condition, not only to stop the vehicle, braking comfortability influence the comfort ride. In research by Antony and Praveen, (2015), they developed the PMSM drive for servo applications where the emphasis is on smooth and accurate speed control in the four quadrants using the MATLAB simulation environment as shown in Figure 2.24. The PI controller is so designed that the motor speed tracks the reference speed accurately. The machine is made to operate in the forward and backward motoring and generative modes. In the generative mode of operation, dynamic braking is implemented by chopper resistance control so as to avoid the rise in DC link bus voltage and thus safeguard the DC link capacitor.

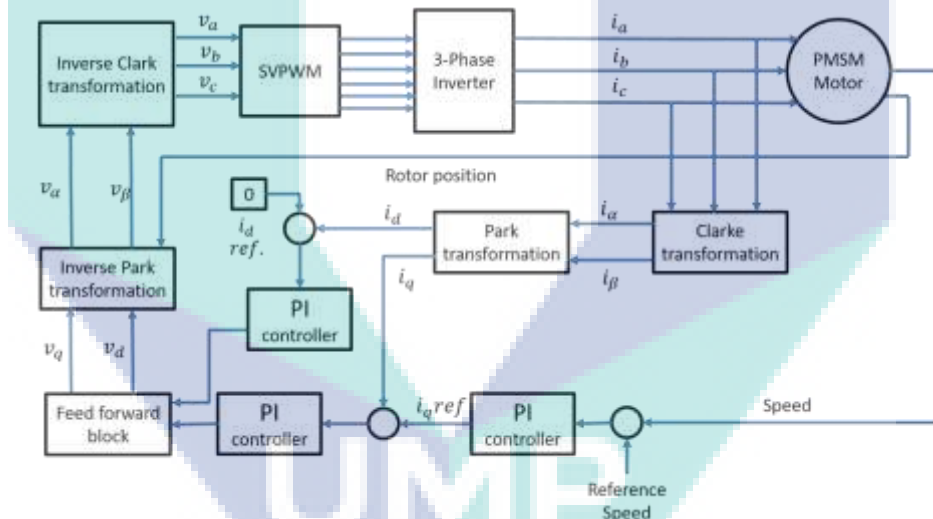


Figure 2.24 Block diagram of Permanent Magnet synchronise Motor(PMSM) drive

However, there is a disadvantage of using this braking type which is that dissipated heat energy in resistor caused a rapid change during braking at high speed. Thus, in research of Chung and Kim, (2014), the braking resistor of roof type electric braking design system using for railway carriage was proposed. The thermal analysis was conducted on the simplified 2-dimension model of roof type resistors using computational fluid dynamics (CFD) software. From the result, the increment rate of thermal was reduced during consumed energy.

Yang et al., (2010) proposes a new converter protection method, primarily based on a series dynamic resistor (SDR) that avoids the doubly-fed induction generator (DFIG) control being disabled by crowbar protection during fault conditions. A combined converter protection scheme based on the proposed SDR and conventional crowbar is analysed and discussed. The main protection advantages are due to the series topology when compared with crowbar and DC-chopper protection. Various fault overcurrent conditions (both symmetrical and asymmetrical) were analysed and used to design the protection in detail, including the switching strategy and coordination with crowbar, and resistance value calculations. The simulation results show that the proposed method was advantageous for fault overcurrent protection, especially for asymmetrical faults, in which the traditional crowbar protection may malfunction.

Using the linear induction motor (LIM) that proposed by Sakamoto et al., (2012) reduce the heating during braking at high speed using dynamic braking in eddy current brake systems in locomotive. The LIM reduces rail heating and uses an inverter for self-excitation. The estimation of the performance of a LIM was conducted in experimental results of a fundamental test machine and confirmed that the LIM generates an approximately constant braking force under constant current excitation. At relatively low frequencies, this braking force remains unaffected by frequency changes. The reduction ratio of rail heating is also approximately proportional to the frequency. From this method, authors also confirmed that dynamic braking resulting in no electrical output can be used for drive control of the LIM. These characteristics are convenient for the realization of the LIM rail brake system.

Although dynamic braking is capable of providing high efficiency braking in an electrical transport, the studies on dynamic braking have become less trendy because of poor energy management. Hence, the study of electrical braking turns to regenerative braking which can preserve the energy generated by the motor as well as increasing the dynamic motion (González-gil et al., 2013). Furthermore, the generated dynamic braking force cannot be controlled directly. As a result, this braking system is unsuitable to be used as an automatic control system for Electric Powered Wheelchair (EPW) especially for controlling the speed when descending on a slope.

ii. *Regenerative Braking*

Research on regenerative braking (RB) is one of the most popular topics. In contradiction to the rheostatic braking where energy is dissipated in resistor and losses as heat, the regenerative braking is an energy recovery mechanism which slows a vehicle by converting the kinetic energy into a form of energy which can be either used immediately or stored until needed as shown in Figure 2.25. Equation 2.7 shows the braking torque function when the regenerative braking is applied in the electrical motor. In this mechanism, the electric motor uses the vehicle's momentum to recover the energy that would be otherwise lost to the brake discs as heat. In the regenerative braking system, there are two conditions that must be satisfied in order to perform the regenerative braking condition (Rakesh & Narasimham, 2012).

1. Back EMF should be greater than the terminal voltage (supply).
2. Current must flow in reverse direction to the voltage supply current.

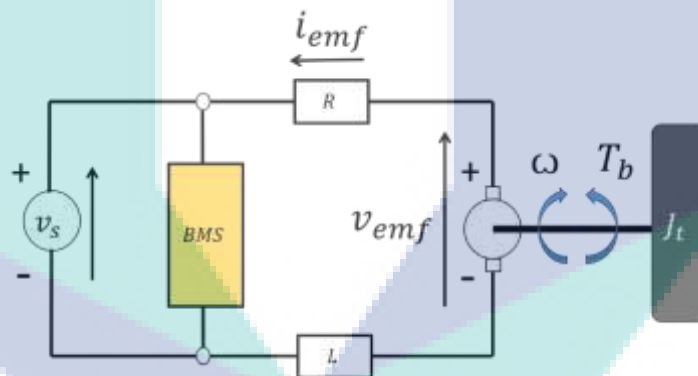


Figure 2.25 Regenerative braking operation

$$V_{supply}(t) = V_{emf}(t) - (R_{internal} + R_{supply}) \cdot i_{emf}(t) \quad 2.6$$

$$T_b(t) = k_t \cdot i_{emf}(t) = k_t \cdot \frac{V_{emf} - V_{supply}}{(R_{internal} + R_{supply})} \quad 2.7$$

Where;

$$R_{supply} = \text{Internal resistance in battery}$$

There are different parameters are analysed according to which control such as slip ratio, road gradient force, state of charge and etc. Thus, research of RB can be classified into two categories which are regenerative efficiency and to save the generation sources. In other research, regenerative braking also is used to improve braking performance and driving comfort (Yoong et al., 2010). Various controllers assist calculation of these parameters properly, enhancing the electric vehicle stability, braking performance (L. Li et al., 2016; Wang et al., 2015) and energy recovery (G. Xu et al., 2016).

Control Strategy in Regenerative braking

i. Low back EMF generation

The common problem regarding regenerative braking for the low-speed transportation, is when the back EMF is small than the terminal voltage that cause the battery not to be charged and leads to no braking effect. In a research that is presented by Lin et al., (2010), a bi-directional converter is applied to an electric bike. The main structure is a cascade buck-boost converter (see in Figure 2.26), which transfers the energy stored in battery for driving motor, and can recycle the energy resulted from the back electromotive force (EMF) to charge the battery by changing the operation mode. Moreover, the proposed converter can also serve as a charger by connecting with AC line directly. Besides, by using single-chip DSP TMS320F2812 approved as a control core to manage the switching behaviours of each mode and to detect the battery capacity.

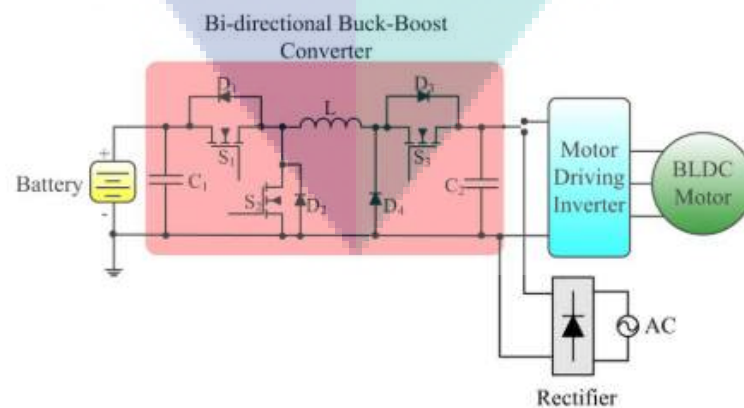


Figure 2.26 Implement of Bi-directional Buck-Boost converter electrical drive

In other research to increase the back EMF, Mehta and Hemamalini, (2017) also proposed a control strategy by using the cascade bi-directional buck-boost converter to ensure that the regenerative braking is functioning. From the result, more energy is stored in the battery during the regenerative braking phase even at low speed. Thus, by implementing this converter, the average power stored by the battery is increased by 2.5 times and reducing the stopping time at the same time.

ii. Overcharging

The other problems in regenerative braking is the generated power for charging the battery. It is unstable and can lead to overcharge which caused faulty and damage to the battery (Gadewar & Jain, 2017). Hence. The flow of current energy that is generated by back EMF needs to be controlled by using a proper energy restore method. Asakura et al., (2009) proposed a control method using cascade pulse width modulation (PWM) converter for state of charge (SOC) balancing of the battery units from overcharging during recharging phase. Experimental was conducted from a 200 V, 10 kW, 3.6 kWh NiMH battery units. The result shows when every battery energy recovery is under SOC, it can be balanced and no overcharging was reported by using this control method.

Berger et al., (2015) proposed pseudo-cascade controlled Insulated-Gate Bipolar Transistor (IGBT) chopper which is used to protect the battery against surge line charging current and the DC-Link against overvoltage while allowing maximum braking capacity and maximum battery charging efficiency. The experiment is conducted by using a Powerex IGBT PM200DVIA120 for switching device and NI Compact RIO module interfaced with LabVIEW for the PWM signal calculation. From the result, the proposed method can protect the battery during a regeneration mode over the entire battery state of charge (SOC) and temperature operating range.

Torre et al., (2015) proposed a novel mixed integer linear programming formulation. This formulation is to optimize the sizing of energy storage during regenerative braking in electric transportation systems that includes the counting of battery cycles. From the simulation, the result shows high power density energy capacity can be captured by ultracapacitors in other to protect the batteries from overcharging. The study by Naseri et al., (2017) mentioned the advantage of implementing hybrid energy storage system (HESS) in an electric vehicle that used BLDC motor. HESS, which consist

of ultracapacitor and batteries, offered battery life safety during the regenerative process with the appropriate switching algorithm. The result from State of Charge (SOC) shows there is no overcharging during regenerative braking and energy is harvested in super-capacitor using the appropriate switching template of the inverter.

iii. RB as the dynamic control

Apart from being used as energy recovery, the regenerative braking also is used for the dynamic motion enhancement. In the experiment conducted by Peng et al., (2008), they have studied the co-operative control of regenerative braking and mechanical friction braking. The Hardware In Loop (HIL) was developed by combining MATLAB Simulink model of the Electric Wire Braking (EWB), motor, battery and the vehicle with the actual vehicle model. They found the proposed regenerative braking scheme algorithm prevent the tire from locking during braking at low adhesive road coefficient.

Peeie et al., (2016) investigated the braking performance using a combination of ABS and regenerative braking. A simulation model of ABS and regenerative brake control using MATLAB Simulink was constructed to prevent the tires from lock during braking on icy road condition. Authors found ABS and regenerative brake control can improve the braking performance, stability and safety of the small EVs.

Zhu et al., (2016) proposed regenerative brake and mechanical brake co-operatively which to maintain the constant speed and the braking energy can be regenerated as much as possible when vehicles travel downhill. The mathematical model of the braking system is established, and the adaptive model predictive control method is adopted to control the speed of vehicles. The simulation results show that the regenerative braking system and the mechanical braking system can be used coordinately by the adaptive model predictive control; the braking energy can be recovered as much as possible under the premise of ensuring the downhill speed constant. And the control system has strong stability and robustness. Moreover, due to the limits of the acceptable power of batteries, the brake mode is switched between the electromechanical composite braking system and mechanical braking system according to the SOC of the batteries. When the SOC is higher than a certain value, the regenerative braking system is closed, and the brake mode is switched to the mechanical braking mode automatically, so the safety of vehicles can be ensured.

Chen et al., (2018) proposed a control of regenerative braking systems for four-wheel-independently-actuated electric vehicles. Based on the measurement of yaw rate and wheel angular velocities, the vehicle longitudinal velocity can be obtained from the modular observer and the estimation error is proved to asymptotically converge to zero. The upper layer controller is designed to track the desired vehicle velocity and the lower layer controller is designed to track the signal from the lower layer controller and to improve the energy recovery. The simulation results show that the proposed system can not only track the desired velocity but also improve the energy recovery of vehicles.

Based on the previous study, the advantages in regenerative braking such as recovery energy and efficient braking mechanism make this braking system still practical. It can be said that the regenerative braking system is suitable for high-speed transportation due to the back EMF produced is satisfied with the regenerative condition. This will allow the battery to be charged and generated the braking torque. Meanwhile, the low-speed transportation which produced lower back EMFs required an external system such as a buck-boost converter to increase the back EMF for the charging rate or braking purposes. It is very impractical to apply in Electric Powered Wheelchair (EPW) which substantially to the cost. Hence, regenerative braking performance for EPW is not carried out in this research.

iii. Plugging braking

Plugging braking also called as “reverse voltage braking”, “reverse current braking” or “counter current braking” is a method of braking obtained by reversing the applied supply voltage, so that the input voltage is in the same direction of the back EMF in forcing armature current in reverse direction (Sarkar & Mukher Jee, 1992). This reversed current will have impact on torque, thus producing deceleration. Plugging provides faster braking response because braking torque is at high level as the magnitude of current during this braking is high (Pan et al., 2002). When reverse voltage is applied for stopping the locomotive the supply must be disconnected at an instant where speed is close to zero. Otherwise it will rotate in reverse direction (Sarkar & Mukher Jee, 1992).

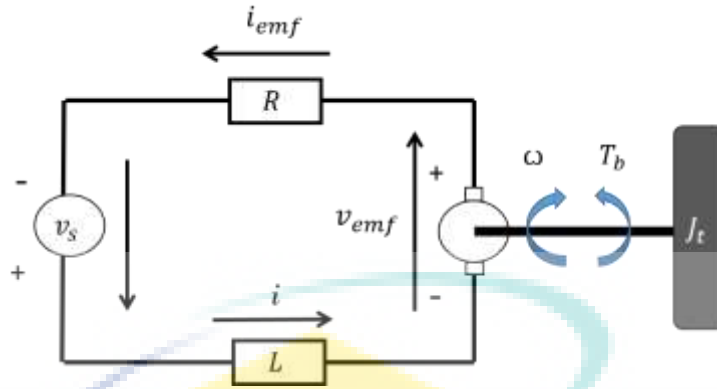


Figure 2.27 Plugging braking operation

$$V_{plug}(t) + V_{emf}(t) = (R_{internal} + R_{supply}) \cdot i_{emf}(t) \quad 2.8$$

$$T_b(t) = k_t \cdot i_{emf}(t) = k_t \cdot \frac{V_{plug}(t) + V_{emf}(t)}{(R_{internal} + R_{supply})} \quad 2.9$$

Where;

$$V_{plug} = \text{Plugging voltage}$$

Control strategy in plugging braking

Halim and Almarshoud, (2008) suggested versatile electronic method to control speed and brake by using reverse chopping current. The computed performance characteristics of a single-phase motor driven by the proposed converter reveal that high starting torque is achieved at low starting current. The direction of rotation could be reversed when plugging braking is possible. High frequency chopping results in low motor current harmonic contents, and consequently lesser copper losses and good efficiency. The AC chopper does not adversely affect the displacement angle of the current, as does the natural commutation method.

The harmonic currents reflected on the network are relatively large compared with the other methods, especially the natural commutation method. Nevertheless, they can be easily filtered as they are of higher orders. It is recommended to include the iron and switching losses in future works for accurate evaluation of the motor efficiency.

In the plugging braking, the control strategy is only focus on reducing the speed of electrical transportation or machine. Yang and Chen, (2011) investigated rapid electric braking scheme for high speed motor by using phase excitations current to dissipate excessive rotor kinetic energy so that the DC link voltage is restricted to a safe range. The current can be controlled with open-loop schemes. The proposed technique also can be used in low-end variable speed drives where rectifiers are used to convert AC to DC power source. Experimental results shown that both schemes can effectively suppress DC link voltage as the motor decelerated from 5000rpm with different deceleration times.

Elkholy and Elhameed, (2015) investigated the optimum values of the applied voltage and frequency during braking to stop the motor in a certain time with minimum braking energy losses to limit any excessive thermal heating. Braking of three phase induction motors is required in many industrial applications. Authors introduced braking of three phase induction motors using particle swarm optimization (PSO) technique and compared with that obtained using plugging braking method. They found that the proposed technique gave lower braking energy and shorter braking time. The braking energy losses with the proposed method are about 20% of the plugging braking energy losses with the same braking time.

Somrajan and Sreekanth, (2016) developed an electric braking for EV has been developed using plugging brake concept. In this work DC motor drive fed by bidirectional DC-DC converter and PI controller is modelled using Simulink. They found that plugging brakes able to stop the vehicle at the instant, which seems to be equivalent or more accurate than mechanical brakes. Thus, plugging braking provides an alternative for mechanical brakes in EV. From the observed results, EV running at a speed of 120 rad/sec is brought to halt at zero rad/sec when plugging brakes were applied.

Obed et al., (2016) proposed simulation model using MATLAB Simulink of plugging braking system on two Permanent Magnet Synchronous Motor (PMSM) that was used as traction motors in subway train. The plugging braking is applied in normal operation of two PMSMs supplied from dual voltage source inverter with Field Oriented Control (FOC) using one PMSM for braking or both motors depending on the speed of the motors. When using one PMSM for plugging brake, the other motor will be disconnected from the source and the mechanical load. Then, the plugging brake is applied when the system is operated in fault tolerant mode and both motors are operated

from five legs voltage source inverter. In fault tolerant operation one motor is used for braking or both motor depending on speed, also when one motor is used for braking the other motor is disconnected from the source and the mechanical load. They found the proposed design can be used in the subway application to provide fast and safe braking. The simulation results show that an effective and efficient plugging braking system which can be designed using PMSM and FOC method.

To improve efficiency control in a vehicle, Li et al., (2018) proposed a new braking strategy based on the driver's braking intention and motor working characteristics in numerical simulations on a quarter-vehicle braking model. The blending braking between regenerative and plugging is adopted by using Model Predictive control (MPC). By adjusting the weight of the MPC cost function, different braking intentions can be achieved. This strategy is able to achieve as much as possible braking energy recovery without violating the driver's braking intention. In the case of the emergency braking, the sliding mode based optimal slip ratio control is adopted and it is able to obtain the shortest braking distance. In the simulation results, the braking strategy using MPC is able to follow the driver's braking intention and is able to recycle more energy than the conventional braking strategy at normal braking condition. In the case of emergency braking, the proposed plugging braking is able to manage the speed and slip ratio of vehicle

However, the improper controlling in plugging braking will cause the system to become failure. As mentioned in study of Sun and Xu, (2018), the use of an inappropriate braking counter current causes broken to the rotor bar and the increasing of load oscillation in Induction Motors will increased. Hence, this causes traction and braking efficiency to decrease.

There are several researches had been done to encounter this problem. In study on Soleimani et al., (2018), they presented a novel technique for the online detection of broken rotor bar(s) (BRBs) in induction motors, based on the analysis of the air-gap rotational magnetic field (RMF), being it indirectly sensed using the voltages induced in dual search coils installed in several stator regions. The induced voltages allow obtaining three differential voltages which reveal the symmetricity level of the mentioned field along the stator circumference. Under the presence of the broken bar, the RMF is

disturbed by the rotor magneto-motive force, being these disturbances detected through the fundamental components of the differential voltages using a new time-domain analysis technique. The proposed diagnostic approach is verified by finite element analysis and also by several experimental tests. A high sensitivity and robustness in the face of unbalanced voltage sources and motor load level variations are the main advantages of the proposed technique. Moreover, it is a secure method for BRB detection, easily implementable in low-cost digital signal processing units.

Another research is done by Fišer and Nedeljkovi, (2019) where they detect the broken rotor bar in induction motor based on rotor flux angle monitoring. In that research, authors investigated a particular frequency component in this signal appears from two difference between their rotor flux angles in two different motor estimation models. Consequently, the proposed algorithm is robust enough to load oscillations and/or machine temperature change, and also indicates the fault severity. The method has been verified at different operating points by simulations as well as experimentally.

In general, the research of plugging braking is to reduce the speed of electrical transportation by promising high braking performance. Although this braking causes many energy losses, but in most researches, it is proved that plugging is able to stop the vehicle or machine at a fast and efficient rate. In addition, the variation of produced braking torque from the reverse voltage on electrical motor provides a merit to achieve various kind of control in the vehicle. This is the reason to developed the plugging braking into an automatic control system which capable to enhance the dynamic motion of Electric Powered Wheelchair (EPW) during descending on the slope.

2.6 Active control system

The dynamic motion of the transportation can be enhanced by implementing control system either in passive, active or in both modes. The passive safety consists of airbags, the structure of car body, seatbelts and head restraints, while active safety include electronic stability control (ESC), anti-lock braking systems (ABS) and other Advanced Driver Assistance Systems (ADAS) like intersection collision avoidance (ICA) and lane keeping assistant (LKA). One of the popular active control systems in the vehicle nowadays, especially to control the speed of vehicle during descending on the slope is known as Hill Descent Control (HDC) will be discussed in the next section.

2.6.1 Hill Descent Control (HDC)

During descending on the slope condition or downhill, the speed of vehicle tends to increase and keep accelerate that causing the vehicle to lose the stability (Lu et al., 2016). The braking system is used to control the speed from rapid increase (Shehan et al., 2000). Therefore, one of the conventional techniques to control the increments of speed is by applying and releasing the braking repeatedly. Hence, the speed of vehicle will decrease and maintain at the low speed during descending on slope condition.

Fortunately, there is an automated system that had been implemented in nowadays vehicles are known as Hill Descent Control (HDC) or Downhill Assist Control (DAC)(Farnsworth, 2011; Atsmon et al., 2017). This system also can be categorized as an active control system. The HDC or DAC is utilizing the same network of Anti-Lock Braking System (ABS) which consist of wheel sensors and control modules to apply adequate braking force as it's required (Claussen and Eickhoff, 1999; Shehan et al., 2000). The idea of this control is to maintain the vehicle speed at a set of speed that same goes with the cruise control.



Figure 2.28 Hill Descent Control (HDC) in current vehicle

Sources: Farnsworth, 2011; Atsmon et al., (2017)

The different is, the HDC is only applying the ABS as a system to control the speed of the vehicle during descending on the downhill. In automatic HDC system, the HDC is working when the inclinometer (see in Figure 2.29) is detecting the gradient of the driving road more than set slope per cent. Then, the ABS will be activated and hold until the speed of vehicle is reaching the set speed. Meanwhile, when the speed of vehicle is below than the desired speed, the ABS is release. Normally, the brake will control the acceleration in the range of 1 m/s^2 (Beever & Reynolds, 2017).



Figure 2.29 Type of inclinometer, G sensor for HDC
Source: Beever & Reynolds, (2017)

HDC is also used for low-speed transportation, H.Seki, et al., (2009) was proposed the Novel Regenerative Braking Control of Electric Power-Assisted Wheelchair (PAW) for Safety Downhill Road Driving. As mention by author, the PAW has no braking system to suppress the wheelchair's velocity and brings the dangerous and fearful driving on downhill roads. To encounter this problem, the regenerative braking system with the step-up chopper circuit serially connecting two motors is applied in PAW system as shown in Figure 2.30.

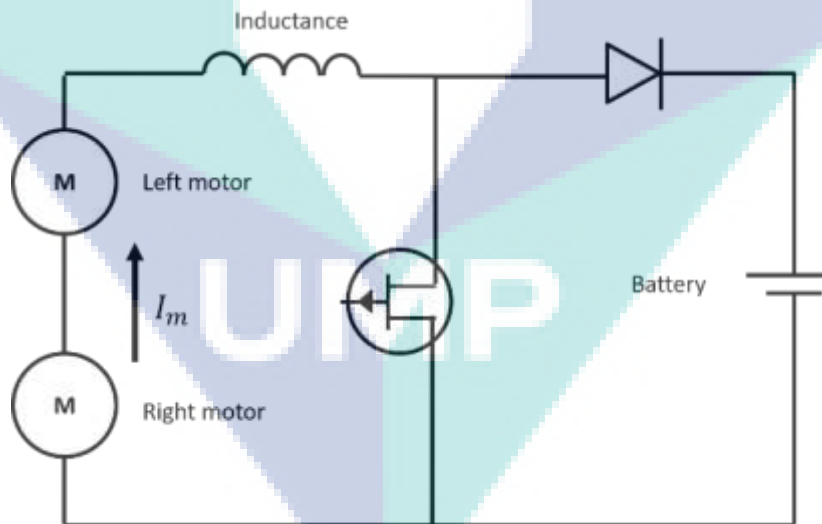


Figure 2.30 Configuration of step-up chopper circuit on the experimental setup

The velocity of the tire is controlled with the variable duty ratio so that it tracks the optimal velocity based on the Minimum Jerk Model. In driving experiments at downhill, the result shows the proposed control system is effectiveness, and the speed of the tire is tracking the desired speed based on the minimum jerk model when descending at 4.5° slope as shown in Figure 2.31.

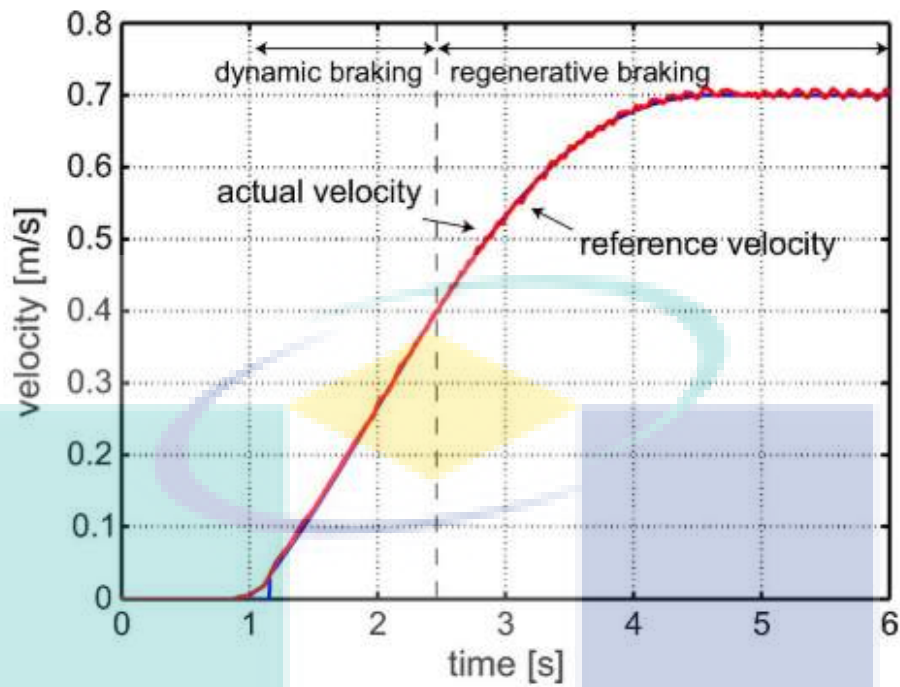


Figure 2.31 Experimental result by applying HDC in electrical wheelchair

Shuyang and Chun (2013) mentioned that HDC is the important system need to apply in heavy transportation. In the research was conducted, authors were introduced the downhill braking condition for an electric drive underground dump truck during engine cranking process. When the truck is going downhill at a low speed, part of the braking energy is consumed by braking resistance system, other energy is changed into AC power by inverter module, the diesel engine is dragged from an idling speed to a high speed by the synchronous motor, energy feedback is realized as shown in Figure 2.32. To achieve synchronous motor starting, a zero-crossing detection and frequency searching method based on rotor speed sensor is used.

Luo et al., (2015) proposed a novel downhill safety assistant control strategy for hybrid electric vehicles, which adapts to the characteristics of different drivers and takes advantage of all braking subsystems of hybrid electric vehicles. Author was mention there is currently no effective downhill safety assistance control technology for hybrid electric vehicles that is effective across the full range of speeds and can take advantage of regenerative braking.

Thus, to improve the vehicle safety, the fuel economy and the ride comfort for the full speed range, a coordinated control strategy for the electric motor's braking subsystem, the engine's braking subsystem and the hydraulic braking subsystem is developed, which includes six braking assistant modes, an identifying strategy and torque control of the electric motor based on coordinated control strategies. The results from simulations and experimental show that the proposed control strategy can improve the vehicle safety and ride comfort in hybrid electric vehicles during downhill driving.

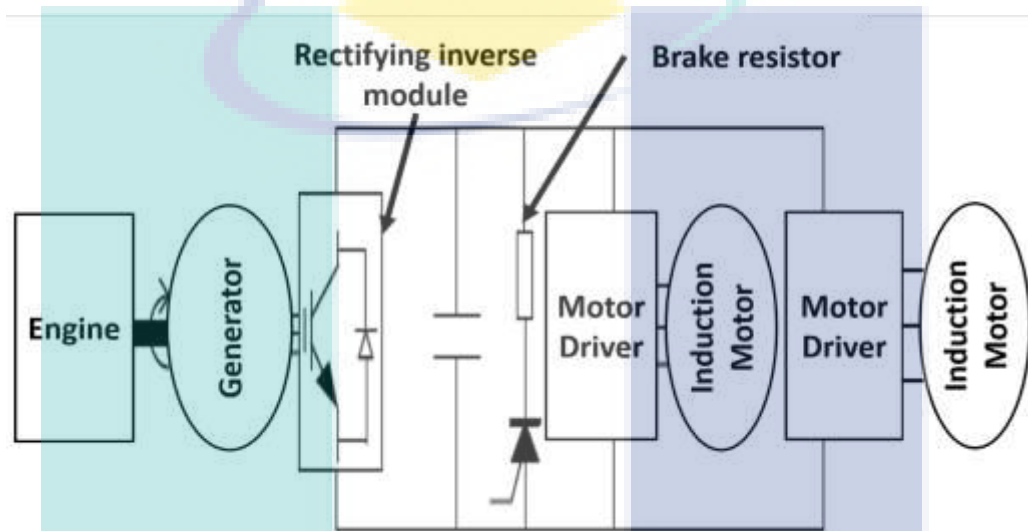


Figure 2.32 Proposed electric drive system in heavy truck

In others research, to increase the efficiency of HDC, Guo-Zhu et al., (2016) proposed the co-operative between regenerative and mechanical braking to maintain the constant speed during descending on the downhill. From the result, the speed can be maintained at the set speed by using the co-operative braking system mechanical and regenerative. Also, the braking energy can be recovered as much by using the regenerative braking technique.

The HDC or DAC utilized the mechanical braking system to control the speed. Xu et al., (2017) was mention the disadvantages that used the mechanical braking as HDC in the heavy truck which caused the raised of temperature on the brake drum. Consequently, he was proposed a hill descent braking strategy using the combination of the engine braking and the hydraulic retarder braking. The research result shows that the brake drum's temperature decreases by 69.9°C and reaches 193.1°C after the heavy truck goes down the chosen slope with the combined braking strategy.

In overall, from the reviews have been constructed, an active system such as Hill Descent Control is very important in transportation system. This not only enhances security, but also offers comfort ride to users. In addition, by using a braking electric as a control based for HDC, it makes the system suitable for use in the EPW which drive by electrical motor. Using this system, it is expected to solve problems related to EPW when down the slope.

2.7 Summary of the review

This review has provided a multifaceted frame work for addressing issues related to powered mobility. Electric Powered Wheelchair (EPW) comes in many forms according to the operation, user input and sensor input used in that EPW. The goal of development is to facilitate independent dynamic mobility and to improve the individual's ability to engage in meaningful life activities. This review has explored the development and technology that had been used in powered mobility. An attempt was made to summarize the literature within the past research of EPW, present research of EPW and dynamic control enhancement which consist of stability control, axial control, longitudinal control and lateral control.

Besides that, this review exposed about the importance to implement the braking system in vehicles, especially in EPW. There are many types of braking system that can be applied in EPW. Not only mechanical braking system, the electrical braking system is also possible to be used as the stopping medium since the EPW is driven by the electrical motor. Table 2.3 shows the summaries of mechanical and electrical braking system that can be as a reference for researchers to develop braking system in EPW. Since EPW is driven by the electrical motor, one of the novelties that can be proposed in this research is to control the speed at slope condition by using the electrical braking that is also known as Hill descent control (HDC).

Table 2.3 Comparison between the mechanical and electrical braking

Braking characteristic	Mechanical	Regenerative	Dynamic	Plugging
Important concept	Enough gripping force to brake lever	Back EMF > terminal voltage (voltage boosting)	Suitable resistor	Suitable Reverse current
Energy restore/losses	Energy loss due to frictional force	Energy store – battery Super-capacitor (prevent overcharging)	Energy loss-dissipated on resistor	Energy loss-dissipated inside motor component
Braking until stop	Yes.	Depend on storage capacity	Yes	Yes, voltage need to cut-off to avoid reverse rotation
Braking regime effective	Effective at all state speed	At a certain speed that produces higher back EMF than the terminal voltage	Effective for all state speed	Effective for all state speed
Braking response	The higher gripping per cent will produce higher braking torque that causes EPW quickly stopped	slow	depend on resistor ohm value high ohm – fluctuating low ohm – not well decelerate	Fast (depend on amount reversing voltage/current)
Controlling speed	Need to install external actuator for controlling the speed	Not appropriate	controlling via variable resistance	controlling via variable reverse current/voltage
Cost	High cost and need to maintain the brake pad regularly	Depend on Battery Management System (BMS) and battery/supercapacitor	Depend on numbers of resistor used	-
Type of motor	-	DC	AC/DC	AC/DC

CHAPTER 3

METHODOLOGY

3.1 Introduction

In methodology, the explanation on procedures of analysis are discussed in detail. Electric Powered Wheelchair (EPW) modelling, validation and braking controller design had been done to solve the problem in EPW. This chapter also clarify the numerical analysis process by using MATLAB Simulink simulation tools. There flow charts are presented to keep track of the project whenever there is a problem or misconduct.

3.2 Project flow chart

Based on the project, the flow chart will be a guide to tackle any problem. It is also a start off point to identify the progress of the whole project with some detail. When any problems arise, it will be faced and identified. And then the issues are clarified and finally solved. As soon as the goals are set, the scope of studies is to focus on keeping track of the project. It acts as a baseline to limit the specified problem. The flow chart of this project is shown in Figure 3.1, Figure 3.2 and Figure 3.3.

In this project, the tasks are divided into three phases. In the first phase, after the literature review is done, the experiment of dynamic behaviors of EPW by using electrical braking system is conducted. Before conducting the experiment, the conditions and instruments is set up. The slope conditions such as angle and length are measured by using angle sensor and measuring tape respectively. Then, it is important to clean the surface of slope form any dirt before running every test. In this experiment, there are two kind of sensors that are used which are speed and voltage. These sensors also needed to be calibrated before running any test in order to acquire the correct and precise data.

Next, the experiment of dynamic behaviors consists of travel distance, speed of tires, speed of EPW and slip ratio are analyzed by using electrical braking are conducted. The electrical braking can be categorized into three types which are; regenerative, dynamic and plugging braking. The experiment is conducted at slope condition in three different initial braking speeds which are 0 m/s, 1 m/s and 2.5 m/s. The rationale to conduct the experiment in different braking speed mode is to illustrate the driving method of EPW's users during descending in slope condition. Then, data is recorded that include travel distance, tire speed, EPW speed and slip ratio.

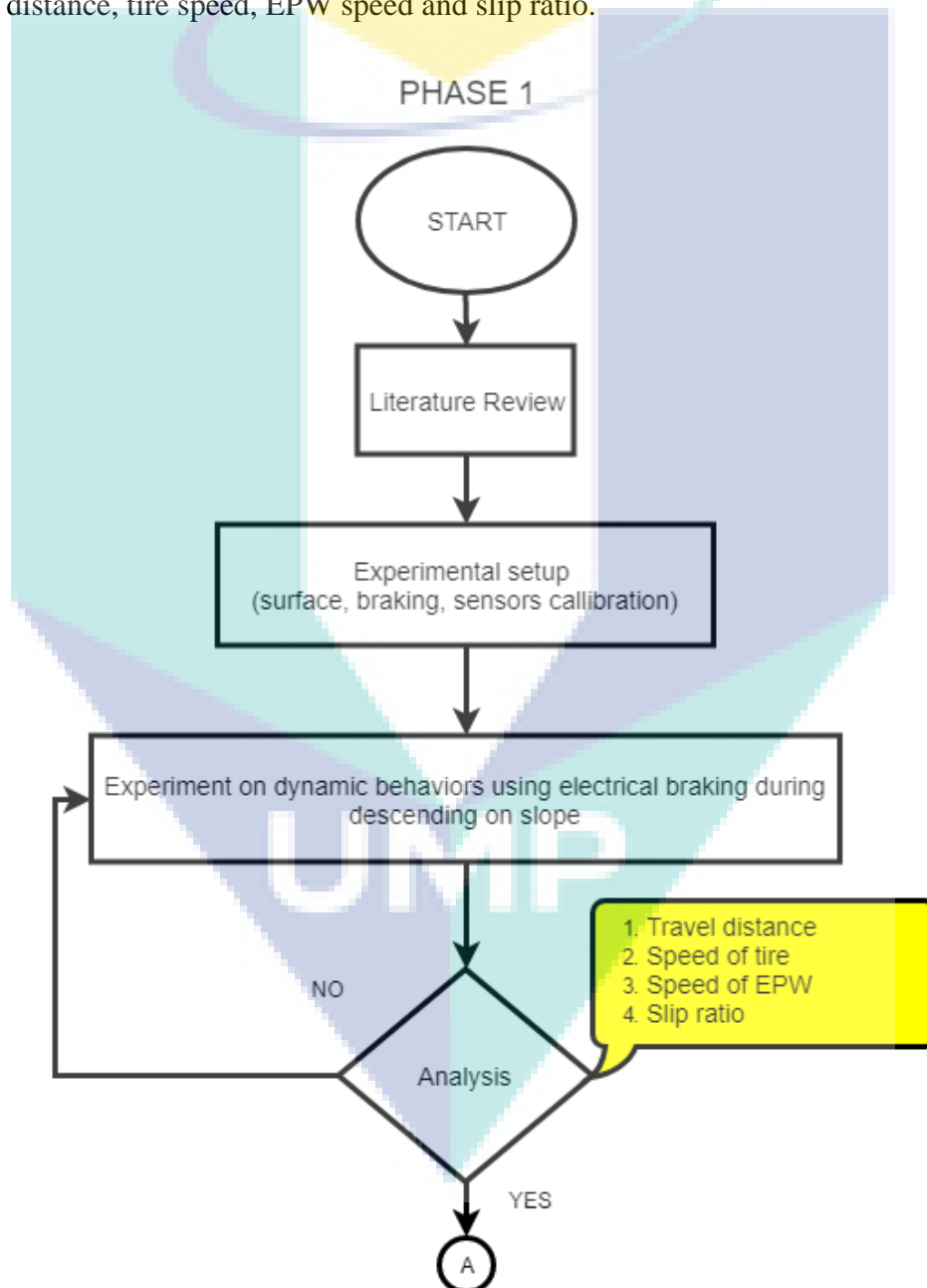


Figure 3.1 Flow chart of EPW project for Phase 1

The purpose of this first phase is to investigate the dynamic behavior between during braking using electrical braking. Besides that, it is also done to choose the appropriate electric braking either regenerative, dynamic or plugging to be used as automatic electric braking in second phase.

In the second phase, from the chosen electrical braking in phase 1, the electric motor braking controller is designed in Myrio-Labview environment. The Proportional Derivative and Integral (PID) controller is selected to be used to control the speed of EPW during descending on the slope condition. In this experiment, the active braking controller to control the speed is conducted at initially 0 m/s because of safety reason. The speed and voltage plugging input are analyzed during descending on slope. The PID gain is needed to be tuned when the speed output does not meet the desired speed by using empirical method.

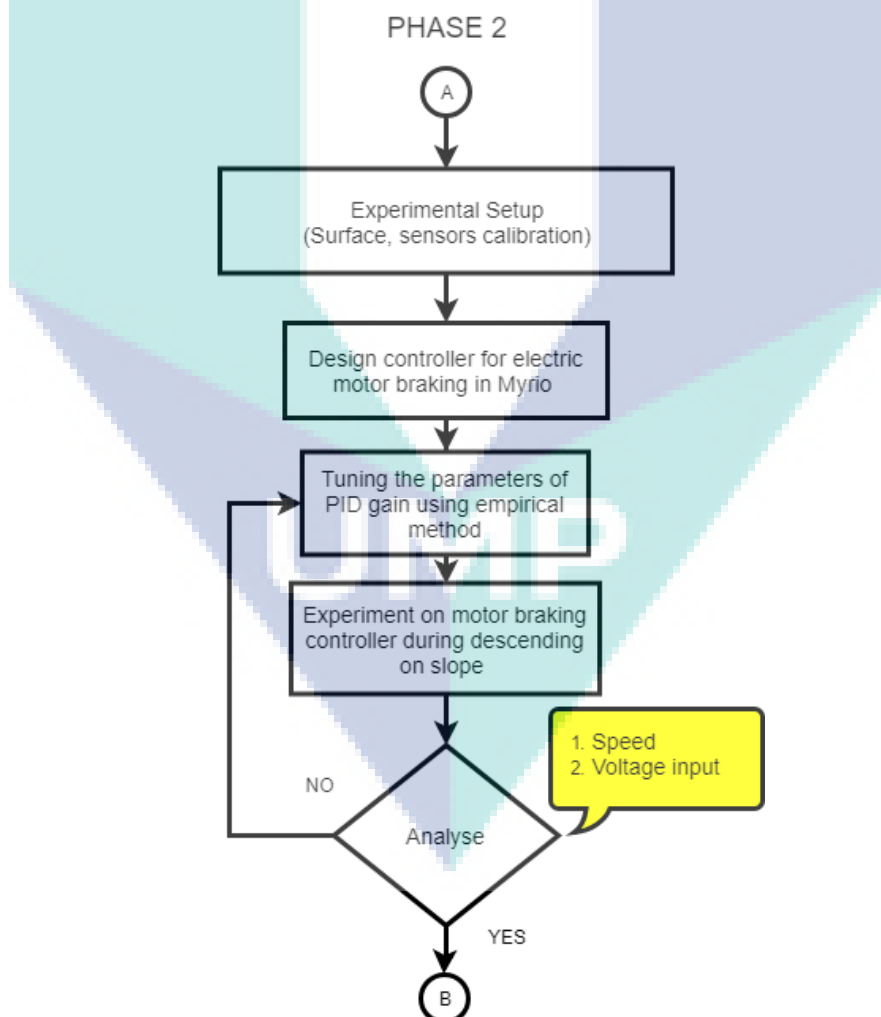


Figure 3.2 Flowchart for Phase 2

At the last phase, it is important to solve the limitation in phase two by designing and investigating the motor braking controller performance during descending at high initial speed using simulation approach.

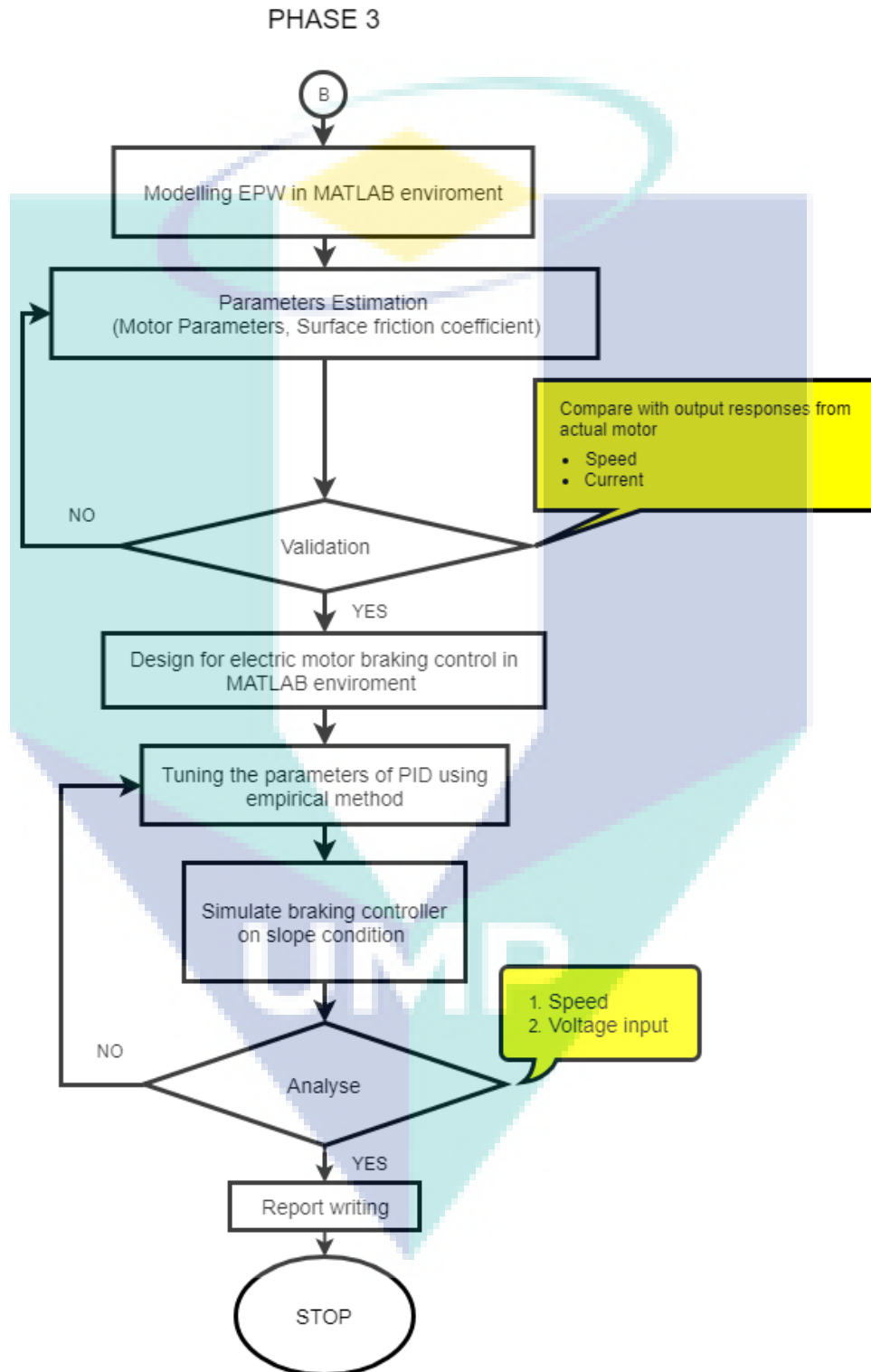


Figure 3.3 Flowchart of Phase 3

The mathematical modelling of Electric Powered Wheelchair (EPW) is developed in MATLAB Simulink environment based on related dynamic equation. Next, the unknown parameters such as internal resistance and moment of inertia of motor in mathematical modelling are estimated by using fitting curve technique. After that, the output response including speed and current between mathematical model and actual model are validated and calibrated using appropriate calibrate parameters technique.

Thereafter, the electric motor braking controller is designed in MATLAB Simulink environment. The Proportional Derivative and Integral (PID) controller is selected to be used to control the speed of EPW during descending on the slope condition. In the simulation, the plugging braking control is simulated at initial speed of 2.5 m/s. The speed and voltage plugging input are analyzed during descending on slope. The PID gain is needed to tune same parameters as experimental work when the speed output does not meet the desired speed.

3.3 Electric Powered Wheelchair specification and instrumentation

Figure 3.4 and Table 3.1 show the Electric Powered Wheelchair (EPW) model and specification used in experimental analysis model.

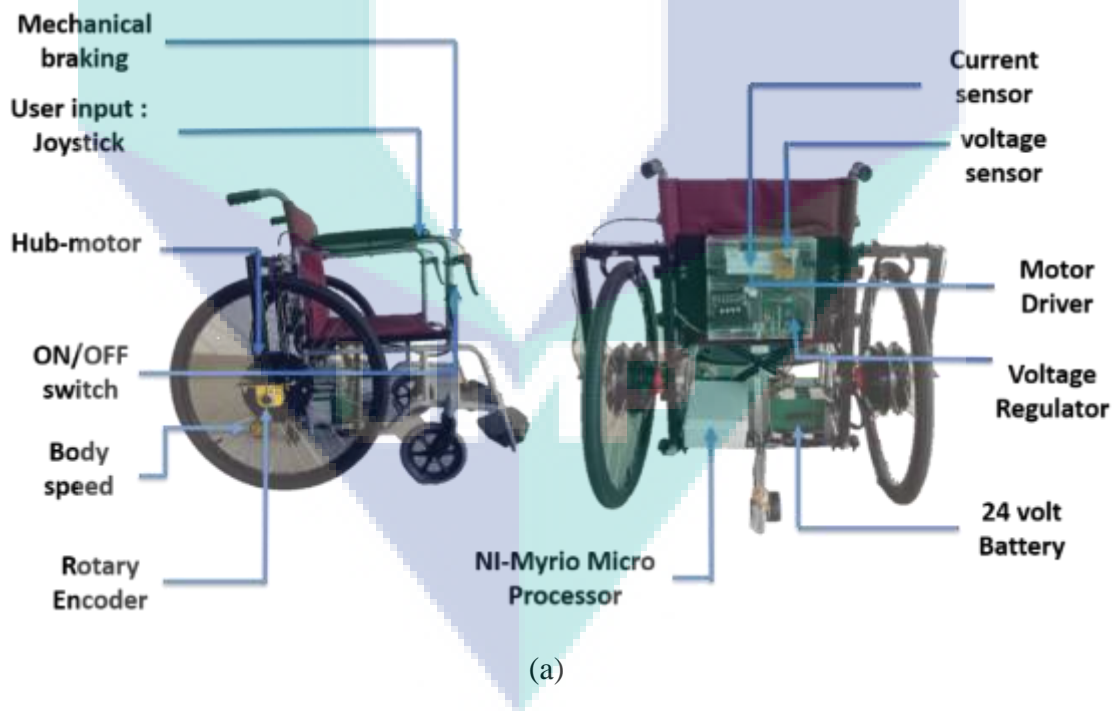


Figure 3.4 Experimental Electric Powered Wheelchair model

Table 3.1 Specification of Electric Powered Wheelchair (EPW)

Feature	Specification
Type of motor	In-wheel Brushless DC
Maximum speed (m/s)	2.7
Operating voltage (Volt)	12~36

The operation of this EPW is same as others Powered Wheelchair. This EPW is operated with 24 V battery supply and navigated by using joystick. The joystick will send the signal to motor driver and operate the motors to move the EPW. In addition, this EPW is equipped with many kinds of sensors as shown in Figure 3.5a and 3.5b which are speed encoder to measure the tire speed, current sensors to measure current value and direction flow in motor, and voltage sensor to measure voltage value. The data signal from sensors will be logged and processed in NI-Myrio Microprocessor.



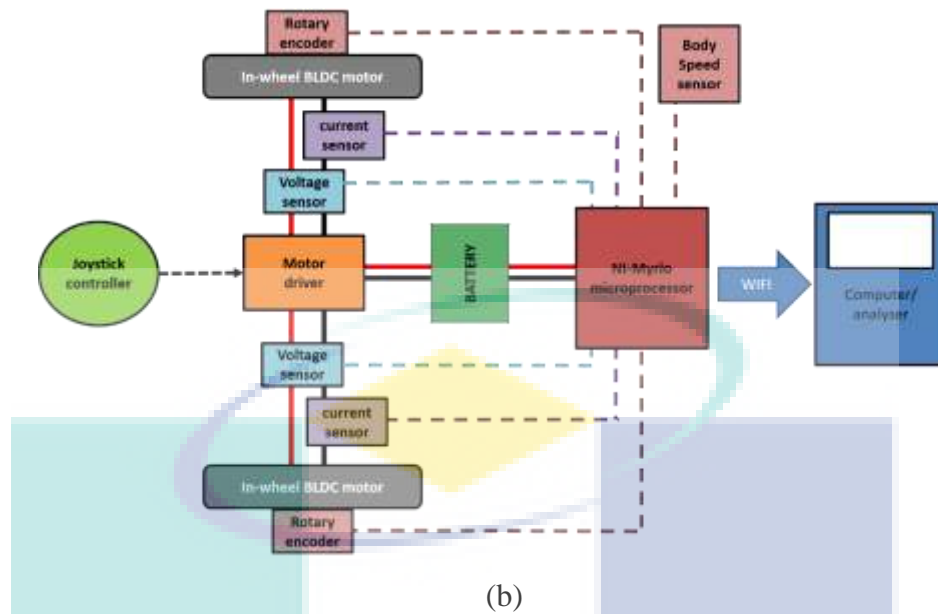


Figure 3.5 Parts and sensors used in EPW

3.3.1 Electrical drive system: BLDC motor

In this project, Brushless DC (BLDC) motor was chosen as drive system because of several reasons. Compare with other kinds of motors, the BLDC motor has lots of advantages, such as higher permanent magnet utilization, large motor torque, higher efficiency and reliability. Therefore, the BLDC motor plays an important role in product quality improvement, service life extension and energy saving (Kirtley, 2003). Figure 3.6 shows the in-wheel BLDC motor used as a drive system in this EPW project.



Figure 3.6 In-Wheel BLDC motor for EPW

The main design principle of a BLDC motor is to replace the mechanical commutator by using electrical switch circuit. In traditional DC motor, the brushes are used for commutation, making the direction of the main magnetic field and the armature magnetic field perpendicular to each other when the motor is running. The BLDC motor's structure contains a stator with armature winding and a rotor with a permanent magnet, which is similar to Permanent Magnet Synchronous Motor (PMSM). Figure 3.7 shows the main parts of the BLDC motor.

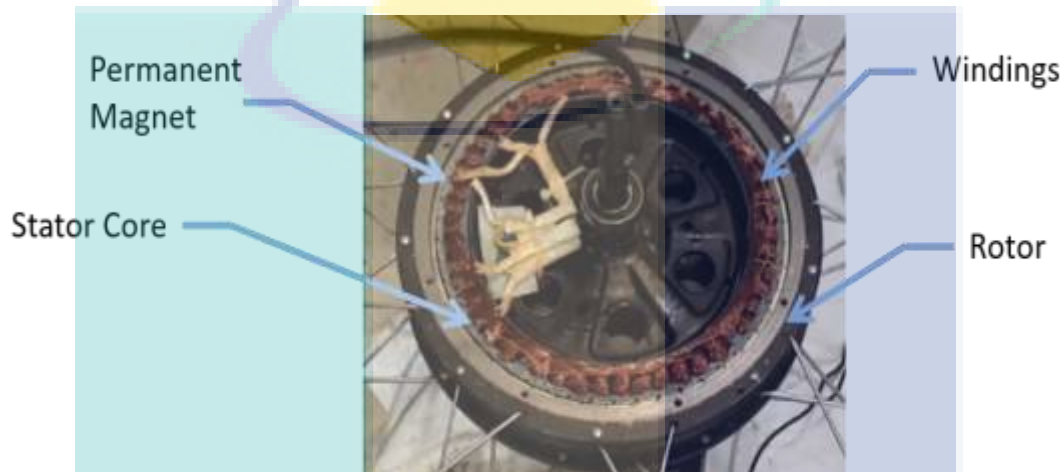


Figure 3.7 Parts inside in-wheel BLDC motor

There are two common types of the BLDC motor which are shown in Figure 3.8. A single-phase motor has one stator winding wound either clockwise or counter-clockwise along each arm of the stator to produce four magnetic poles as shown in the above figure. A three-phase BLDC motor has three windings. Each phase turns on sequentially to make the rotor revolve. In this research, single phase of BLDC is used for the Electric Powered Wheelchair (EPW).

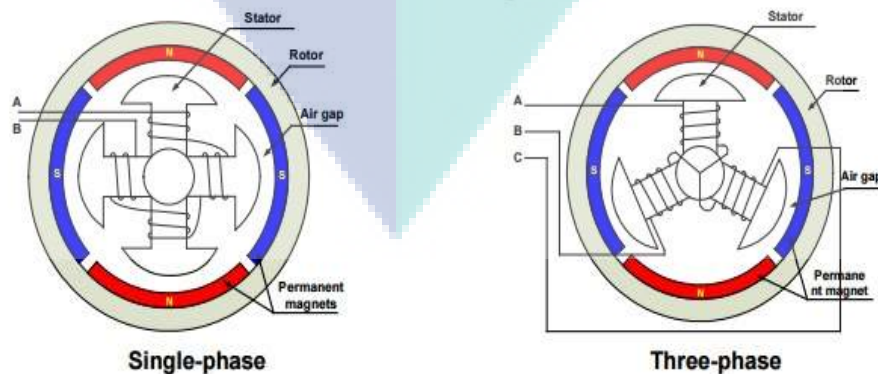


Figure 3.8 Phase type of BLDC

3.3.2 Motor driver Smart Drive Duo 30

Figure 3.9 shows the motor driver which had been used in this EPW project. Smart Drive Duo-30 is one of the latest smart series motor drivers designed to drive medium power electric motor with current peak capacity up to 80 Amp for a few seconds and 30 Amp for continuously run. This driver is designed for controlling differential drive small scale transportation system especially EPW.

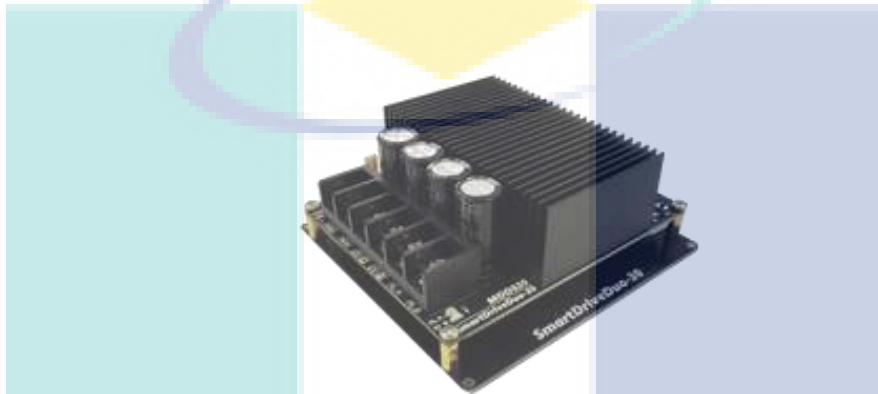


Figure 3.9 Two outputs motor driver provided by Cytron

This driver can be controlled using analog joystick or microcontroller by using PWM. The MOSFET inside the motor driver can be switched at 18 KHz which is to ensure quiet operation and no whining sound during switching the frequency. Table 3.2 shows the specification of SDD-30 motor driver provided by Cytron.

Table 3.2 Operating condition for SDD-30 motor driver

Features	Specifications
Compatible input	3.3 and 5V
Motor Channel	2
Operating voltage (VDC)	7 to 35
Peak Current (A)	80
Continuous current (A)	30

3.3.3 Battery

The Electric Powered Wheelchair moves at a very high speed and causes danger to the user. Hence a lower voltage battery is chosen to reduce the speed of the EPW and higher current peak to prevent from overcurrent to the motor driver. Even operating voltage of motor driver and electrical motors up to 36V, the 24V capacity battery is selected due to safety concern. Figure 3.10 shows the 12V lithium battery that used in the EPW. The battery is needed to connect in series way to form 24V.



Figure 3.10 12V Lithium GP battery

3.3.4 2 level speed control Joystick

Figure 3.11 shows the joystick as a user input for Electric Powered Wheelchair (EPW). Just like a joystick on the game console, this type of joystick can control x, y and z dimensions input by this joystick module. It can be considered a combination of potentiometers and one button.



Figure 3.11 Multi-axis Joystick

3.3.5 Rotational speed encoder

The rotary encoder that is used in this project is the B106 Rotary Encoder by Cytron Technologies as shown in Figure 3.12. Specification of the encoder is as listed in Table 3.3.



Figure 3.12 B106 Rotary Encoder

Table 3.3 Table of specification for rotary encoder

Electrical Specification	Output
Output signals	A, B, Z
Response frequency	0~100KHz
Supply Voltage	5~24 VDC
Pulse reading	2000 PPR
Mechanical Specification	Output
Maximum shaft speed	6000 rpm
Rotor moment of inertia	$1.5 \times 10^{-3} \text{ Kg/ms}^{-2}$
Weight	130g
Working life	MTBF \geq 25000h (+25°C, 2000rpm)

This type of rotary encoder is suitable for this particular project as the 5V operating voltage suits the LabView-Myrio and the 6000 Rpm maximum shaft speed is more than enough for the use of this project. The 2000 pulses per rotation ensure that the rpm reading of the encoder is accurate.

3.3.6 Oscilloscope: Voltage measuring

U1620A oscilloscope is the handheld oscilloscope with a VGA display. This 100/200 MHz handheld oscilloscope offers the floating measurement capability with two CAT III 300V isolated channels.

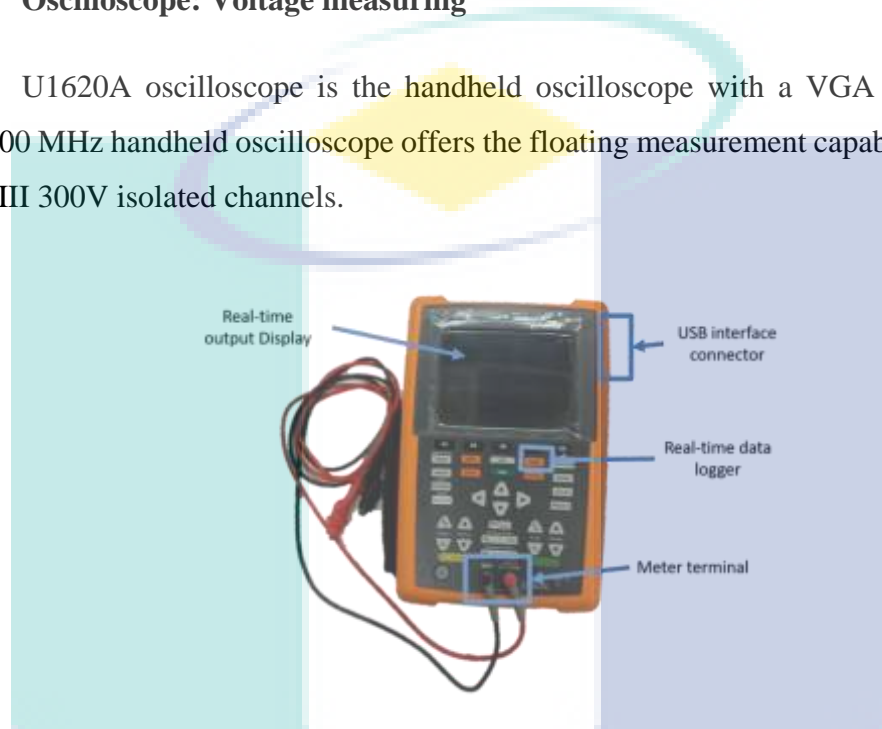


Figure 3.13 Hand held oscilloscope for voltage measurement

With up to 2 GSa/s sampling rates and 2 Mpts memory depth, it captures more waveform from the signal such as pulse width modulated circuit, in rush, transient, and the motor starts up sequences. The benchtop-like display and dual window zoom allow the user to quickly identify problem areas and zoom in for more detailed analysis. In this project, a real-time multimeter logger function is used to determine the voltage signal generated.

3.3.7 Current sensors

To measure the current, ACS712 type current sensors are used for this EPW project as shown in Figure 3.14. They are used to measure the current flowing into the motor during accelerating and braking up to 30 Amp. It also can sense the current flowing direction, especially while reversing the polarity of the voltage. Table 3.4 shows the specification of the ACS712 current sensor. Current sensors are connected in series between the motor driver and BLDC motor.



Figure 3.14 AC712 current sensor

Table 3.4 Specification of AC712 current sensor

Features	Specifications
Supply Voltage	5V dc Nominal
Measurement Range	-30 to +30 Amps
Voltage at 0Amp	VCC/2 (nominally 2.5VDC)
Scale factor	66mV per Amp

3.3.8 Voltage sensors

The voltage sensors need to be connected in a parallel way to measure the voltage during operation. There are many types of voltage sensors in the market based on the application. Figure 3.15 shows the typical voltage sensor for the lower voltage application. However, most of lower voltage sensors have many disadvantages such as disability to measure voltage more than the requirement. This sensor also cannot measure the voltage in reverse polarity.



Figure 3.15 Voltage sensor by Arduino

By using the handheld oscilloscope, the highest voltage recorded is almost 35 volts during free rolling descending on the slope. Thus, this sensor is not applicable to be used in this experiment. However, by applying voltage divider technique as shown in equation below, the voltage measured can be changed. In this project, the voltage sensor can be measured up to 55 V. The full wave rectifier is designed in this sensor to prevent reversed polarity during measurement of the voltage. Equation 3.1 shows the fundamental equation of voltage divider for the voltage sensor. Figure 3.16 and Figure 3.17 show the voltage sensor with full wave rectifier that had been fabricated for this project. Table 3.5 shows the specification of differences in common voltage sensor and the modified voltage sensor.

$$V_{measured} = V_{analog} \frac{(R_1 + R_2)}{R_2} \quad 3.1$$

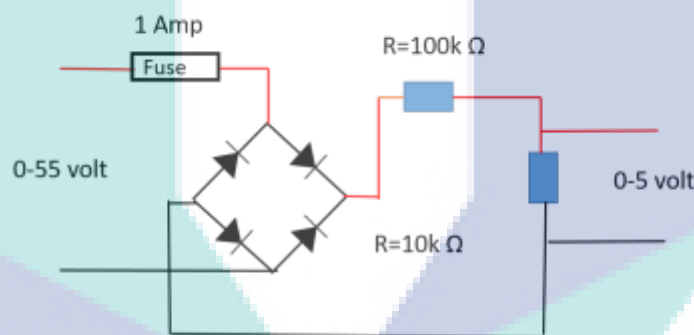


Figure 3.16 Circuit schematic of modified voltage sensor for reverse polarity prevention

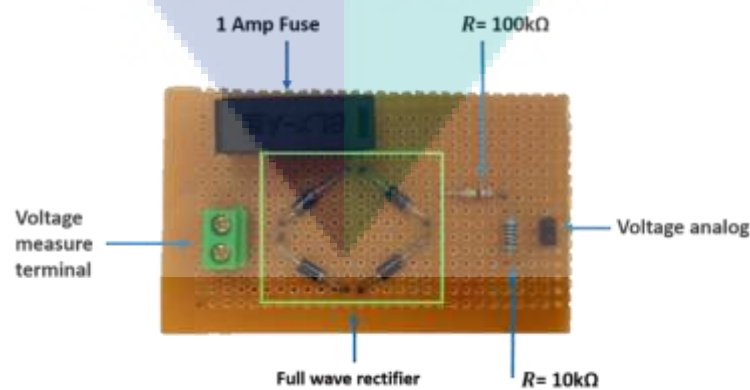


Figure 3.17 Modified voltage sensor with full wave rectifier

Table 3.5 Specification of common voltage sensor for low voltage uses

Features	Specifications	
	Common voltage sensor	Modified voltage sensor
Voltage measured (volt)	0-25	0~35
Voltage polarity	forward polarity only	Both polarity
Scale factor	4.8	7.2

3.3.9 Body speed by using third wheel

There are many types of devices that can be used to measure the speed of body/EPW. The commonly used sensor is a Global Positioning System (GPS). However, this type of sensor is only suitable for outdoor uses and not suitable for EPW where the experiment is conducted in a closed environment. Hence, the other technique to measure the speed of body/EPW is by using the third wheel that is installed at the middle back of EPW.



Figure 3.18 Body speed sensor using third wheel

The third wheel is made up of the rotary encoder, small wheel and weighing. The purpose of this third tire is to measure the translation speed of body/EPW by multiplying the rotational speed of wheel (ω) with the radius of the third wheel. Experiments had been done to validate the third wheel as a device to measure the body speed.

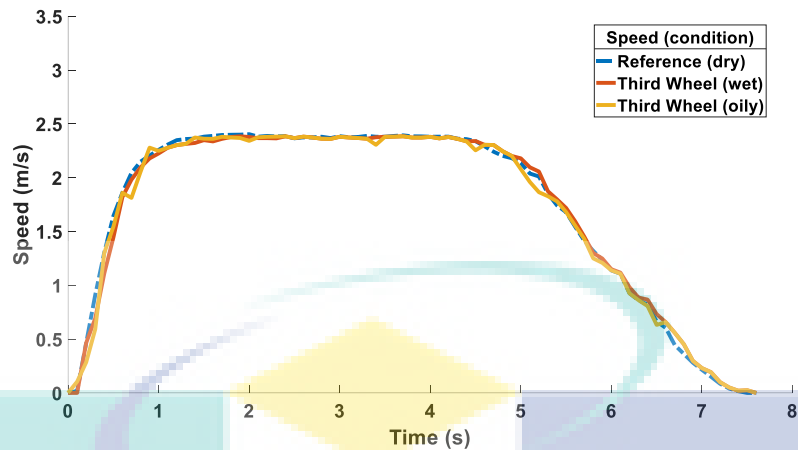


Figure 3.19 Characteristic speed of third tire in different surfaces

Figure 3.19 shows the speed characteristic of the third tire to measure the body speed in different surfaces. The experiment proves that the third wheel does not slip and the speed characteristic follows the reference speed even in the poor adhesion surface (oily). Therefore, the third tire is valid to be used as the device to measure the body speed of EPW for the experiment purpose.

3.3.10 Myrio Microprocessor Control Unit (MCU)

Figure 3.20 shows the Myrio embedded device that provides reconfigurable I/O on both sides of the device in the form of MXP and MSP connectors that allow implementing multiples design concept with one device. It also includes analog outputs for the sensors acquire purpose. In this project, there are three types of sensors being used which are; rotary encoder, voltage and current sensor that can also be measured and log in real-time as shown in Figure 3.21.

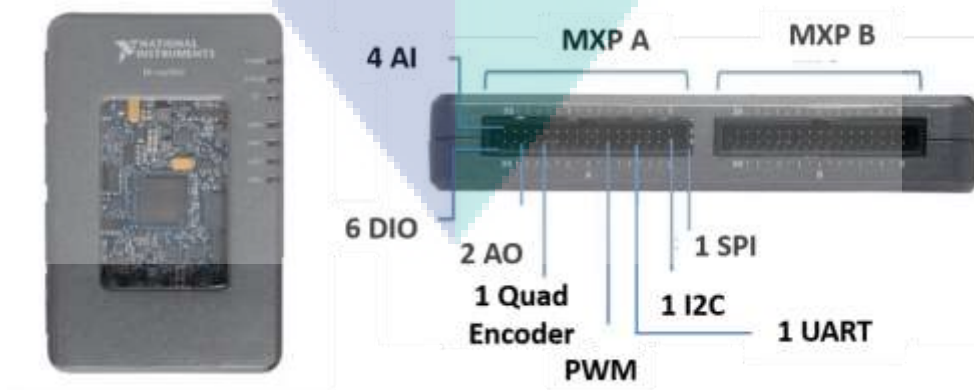


Figure 3.20 Myrio microprocessor module part

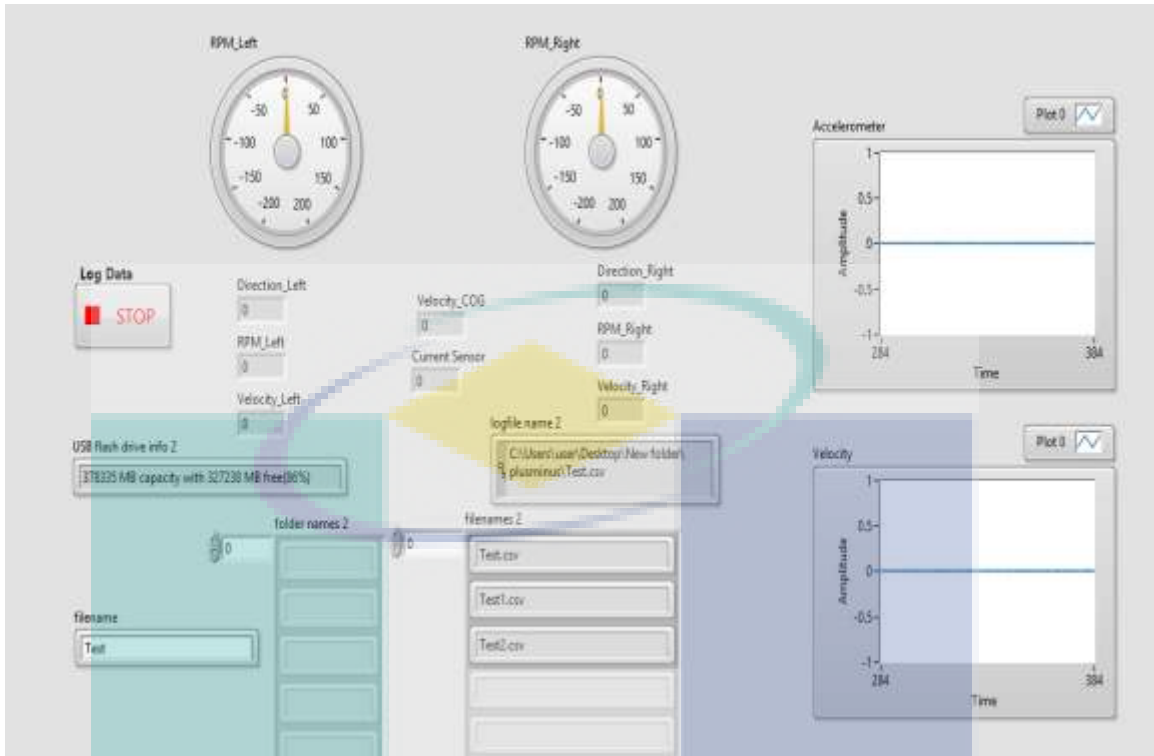


Figure 3.21 Real time control panel and data logger

3.4 Data analyse technique

To analyse the precise data, many techniques can be used. In this analysis, lower and upper boundary technique by using standard deviation calculation is used to collect precise data (F, Dunn, 2005). Equation 3.2 shows the standard deviation formula where \bar{x} is the mean or average for every experiment in each sampling time, t_s . The x_n is data for each experiment in each time sampling, t_s and n is the number of the experiment.

$$\sigma = \sqrt{\frac{\sum |x_n - \bar{x}|^2}{n-1}} \quad 3.2$$

σ = Standard deviation

\bar{x} = Mean/ average

x_n = Data of experiment for each sampling time

n = sample

Equation 3.3 shows the formula for the lower and upper boundary for each time sampling, t_s . The experimental data is accepted when the data in each sampling time is between the lower and upper boundary value as shown in Figure 3.22.

$$\text{Lower and upper value} = \bar{x} \pm \sigma$$

3.3

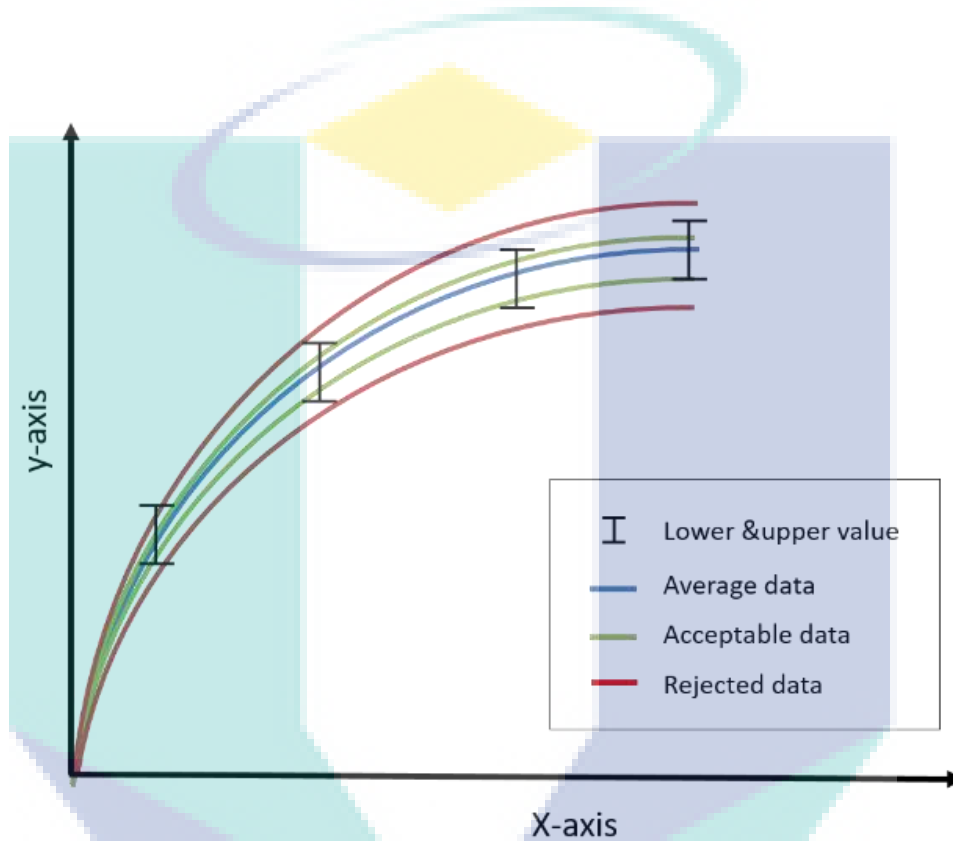


Figure 3.22 Illustration of Data acceptable

3.5 Slope condition setup

The experiment that is conducted on the slope for the wheelchair located at Students Activity Centre in Universiti Malaysia Pahang (UMP) is as shown in Figure 3.23. At first, the condition of experiment site needs to be confirmed by identifying the degree and length of slope. According to Malaysia Standards (MS), there are several standards for the slope of wheelchair that needs to be followed.



Figure 3.23 Slope condition for wheelchair at UMP

The first requirement is the slope percent of not more than 1:12 ratio. Then, the rise of slope is not more than 30" (0.76 meter) (Aqmar et al., 2018). However, in this experiment, the degree of slope is set more than MS-1184 requirement which is 8.1-degree average that can be measured by using tilt sensor (Figure 3.24). Next, the length of the slope is set at 5.4 meters based on the maximum rise standardized by MS-1184. The details of slope are shown in Figure 3.25 and Table 3.6.



Figure 3.24 Tilt meter sensor

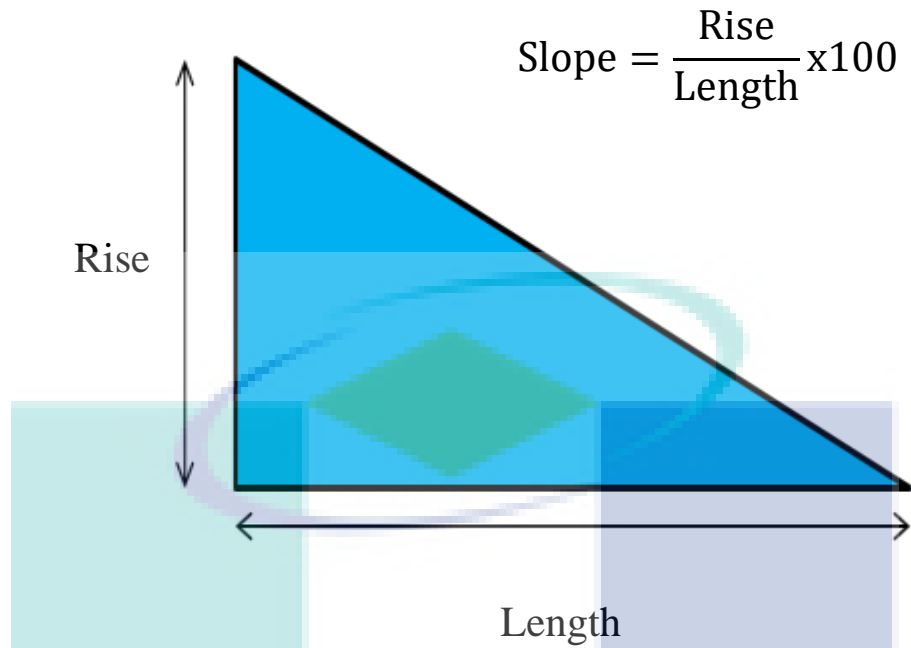


Figure 3.25 Slope setting for experiment base on MS-1184 requirements

Table 3.6 Slope setting information for experiment base on MS-1184 requirements

	Specification
Slope	8.1° (measure using tilt sensor)
Rise	0.76 meters (MS-1184 requirement)
Slope length	5.4 meter
Surface condition	Dry mosaic

3.6 Electrical braking analysis procedure

In the electrical braking analysis, this project focuses on three types of electrical braking which are; Regenerative, Dynamic and Plugging. The aim to conduct this experiment is to analyses the EPW behaviors consist of distance travel, speed of tires, speed of EPW and slip ratio during braking on the slope condition. In this experiment, several parameters are fix for the data consistency and accuracy such as weight of patient (75 kg) and longitudinal motion.

3.6.1 Regenerative braking analysis

The dynamic behaviors analysis using regenerative braking is not conducted because of several factors as pointed at below.

- Short Regenerative braking torque produced due to small Back EMF generated during descending on the slope and not practical to apply for the small transportation like EPW
- Limitation for BMS installation due to high cost (Affanni et al., 2005).

However, there is an analysis had been conducted to investigate the regenerative effectiveness during descending on the slope for EPW which to prove this type of electrical braking is not appropriate to be applied in EPW. To conduct the regenerative braking effectiveness, the analysis procedures are stated as below:

1. The slope conditions are set based on Table 3.6.
2. The sensors and microcontroller are set up and calibrated as shown in Figure 3.26 wiring schematic.
3. The voltage is started to record when the EPW is ready at the top of slope condition, 0 m.
4. The EPW is released from the top of slope at the initial speed 0 m/s without applied any braking force (free rolling).
5. The travel distance, speed of tires, speed of EPW and voltage generation are recorded until EPW reached at 5.4 m slope distance which to analyses the regenerative effectiveness.
6. The experiment is repeated at least ten times for the accuracy and precise data acquired using the correct data analysis technique as discussed in section 3.4.

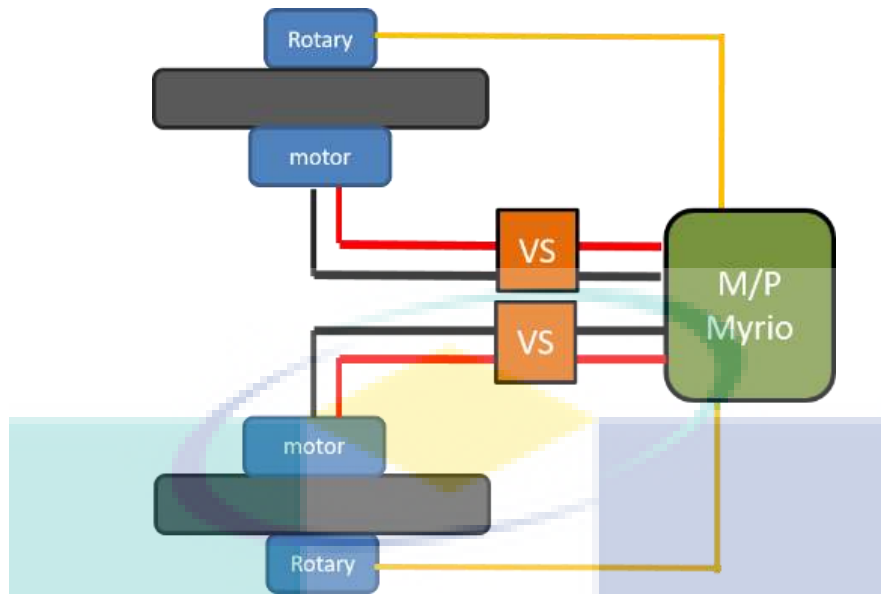


Figure 3.26 Wiring schematic for regenerative voltage experiment

3.6.2 Dynamic braking analysis

There are three initial speed for dynamic braking to be applied when EPW is descending on the slope which are 0 m/s, 1 m/s (medium) and 2.5 m/s (high). Figure 3.27 below shows the experiment setup schematic for the dynamic braking analysis. Basically, the main switch will be closed in order to perform the dynamic braking.

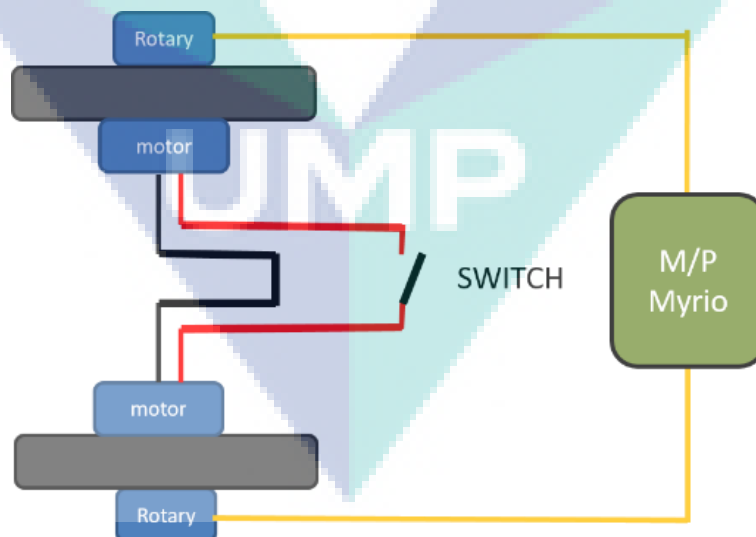


Figure 3.27 Dynamic braking experiment setup

i. Dynamic braking experimental procedures at initial speed 0 m/s

1. The slope conditions are set based on Table 3.6.
2. The sensors, microcontroller and main switch are setup as shown in Figure 3.27 wiring schematic.
3. The EPW is released from the top of slope, 0 m at the initial speed 0 m/s and main switch is closed to perform the dynamic braking.
4. The travel distance, speed of tires, speed of EPW and slip ratio are recorded until EPW stopped or reached at 5.4m slope distance.
5. The experiment is repeated at least ten times for the accuracy and precise acquired data using the correct data analysis technique as discussed in section 3.4.

ii. Dynamic braking experimental procedures at initial speed 1 m/s and 2.5 m/s

1. The slope conditions are set based on Table 3.6.
2. The sensors, microcontroller and main switch are set up as shown in Figure 3.27 wiring schematic.
3. The EPW is ride at constant speed 1 m/s on 0° slope condition (See Figure 3.28).
4. The main switch is closed to perform the dynamic braking when EPW entered slope condition, 0 m (See Figure 3.28).
5. The travel distance, speed of tires, speed of EPW and slip ratio are recorded until EPW stopped or reached at 5.4 m slope distance.
6. The experiment is repeated at least ten times for the accuracy and precise acquired data using the correct data analysis technique as discussed in section 3.4.
7. The experiment is repeated with the same procedure 1 to 6 for dynamic braking analysis at initial speed 2.5 m/s.

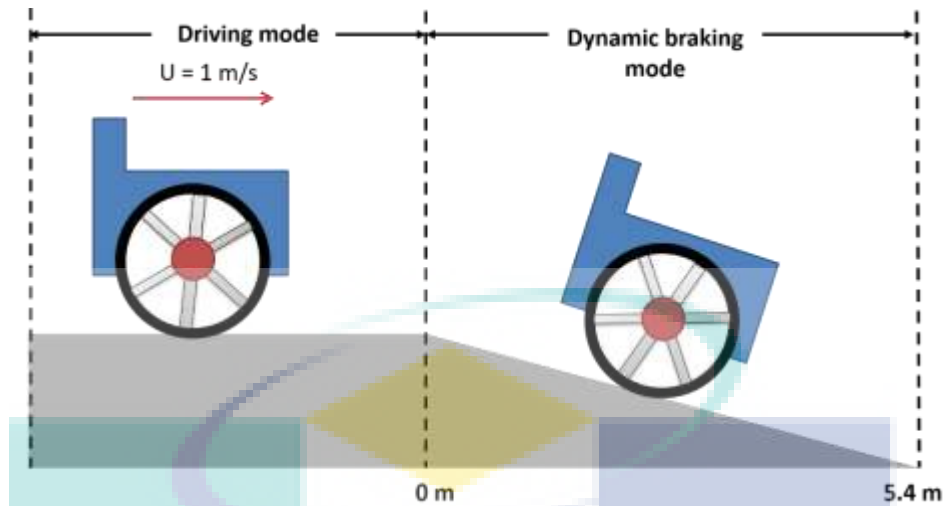


Figure 3.28 Dynamic braking analysis procedure

3.6.3 Plugging braking analysis

The last type of electrical braking to be analyzed is known as plugging braking or reverse polarity braking. For this method, the polarity of the supply voltage (battery) is reversed by using voltage regulator as shown in Figure 3.29. As a result, the back EMF that produces the reverse current is doubled with the current that produced by reversed polarity from the voltage supply. Thus, the braking torque is generated to reduced and stopped the speed of EPW. There are three initial speed for plugging braking are applied when EPW is descended on the slope which are 0 m/s, 1 m/s and 2.5 m/s.

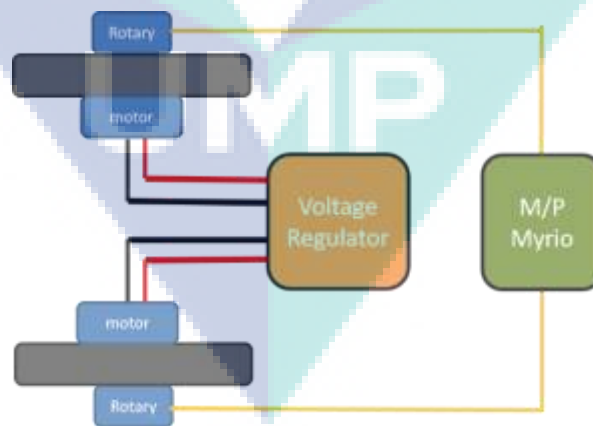


Figure 3.29 Plugging braking experiment setup

i. Plugging braking analysis procedures at initial speed 0 m/s

1. The slope conditions are set based on Table 3.6.
2. The sensors, microcontroller and voltage regulator are set up as shown in Figure 3.29 wiring schematic.
3. The EPW is released from the top of slope, 0 m at the initial speed 0 m/s and voltage regulator with plugging (reversed) voltage 0.5V is switch on to perform the plugging braking.
4. The travel distance, speed of tires, speed of EPW and slip ratio are recorded until EPW stopped or reached at 5.4m slope distance.
5. The experiment is repeated at least ten times for the accuracy and precise acquired data using for the each plugging voltage.
6. The experiment is repeated at with the same procedure from 1 to 5 for the 1.5 V, 2.5 V, 3.5 V and 4.5 V plugging voltage.

ii. Plugging braking experimental procedures at initial speed 1 m/s and 2.5 m/s

1. The slope conditions are set up based on Table 3.6.
2. The sensors, microcontroller and voltage regulator are set up as shown in Figure 3.29 wiring schematic.
3. The EPW is ride at constant speed 1 m/s on 0° slope condition (See Figure 3.30).
4. voltage regulator with plugging voltage 0.5V is switch on to perform the plugging braking when EPW entered slope condition, 0 m (See Figure 3.30).
5. The travel distance, speed of tires, speed of EPW and slip ratio are recorded until EPW stopped or reached at 5.4m slope distance.

6. The experiment is repeated at least ten times for the accuracy and precise acquired data using for the each plugging voltage.
7. The experiment is repeated at with the same procedure 1 to 6 for the 1.5V, 2.5V, 3.5V and 4.5V plugging voltage.
8. The experiment is repeated with the same procedure 1 to 7 for plugging braking analysis at initial speed 2.5 m/s.

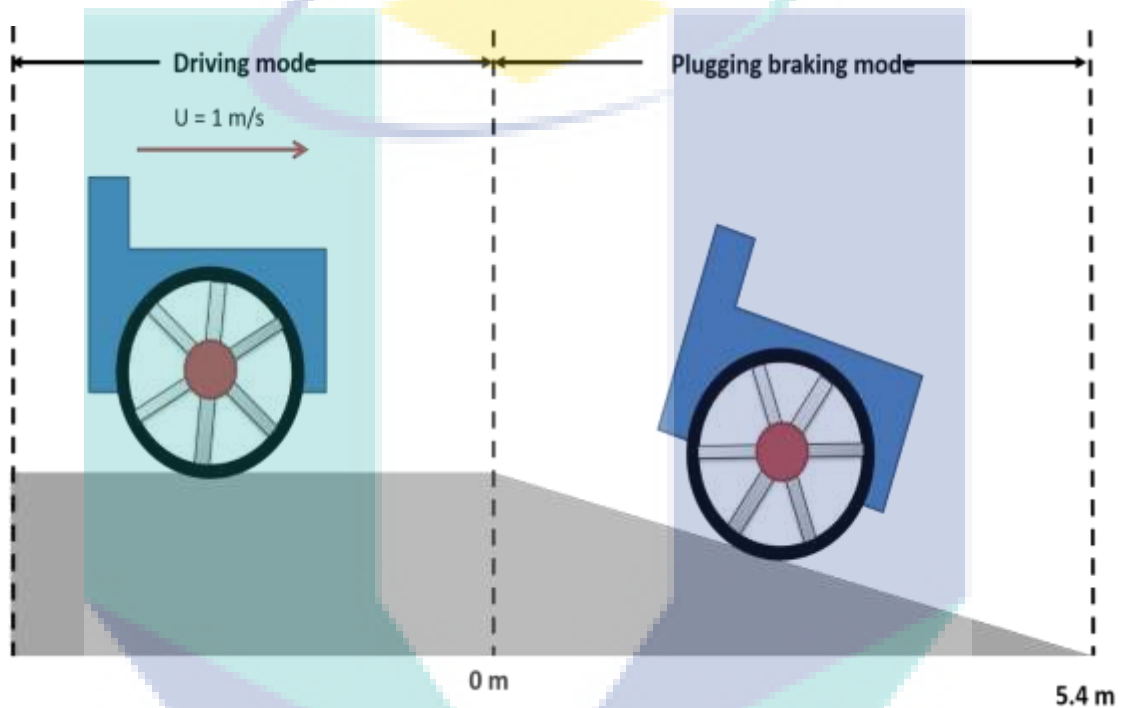


Figure 3.30 Plugging braking analysis

3.7 Real-time experimental on active braking control system

In the second phase, the active braking control is developed in real time application. This technique also known as hardware in the loop. Figure 3.31 shows the schematic setup for real-time control on active braking control. The Myrio is used as the microprocessor since the processor frequency is supported until 40 KHz. From the figure below, the speed of tire that is acquired from the analog output is compared with the desired speed as the error term for the PID controller. The correct input from the PID is transfer as PWM for the voltage control information in duty cycle form.

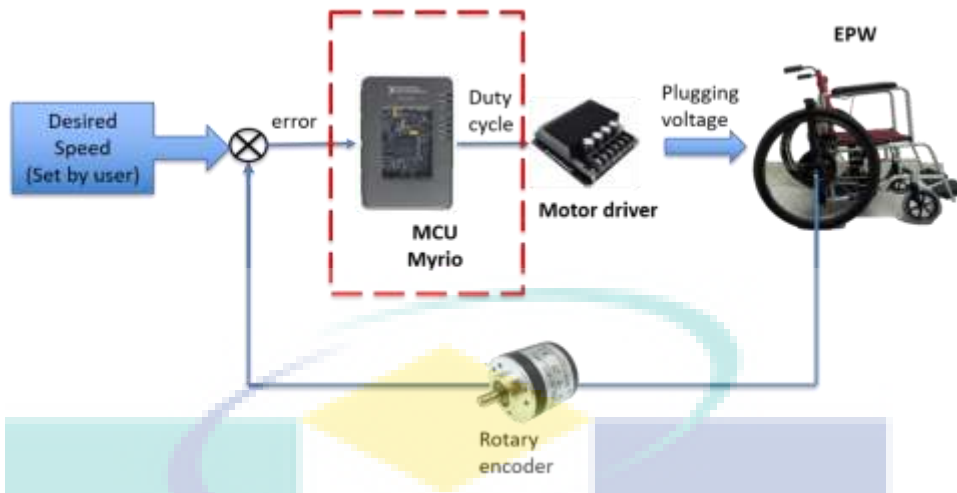


Figure 3.31 Plugging control setup

In this experiment, the same slope location in previous braking analysis is used. The EPW is released from the top of the slope at the initial speed 0 m/s which is same as free rolling analysis. When the speed approaches the desired speed, the braking control is automatically activated. The experiment is only conducted in initial braking speed 0 m/s for the safety reason and to avoid the motor driver from overheating that causes default to the electronic component inside the motor driver. For this project, the PID gains are tuned by using the empirical method that discusses in the next section.

3.7.1 Tuning of PID

The PID control is selected as the controller for EPW speed control during descending on the slope due to simplicity. Figure 3.32 shows the schematic diagram of the PID controller. A PID controller is a combination of three gains which are proportional (P), integral (I) and derivative (D).

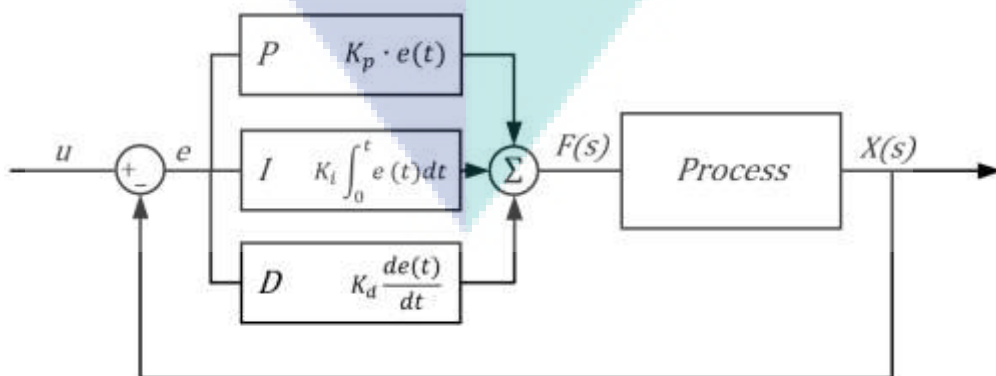


Figure 3.32 PID controller structure

Equation 3.4 shows the control input for the plant. By using the state feedback control method, the desired and actual angular speed of the tire are compared as the error, $e(t)$ term for the PID controller.

$$V_{input}(t) = K_p \cdot e(t) + K_i \cdot \int e dt + K_d \frac{de}{dt} \quad 3.4$$

Where:

$$e(t) = \omega(t)_{desired} - \omega(t)_{actual}$$

k_p = Proportional gain

k_i = Integral gain

k_d = Derivative gain

Each gain in PID controller plays their role. The purpose of the P controller is to calculate the term proportional to the error. The higher P gain that gives to the controller, the faster response to the time rise. However, the system will be overshoot and caused steady-state error to the system.

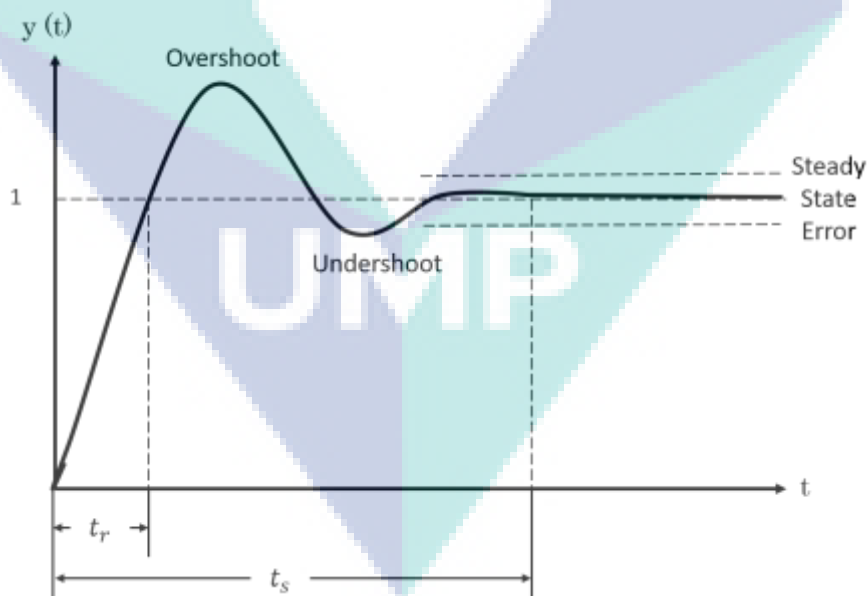


Figure 3.33 System response characteristic

Meanwhile, the I controller is to calculate a term proportional to integral of error. An integral controller gives great reduce to steady state error (SSE) between desired and actual response. The D controller is to calculate a term proportional to derivative of error.

A derivative control term often produces a faster response and reduce the overshoot. Table 3.7 shows the system response when each gain value is increased.

Table 3.7 Effect of system response by increasing the gain

Parameter Increase	Rise time (Tr)	Overshoot (OS%)	Settling time	Steady state error
Kp	decrease	increase	Small change	decrease
Ki	decrease	increase	increase	Great reduce
Kd	Small change	decrease	decrease	Small change

In this experiment, the PID controller on active braking control is set based on demand response that is stated in Table 3.8.

Table 3.8 Responses characteristic

Responses characteristic	Parameter characteristic
Overshoot	< 5 %
Settling time	< 3 s
Steady state error	± 0.05

3.8 EPW mathematical model plant

The numerical analysis starts by focusing on developing the mathematical model of Electric Powered Wheelchair (EPW) as shown in Figure 3.34 based on the related dynamic equations. MATLAB Simulink is used in this project to model the mathematical EPW. Recently, numerical analysis by using the simulation approach is the most popular concept among researchers to do an analysis. Not only it saves the cost, it can also save the time of analysis instead of using the real model that has high possibility of try and error (Pavasson et al., 2014).

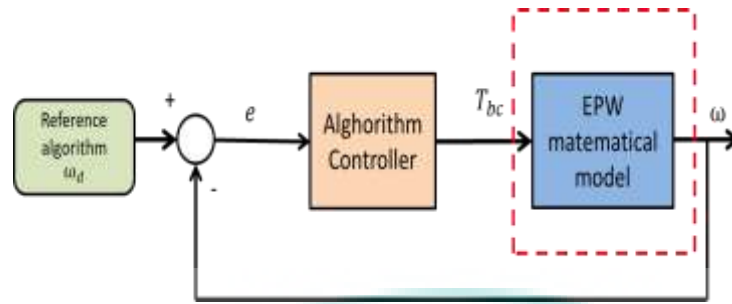


Figure 3.34 Mathematical model of EPW

Since Electric Powered Wheelchair (EPW) is driven by electric motor, mathematical modelling of EPW is divided into two parts which are electrical and mechanical part as shown in Figure 3.35.

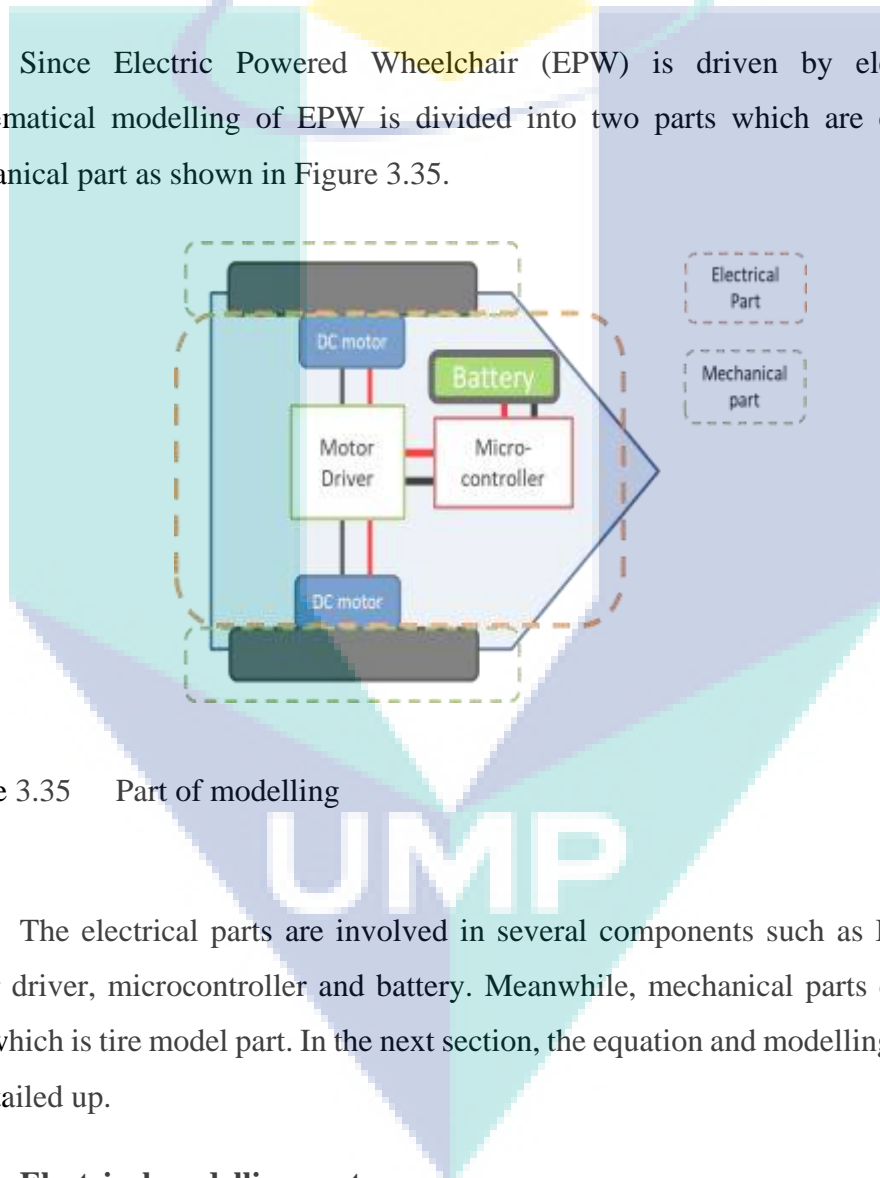


Figure 3.35 Part of modelling

The electrical parts are involved in several components such as BLDC motor, motor driver, microcontroller and battery. Meanwhile, mechanical parts consist of the load which is tire model part. In the next section, the equation and modelling of EPW will be detailed up.

3.8.1 Electrical modelling part

In this section, a single phase of brushless DC motor electrical part is discussed and modelled. To derive an equation model of the motor's behavior, the details of the commutation and motor driver are ignored. The modelling is only focused on electrical and mechanical power. The stator of the motor is assumed to have a single coil

characterized by an inductance L due to the windings and resistance R due to dispersions in the conductor as shown in Figure 3.36.

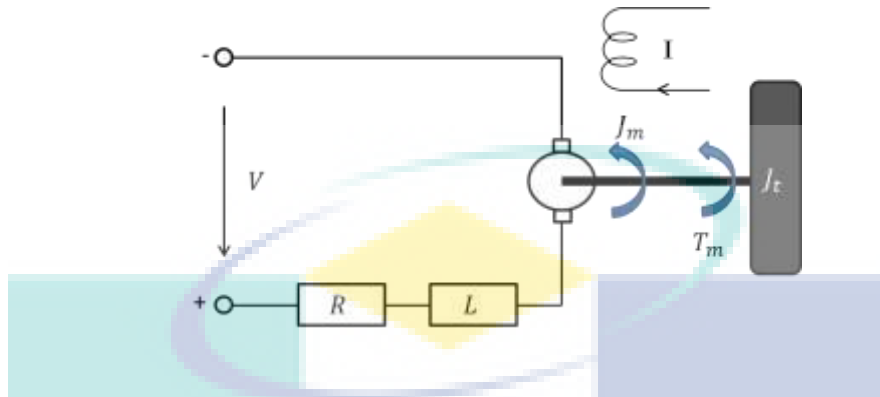


Figure 3.36 Electrical Part of BLDC

The modelling starts from the power equivalent as equation 3.5. The total power in is equal to the total of power out. In this case, power in comes from DC supply (battery) and output power is also known as total power loss.

$$\sum p(t)_{in} = \sum p(t)_{out} \quad 3.5$$

When the supply is connected to the electrical motor, the electrical power is supplied into the motor as iV , where i is the current through the motor and V is the voltage across the motor. Usually, the motor converts some of this input power to mechanical power, $\tau\omega$ where τ and ω are the torque and rotational speed of the output shaft respectively. In electrical part, the motor is described by a resistance, R between the two terminals as well as an inductance L due to the coils.

The resistance of the motor coils dissipates power i^2R as heat. The motor also stores energy $1/2(Li^2)$ in the inductor's magnetic field, and the time rate of change of this is $Li(di/dt)$, the power into (charging) or out of (discharging) the inductor. Finally, power is dissipated as sound, and heat is known as other power loss at the bearings between the motor shaft and the housing. In SI units, all these power components are expressed in Watts, W . Combining all these factors provides a full accounting for the electrical power put into the motor:

$$iV = i^2R + Li \frac{di}{dt} + \tau\omega + (\text{others power losses}) \quad 3.6$$

Ignoring the last term of power losses, the simple motor model can be written in terms of power as equation 3.7 below.

$$iV = i^2R + Li \frac{di}{dt} + \tau\omega(t) \quad 3.7$$

From the equation 3.7, the other relationships can be derived in form of voltage by dividing both sides by current, i term to form voltage relation as equation 3.8.

$$V(t) = i(t)R + L \frac{di(t)}{dt} + \frac{\tau}{i(t)}\omega(t) \quad 3.8$$

The ratio τ/i is a constant, an expression of the Lorentz force law for the particular motor design. This constant, relating current to torque, is called the torque constant, k_t as shown in equation 3.9. The torque constant is one of the most important properties of the motor. The SI units of k_t are Nm/A.

$$k_t = \frac{\tau}{i(t)} \quad \text{or} \quad \tau = k_t i(t) \quad 3.9$$

The motor model in equation 3.8 can be expressed in torque constant term as shown in equation 3.10.

$$V(t) = i(t)R + L \frac{di(t)}{dt} + k_t\omega(t) \quad 3.10$$

The term $k_t\omega$, with units of voltage, is called the back-EMF where EMF is known as *Electromotive Force*. It is also called as “back-voltage”. It is easy understand Back-EMF concept by spinning the motor and measure the voltage at output terminal. The measure voltage/generated voltage is known as back-EMF. For example, assume that the motor’s terminals are not connected to anything (open circuit). Then $i(t)$ and $di(t)/dt$ is assumed to be zero. Thus, equation 3.10 can be reduced to the equation 3.11. In this condition, motor is known as a generator that produces the back-EMF when the EPW descends with free rolling on the slope.

$$V(t) = k_t\omega(t) \quad 3.11$$

3.8.2 Mechanical modelling part

Figure 3.37 shows the dynamic motion of EPW. Assume tire is free rolling at the slope condition which means that the EPW is moving without giving any external torque or forces. During descending on the slope, EPW tends to move downward on the slope. This is because of the existence of gravity weight ($mg \sin \theta$) at x-component. The gravity weight at x-component will pull the EPW down and the gravitational torque T_g is generated.

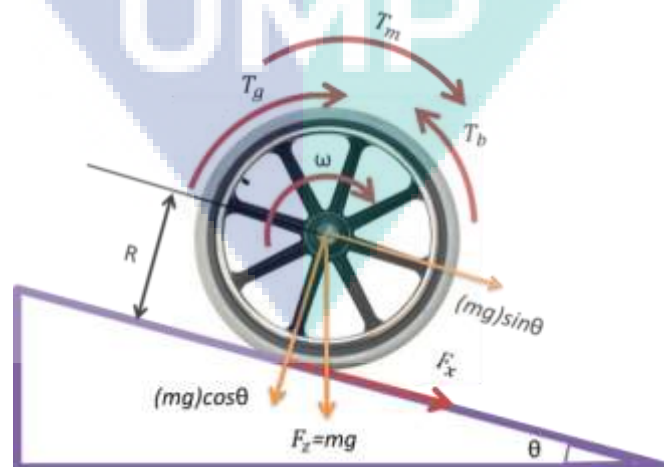


Figure 3.37 Mechanical part modelling

The dynamic equations for the tire rotating motion is shown in equation 3.12 where $d\omega/dt$ is the wheel angular acceleration time derivative, T_m is the motor input torque, T_L is the load torque which the total of initial torque in motor and frictional torque. B and ω is bearing constant and rotational speed respectively. J is the total moment inertia from motor, J_m and tire moment of inertia, J_t and T_b is braking torque.

$$\frac{T_m(t) + T_g(t) - T_L(t) - T_b(t) - B\omega(t)}{J} = \frac{d\omega(t)}{dt} \quad 3.13$$

$$T_L(t) = T_{int}(t) + T_F(t)$$

$$J = J_m + J_t$$

Equation 3.13 can be expanded as equation 3.14 where T_m is the product of current, I and torque constant, k_t . T_g is the product of weight force at x-component and tire radius, R_t . At the same time, the resistance torque is known as friction torque, T_F is obtained from product of longitudinal friction, F_x and tire radius, R_t .

$$\frac{k_t I(t) + mg \sin(\theta) R_t - [T_{int}(t) + F_x(t) R_t] - T_b(t) - B\omega(t)}{J_t + J_m} = \frac{d\omega(t)}{dt} \quad 3.14$$

For the braking torque, T_b there is only one type of electrical braking concept will be simulated in this project which is plugging. During EPW descending on the slope, the back EMF that carried current will be produced as discussed in equation 3.11. By changing the polarity of armature voltage immediately, the current direction will be changed and opposed to the current carried by back EMF voltage. Thus, the braking torque is produced when the plugging braking is given to the electric motor as shown in equation 3.8. Usually, the electrical braking will be simplified as equation 3.19 where C_{reg} is regeneration coefficient and ω is rotational speed (Peeie et al., 2013).

$$T_b = -C_{reg} x \omega \quad 3.15$$

3.8.3 EPW Dynamic modelling

A simple EPW model for longitudinal motion is shown in Figure 3.38. The longitudinal dynamics can be obtained by assuming that EPW mass is distributed on right and left wheel equivalently. The dynamic of front tire can be neglected due to the small vertical force acting on it and no driven mechanism. Since EPW moves in low speed and no cornering condition, the lateral, yawing, pitch, and roll dynamics also can be neglected.

The dynamic equations for the longitudinal EPW motions are derived using Newton's Second Law as stated in equation 3.16 which is the total of forces acted on x-axis of the EPW body is equal to the product of EPW mass and acceleration. Dynamic of model can be simulated by totaling up the forces that acted on right and left tire which are given as F_{xR} and F_{xL} respectively. Longitudinal acceleration, \dot{u}_x of EPW can be determined from dividing total forces with mass of EPW as shown in equation 3.17 and longitudinal velocity, u_x can be obtained by integrating the \dot{u}_x .

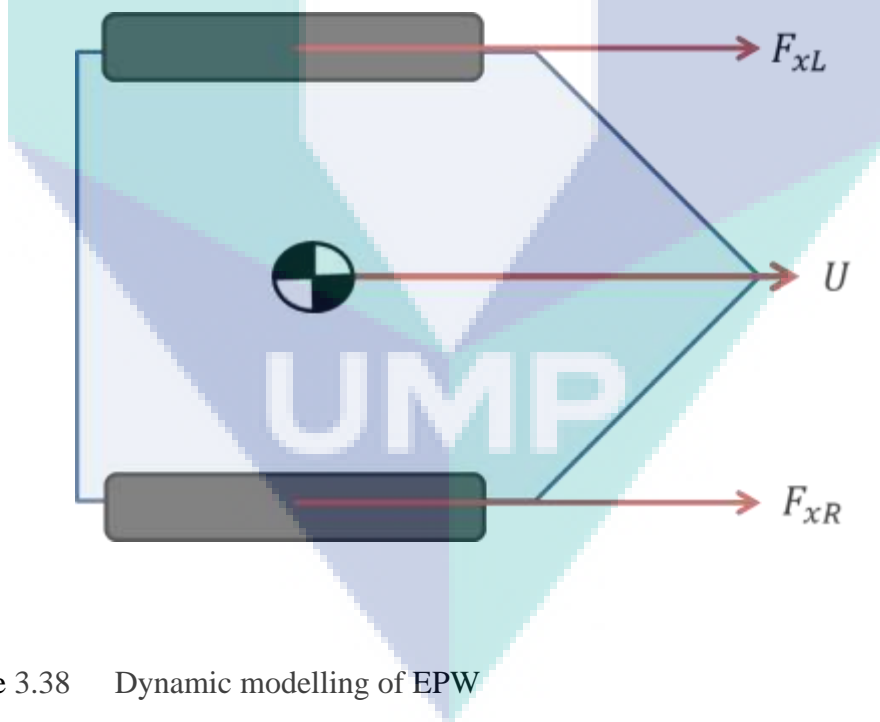


Figure 3.38 Dynamic modelling of EPW

$$\sum F_x = m_{EPW} \dot{u}_x \quad 3.16$$

$$\frac{F_{XL} + F_{XR}}{m_{EPW}} = \dot{u}_x \quad 3.17$$

When a driving motor torque, T_m is applied or gravity torque, T_g exist, the driving force will be developed at the contact patch between tire and road. The distance the tire travels when it is subjected to a driving force will be less than when it is in free rotation. This phenomenon is referred to as the wheel slip. The wheel slip is defined as the relative difference between a driving wheel's angular velocity and the vehicle velocity is known as slip ratio as derived in equation 3.18 (Peeie et al., 2014).

$$\rho_{accelerating} = \frac{R_t \omega - U}{R_t \omega} \quad 3.18$$

$$\rho_{braking} = \frac{U - R_t \omega}{U}$$

Adhesion characteristics of tire and road can be expressed by the concept of slip ratio. Utilizing slip ratio, the relationship of the slip ratio and the friction coefficient between the tire and the road can be approximated and described as equation 3.19, which is called $\mu-\rho$ function. Where k is the parameter of the road condition.

$$\mu_{acc} = 1.05k\{e^{-45\rho} - e^{-0.45\rho}\} \quad 3.19$$

$$\mu_{brk} = -1.15k\{e^{-35\rho} - e^{-0.35\rho}\}$$

$$k_{dry} = 0.8$$

$$k_{icy} = 0.12$$

The function of equation 3.19 can be illustrated as Figure 3.39 where blue line is when the road condition for asphalt dry is approximate to 0.8. Meanwhile, the red line

indicates when the road is in icy condition. These curves are very important in the slip ratio control design which to determine the optimum slip ratio for the tires from skidding.

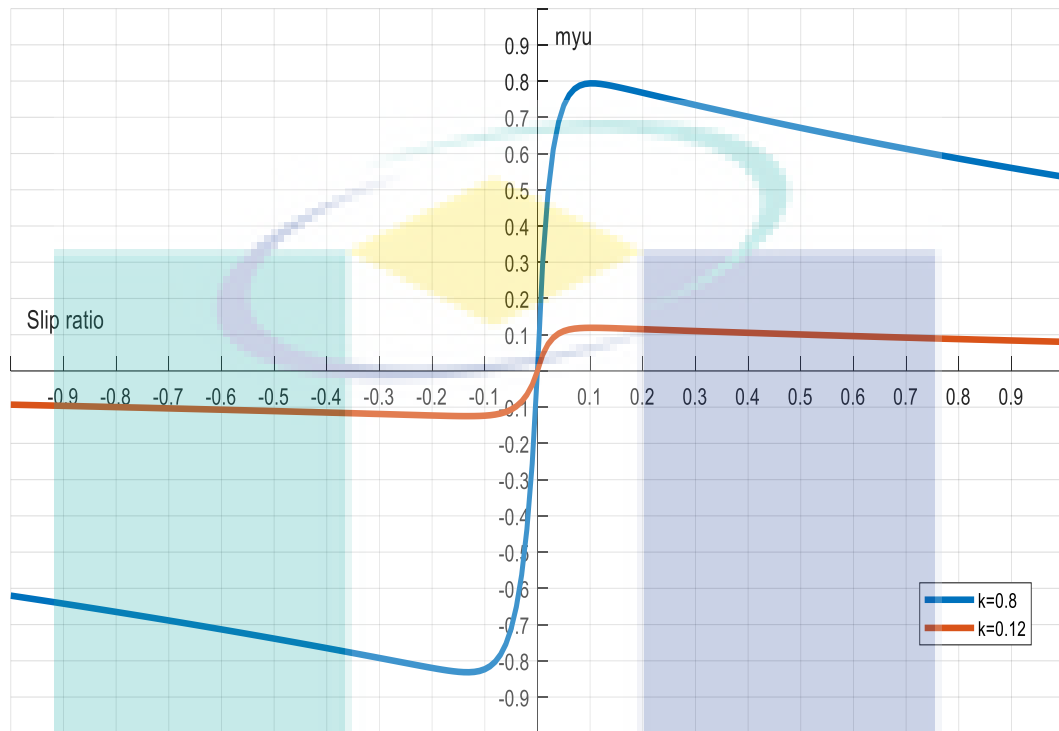


Figure 3.39 Myu-Slip curve
Sources: (Bera et al., 2011)

$$F_x = \mu(\rho) \times F_z \quad 3.20$$

$$F_z = mg \quad 3.21$$

Subsequently, the friction force F_x can be calculated as equation 3.20 after calculating the friction coefficient μ from utilizing $\mu - \rho$ curve, where F_z is the normal force reaction on the tire. The overall simulation between the electrical and mechanical part is shown in Figure 3.40.

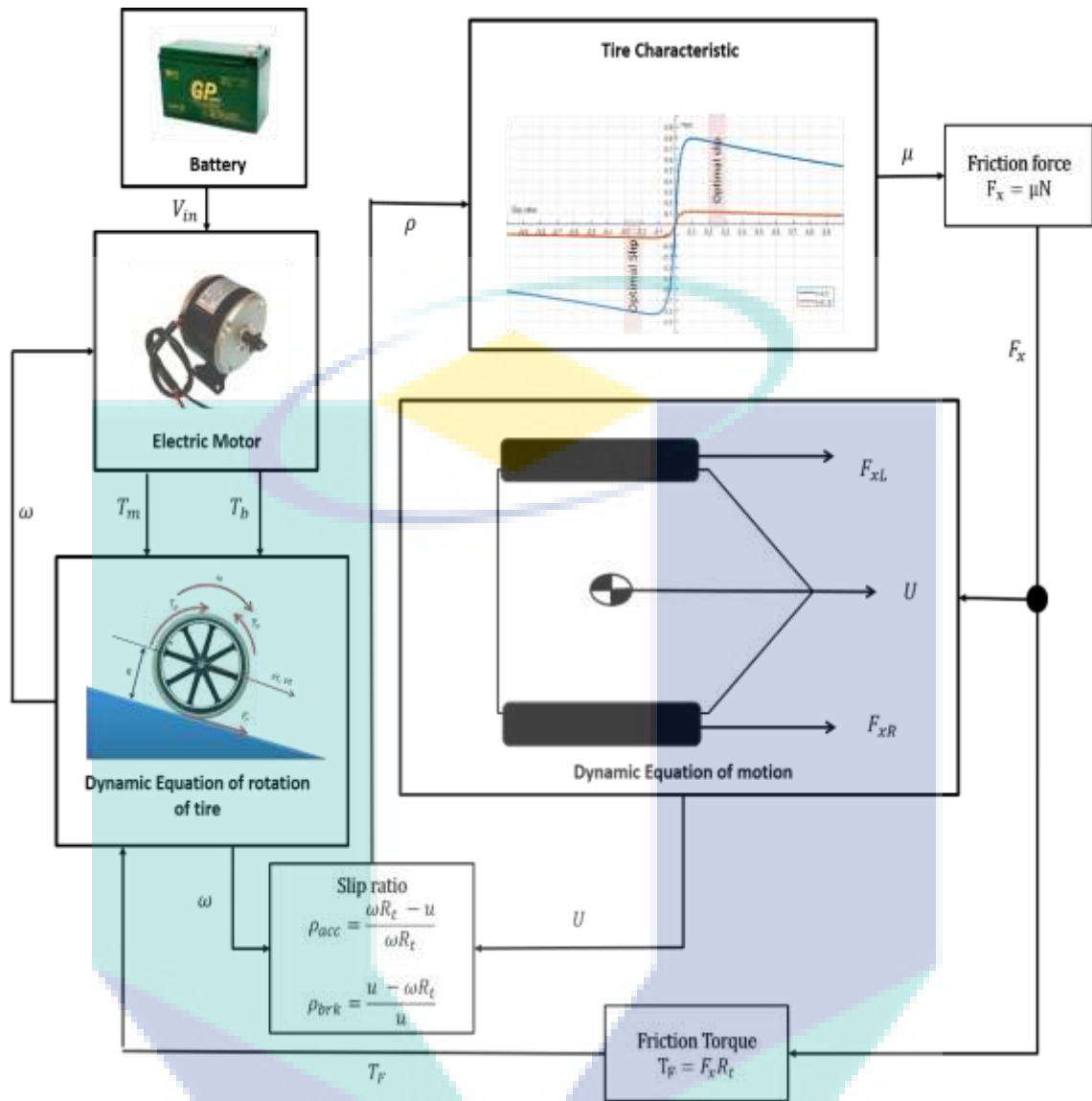


Figure 3.40 Single model tire simulation analysis flow

3.9 Experiment of parameters estimation

To run the simulation, the parameters are needed to estimate and verify. Parameter verification is very important for the modelling work before designing the control system. This process will determine the similarity of output responses between modelling system and actual system. This section focuses on estimating the model parameters of a brushless DC motor through experiment to develop a linear model of the system. Open-loop experiments need to be performed in order to estimate parameters through the response of sensors and motor behaviour.

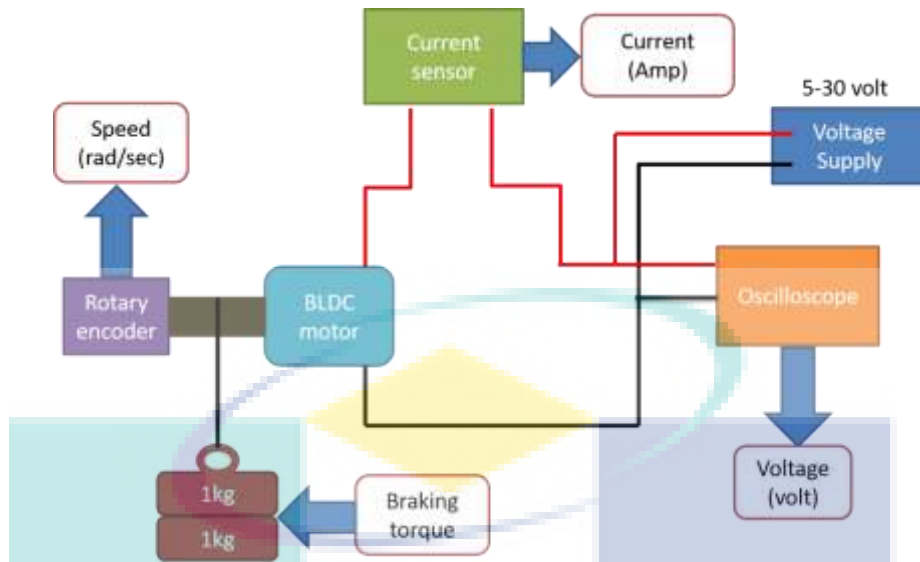


Figure 3.41 Schematic diagram set up for estimating parameters experiment

Experiment for estimating initial parameters of the motor is set up as Figure 3.41 and Figure 3.42. Input DC Voltage supply is used to supply the voltage into BLDC motor to generate the constant voltage. The actual input voltage is measured by using an oscilloscope. Then, the current sensor is connected in series between motor and input voltage supply for the current sensing purpose. To acquire data of the rotational speed, rotary encoder is used in this experiment in the unit of radian per second. All the output data will be logged/saved in the data logger system.

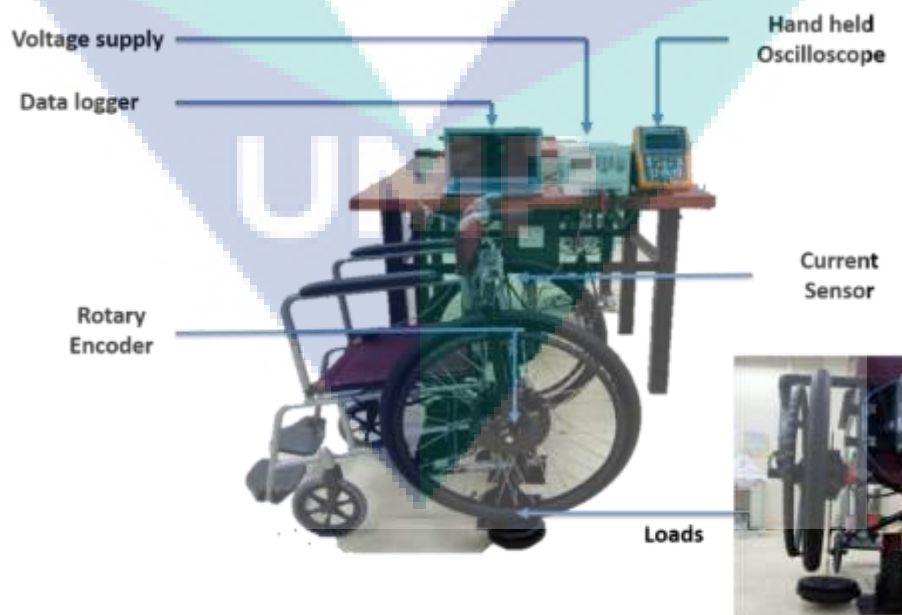


Figure 3.42 Schematic diagram and experiment equipment setup

3.9.1 Estimation of Resistance (R) and Torque Constant (k_t)

Recall back from equation 3.10, the resistance and torque constant can be determined by manipulating certain input. The torque constant, k_t which is the coupling parameter between electrical and mechanical model part. When the constant DC voltage is given, current will become a steady state condition and there is no change of current rate, so that the inductance term can be neglected to form equation 3.22. If every term in equation 3.22 is divided by $i(t)$ to form as $y = mc + c$ linear equation which $y = V(t)/i(t)$ and $x = \omega(t)/i(t)$ where $m = k_t$ and $c = R$ as shown in equation 3.23.

$$V(t) = i(t)R + L \frac{di(t)}{dt} + k_t \omega(t) \quad 3.22$$

$$\frac{V(t)}{i(t)} = k_t \frac{\omega(t)}{i(t)} + R \quad 3.23$$

The voltage and steady state current output can be determined by an oscilloscope and current sensor respectively. The speed can be acquired from the rotary encoder sensor. Voltage needs to be applied in many values in order to obtain the different current and rotational speed.

3.9.2 The estimation of bearing (B) and initial torque constant (T_{int})

Parameters of bearing, B and initial load torque, T_{int} is known as the mechanical part parameters. Recall back from equation 3.13, by neglecting the effect of friction, braking, and generation torque, equation can be rearranged and derived as below:

$$T_m(t) = J \frac{d\omega(t)}{dt} + B\omega(t) + T_{int} \quad 3.24$$

If the current in steady state condition, it can be assumed constant. The motor torque will also become constant because of the relation of $T_m = k_t i(t)$. At the steady state speed condition, there are no changes of speed rate and the $d\omega(t)/dt$ can be

assumed as zero. Rearrange the equation in terms of $y = mx + c$, the linear equation is derived as equation 3.25 where $y = k_t i(t)$ which k_t can be determined from the previous estimation, $x = \omega(t)$, $m = B$ and $c = T_{int}(t)$.

$$\frac{d\omega(t)}{dt} \approx 0 \text{ Steady state}$$

$$T_m(t) = B\omega(t) + T_{int}$$

3.25

3.9.3 The estimation of moment of inertia, J

The last parameter to estimate is known as moment of inertia. There are many methods to identify this parameter. In this project, we used the different braking load concept to determine J parameter. When the motor starts to rotate, at the transient or coasting (cut-off voltage) phase, $d\omega/dt$ is assumed cannot be zero as shown in Figure 3.43.

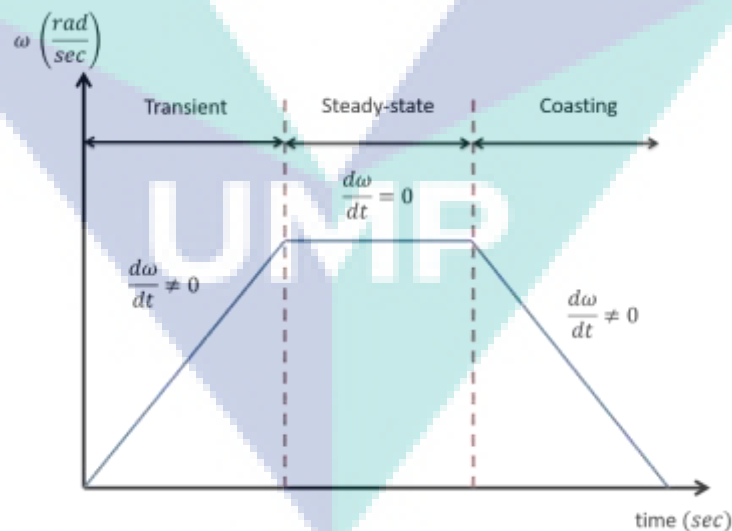


Figure 3.43 Phases of DC motor operation

Thus, the parameter J can only be determined during these two phases. In other hand, it is difficult to determine parameter J during a transient phase because the time is

short to record the sample, so that, the parameter J is determined at a coasting phase which is after the applied voltage is cut off. When the supply is cut off, by giving different external load (braking torque), the rate change of rotational $d\omega/dt$ will be different respectively as shown in Figure 3.44.

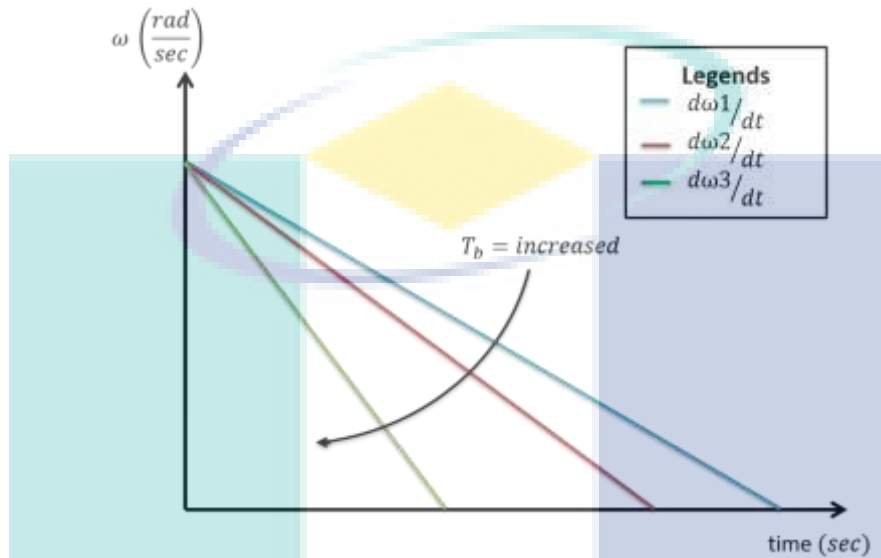


Figure 3.44 Different of braking speed by applied different braking torque

From the linear equation $y = mx + c$, the linear equation of mechanical part can be rearranged as equation 3.26 below.

$$-B\omega(t) - T_b(t) = J \frac{d\omega(t)}{dt} + T_{int}(t) \quad 3.26$$

Where;

$$y = -B\omega(t) - T_b(t)$$

$$x = \frac{d\omega(t)}{dt}$$

$$m = J$$

$$c = T_{int}(t)$$

At the same time, the rotational speed is recorded for each different applied braking torque. Table 3.9 can be used as the guideline to perform the experiment of

estimating the parameter J . The rotational speed can be determined to form the one-point time. For example, data of rotational speed is taken at $t = 1$ second in this project.

Table 3.9 Data sheet to find J parameter

Applied mass (kg)	Braking torque ($T_b = \text{Radius} \times \text{mass}$)	$d\omega/dt$	Rotational speed, $\omega(t)$
10			
5			
3			

3.10 Model validation

Once the parameters are estimated, they should be validated by using simulated model based. The most common method to validate the parameters is by simulating output responds between experiment and mathematical model with respect to different input. Before results analysis and validation, one must clearly understand the desired aim of the model. In other words, what output should have great precision, and where some errors may be tolerated. Equation 3.27 shows the standard error tolerated technique to validate the output responses between experiment and modelling. Data are verified if the modelling data is less than 10% in error range (Nazri et al., 2019).

$$\text{Model Validation} = \left| \frac{\text{experiment} - \text{simulation}}{\text{experiment}} \right| \times 100 \leq 10\% \quad 3.27$$

Several test scenarios should be defined to validate the model, and the chosen tests should represent the motor behavior in different significant situations. For example, if the model is needed to design the longitudinal control, a scenario of a straight-line motion should be prepared. In this project, the validation outputs response includes:

1. Rotational speed (rad/s)
2. Current (Amp)

3.10.2 In-wheel BLDC electrical motor model validation

Simulation models of the BLDC motor and the motor driver are established in MATLAB Simulink. Initial estimated parameters value is implemented in the simulation model and evaluated by observing the real-time response of the BLDC motor. The accuracy of simulation results with the real-time response can be enhanced by using the parameter-calibration tool in the MATLAB-Simulink software. In this tool, the iteration of the unknown parameter also such as inductance parameters are determined and calibrated based on experiment and simulation output.

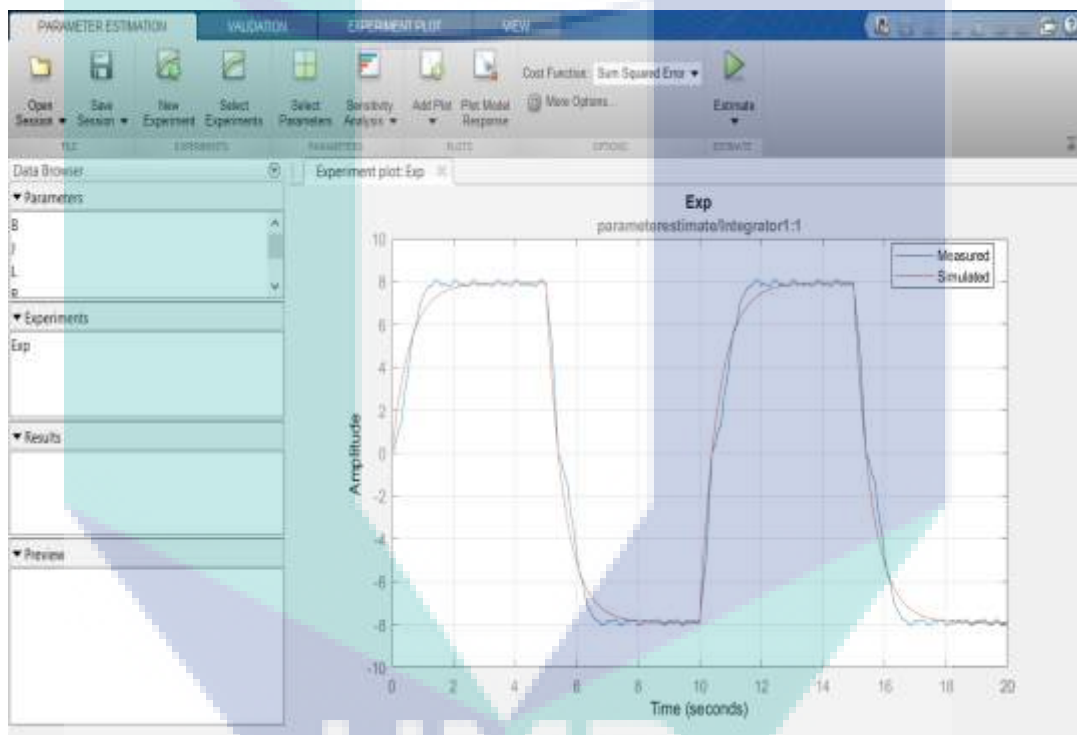


Figure 3.45 Parameters calibration tool in MATLAB Simulink

3.10.3 Road Surface parameter, k validation

Recall back from equation 3.19, the optimum parameter of k need to estimate in order to identify the friction coefficient μ for EPW during braking on dry mosaic condition. Parameter k very important to estimate for the braking control simulation during descending on the mosaic slope. According to the experiment that had been conducted by El-Sherbiny et al. (2012), the friction between rubber and dry ceramic/mosaic is ranged between 0.43~0.53 as shown in Figure 3.46.

Since surface coefficient, k is single parameters to be estimated, example iteration table as shown in Table 3.10 can be used to estimate the optimum “ k ” value for mosaic condition by comparing the error per cent of slip ratio between experiment and simulation. In the simulation setup, the configuration for sampling time is set 0.1 seconds which is the same as sampling time in experiment. Then, the initial speed is set 2.5 m/s during braking condition. In this simulation, the plugging voltage (reverse voltage) is set in two modes which are -4.5V and -2.5V. The surface coefficient, k is set in range 0.43~0.53.

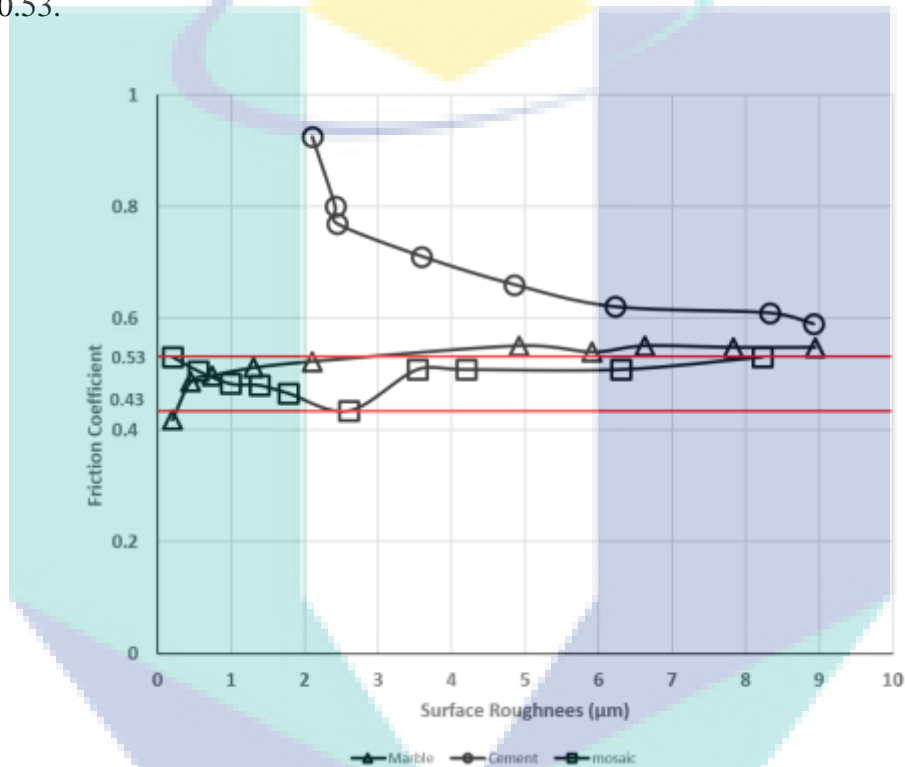


Figure 3.46 Friction coefficient range on mosaic surface

Sources: (El-Sherbiny et al., 2012)

Table 3.10 example table for optimum surface coefficient, k estimation

Estimated road surface, k iteration	Ave. Slip ratio error (%)
0.43	
↓	
0.53	

3.11 EPW Plant design by using state space method

In modern control theory, the motion state of control system relies on its state equation. The state-space equation method is one of the most important analysis methods in modern control theory. From the state equation, we can get all the independent variables and then determine all the motion states of the system. A group of first-order differential equation with state variables is used in the state-space method to describe the dynamic characteristic of the system. Since it is helpful to the realization of different digital control algorithm, the state-space method is becoming more and more popular in designing control systems with the fast development of computer techniques.

In recent years, computer on-line control system such as optimal control, Kalman filter, dynamic system identification, self-adaptive filters and self-adaptive control have been applied to motor control. All these control techniques are based on the state equation. The state equation of DC motor can be obtained by the algebraic transformation of the differential equation model. To describe a system in a linear motion, the equation 3.10 and 3.13 can be transformed to the following equivalent linear state-space as shown in equation 3.28.

$$\dot{x} = Ax + Bu \quad 3.28$$

$$y_1 = C_1 x = I \quad 3.29$$

$$y_2 = C_2 x = \omega$$

$$C_1 = [1 \quad 0] \quad 3.30$$

$$C_2 = [0 \quad 1]$$

where,

$$A = \begin{bmatrix} -\frac{R}{L} & -\frac{K_t}{L} \\ \frac{K_t}{J} & -\frac{B}{J} \end{bmatrix} \quad 3.31$$

$$x = [I \quad \omega]^T \quad 3.32$$

$$B = \begin{bmatrix} \frac{1}{L} & 0 \\ 0 & \frac{1}{J} \end{bmatrix} \quad 3.33$$

$$u = [v \quad (T_g - T_L - T_f)]^T \quad 3.34$$

Here, equation 3.31 and equation 3.33 can be simplified equation below.

$$A = \begin{bmatrix} a & b \\ c & d \end{bmatrix} \quad 3.35$$

$$B = \begin{bmatrix} e & 0 \\ 0 & f \end{bmatrix} \quad 3.46$$

Where;

$$a = -\frac{R}{L}$$

$$c = \frac{k_t}{J}$$

$$e = \frac{1}{L}$$

$$b = -\frac{k_t}{L}$$

$$d = -\frac{B}{J}$$

$$f = \frac{1}{J}$$

In the state-space equation, x is a system state, u is a scalar representing the input of the system and y is a scalar representing the output of the system. The matrices A , B and C determine the relationships between state and input and output variables. The block diagram of this plant system is shown in Figure 3.47.

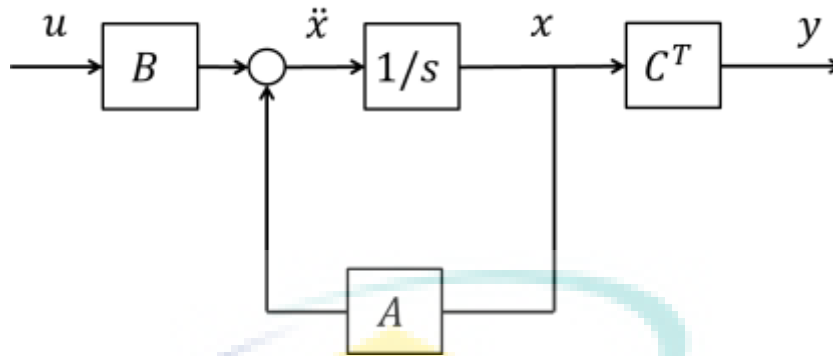


Figure 3.47 Block diagram state space of EPW

3.12 Simulation of motor braking controller using plugging braking concept

The other method to analyse the speed response of automatic braking controller during descending on slope is by using simulation approaches. Since there is a limitation on experiment as mentioned at Section 3.7, where motor braking cannot be performed in high speed, this method can save the time and cost of analysis.

Figure 3.48 shows the complete plant with the feedback controller. As shown in figure, u is the input voltage, V is the main control input for this plant. Thus, to control the speed of EPW during descending on the slope, the type of electrical braking that can be applied is plugging braking which is by reversing the polarity with certain control voltage amount.

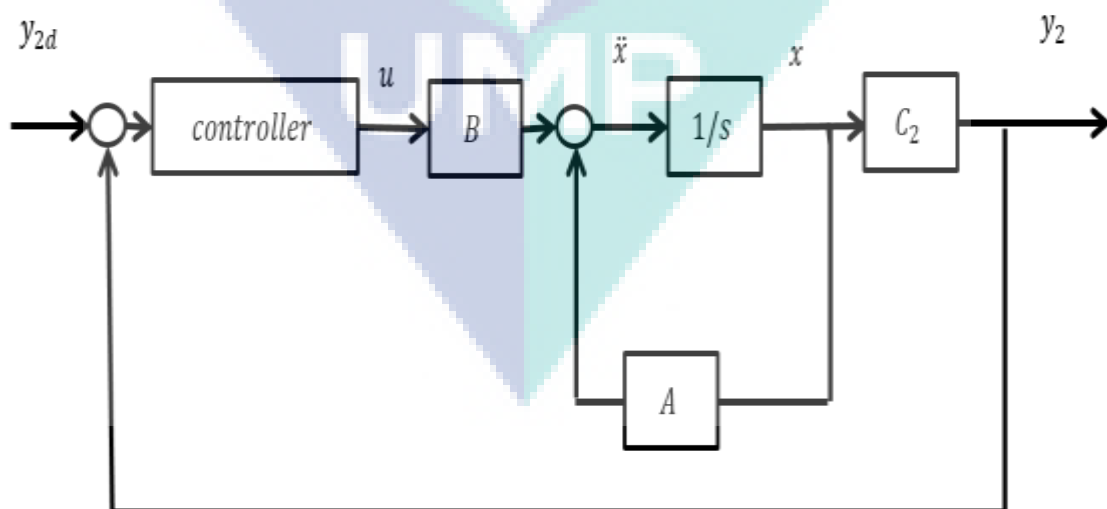


Figure 3.48 Block diagram control of EPW

To analyse the automatic braking control during descending at slope condition, the verified EPW model is used in this simulation. At the beginning of the simulation, the EPW is drive at a constant speed of 2.5 m/s at 0° dry mosaic slope. After a while, the condition slope is changed into 8.1° . At the same time, the automatic braking control/HDC is automatically activated and tracks the desired speed 0.6 m/s until end of slope. The gain in PID gain is tuned by using empirical method based on previous Table 3.8.

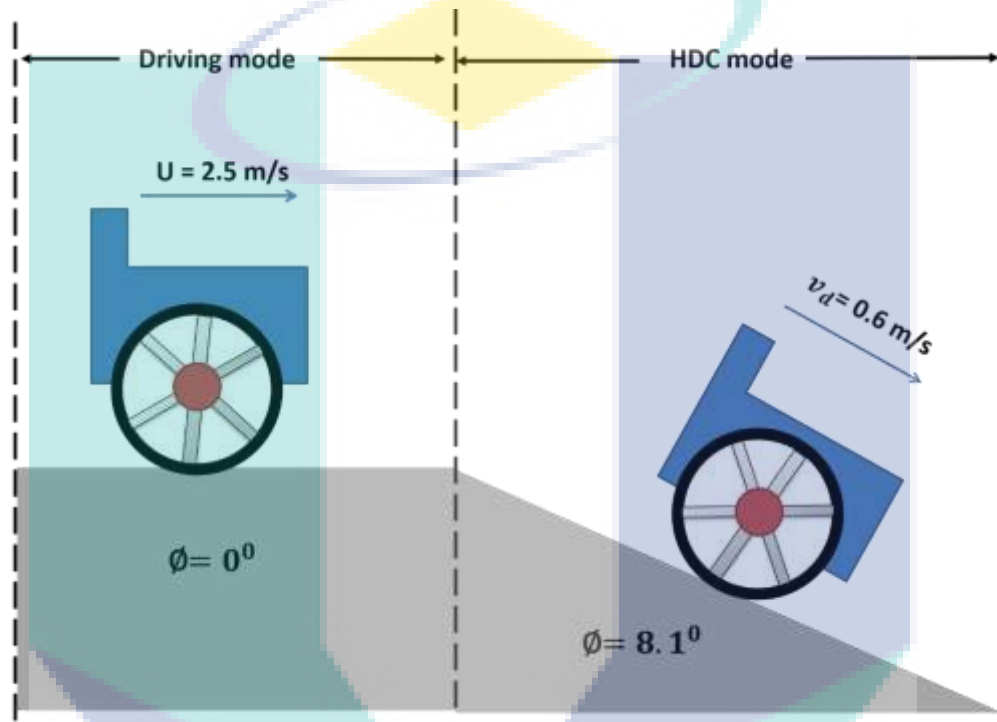


Figure 3.49 Plugging control simulation illustration

UMP

CHAPTER 4

RESULTS AND DISCUSSION

4.1 Introduction

This chapter discussed the results obtained from the experimental and simulation works that had been conducted phase by phase. For the first phase, the discussion is suggestive to the dynamic behavior of the EPW when different electrical braking systems are applied on sloped surfaces. Next, in the second phase, the development of active braking control system in real time is shown which proved that the Hill Descent Control integrated with plugging braking can control the speed of EPW during descents on slopes automatically. In the third phase, the result of parameters estimation by using fitting curve and model validation are discussed in detail. Lastly, the results of the active braking system constructed in simulation is presented well in the last section.

4.2 Analysis of EPW dynamic behaviour using different electrical braking

4.2.1 Regenerative braking analysis

Regenerative braking is a braking system using regenerative voltage (back EMF) that opposes the voltage supply. The condition for regenerative occurs when the regenerative voltage (back EMF) is higher than the terminal voltage (supply). However, the braking performance for the regenerative braking was not conducted in this research because of several reasons that had been discussed in the previous section. Nonetheless, the voltage generation (back EMF) was analyzed to investigate the regenerative braking effective region during free rolling in sloped surfaces.

First, the experiment was conducted at the slope ($\theta = 8.1^\circ$) which is more than the requirement provided by Malaysia Standard (MS). The purpose of choosing a higher

slope is to prove that regenerative braking is not suitable to be applied as primary braking for Electric Powered Wheelchair (EPW) even in a higher slope. Figure 4.1 shows the travelled distance of EPW when free rolling during descent on sloped surfaces. From the plotted data, it can be observed that the distance travelled by the EPW is steadily increasing over time until 5.4m distance of slope. This happens because there is no braking applied during descent on the sloped surface. As a result, the EPW kept moving. The recorded time taken for EPW to reach 5.4 m of slope length is 3.6s.

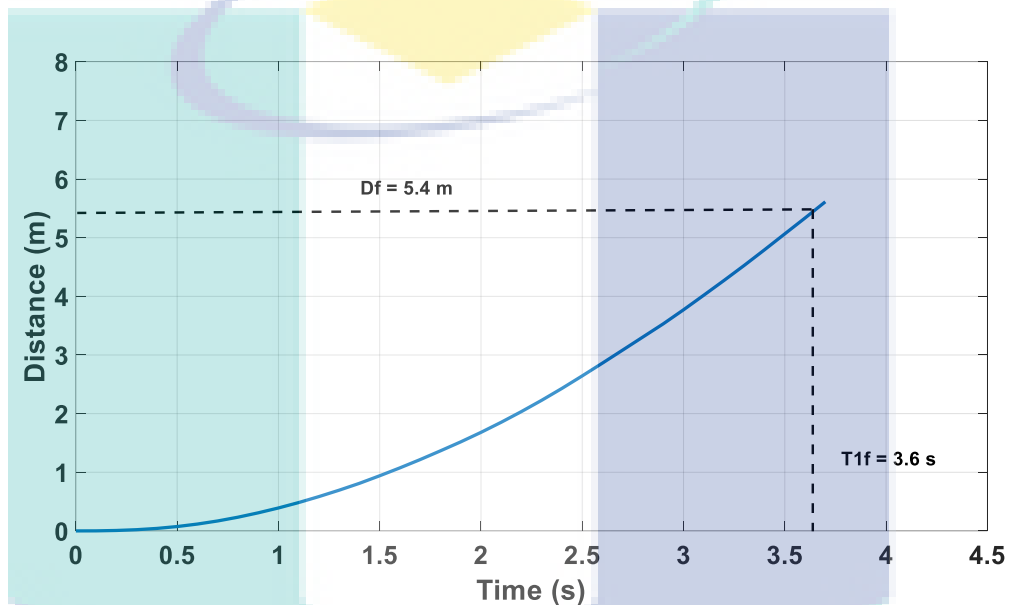


Figure 4.1 Distance travel for free rolling analysis

Figure 4.2 shows the speed of the EPW when released from the top of a dry mosaic sloped surface. The blue line is represented as the speed of EPW. The red and green line is indicated as the speed for right and left tire respectively. From the plot, it shows that the speed of the tire and EPW gradually increased in the same pattern which obeys the Newton's first law that a higher force subjected in an object will cause the body to accelerate fast. In this case, when the EPW is released from the top of the slope, the pulling gravitational force is as high as the angle of slope. Thus, this situation leads to the speed of EPW to increase quickly and accelerated fast. At 3.6s, the final speed of EPW, the right tire and left tire was recorded at 2.71 m/s, 2.73 m/s and 2.74 m/s. This situation also happened to people who suffers from a weak hand grip. The speed of EPW will keep increasing and it is dangerous for the EPW user because it can lead to serious injuries.

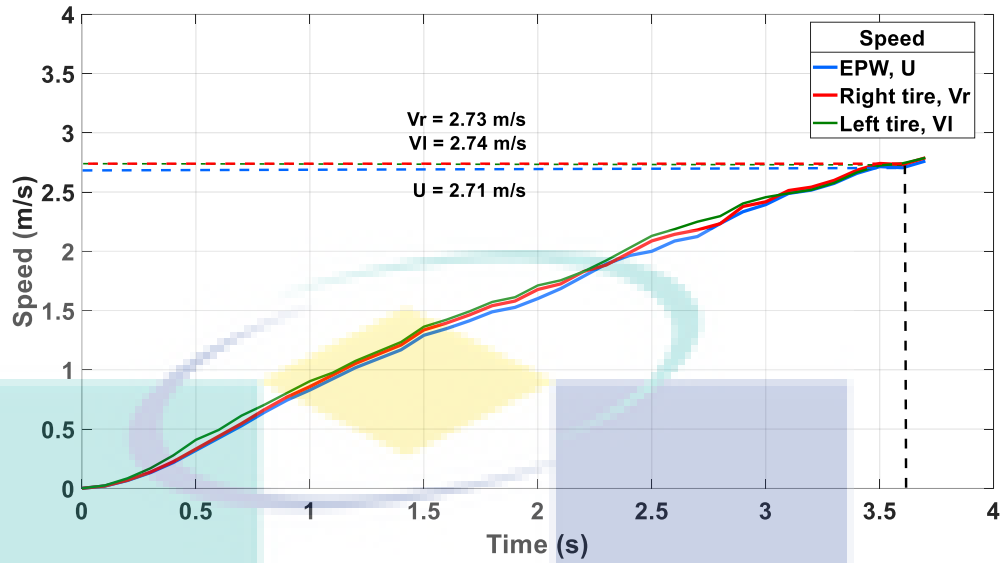


Figure 4.2 Speed of EPW and tire during free rolling at dry mosaic condition

Figure 4.3 demonstrates the behaviour of the back EMF of a left and right electrical motors during free rolling descent on a slope. The purpose is to acquire the back EMF on the left and right tire in proving that the back EMF is not sufficient to perform regenerative braking.

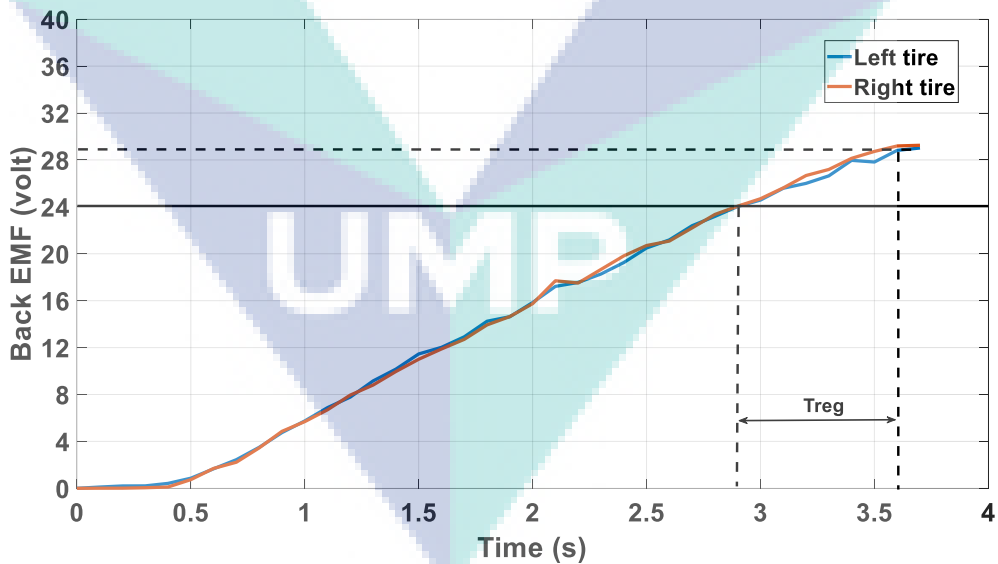


Figure 4.3 Back EMF generation of EPW during descending at slope on dry mosaic surface condition

As shown in Figure 4.3 above, the blue and red solid line indicate the left and right motor respectively. Both plots show the same pattern and almost the same values of back EMF. As noted, when the speed of EPW and tire are increased, the back EMF voltage will also keep increasing. This is because the voltage generation is directly proportional to the speed of tire as shown in equation 3.11. In this condition, the electric motors are operated as generators. At the time of 3.6s, the back EMF voltage generation was acquired as 28.8 V by using the voltage sensor.

As is the principle of regenerative braking, the regenerative braking will occur when the regenerative voltage (back EMF) is higher than the voltage supply or battery (Rakesh & Narasimham, 2012). Thus, to illustrate the regeneration regime state, the horizontal line at 24V is drawn along the graph to represent 24 V terminal supply. The purpose of these lines are to show the region of regenerative braking effectiveness.

Ideally, the terminal supply (battery) is assumed in full capacity. However, in the real situation, the capacity of battery may be dropped due to frequent use. Referring to Figure 4.3, the back EMF is generated and proportionally increased when the EPW moved in a descending order on the slope. Below the 24 V horizontal line, the regenerative braking does not occur. Hence, the regenerative braking occurs when the back EMF is more than the 24V horizontal line. As shown in the figure, the regenerative braking starts to be effective at 2.9 s. T_{reg} is noted as the effective duration of predicted regenerative braking to occur regionally. The recorded duration of effective regenerative braking to occur is 0.73 s as shown in Table 4.1.

Table 4.1 The effective of regenerative braking to be occurred

	Output
Terminal supply (volt)	24
Minimum speed for voltage generated (m/s)	2.4
Duration effectiveness of regenerative braking (s)	0.73

From the plotted graph of regeneration voltage, it can be identified that the regeneration of voltage (back EMF) depends on the rotation speed of tire. A higher rotational speed of tire will produce a higher back EMF. In conclusion, from the analysis

that has been conducted, it is proved that regenerative braking is not suitable to be applied as a braking system in low speed transportations especially the Electric Powered Wheelchair (EPW) due to lack of effectiveness in the regeneration of voltage duration.

4.2.2 Dynamic braking analysis

i. Distance travel

Figure 4.4 shows the three plots of travel distance for EPW when dynamic braking is applied during descent on slopes at different initial braking speed. As shown in the figure, the overall plots of distance travelled exceed 5.4m of the slope length. The blue plot is indicated as the travel distance of EPW when the braking is applied initially at 0 m/s. At a distance of 5.4 m, the time was recorded as 27.6s. Next, the shown red plot is indicated as travel distance of EPW when dynamic braking is applied at the speed of 1m/s. From the plot, it shows that the duration of EPW to reach 5.4m was recorded at 21.2s respectively. Lastly, the green plot indicates the dynamic braking applied at an initial speed of 2.5m/s. In this braking speed condition, the time taken for EPW to reach 5.4m slope is shorter than others which is 18.4s.

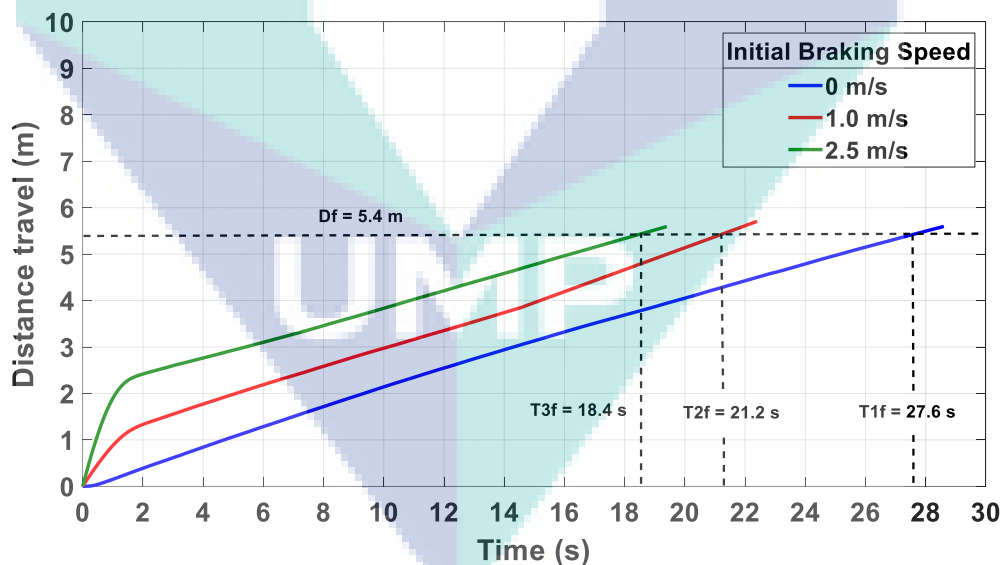


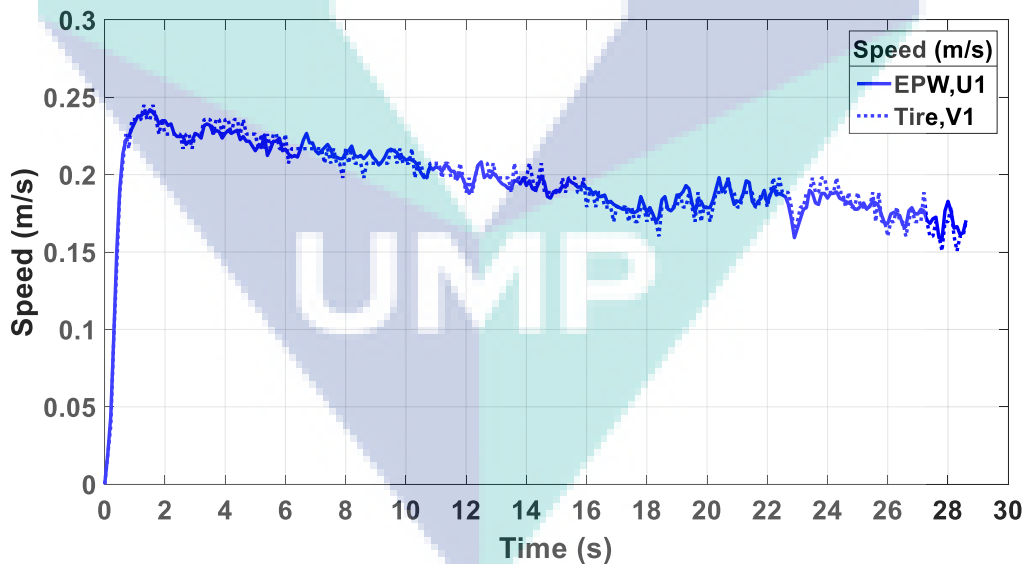
Figure 4.4 Distance travel at different initial braking speed.

The difference of travel distance happened because of the effect of momentum during braking at different speed. A higher braking speed will cause higher momentum and take a shorter time to reach the 5.4m slope. From the shown figure of travel distance, although braking had been applied, the EPW was still travelling until it reached the 5.4m

of slope length. This is because, the gravitational torque, T_g is higher than the braking torque, T_b which forced the EPW to keep descending on the slope.

ii. *Speed of EPW and tire analysis*

Figure 4.5 (a) shows the speed of EPW and its tires when dynamic braking is applied at an initial braking speed of 0m/s. As it goes down the slope, the pattern of EPW and the tires' speed are almost the same. Besides that, both of the speed is slightly reduced by time. This happened because of the braking torque produced from the dynamic braking operation of the electrical motor. As mentioned in equation 2.3, the braking torque produced by electrical braking depends on the speed, ω of the tire that corresponded to the current, i_{emf} . Since the speed of EPW is reduced, the braking torque produced from dynamic braking is also reduced. Thus, the EPW is still descending on the slope because the gravitational torque, T_g that pulls the EPW down is higher than the braking torque, T_b produced by dynamic braking. In other words, the internal resistance inside the motor is a small value in which a low current has been resisted and caused lower produced braking torque as mentioned in equation 2.5.

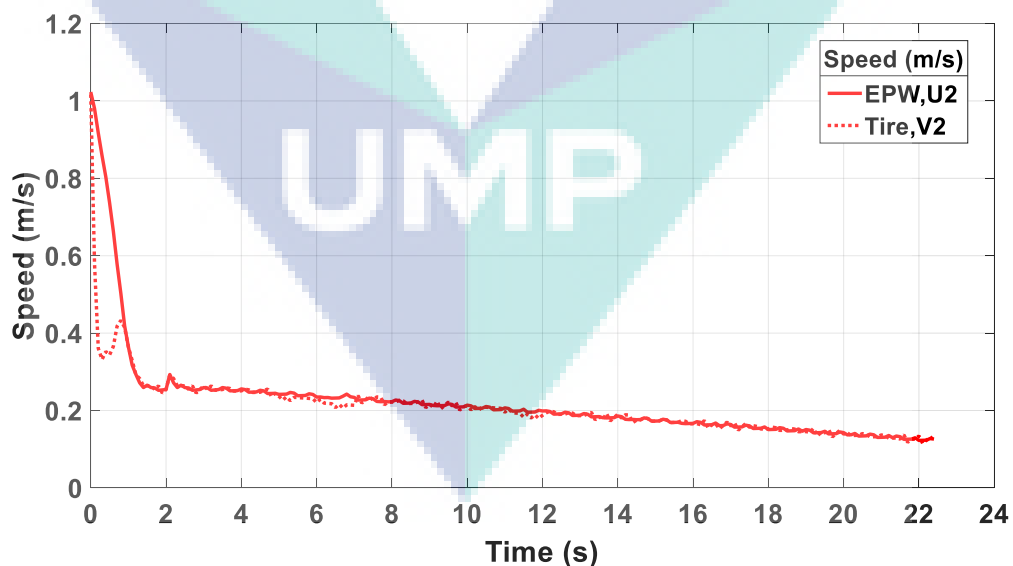


(a)

Figure 4.5 (b) and (c) show the speed of EPW and its tires when dynamic braking is applied at different initial braking speed which are 1m/s (red) and 2m/s (green). The red and green dotted lines are indicated as EPW speed for the initial braking at the speed

of 1m/s and 2.5m/s respectively. Meanwhile, the red and green solid lines are represented as speed of the tires when braking at the initial speed of 1m/s and 2.5m/s correspondently. In general, both patterns of speed behaviours of EPW are the same. As shown in the speed of tire when braking at 1m/s and 2.5m/s, the speed is quickly decreased when the dynamic braking is applied. However, the speed of tire for the green line decreased more than the red line. As discussed before, this is because the braking torque, T_b that was applied depended on the rotational speed of tire that corresponded to the current resisted by resistance.

Because of the difference of braking torque generated, the speed of EPW for both of the initial braking speeds also show a difference in deceleration. The speed of EPW for braking at 1 m/s (red) and 2 m/s (green) decelerated in 1.63s and 1.72s respectively. After a while, both plots show the pattern of EPW and the tires' speed are almost the same as it goes down the slope and both of the speed are slightly reduced by time. This happens because the braking torque that is produced from the dynamic braking operation of the electrical motor depends on the speed of tire. Since the speed of EPW is reduced, the braking torque that is produced from dynamic braking is also reduced. Thus, the EPW is still descending on the slope because the gravitational torque, T_g that pulls the EPW down is higher than the braking torque, T_b produced by dynamic braking.



(b)

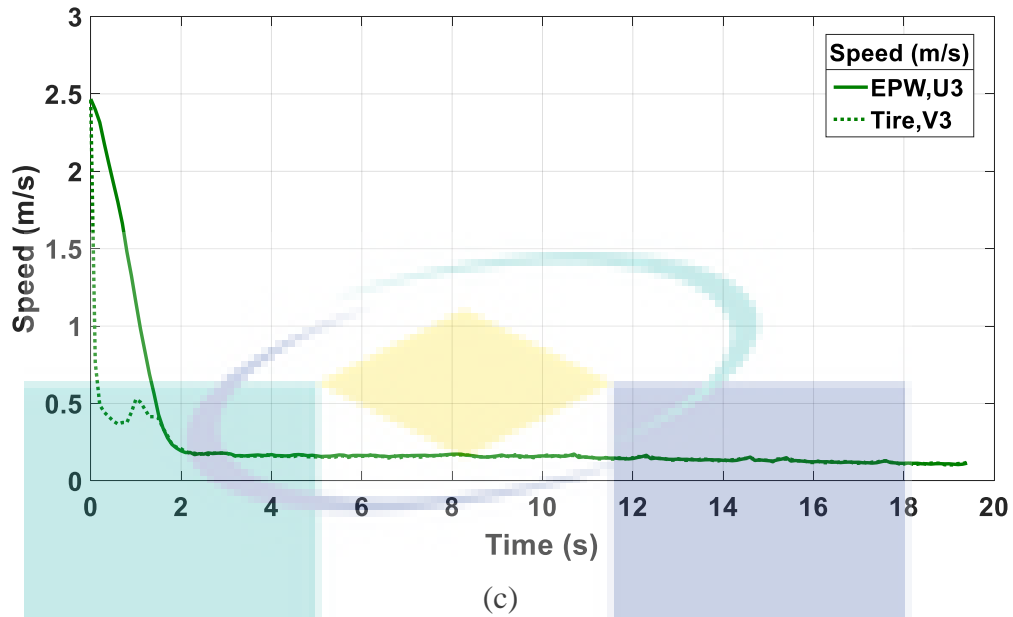


Figure 4.5 Speed of tire and EPW during dynamic braking at different initial braking speed: (a) 0 m/s (b) 1 m/s (c) 2.5 m/s.

iii. Slip ratio analysis

Slip ratio that is plotted in Figure 4.6 (a) and (b) is used to identify the slip behaviour speed of the tire and EPW. The blue, red, and green plots indicate the slip ratio during braking at 0 m/s, 1 m/s and 2.5 m/s respectively. The solid blue plot recorded the lowest slip at average below the optimal dynamic slip ratio (0.2). This happens because the braking torque produced from the dynamic braking during braking at an initial speed of 0 m/s is lower. Thus, slipping of the tire does not happen when braking at 0 m/s.

Meanwhile, when dynamic braking is applied at 1m/s, the slip ratio which is indicated as a solid red plot shows that the tire is almost locking when braking is applied on a sloped surface. As shown in Figure 4.6 (b), the slipping duration is recorded as 0.72s. This shows that the torque braking produced by dynamic braking in this condition is higher than when braking at an initial speed of 0 m/s.

Next, the solid green plot shows the slip ratio when braking at 2.5 m/s. This is the highest slip that is recorded compared to the other slip ratios. This slip ratio exceeds the optimal dynamic slip ratio (0.2). The slip duration is recorded as 1.4 s. This happens

because the braking torque produced from the dynamic braking during braking at an initial speed of 2.5 m/s is higher and caused the tire to be quickly reduced.

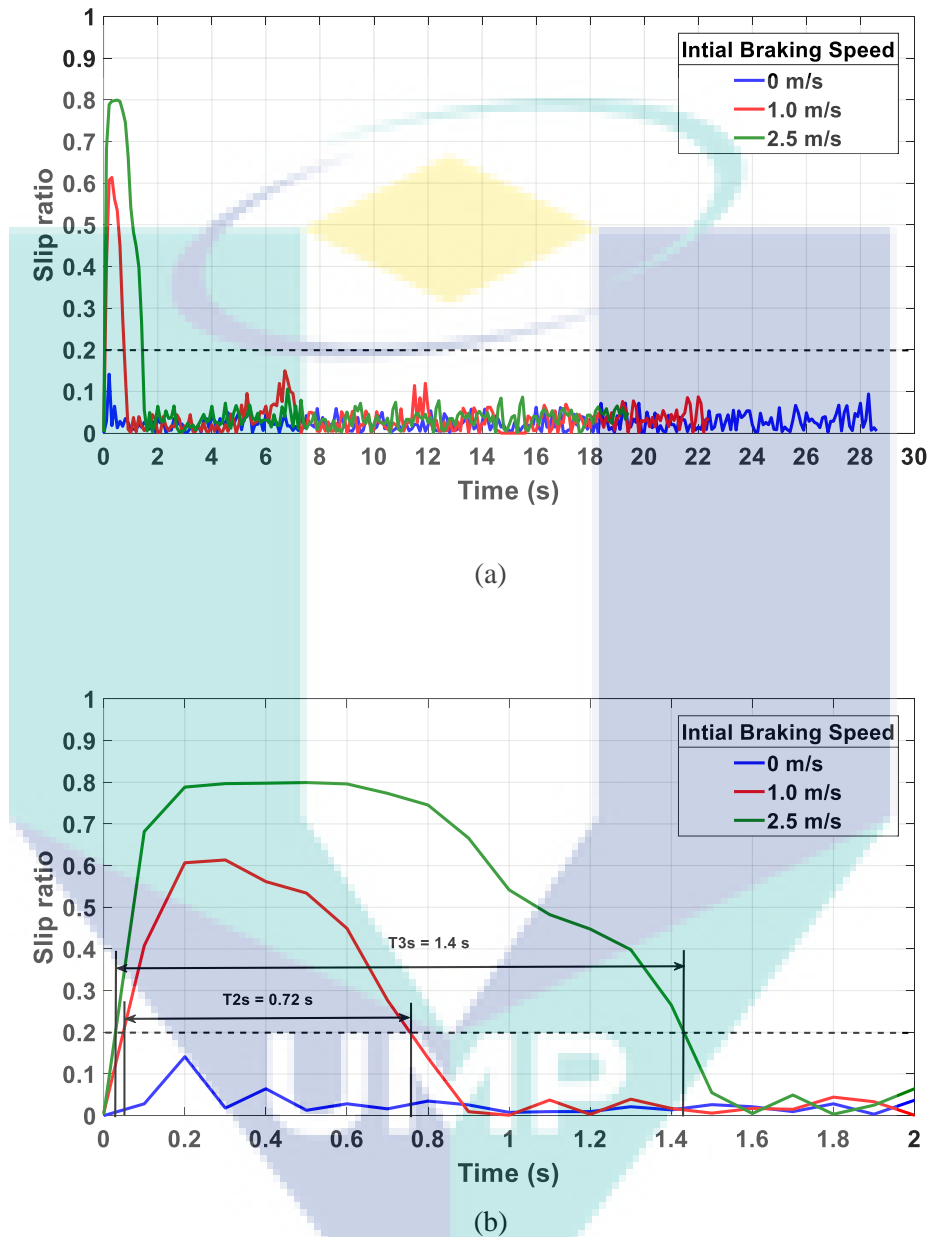


Figure 4.6 (a) Slip ratio during dynamic braking at initial different initial braking speed (b) scale up slip ratio

In general brief, the braking torque is produced when the current that is carried by back EMF is resisted to the internal resistance in motor coils by shortening the positive and negative terminal. From the dynamic braking results, it can be observed that the braking effect is dependent on the initial rotational speed of tire during braking. For an

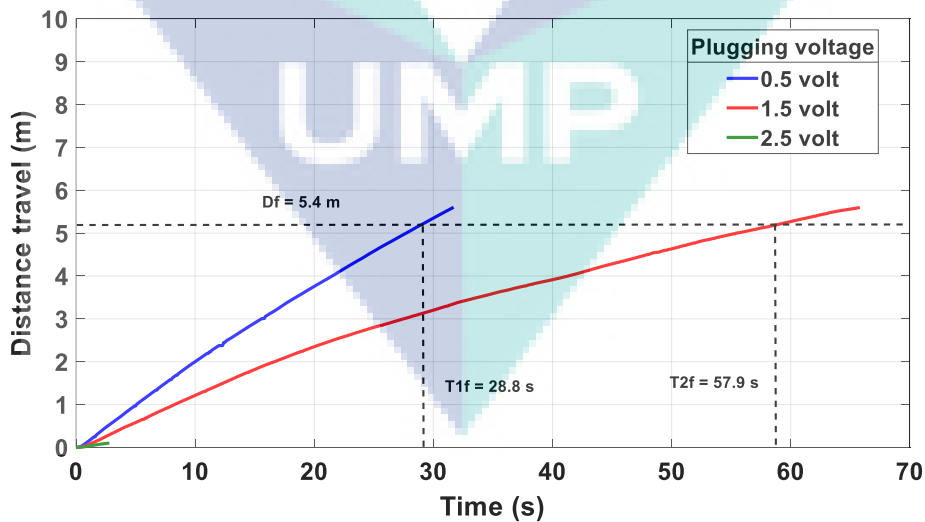
example, in a situation when the dynamic braking is applied at an initial speed of 2.5 m/s, the braking torque is higher because the flow of current to be resisted is higher. This is because the braking torque is directly proportional to the rotational speed of motor. From the results, it is clearly shown that the dynamic braking can be considered to be applied as the braking mechanism in the EPW. However, this braking type is not suitable to be used as the primary braking since the braking effect depends on the speed of tire. In overall analysis, the EPW still moved even when the dynamic braking is applied.

4.2.3 Plugging braking analysis

Braking at initial speed 0 m/s

i. Distance travel at different plugging voltage

Figure 4.7 (a) and (b) show the travelled distance of EPW when different plugging voltage is applied during descent on a sloped surface. The blue, red and green lines in the graph indicate the EPW travelled distance when the plugging brake is 0.5 V, 1.5 V and 2.5 V, respectively. It can be seen that the travelled distance for 0.5 V and 1.5 V is greater than the set distance, which is 5.4 m. However, the EPW only took 0.1 m to stop when the 2.5 V plugging brake is applied. From this result, it can be understood that a high plugging voltage is needed to stop the EPW quickly.



(a)

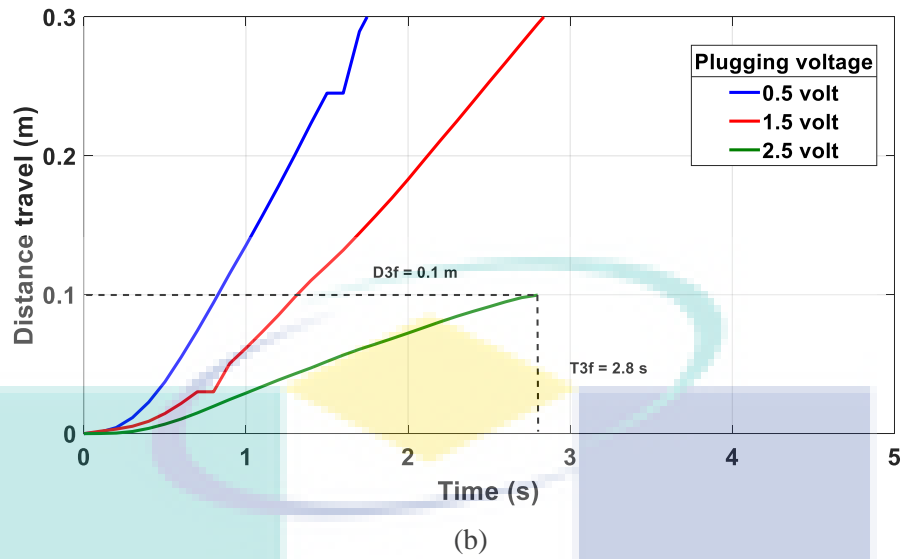


Figure 4.7 Distance travel for different plugging braking at initial speed 0 m/s

ii. Speed of EPW and tire

Figure 4.8 shows the speed of tire and EPW when the 0.5 V, 1.5 V and 2.5 V plugging voltage was applied at the initial speed of 0 m/s. The solid line indicates the speed of EPW, while the dashed line indicates the rotational speed of the tire. Each color represents the difference plugging voltage, such as blue for 0.5 V, red for 1.5 V and green for 2.5 V.

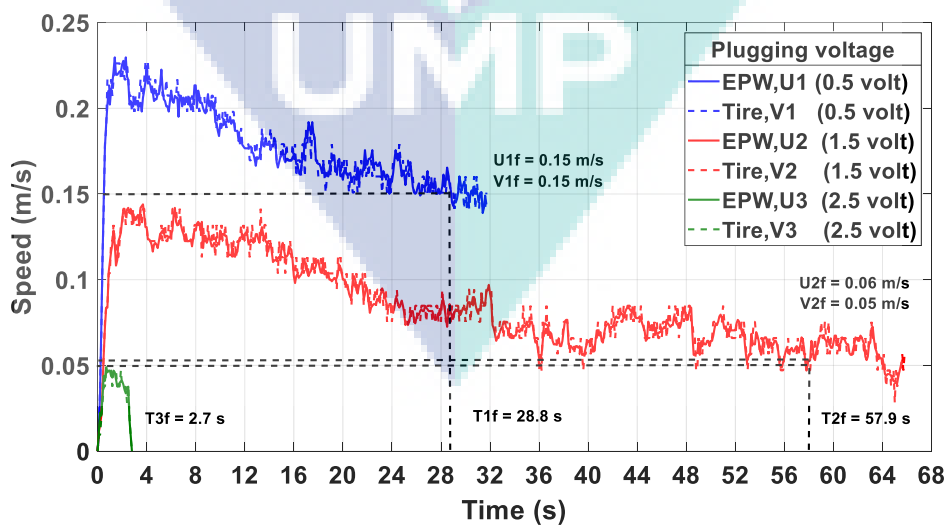


Figure 4.8 Speed of EPW and tire braking at different plugging voltage

From the figure above, the speed of EPW and tire for each plugging brake decrease gradually. There is no tire lock-up, and it can be said that the EPW was braking smoothly. For the 0.5 V, the time for EPW to reach 5.4 m is 28.8 s, while the time for 1.5V to reach 5.4 m is 57.9 s. Based on equation 3.14, the time taken for EPW to decelerate for 1.5 V is greater than 0.5 V, due to the summation of torque at the wheel for 1.5 V being lower than 0.5 V. Although the torque braking for 1.5 V is greater than 0.5 V, the gravitational torque, T_g is still larger than the torque braking. Consequently, the tire is still rotating while descending on the slope. In contrast, the 2.5 V plugging brake only took 2.7 s to stop due to the larger braking torque produced compared to the gravitational torque.

iii. *Slip ratio analysis*

The analysis of slip ratio is to determine the speed behaviours between the tires and EPW. The EPW can be defined in slip condition when the slip ratio is more than the optimal value which is 0.2. Figure 4.9 below shows the slip ratio plots when different plugging braking or reverse voltage is applied to the electric motor. The blue, red and green plots are indicated as plugging voltage 0.5 V, 1.5 V and 2.5 V respectively. Generally, the overall plots show that the slip ratio values fluctuate under the optimal slip ratio value. It can be observed that when the EPW descends on the slope at the initial speed of 0m/s, the tire did not slip even when a higher plugging voltage is given.

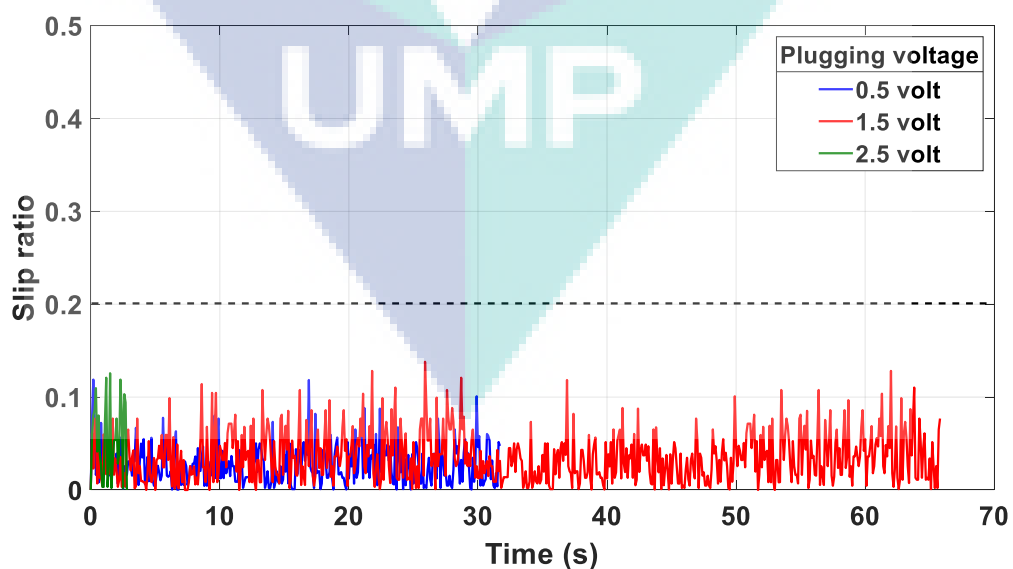
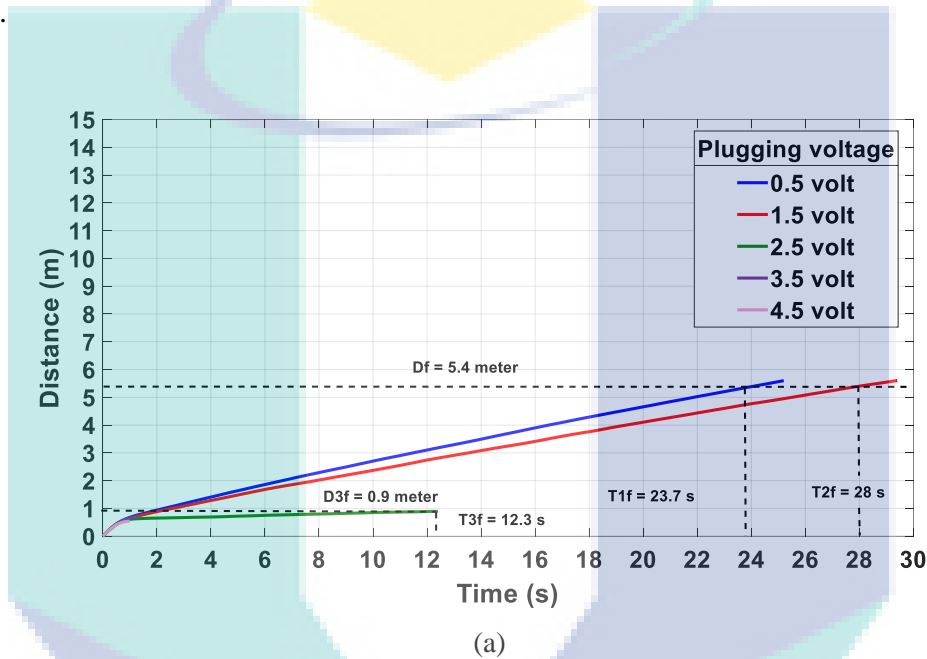


Figure 4.9 Slip ratio for different applied plugging voltage at initial speed 0 m/s

Braking at initial speed 1 m/s

i. Distance travel

Figure 4.10 (a) and (b) show the travelled distance of EPW when plugging braking is applied with various reverse voltages during descent on the slope at 1m/s initial braking speed. The blue, red, green, purple and pink plot indicate the travelled distance of EPW when the 0.5 V, 1.5 V, 2.5 V, 3.5 V and 4.5 V plugging brake are applied on the electric motor.



In Figure 4.10 (a), the 0.5 V and 1.5 V plugging braking plots show the distance travelled by EPW is more than the maximum length of slope (5.4 m) set by the ADA regulation. It shows the time taken for 0.5 V and 1.5 V to reach 5.4 m was recorded at 23.7 s and 28 s respectively. In contrast, the travelled distance for 2.5 V, 3.5 V and 4.5 V plugging voltage are recorded to be less than the ADA slope length requirement as shown in Figure 4.10 (b). When the 2.5 V plugging voltage is applied, the EPW stopped at 0.9m in 12.3 s. Next, the stopping time and distance for 3.5 V plugging voltage were recorded at 1.27 s and 0.68 m. By increasing the plugging voltage at 4.5 V, the travelled distance became shorter at 0.55 m in 1 s.

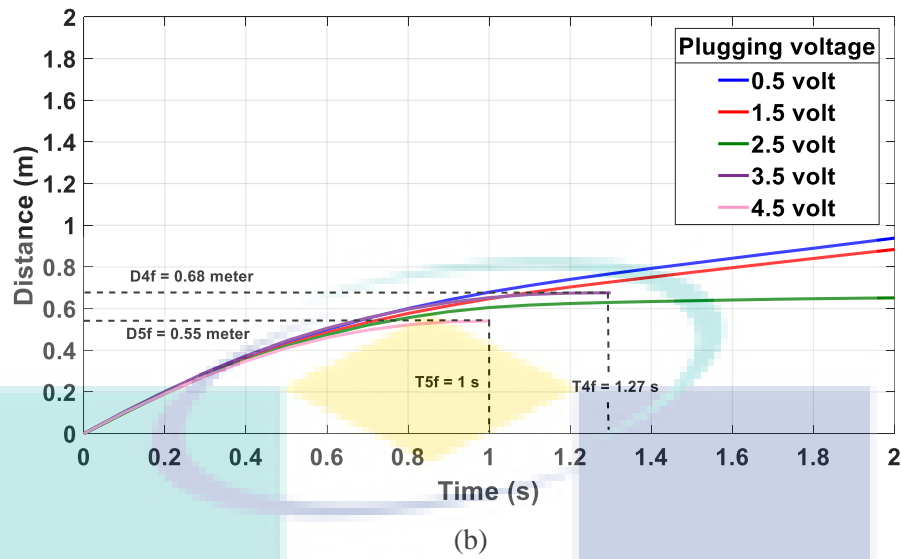
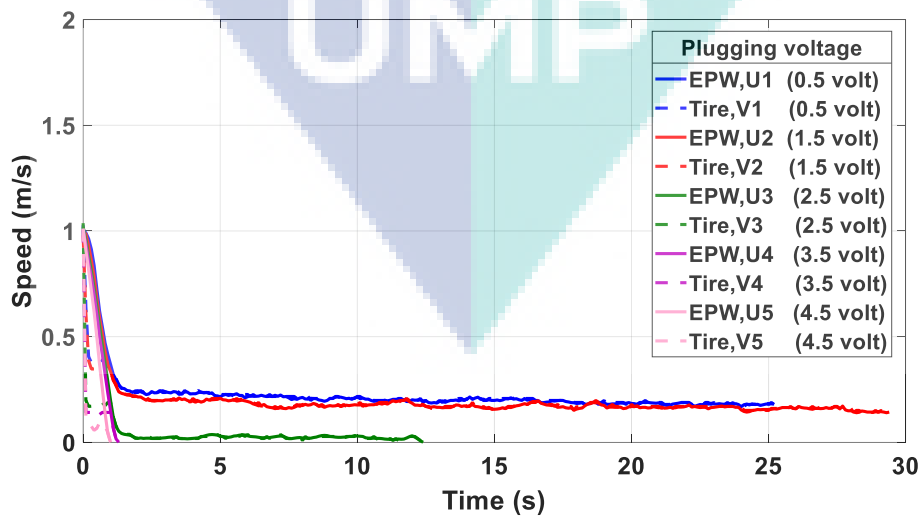


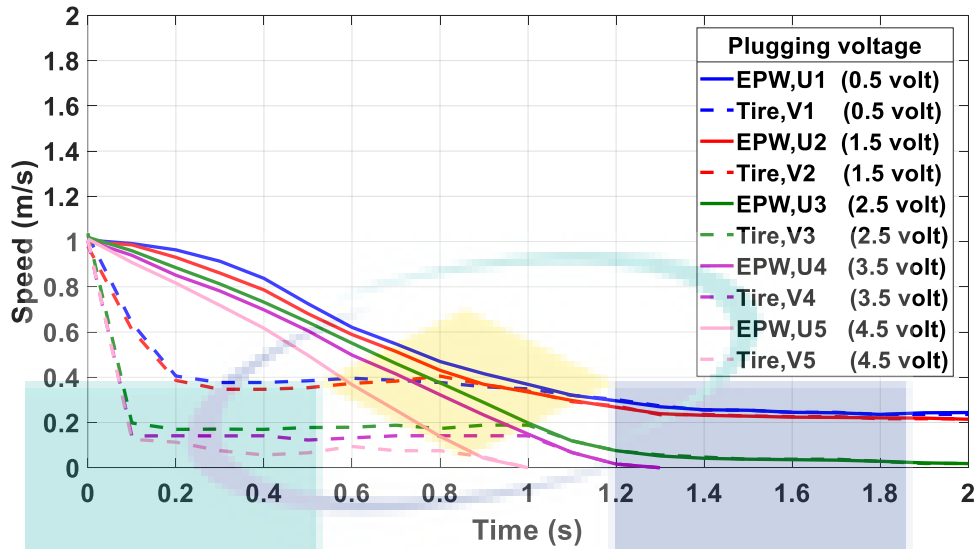
Figure 4.10 Distance travel for different applied plugging voltage at initial speed 1 m/s

ii. Speed of EPW and tire

Figure 4.11 (a) and (b) show the speed of tire and EPW when the plugging braking 0.5 V (blue), 1.5 V (red), 2.5 V (green), 3.5 V (purple) and 4.5 V (pink) were applied at an initial speed of 1 m/s. The solid and dashed line indicate the speed of EPW and tire respectively.



(a)



(b)

Figure 4.11 Speed of EPW and tire when different

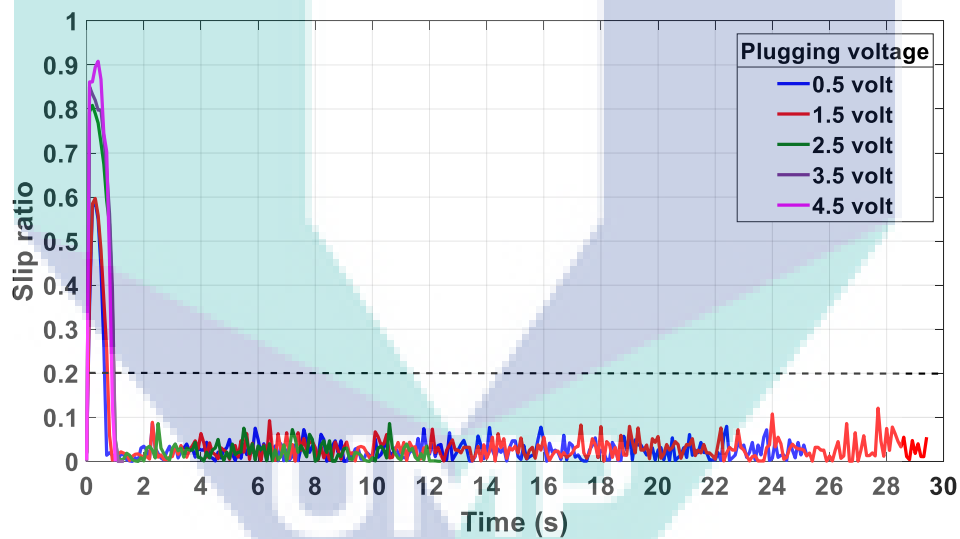
As shown in Figure 4.11 (a), when the plugging braking was applied at 0.5 V, the speed of the tire decreased rapidly from 1 m/s to 0.4 m/s in 0.2 s. Then, the speed of the tire slightly decreased but still moved from 0.4 m/s to 0.3 m/s in 23.5 s. Meanwhile, when the speed of EPW is decreased gradually from 1 m/s to 0.32 m/s in 1.1 s, it slightly decreased similarly to the tire in 23.5 s. Next, when 1.5 V plugging braking was applied at the initial braking speed of 1 m/s, the pattern of the speed of tire and EPW is almost the same as 0.5 V. The tire speed dropped from 1 m/s to 0.4 m/s in 0.2 s and then slowly decrease from 0.4 m/s to 0.2 m/s in 29 s.

Different from the 0.5 V and 1.5 V, the 2.5 V plugging braking caused the EPW to stop at the slope as shown by the green line. The tire speed quickly reduced from 1 m/s to 0.2 m/s in 0.1 s and then was at a constant at 0.2 m/s until 1 s. After that, the tire speed slowly reduced and stopped at 12.5 s. The EPW speed steadily decreased from 1 m/s to 0.1 m/s in 1.2 s. After a while, the speed is slightly decreased similar to the tire speed and also stopped at 12.5 s. By increasing the plugging voltage to 3.5 V and 4.5 V, the tire and EPW speed patterns are the same as 2.5 V, where the only difference is the time taken for EPW and tire to stop. The recorded stopping time for 3.5 V and 4.5 V at the initial braking speed of 1 m/s is 1.3 s and 1s respectively.

It can be understood that when a larger plugging braking is applied to the wheel, it will produce larger braking torque. As a result, the speed of tire will decrease abruptly and the EPW will be decelerated faster and take a shorter time to stop. However, at a lower plugging voltage of 0.5 V and 1.5 V, the EPW will decelerate at a certain time and then continue descending on the slope. This happens due to the existence of gravitational force that pulls the EPW downward on the slope.

iii. Slip ratio analysis

Figure 4.12 (a) and (b) show the tire slip behaviour when different plugging braking is applied to the electric motor at an initial braking speed of 1m/s. The blue, red, green, purple and pink indicate the slip ratio when 0.5 V, 1.5 V, 2.5 V, 3.5 V and 4.5 V plugging voltages are applied. The overall slip ratio results show the tire slipped when plugging braking has been applied for a while.



(a)

When the plugging voltage 0.5 V is applied, the slip duration becomes short at 0.59 s. The maximum recorded slip ratio is almost 0.6 at 0.3 s. As the plugging voltage is increased to 1.5 V, the duration of slip ratio becomes longer at 0.68 s. The recorded maximum slip ratio is almost 0.6 at 0.3s. Next, the duration and maximum slip for 2.5 V is recorded at 0.92 s and 0.8. The 3.5 V plugging voltage's longest duration slip is 0.93 s, and the maximum slip ratio of 0.85 was recorded. When a higher plugging braking at 4.5 V was applied, a higher maximum slip was recorded at 0.9. However, the duration of the slip is shorter than 2.5 V and 3.5 V, which is at 0.86 s.

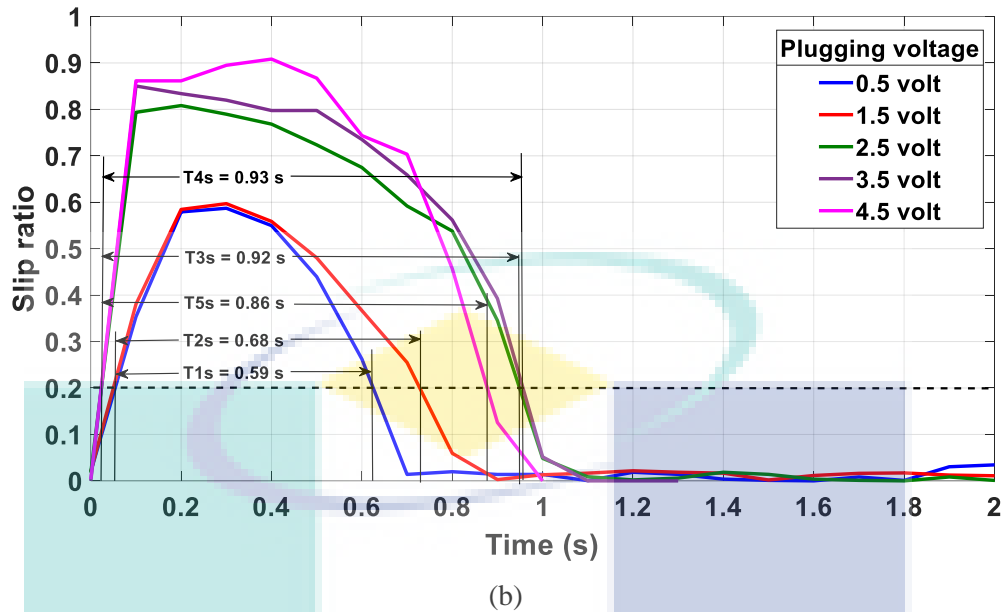
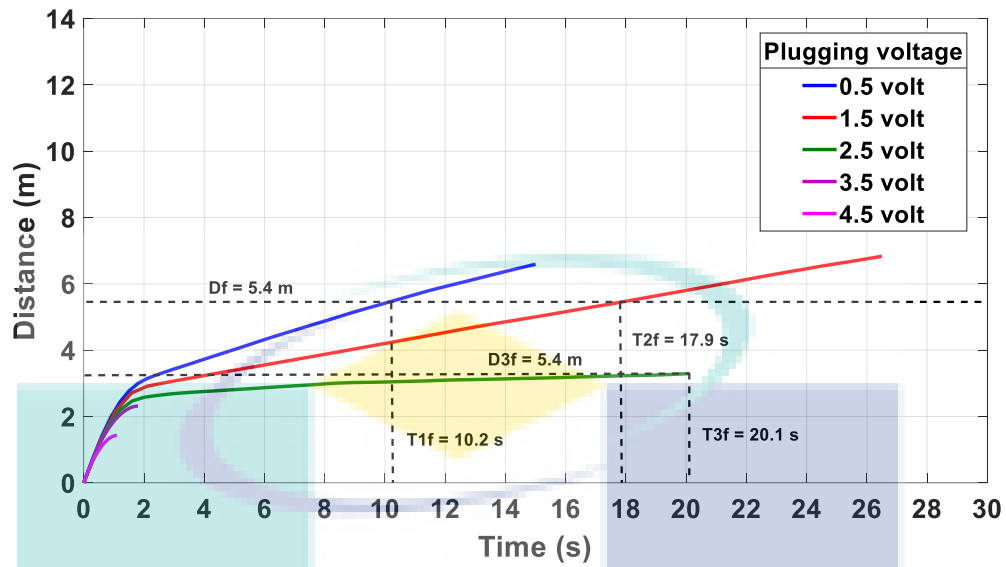


Figure 4.12 (a) Slip ratio for different plugging braking (b) zoom in for slip ratio

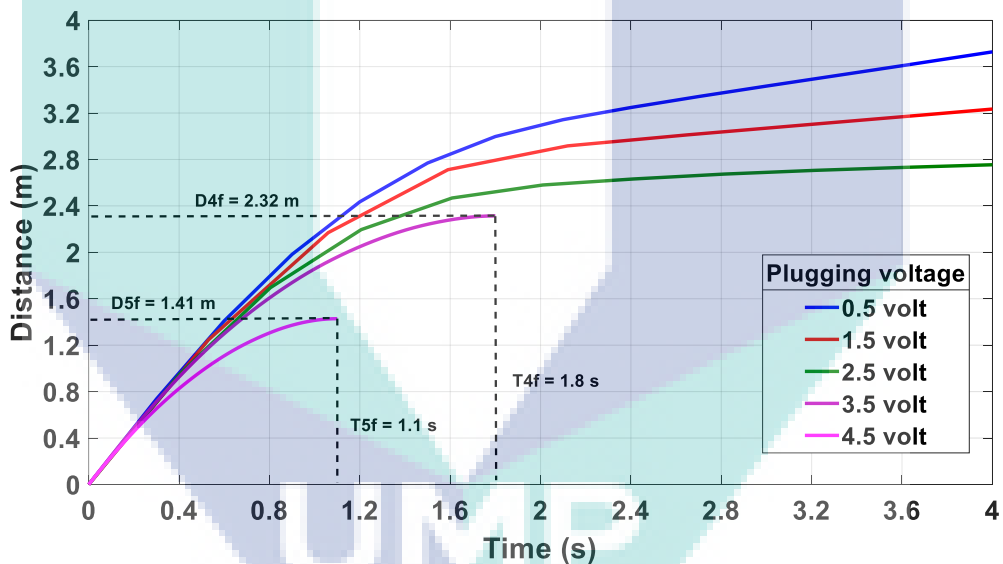
Braking at initial speed 2.5 m/s

i. Distance travel

Figure 4.13 (a) and (b) show the travelled distance of EPW when different plugging braking is applied during descent on a slope at 2.5 m/s initial braking speed. Five different plugging voltages are applied which are 0.5 V, 1.5 V, 2.5 V, 3.5 V and 4.5 V that are indicated as blue, red, green, purple and pink lines respectively. In Figure 4.13 (a), the 0.5 V and 1.5 V plugging braking plots show that the distance travelled by the EPW is more than the required length of slope (5.4 m) set by the SM-1184 regulation. Both scenarios show that the time taken for 0.5 V and 1.5 V to reach 5.4 m is recorded at 10.2 s and 17.9 s respectively. However, the travelled distance for 2.5 V, 3.5 V and 4.5 V plugging voltage are recorded less than the SM-1184 slope length requirement as shown in Figure 4.13 (b). When 2.5 V plugging voltage is applied, the EPW stopped at 3.2 m in 20.1 s. Next, the stopping time and distance for 3.5 V plugging voltage were recorded at 1.8 s and 2.32 m. By increasing the plugging voltage to 4.5 V, the travelled distance becomes shorter at 1.41 m in 1.1 s.



(a)



(b)

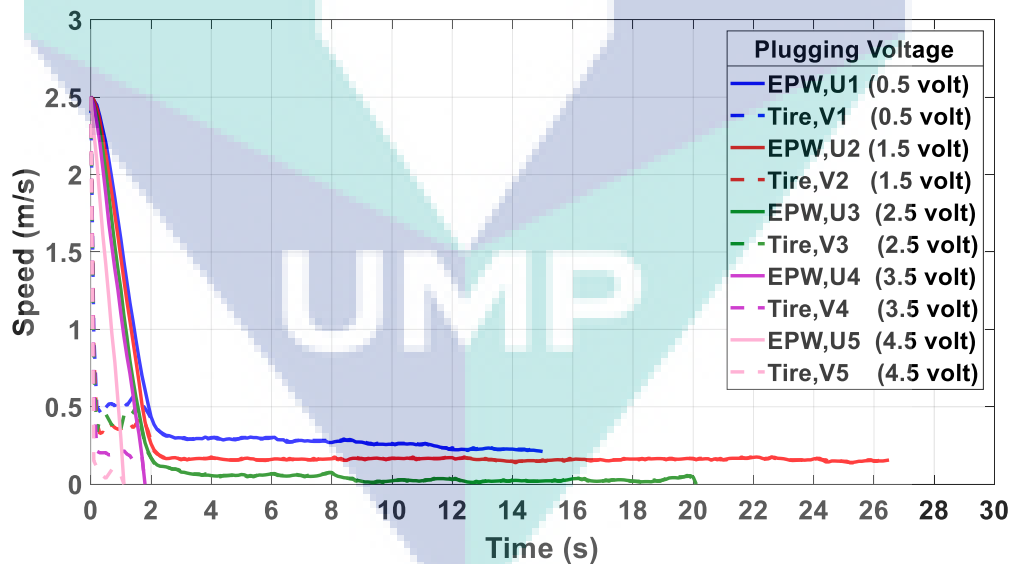
Figure 4.13 (a) Distance travel when different plugging is applied at initial speed 2.5 m/s (b) zoom in for distance travel.

From the travelled distance plot, it can be determined that the stopping distance of EPW will become shorter as the plugging voltage increases. When a lower plugging voltage is given to the electric motor such as 0.5 V and 1.5 V, the EPW will not stop before the required length of the slope.

ii. *Speed of EPW and tire*

Figure 4.14 (a) and (b) show the speed of tire and EPW when the plugging braking 0.5 V (blue lines), 1.5 V (red lines), 2.5 V (green lines), 3.5 V (purple lines) and 4.5 V (pink lines) are applied at the initial speed of 2 m/s. The solid and dashed line indicate the speed of EPW and tire respectively.

As shown in Figure 4.14 (a), when the plugging braking is applied at 0.5 V, the speed of the tire is rapidly decreased from 2 m/s to 0.5 m/s in 0.2 s. Then, the tire constantly rotated at a speed of 0.5 m/s in 1.8 s and decreased steadily from 0.5 m/s to 0.25 m/s in 13 s. Meanwhile, the speed of EPW decreased gradually from 2.5 m/s to 0.42 m/s in 2 s and slightly decreased similarly as the tire speed in 13 s. Next, when 1.5 V plugging braking is applied at the initial braking speed of 2.5 m/s, the pattern speed of tire and EPW is almost the same as 0.5 V. The tire speed is dropped from 2.5 m/s to 0.4 m/s in 0.2 s and decreased steadily from 0.4 m/s to 0.2 m/s in 29 s. The speed of EPW also decreased steadily from 2.5 m/s to 0.42 m/s in 2 s and then slightly decreased similar to the tire speed in 26.4 s.



(a)

Different than the 0.5 V and 1.5 V, the 2.5 V plugging braking EPW stopped at the slope as shown by the green line. The tire speed rapidly dropped from 2.5 m/s to 0.38 m/s in 0.2 s and then at a constant of 0.38 m/s in 1.6 s. Subsequently, the tire speed slowly reduced and stopped at 20.1 s. The EPW speed decreased steadily from 2.5 m/s to 0.57 m/s in 1.55 s. After a while, the speed slightly decreased similar to the tire speed and also stopped at 20.1 s. By increasing the plugging voltage to 3.5 V and 4.5 V, the tire and EPW immediately stopped. The recorded stopping time for 3.5 V and 4.5 V at the initial braking speed of 2.5 m/s is 1.8 s and 1.1 s respectively.

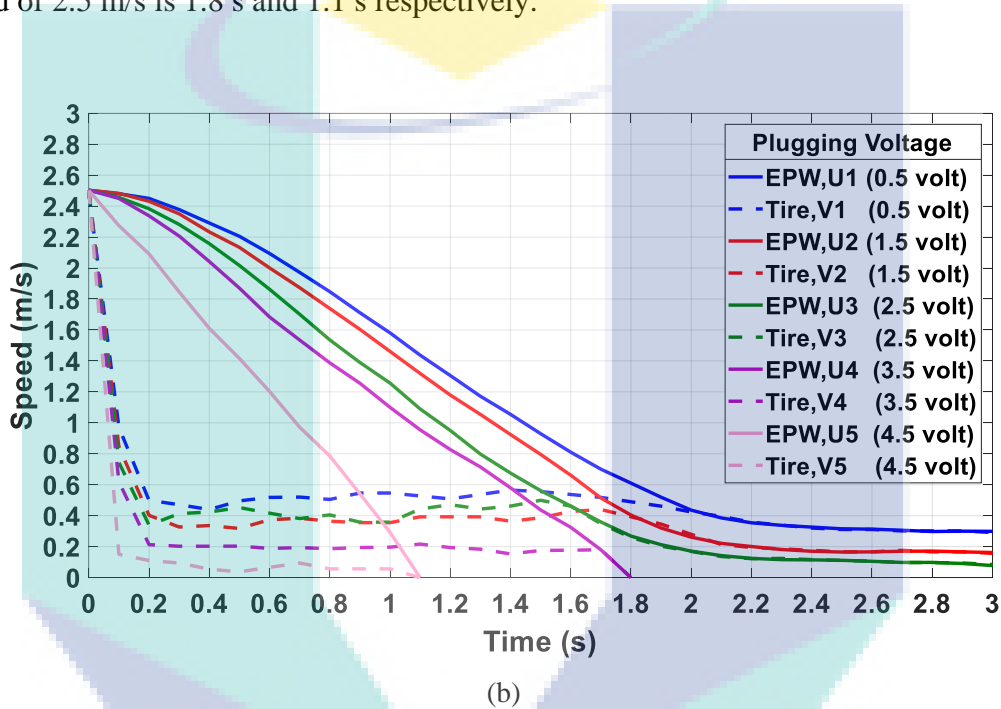
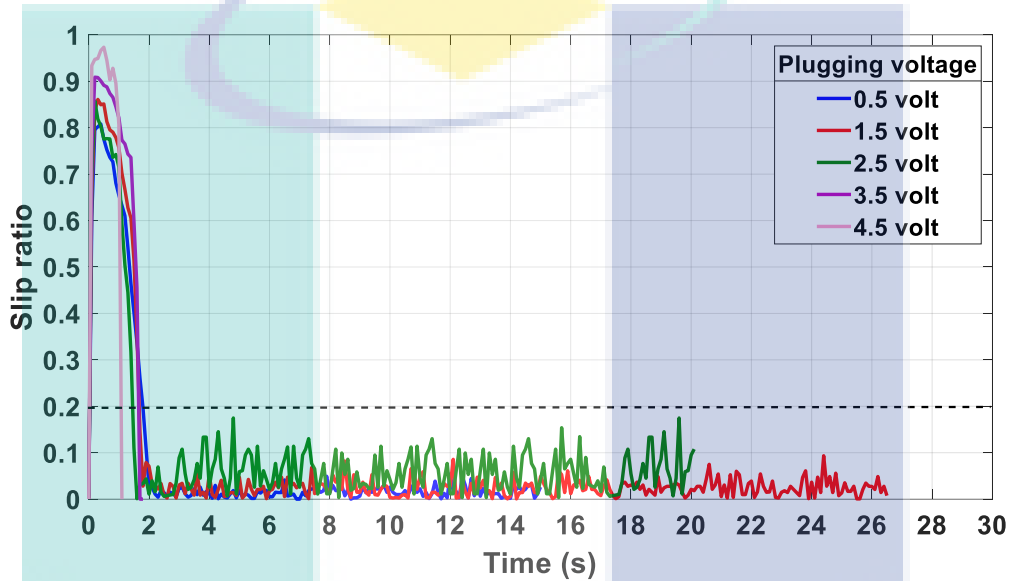


Figure 4.14 (a) Speed of EPW and tire during plugging voltage is applied at speed 2.5 m/s. (b) zoom for speed of EPW and tire.

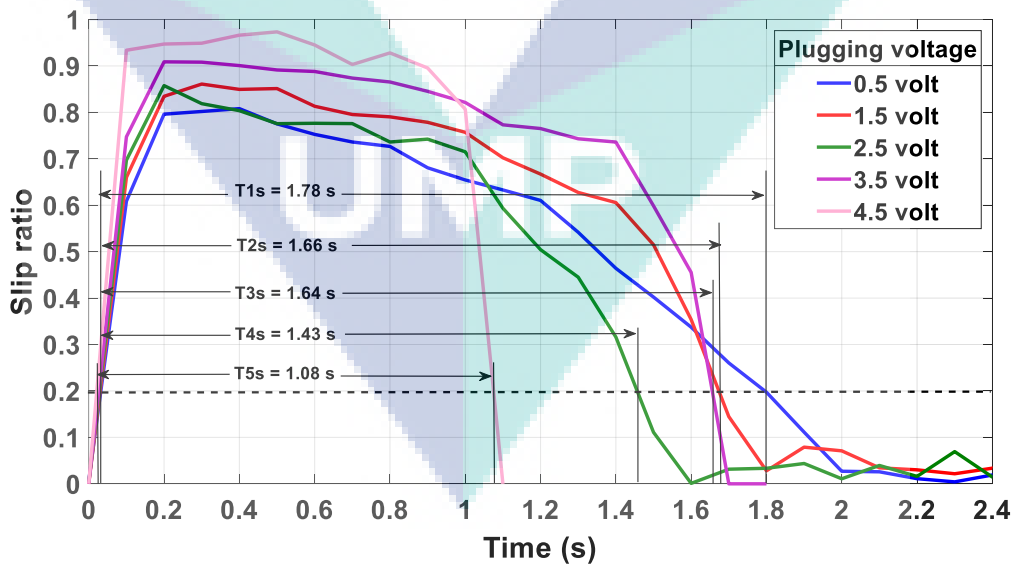
From these plugging braking analysis, it can be concluded that when a higher reverse voltage or plugging braking is applied to the electric motor, it will produce a larger braking torque. In consequence, the speed of the tire will decrease abruptly and the EPW will decelerate faster and stop quicker. However, at a certain lower plugging voltage such as 0.5 V and 1.5 V, the EPW will decelerate at a certain time and then continue descending on the slope. This happens due to the existence of gravitational force that pulls the EPW on the downward slope.

iii. Slip ratio analysis

Figure 4.15 (a) and (b) show the tire slip behaviour when different plugging braking is applied at the initial braking speed of 2.5 m/s. The blue, red, green, purple and pink represent the slip ratio when 0.5 V, 1.5 V, 2.5 V, 3.5 V and 4.5 V plugging voltage are applied. The overall slip ratio results show that the tire slips when plugging braking is applied for a while.



(a)



(b)

Figure 4.15 Slip ratio analysis when different plugging braking are applied

When the plugging voltage of 0.5 V is applied, the maximum recorded slip ratio is lower than the others which is 0.8 at 0.4 s. However, the time taken for the slip duration is longer at 1.78 s. As the plugging voltage is increased to 1.5 V, the duration of slip ratio becomes 1.66 s. The recorded maximum slip ratio is almost 0.8 at 0.3 s. Next, the duration and maximum slip for 2.5 V is recorded at 1.43 s and 0.83. The 3.5 V plugging voltage has the longest duration slip at 0.93 s, and the maximum slip ratio 0.85 is recorded. When a higher plugging braking which is 4.5 V is applied, the highest maximum slip is recorded at 0.9 which almost resulted in a tire lock. The duration of slip is shorter than other plugging braking which is at 1.08 s.

In general, from the analysis of braking by using plugging, this braking type is a versatile electrical braking because it can give different braking torque when the reverse voltage is changed. A higher reverse voltage will produce higher braking torque. For example, from the data of speed observed during braking at the initial speed of 0m/s, the EPW is still moving when the lower reverse voltage is applied. The EPW immediately stops when the plugging voltage is increased up to 3.5 V. The various plugging voltage also causes various slip ratio during descent on the slope. It can be determined when the plugging braking is applied at the initial speed of 2.5 m/s, the slip ratio duration is longer when the reverse voltage is increased. In conclusion, this type of braking is suitable to be used as a braking system in the EPW. Moreover, various voltage from plugging give the advantage in control work to control the speed of EPW during descent on sloped surfaces.

4.3 Real time control for EPW during descending on slope using plugging braking technique

The purpose of this plugging braking control system is to maintain the speed of EPW during descent on sloped surfaces at a certain desired speed. Figure 4.16 shows the travelled distance when the plugging control is applied during descent on a sloped surface at the initial speed of 0 m/s. The travelled distance exceeded the length of the slope set by SM-1184 when using plugging voltage control. The duration for EPW to reach 5.4 m was recorded at 9.5 s.

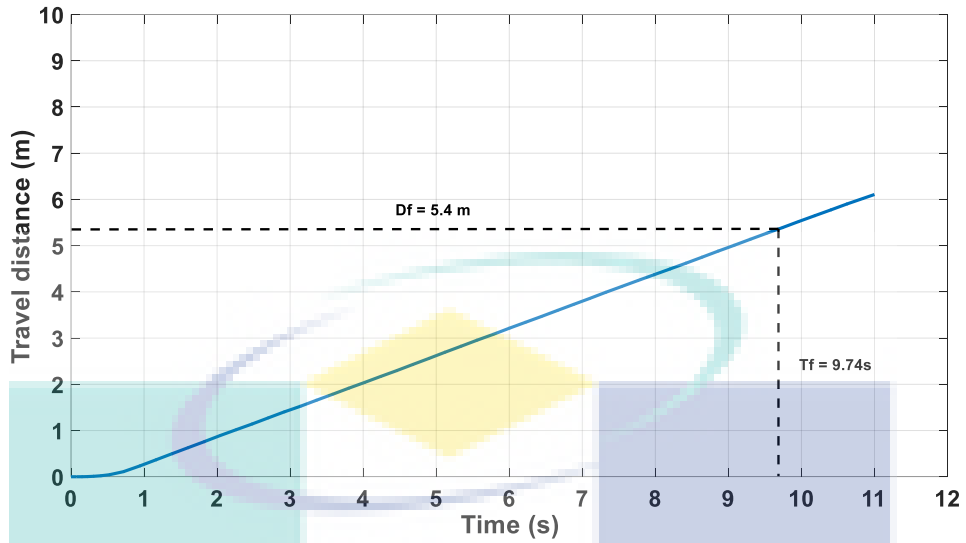


Figure 4.16 Distance travel by using plugging voltage control at initial speed 0m/s

Figure 4.17 shows the speed of tires and EPW when the plugging control is applied on a sloped surface. As shown in the figure, the blue dashed line represents the desired speed that can be set by the user. In this experiment, the speed is set at 0.6 m/s for safety reasons. The solid red, yellow and purple lines represent the speed of the EPW, right tire and left tire respectively.

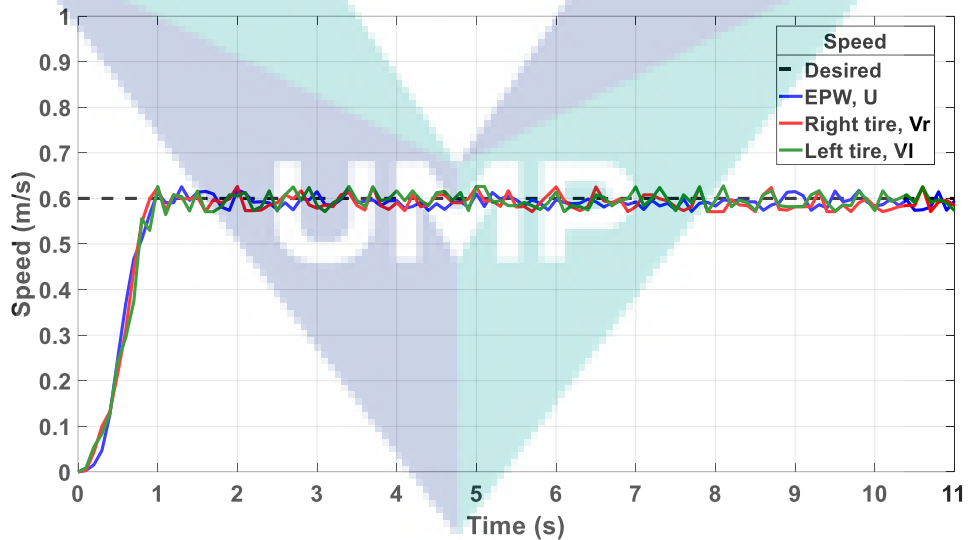


Figure 4.17 Speed of EPW and tire using plugging voltage control at initial speed 0m/s

The speed of tire and EPW increased from 0 m/s to 0.6 m/s in 1s when the EPW is released from the top of the slope. At 0.9 s, the plugging control is activated, and the speed is maintained and fluctuated at 0.6 m/s when descending along the slope. From this graph, it can be understood that the speed of tire and EPW can be maintained at a desired speed when descending on slopes by applying the plugging braking which is by controlling the reverse voltage in the electric motor.

The Figure 4.18 shows the control of plugging voltage when descending on a sloped surface. The blue and red line represent control plugging voltage for the right and left motor. As shown in Figure 4.18, the recorded plugging voltage is zero at a certain time. This is because the plugging controller is not activated in this duration. When the speed reaches the desired speed of 0.6 m/s, the plugging controller is activated. In the beginning, the plugging voltage is recorded at a higher value which is almost -1.7 V. This happens because a high braking torque or plugging voltage is applied to the motor. Then, the voltage gradually decreased and fluctuated. At 2.3 s, it seems that the plugging voltage maintained and fluctuated at an average of -0.3 V.

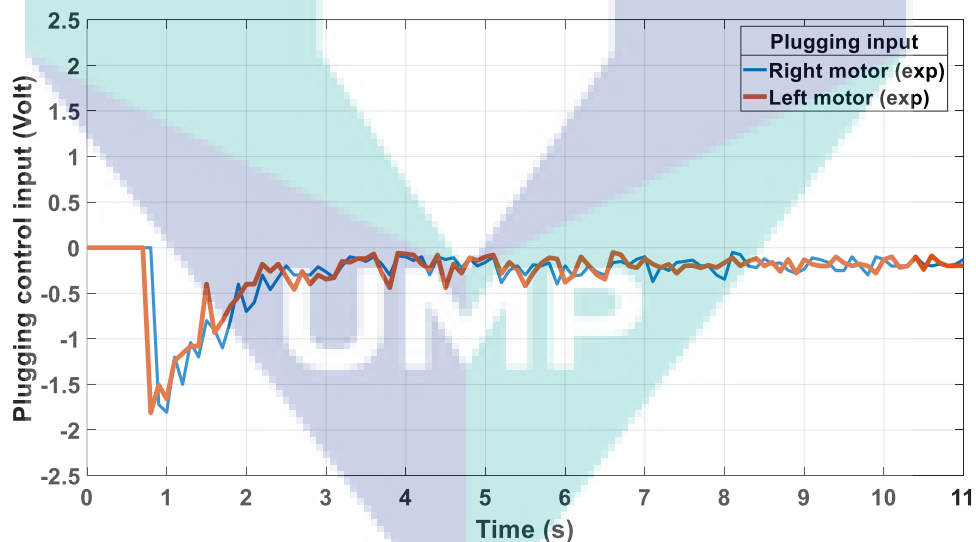


Figure 4.18 Control input of plugging braking during braking at initial speed 0 m/s

The amplitude response of control can be determined by dividing the output and input values of speed. Figure 4.19 shows the example of amplitude response from controlling the speed of tire. The amplitude response is used as a reference to tune the PID gain based on requirements in Table 3.8. From the figure below, when the controller

is activated at 0.9 s, the amplitude response does not show the overshoot values. The response of speed also settled in a short period. From the steady state error analysis, it shows that the fluctuation of speed when maintaining the speed is in range of steady state error boundary.

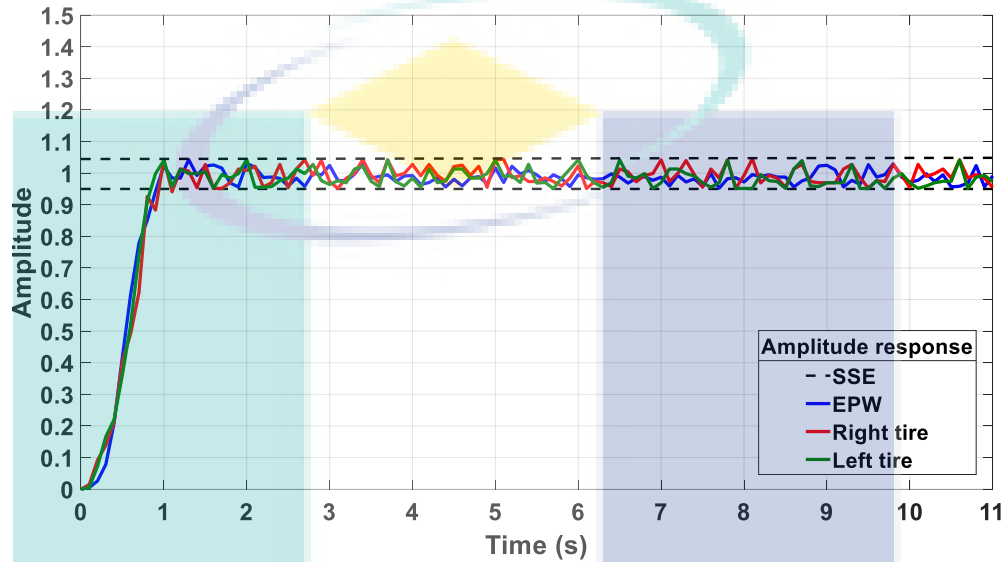


Figure 4.19 Amplitude response of controlling the speed

In the second phase, the purpose is to investigate motor braking controller performance when descending on sloped surfaces in real time analysis. The experimental result of control showed that the speed can be maintained at the desired speed of 0.6 m/s. However, when the speed reaches the desired speed, a small fluctuation happens. This is caused by mechanical constraints such as tire inertia. The experiment of control is only conducted at 0 m/s because of the limitation of the motor driver. When the motor braking controller is investigated at the initial speed of 2.5 m/s, due to the large back EMF produced during descent on the slope, it causes the motor driver to be overheated and broken down. Thus, the simulation approach is used in order to analyse the performance of active braking control during braking at an initial high speed.

4.4 The Initial estimation of the Electric motor Parameters

In this experiment, when the constant DC voltage was supplied to the BLDC motor, there are different responds speed acquired. Even the EPW has two in-wheel electric BLDC motors, but for this experiment right and left tires are assumed to have the

same parameters, characteristic and the outputs respond. In addition, the experiment is conducted in free friction force (pure motor).

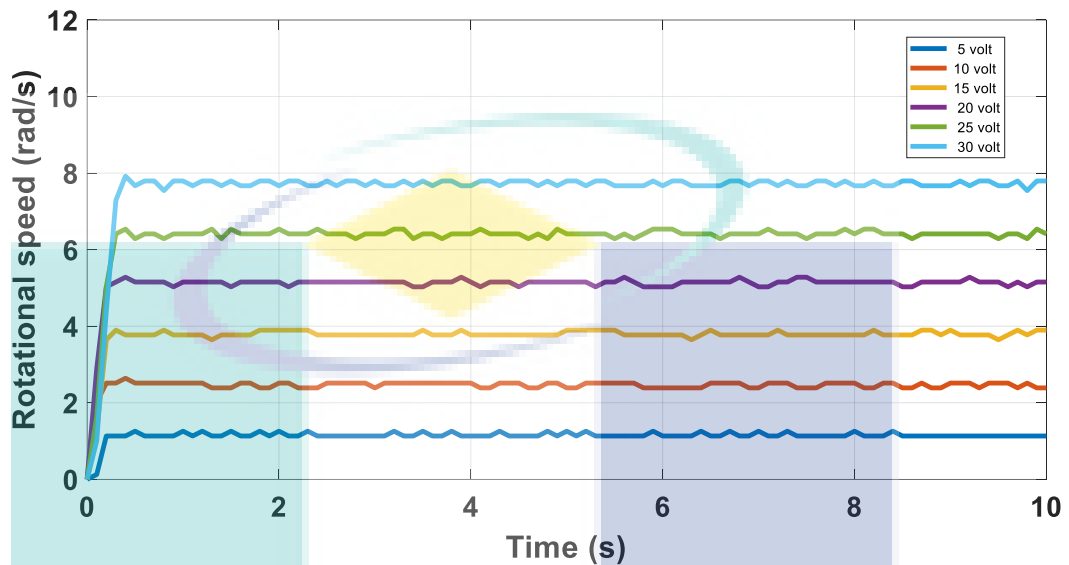


Figure 4.20 Output speed at different supply voltage

Figure 4.20 shows the output speed responses when different voltages are supplied in BLDC motor. There are six different voltages supplied in BLDC motor as shown in Table 4.2. The blue line shows the average output of speed which is 1.417 rad/s when the 5 V DC voltage is supplied. This is the lowest speed this motor can be operated. When the supply voltage is lower than 5 V, motor does not rotate well and only noise sound can be heard. When the supply voltage is increased up to 30 V, output speed is proportionally increased where the average speed is 9.4162 rad/s as shown in light blue line.

Table 4.2 Data distribution of output speed by applied different voltage

Applied Voltage (V)	Speed (rad/s)	current (Amp)
5	1.4170	0.3505
10	3.0420	0.4183
15	4.6576	0.4911
20	6.3168	0.5299
25	7.8424	0.5682
30	9.4162	0.6567

This type BLDC electric motor can be supplied up to 36 V. Nevertheless, when supply voltage is increased until 33 V, the output speed response shows the fluctuation reading. This happens because of the vibration produced from the unbalance rotation from the tire. Thus, to obtain the optimal experiment result, six different voltages are selected which are 5 V, 10 V, 15 V, 20 V, 25 V and 30 V as shown in Table 4.2.

4.4.1 Estimation initial parameters of torque constant and resistance

Recalled back the rearranged estimation equation in 3.23, the linear equation $y = mx + c$ is equivalent to the motor equation is stated as below.

$$\frac{V(t)}{i(t)} = k_t \frac{\omega(t)}{i(t)} + R \quad 3.23$$

The y term is the output which is corresponding to voltage values divided with current values ($V(t)/i(t)$) for the y-axis data and the x term is input which corresponding to rotational speed per current ($\omega(t)/i(t)$) for the x-axis data. The value of parameter torque constant, k_t is corresponding to the m that defined as gradient and the y-intercept is the value for R in linear fitting line. Table 4.3 shows the distributed data of input voltage per current (V/Amp) for the x-axis data and output rotational speed per current (rad/s*Amp) for y-axis data when the different voltages are applied. As shown from the table, the input voltages per current and rotational speed per current are increased proportionally.

Table 4.3 Distributed data for torque constant and Resistance estimation

$x = \omega/I$	$y = V/I$
4.0427	14.2649
7.2724	23.9069
9.4835	30.5419
11.9208	37.7434
13.8030	44.0013
14.3389	45.6841

To estimate the parameters of resistance and torque constant, distributed data in Table 4.3 are plotted as shown in Figure 4.21. The linear fitting line is fitted along scattered data. The linear fitting line for this plot is $V(t)/i(t) = 3.047\omega(t)/i(t) + 1.781$ that equivalent to standard linear $y = mx + c$ equation. The gradient which is $m = k_t = 3.047$ and the y-intercept is resistance, $R = 1.781$. The value of estimated resistance is almost to the measured static resistance which is $R = 1.631$, that is measured by using hand held multi-meter.

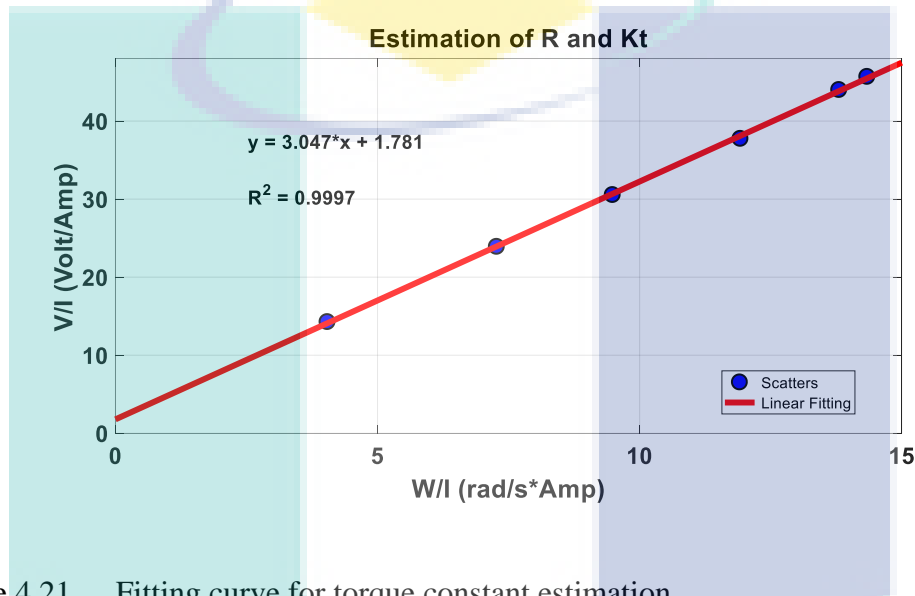


Figure 4.21 Fitting curve for torque constant estimation

By using R-square method, the plot shows the value for $R^2 = 0.9997$, which means that the acquired data in experiment is consistent and equally distributed. The acceptable fitting can be checked by using residual technique. From the residual data information, data of experiment can be classified as acceptable when the residuals are less than ± 0.6 . Figure 4.22 shows torques constant and resistance residual estimation. Residuals data shows that the data are divided equally to three at positive and negative. Data also are below than ± 0.6 .

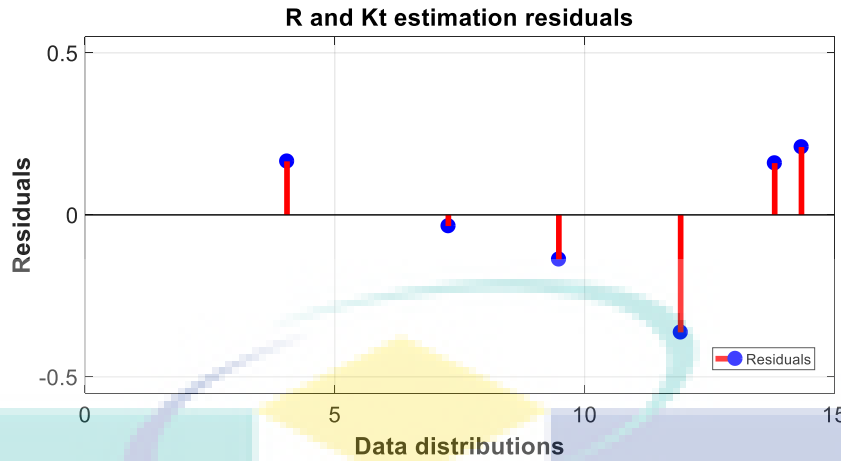


Figure 4.22 Residual estimation of Resistance and Torque constant

4.4.2 Estimation initial of bearing and load torque constant

From rearranged estimation equation in 3.25, this equation is equivalent to the standard form of linear equation $y = mx + c$. The x term is the input which is corresponding to rotational speed, $\omega(t)$ values for the x-axis data and the y term is output which is corresponding to motor torque, T_m for the y-axis data that can be obtained from the product of current, $i(t)$ and previous estimated torque constant, k_t in Section 4.4.1. The value of parameter bearing constant, k_t is equivalent to the m that is known as gradient and the y-intercept is the value for initial load torque, T_{int} in linear fitting line.

$$T_m(t) = B\omega(t) + T_{int} \quad 3.28$$

Table 4.4 shows the distributed data of input rotational speed, $\omega(t)$ (rad/s) for the x-axis data and output motor torque, T_m (N.m) for y-axis data. From the table shown, the input voltages per current and rotational speed per current are also increased proportionally when different are applied.

Table 4.4 Data distribution for Bearing and Load torque constant estimation

$x = \omega(\text{rad/s})$	$y = T_m = K_t I$
1.4170	1.0681
3.0420	1.2746
4.6576	1.4966
6.3168	1.6147
7.8424	1.7313
9.4162	2.0010

Distributed data in Table 4.4 are plotted as Figure 4.23. Based on plotted data, the scattered data are fitted by using linear fitted equation $y = mx + c$ that is equivalent to equation 3.28. The gradient from this equation is m that is equal to bearing constant, $B = 0.1098$ and the y-intercept for this equation is equal to load torque, $T_{int} = 0.933$.

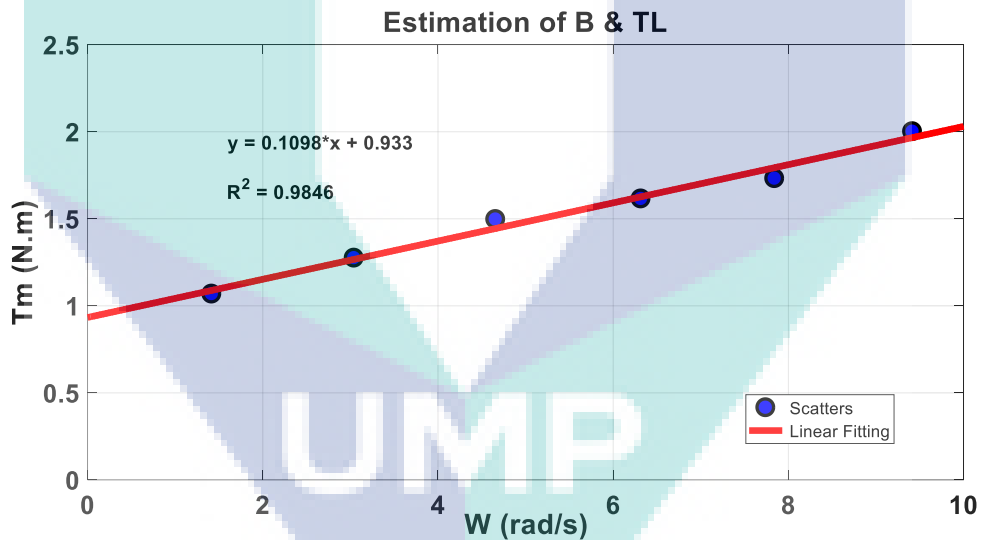


Figure 4.23 Fitting curve for bearing and load torque constant estimation

The R-square information shows that the experiment data are reliable which is $R^2 = 0.9846$ which is more than standard acceptable R-square which is $R^2 = 0.6$. Residual information in Figure 4.24 also shown the fitted line and scattered data are fitted equally. The maximum residual recorded for this experiment is not more than -0.1.

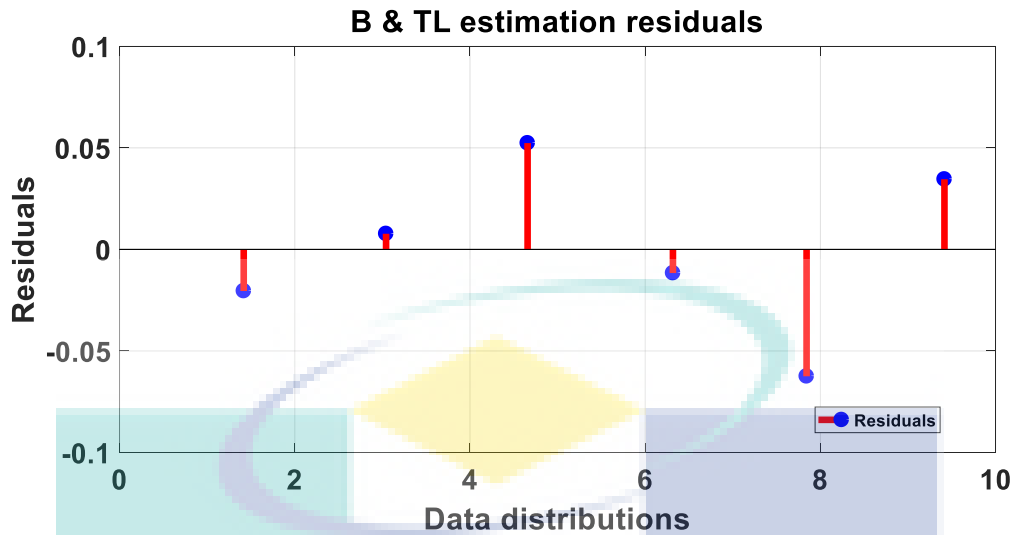


Figure 4.24 Residuals of Bearing and Load torque estimation

4.4.3 Estimation of moment of inertia

The last estimated parameter to discuss is moment of inertia. As mentioned before, there are many methods that can be used to estimate the moment of inertia. In this project, braking torque method is used to determine the moment of inertia for BLDC motor. In this experiment, the applied voltage is set at 30 V and motor is run at constant speed. After the supplied voltage is cut-off, the braking torque is applied until the tire stops to rotate. Table 4.5 shows four different applied braking torque, and its effect to stopping time and deceleration.

Table 4.5 Data distributions by applied different braking torque

T_b (N.m)	Stopping time (s)	$d\omega/dt$ (rad/s ²)
0	2.8	-2.3388
2.5423	2.0	-3.8343
3.5990	1.7	-4.5849
4.8638	1.5	-5.1124

Figure 4.25 shows the relationship between rotational speed and stopping time when different braking torque is applied. The blue line is the tire deceleration when there is no braking torque applied. This condition also is known as coasting where the tire stop

the rotation by its own inertia without applying external load. The stopping time is recorded at 2.8 s, and the deceleration is -2.3388 rad/s^2 .

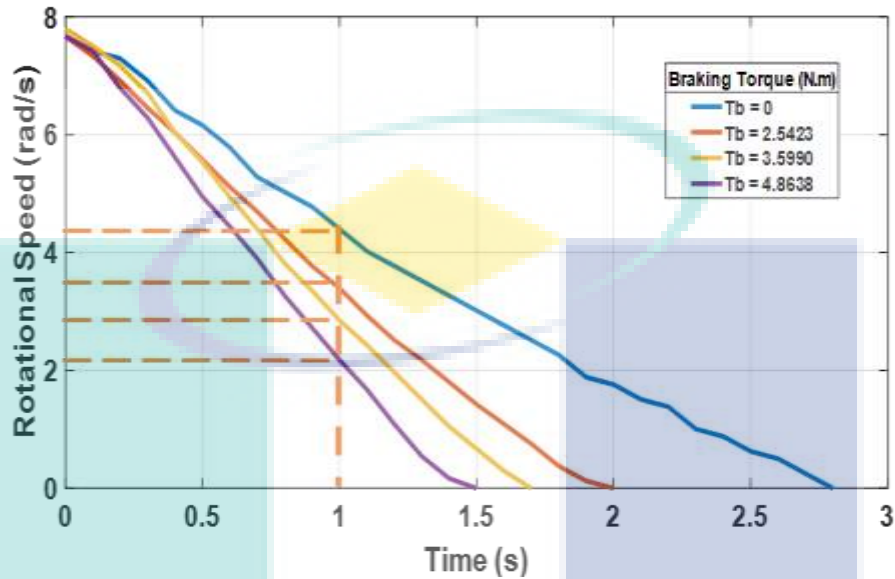


Figure 4.25 Deceleration at different applied braking torque

Meanwhile, the red line shows the deceleration of tire when braking torque, $T_b = 2.5423 \text{ N.m}$ is applied after supply is cut-off. The stopping time is recorded at 2.0 s and tire decelerated faster than the coasting condition which is $d\omega/dt = -3.8343 \text{ rad/s}^2$. Next, the yellow line shows the deceleration of tire when braking torque, $T_b = 3.5990 \text{ N.m}$ is applied. The stopping time is recorded at 1.7 s. There is no big difference in stopping time for this condition, but the tire seems to decelerate faster than the previous condition which is $d\omega/dt = -4.5849 \text{ rad/s}^2$.

Next, the purple line shows the deceleration of tire when braking torque, $T_b = 4.8638 \text{ N.m}$ is applied after supply is cut-off. The stopping time is recorded at 1.5 s, and tire is decelerated, $d\omega/dt = -5.1124 \text{ rad/s}^2$. From the graph, it can be concluded that when the constant applied braking torque is increased, the time taken for the tire to stop is decreased. That means the deceleration will also increase. The dotted line shows the speed of tire at 1 s for the different applied braking torque. At 1s, the rotational speed of tire is recorded 4.1 s, 3.4 s, 2.8 s and 2.2 s in respect to 0 N.m, 2.543 N.m, 3.599 N.m and 4.8638 N.m braking torque. Same with the previous estimation parameters, distributed data in Table 4.5 are plotted according to equation 3.26.

Initially, the y-intercept needs to be set same with initial load torque, $T_{int} = 0.7216$ N.m which had been estimated in Section 4.4.2. For the moment of inertia, J the parameter of the moment of inertia can be estimated from the slope of the linear fitted line in Figure 4.26 which is $m = J = 1.3728$ kg.ms² from the linear fitted $B\omega(t) = 04416 d\omega(t)/dt + 0.721$. R-square information shows the linear fitting is close to the reliable R-square. Nonetheless, linear fitting line is fitted well along the scattered data which $R^2 = 0.9701$.

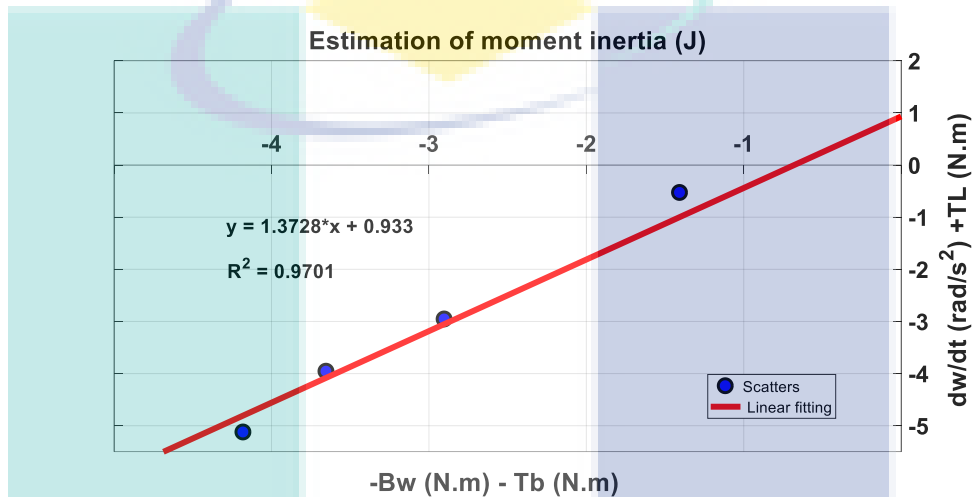


Figure 4.26 Fitting curve for moment inertia estimation

Besides that, residual information estimation of moment inertia in Figure 4.27 shows that data distributed are reliable. All the result of estimated parameters is shown in Table 4.6.

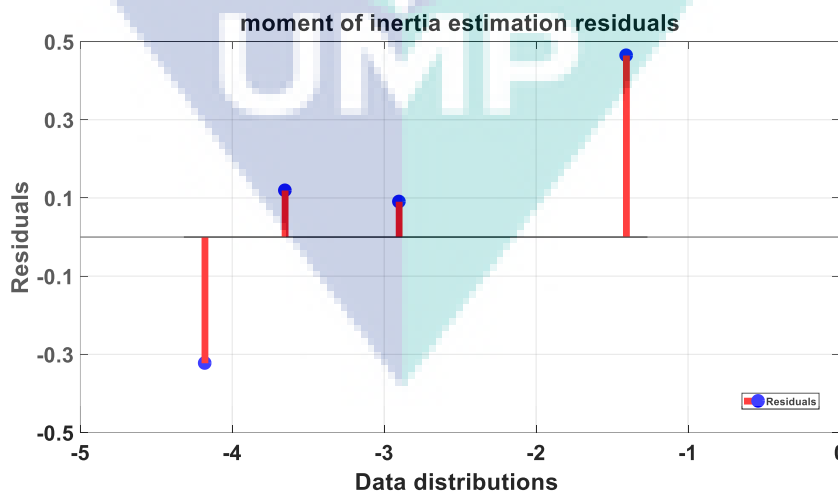


Figure 4.27 Residuals moment inertia estimation

Table 4.6 Estimated parameter result from the fitting line method

R	k_t	B	T_{int}	J
1.781	3.047	0.1098	0.933	1.3728

4.5 BLDC motor parameters validation

Before parameters and responses of BLDC model are validated, the output response data in the experiment such as speed and current need to be analyzed. Firstly, the input supply voltage is set at +24 V and -24 V. The voltage supply changes every 2 s. The purpose to set the input signal in that form is to observe the motor characteristic. In simulation model, +24 V and -24 V signal input is also set and changed in every 2 s by using signal building module. The estimated parameter in Table 4.6 is then simulated in BLDC motor modelling to observe the response of speed and current. In this simulation also, the initial inductance term needs to be set at $L = 0.0001$. This is the standard value used in every parameter estimation of electric motor (Asyraf et al., 2019; Sankardoss & Geethanjali, 2017).

Figure 4.28 shows the output speed response between experiment and simulation by using initial parameters estimation which are plotted as blue and red line respectively. The responses show the big difference between experiment and simulation. The pattern of output speed by using estimated parameters give slow response than analysis. Settling time for experiment and simulation are recorded at 0.13 s and 1.2 s respectively before it becomes steady state. By using the equation in 3.30, the validation of model is based on error percent technique. The data is validated when the error between experiment and simulation is less than 10%. From the error analysis, the error of experiment and simulation is recorded more than 10% which is 54.6%.

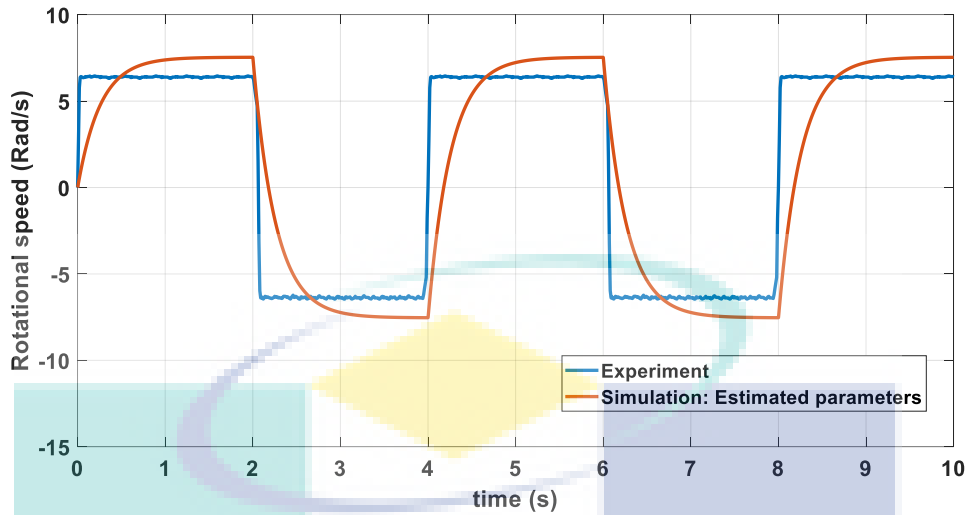


Figure 4.28 Output speed responses between experiment and simulation by using estimated parameters

Meanwhile, Figure 4.29 below shows the output responses of current between experiment and simulation by using the initial estimated parameter. The output current responses also show the big difference between experiment and simulation. The error per cent of output current responses are also more than 10% which is 63.26%. Thus, the parameters need to be calibrated in order to obtain the corresponding response between experiment and simulation.

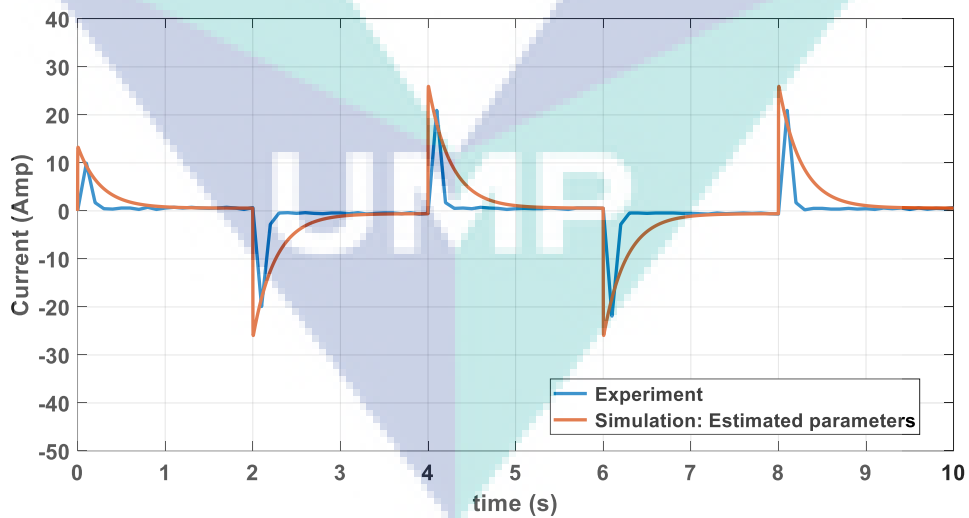


Figure 4.29 Output current responses between experiment and simulation by using estimated parameters

Then, after parameters are calibrated and optimized by using sum of error method provided in MATLAB tool software, the calibrated parameters are simulated again in BLDC motor modelling. Figure 4.30 shows the output speed response between experiment and simulation by using calibrated parameters which are plotted as blue and yellow line respectively.

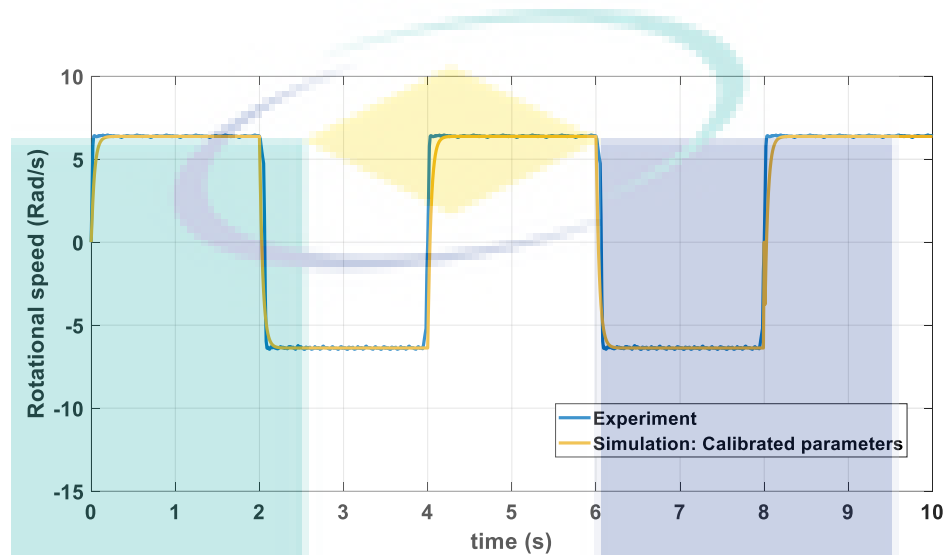


Figure 4.30 Output speed responses between experiment and simulation by using calibrated

The result shows the improvement in corresponding responses between experiment and simulation. The pattern of output speed by using calibrated parameters give the close response as the experiment. Settling time for experiment is recorded at 0.13 s and simulation is recorded at 0.22 s before it becomes steady state. the validation model based on the error between experiment and simulation shows that the correlation responses between experiment and simulation is less than the 10% which is 4.93%.

Next, Figure 4.31 shows the output responses of current between experiment and simulation by using calibrated parameter. The output current responses also show the corresponding between experiment and simulation. The error per cent of output current responses is less than 10% which is 5.65%. The initial and calibrated parameters values are shown in Table 4.7.

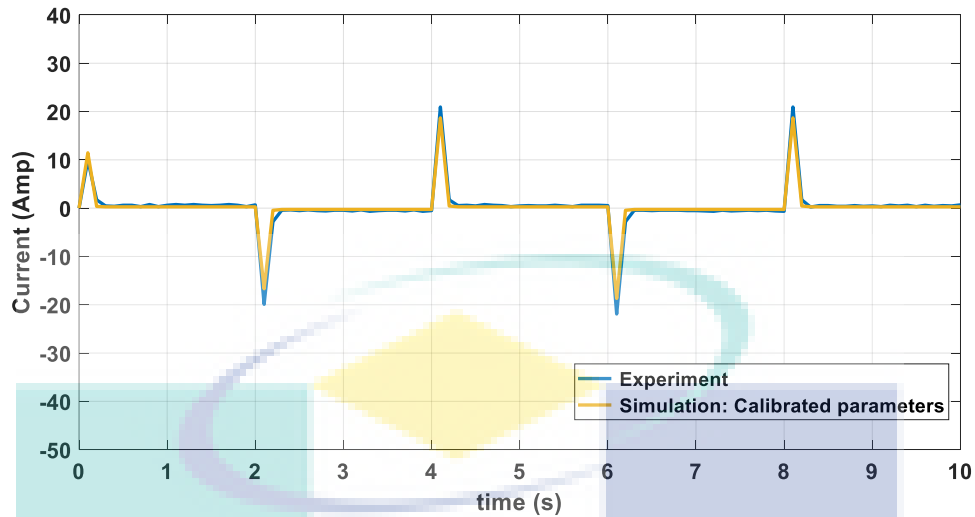


Figure 4.31 Output current responses between experiment and simulation by using calibrated parameters

Table 4.7 Initial estimate and calibrated parameters

Parameters	R	k_t	B	T_L	J	L
Estimated	1.781	3.047	0.1098	0.933	1.3728	0.0001
Calibrated	1.2407	10.264	0.42023	0.8703	1.1924	0.00008
Rate change	0.3034	-7.217	-0.3104	0.8627	0.1804	0.0002

4.6 Surface coefficient validation

The important parameters need to be validated is surface coefficient, k as shown in equation 3.19. Parameter k is the friction coefficient contact between tire and road surface. In theory, the value of friction coefficient, k for the dry ceramic is assumed at 0.43~0.53. To estimate the actual value for k , the experimental study of braking is conducted at dry mosaic surface in order to determine the actual speed characteristic of the tire and EPW. The purpose of actual speed characteristic is for the speed characteristic references in simulation.

Figure 4.32 shows the slip ratio plot when 2.5 V plugging voltage is given to the electric motor at initial speed 2.5 m/s. The blue line indicates the slip ratio that is acquired from the experimental work. The red, green and purple indicate the slip ratio that are analysed in simulation work.

The red line shows the simulated slip ratio from the lowest estimated surface coefficient, $k = 0.43$. At time 0 s to 0.3 s, the characteristic of slip ratio is almost the same with the experimental slip ratio. However, at time 0.3 s to 1.8 s, it shows significant different between simulation and experiment. From the error analysis, the average error between experiment and simulation for $k = 0.43$ is recorded as 13.35% as shown in Table 4.8. The purple line represents simulated slip ratio when the highest estimated surface coefficient $k = 0.53$ is used in the simulation. It also shows the huge difference between simulation and experimental work. From Table 4.8, it is clearly shown that the biggest average error is 24.54%. When the k value is estimated from 0.43 to 0.53, the $k = 0.45$ shows the optimum estimated surface coefficient as plotted in the green line. The simulated slip ratio is seen closely with the experiment in overall time. Table 4.8 also shows that the estimated surface coefficient $k = 0.45$ is the lowest average of error.

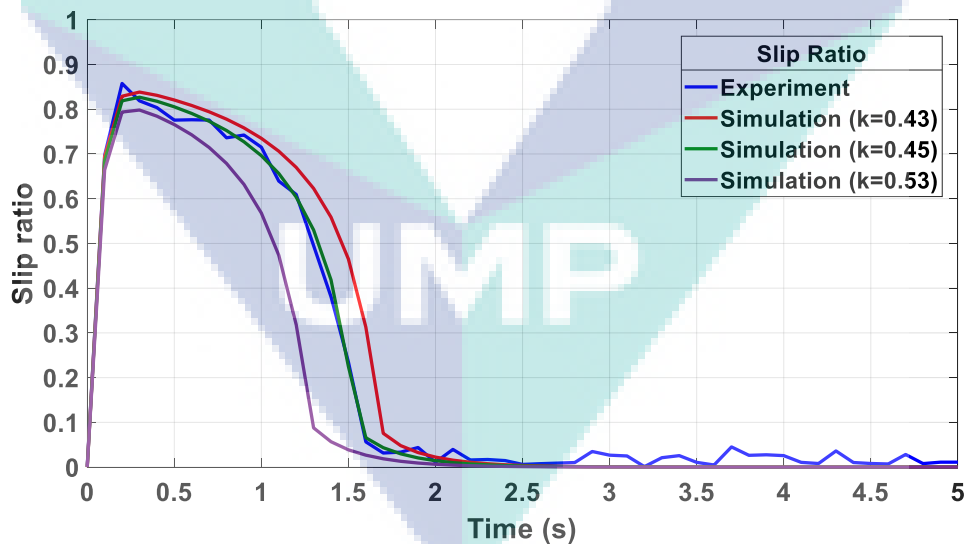


Figure 4.32 Effect of slip ratio by changing the surface coefficient

Table 4.8 Output response error at different estimated iteration road surface, k (plugging voltage, 2.5 V)

Estimated road surface, k iteration	Ave. Slip ratio error (%)
0.43	13.35
0.44	8.52
0.45	3.71
0.46	5.34
0.47	7.24
0.48	12.65
0.49	14.43
0.50	16.44
0.51	17.32
0.52	21.04
0.53	24.54

To verify that the estimated parameter of the surface coefficient $k=0.45$ is the suited value for surface coefficient during braking at dry mosaic in simulation work, the comparison slip ratio between experiment and simulation is conducted once again. However, in this analysis, the 4.5 V plugging braking is given to the electric motor at the initial braking speed of 2.5 m/s. As shown in Figure 4.33, the blue line is indicated as the slip ratio that is acquired from the experimental work. The red, green and purple are indicated as slip ratio that are analysed in simulation work.

The red line shows the previous optimum estimated surface coefficient, $k=0.45$. The simulated slip ratio is seen closely with the overall experiment in 1.1 s. At 1.1 s until stop, error between experiment and simulation can be seen. From the Table 4.9, the average error is recorded at 6.32%. The green line shows the optimum estimated surface coefficient which is $k=0.46$. The simulated slip ratio is seen closely with the experimental work in overall time. Table 4.9 also shows that the estimated surface coefficient $k=0.46$ is the lowest average of error.

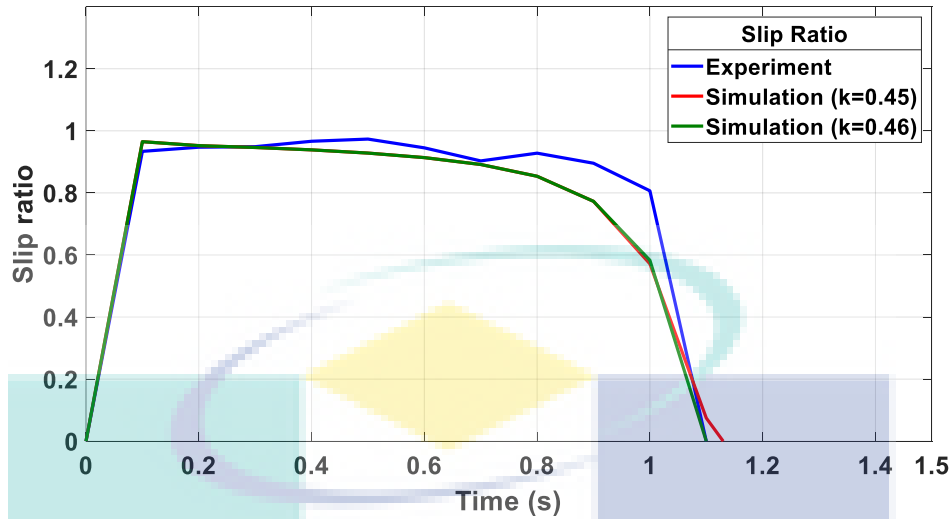


Figure 4.33 Slip ratio response between experiment and simulation

Table 4.9 Output response error at different estimated iteration road surface, k (plugging voltage, 4.5 V)

Road surface, k iteration	Ave. Slip ratio error (%)
0.43	10.12
0.44	8.55
0.45	6.32
0.46	5.47
0.47	8.18
0.48	14.65
0.49	17.13
0.50	19.44
0.51	22.32
0.52	25.04
0.53	27.24

From the analysis, it can be understood that the parameter of surface coefficient is very important to validate. The small changes of k will be affect the output characteristic between experiment and simulation. In conclusion, the optimum value for the surface coefficient, k to use in the simulation is in 0.45~0.46 range for braking at the dry mosaic.

In the conclusion of parameters estimation, all the parameters are estimated by using the fitting curve technique and Root Square Mean (RMS) method. From the results, data are distributed well which the R^2 results exceed 0.9. To validate the output responses, the initial parameters are used in the established mathematical electric motor. However,

when the initial parameters are used, the speed and current responses are not correspondents with the experimental outputs, and the error is determined to be more than 10%. It can be determined that the parameters which are estimated by using fitting curve technique is not convincing to be used as the parameter in the electric motor mathematical model. However, the parameters' accuracy can be determined and improved by using the calibration tool provided by MATLAB. After parameters are calibrated by using the calibration tool in MATLAB, the parameters are used again in the electric motor mathematical model. From the output responses of rotational speed and current, the output error shows less than 10%.

Thus, the calibrated parameters estimation is verified to be used in electric motor mathematical model simulation. The next estimated parameter is surface coefficient, k . From the studies of El-Sherbiny, Hasouna and Ali, the surface coefficient between rubber and dry mosaic are determined in the range of 0.43~0.53. The analysis error is by comparing the slip ratio between experiment and simulation during braking. From the analysis, it can be understood that the parameter of the surface coefficient is very important to validate. The small changes of k parameters will affect the output characteristic between experiment and simulation. In conclusion, the optimum value for the surface coefficient, k to use in the simulation is in 0.45~0.46 range for braking at the dry mosaic. Overall, it can be concluded that the estimated parameters are valid to be used in mathematical model of EPW in order to simulate the dynamic behaviors of EPW that cooperate with the active braking control system at dry mosaic during descending on slope condition.

4.7 Simulation of plugging braking controller during descending on slope using plugging braking technique

To observe the performance of the active braking controller, the controller is analyzed at a high initial braking speed of 2.5m/s. However, due to the limitation in experimental work, the analysis cannot be conducted at the high initial braking speed which can cause damage to the motor driver. Thus, a simulation analysis is used to predict and observe the response of speed and input control when the plugging voltage control is applied at the initial braking speed of 2.5m/s.

4.7.1 Validation of active braking control

Before the simulation of control speed during descent on slope is conducted, the active braking controller is validated. The validation of motor braking controller is by comparing the travelled distance, speed response and plugging control input with real time experiment in Section 4.3.

Figure 4.34 shows the validation of travelled distance when the plugging control is applied during descent on sloped surfaces at the initial speed of 0m/s. The red and blue show the travelled distance by experiment and simulation respectively. Both travel distance is shown in the same pattern and exceeded the length of the slope set by MS-1184 during descent on the slope by using plugging voltage control. The time taken for EPW to reach 5.4m is recorded at 9.5s and 9.7s for experiment and simulation respectively.

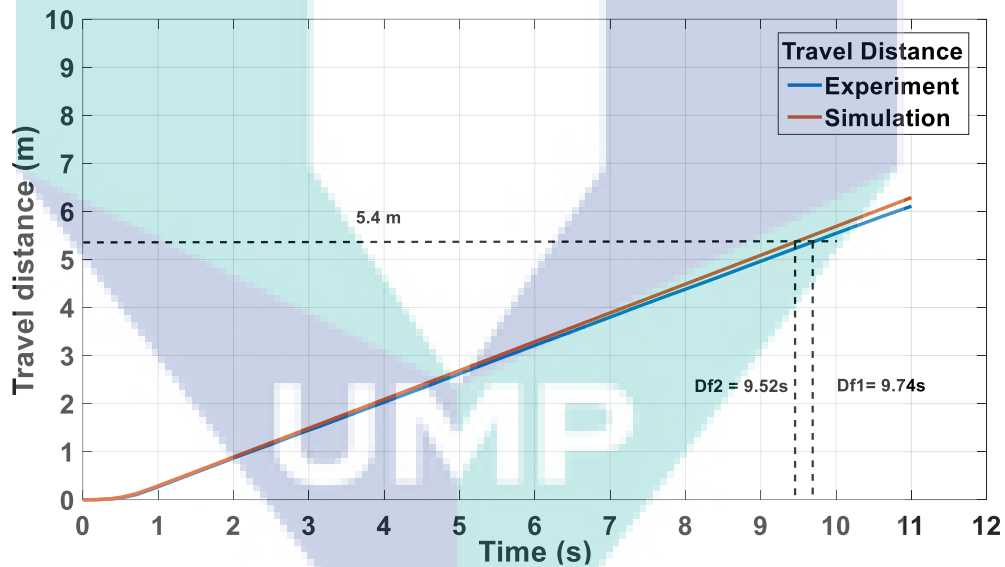


Figure 4.34 Validation of distance travel

Figure 4.35 shows the validation speed of tires and EPW when the plugging control is applied on the sloped surface. As shown in the figure below, the blue dashed line represents the desired speed that can be set by the user. In this experiment, the speed is set at 0.6m/s for safety reasons. The solid red, yellow and purple lines represent the speed of the EPW, right tire and left tire in experimental work. Meanwhile, the red and blue lines indicate the speed of EPW and tire in simulation analysis.

In the experimental work, when the EPW is released from the top of the slope, the speed of tire and EPW increased from 0m/s to 0.6m/s. At 0.9s, the plugging control is activated, and the speed is maintained and fluctuated at 0.6m/s during descent along the slope. While in simulation analysis, when the EPW is released at the initial speed of 0m/s, the speed of tire and EPW also increased from 0m/s to 0.6m/s. When the plugging is activated at 0.8s, the speed is maintained at 0.6m/s. From this graph, it can be understood that the speed of tire and EPW can be maintained at a desired speed during descent on the slope by applying the plugging braking control to the electric motor in experimental work and simulation analysis.

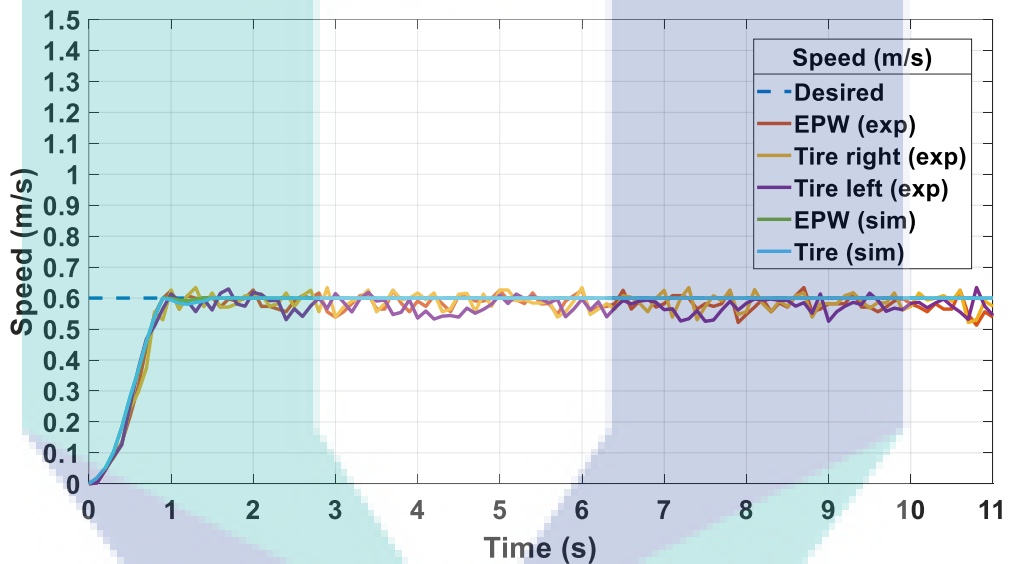


Figure 4.35 validation of speed control

The Figure 4.36 shows the control of plugging voltage during descent on sloped surfaces. The blue and red lines represent the control plugging voltage for right and left motor in experimental work. The yellow line indicates the plugging voltage control in simulation analysis. Generally, the pattern of plugging voltage is the same for both experiment and simulation analysis. As shown in Figure 4.36, the recorded plugging voltage is zero at a certain time. This is because the plugging controller is not activated in this duration.

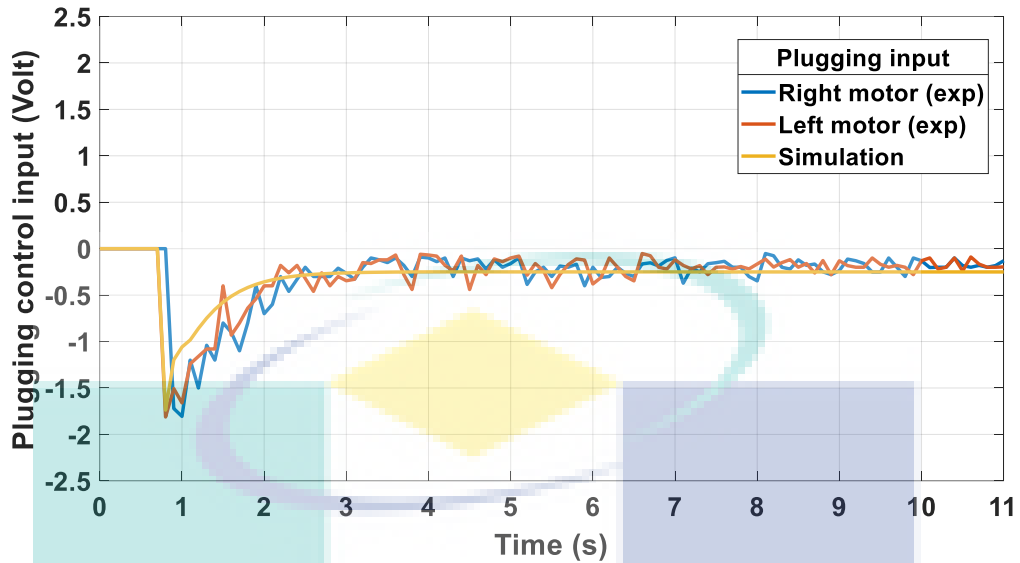


Figure 4.36 Validation of plugging voltage input

When the speed reaches the desired speed of 0.6m/s, the plugging controller is activated. In the beginning, the plugging voltage is recorded at a higher value which is almost -1.7V for experiment and simulation analysis. Then, the voltage gradually decreased and fluctuated. At 2.3s, it shows that the plugging voltage maintained and fluctuated at an average of -0.3 V. The voltage gradually decreased from -1.7V and maintained at -0.3V in simulation analysis. The fluctuation output does not appear in simulation analysis because of the neglect in some disturbances such as switching frequency in the motor drive that causes delay to the system.

From these three figures above, it can be observed that the output responses between experiment and simulation are not alike. However, it can be concluded that the patterns of output responses between experimental and simulation analysis are significantly the same. Thus, the simulation analysis of plugging voltage to control the speed during descent on sloped surfaces can be considered to be used in the next analysis.

4.7.2 Simulation of plugging braking control at high initial braking speed

Figure 4.37 shows the simulation of travelled distance for EPW. In driving mode, the travelled distance is recorded at 12.4m in 5s. Then, when the plugging voltage control is applied at the initial speed of 2.5m/s, the distance of EPW slightly increased and

exceeded the length of slope set by MS-1184. The time taken for EPW to reach 5.4m is recorded at 7.4s as shown in Figure 4.37 (b).

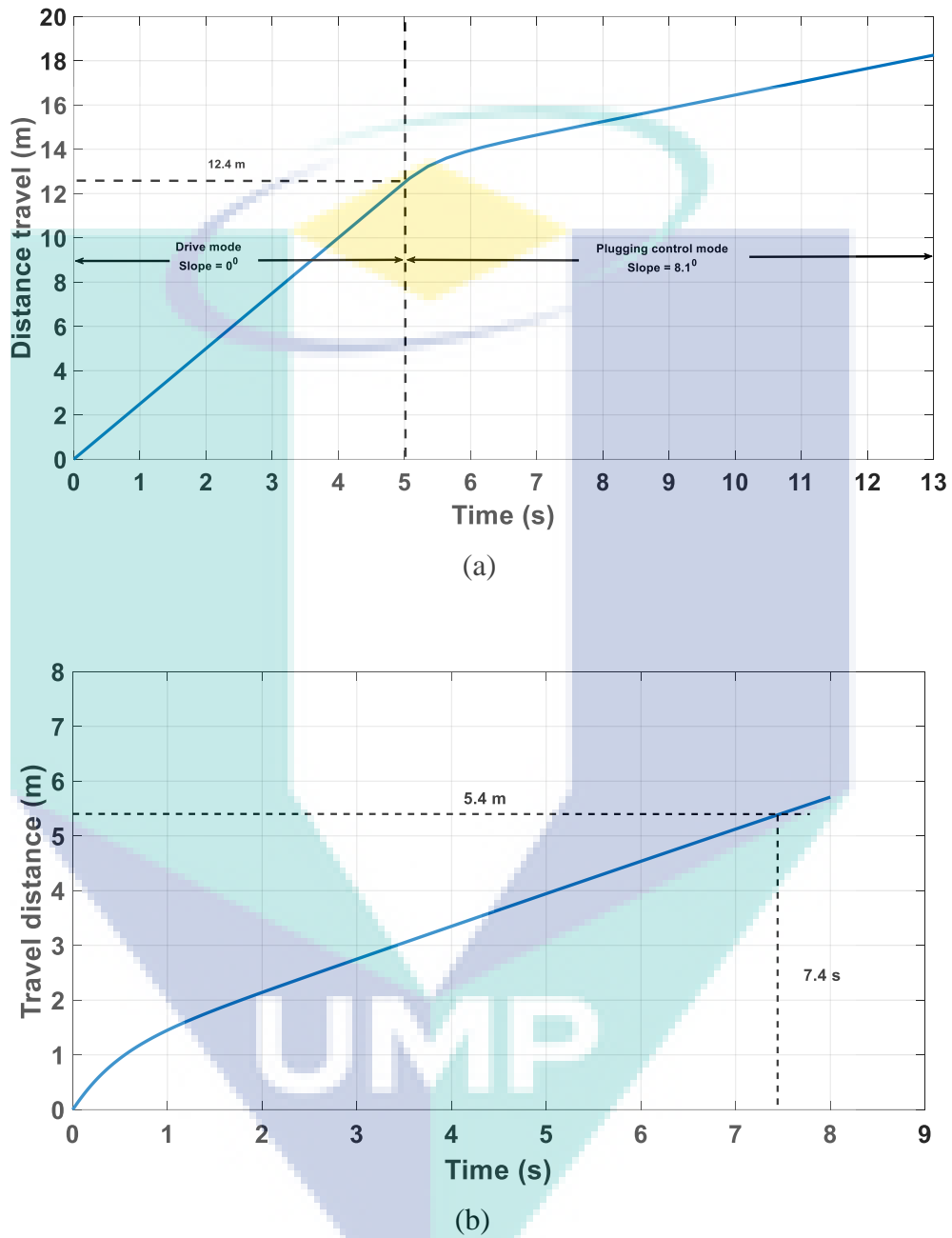


Figure 4.37 (a) Distance travel of EPW (b) Distance travel using plugging voltage at initial speed 2.5m/s

Figure 4.38 shows the speed of tires and EPW. In driving mode, the speed of tire and EPW are the same at 2.5m/s. On a sloped surface, the plugging control is applied at the initial speed of 2.5m/s. As the experimental work, the desired speed is also set at 0.6m/s in simulation analysis that is represented by the blue dotted line.

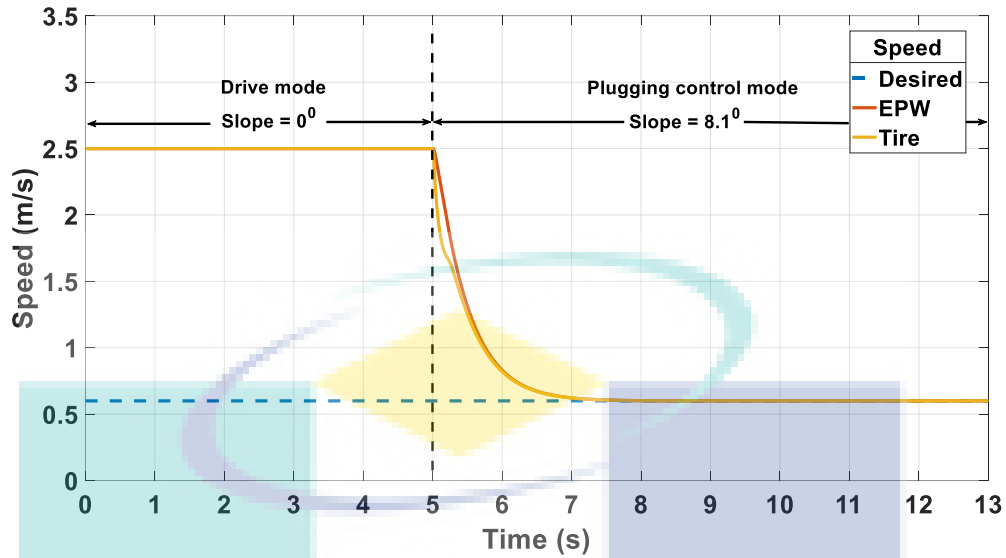


Figure 4.38 Speed of EPW and tire

The solid red and yellow lines represent the speed of the EPW and tire. In the simulation analysis, when the EPW enters a sloped surface at the speed of 2.5m/s, the plugging voltage control is activated. As shown in the figure, the speed of EPW drastically decreased from 2.5m/s to 0.6m/s in 2.2s. Then, the speed of the tire maintained at 0.6m/s during descent along the slope. Next, the speed of the tire dropped from 2.5m/s to 0.6m/s in 2.2s. Initially, in 0.5s, the tire seems to be abruptly decreased. This happens because of the large braking torque produced from the larger plugging voltage. From this simulation, it can be determined that the speed of tire and EPW can be maintained at the desired speed during descent on slope by applying the plugging braking control. The initial larger plugging voltage causes the tire to stop faster due to the larger braking torque produced.

Figure 4.39 shows the voltage input to the motor. In driving mode, 24V input was applied to the electric motor. Meanwhile, when the EPW entered a sloped surface, the plugging voltage control input is activated. The plugging voltage can be determined directly from the input of voltage to the motor in mathematical modelling. As shown in Figure 4.39 (b), when the plugging voltage is applied at an initial speed of 2.5m/s, the plugging voltage is recorded near -3V. Next, the input plugging voltage gradually decreased and remains constant at -0.49V from 6.6s. From the simulation, it is proven that the plugging voltage can be applied at a high speed and control the speed of EPW during descent on sloped surfaces.

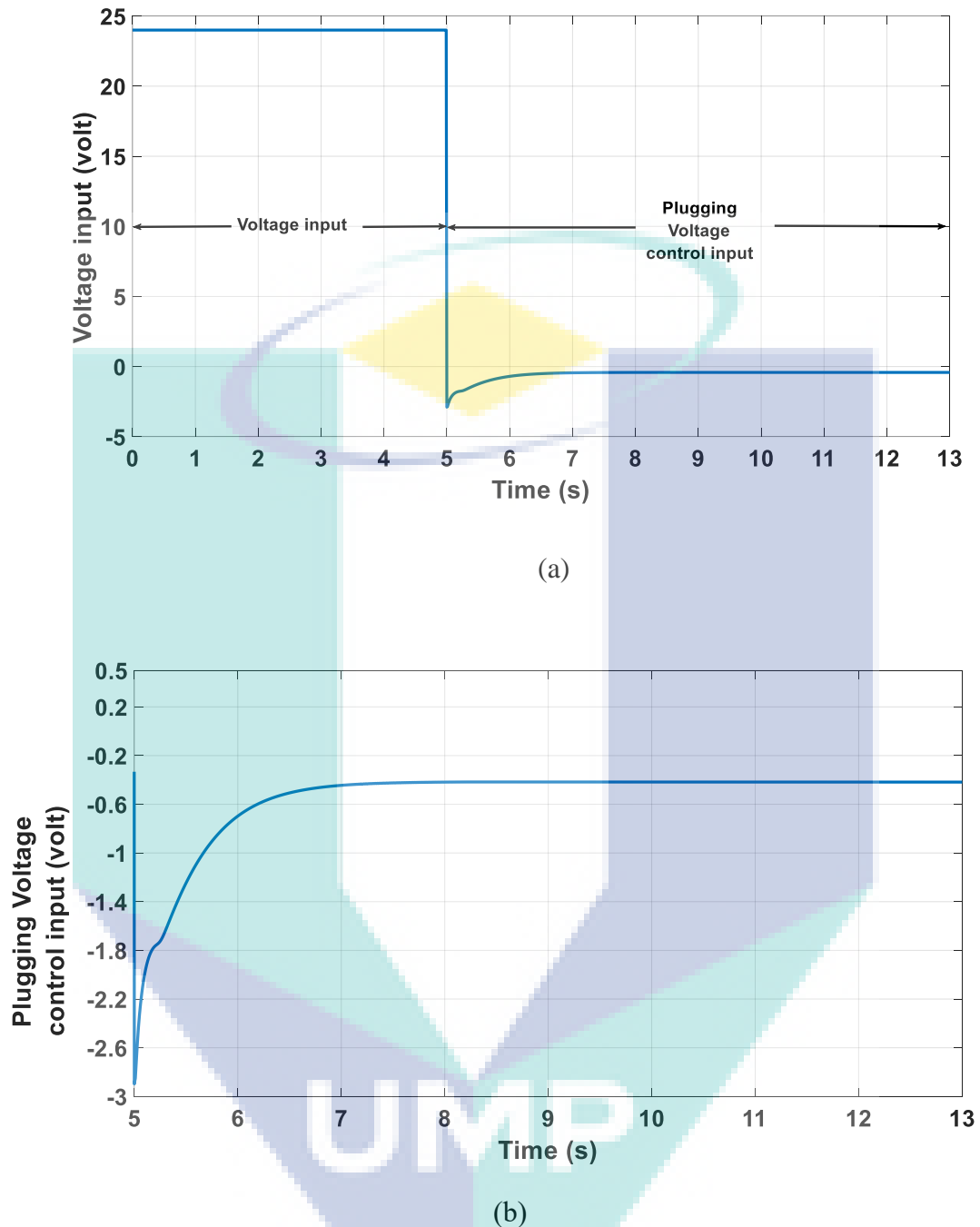


Figure 4.39 (a) Input voltage to electric motor (b) Control input of plugging voltage at initial speed 2.5m/s

Figure 4.40 shows the amplitude response by driving the output and input speed response. The amplitude response plot does not show the overshoot. Moreover, the settling time is 2.3s which is below the required settling time. The plot also shows that the amplitude response is in range of the required steady state error that is set in Table 3.8.

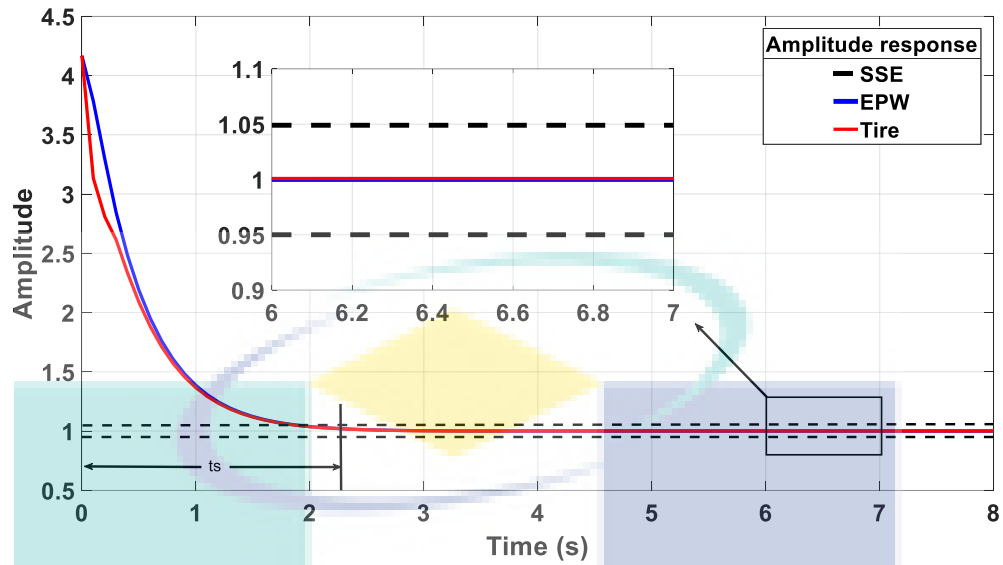


Figure 4.40 Amplitude response of speed

In the third work scope, the simulation method was used to investigate the motor braking during descent on sloped surfaces at the initial speed of 2.5m/s. When the EPW is at a sloped surface, the electric motor braking is activated and reduces the speed of tire and then maintains it at the desired speed of 0.6m/s. It is proven that the plugging braking can control the speed during descent on sloped surfaces at a high initial speed.

UMP

CHAPTER 5

CONCLUSION

5.1 Introduction

The last chapter in this thesis is to summarize the outcomes of this study and to recommend any further improvement. The conclusions are made based on the key found in every phase that consists of braking performance analysis, experiment on electric motor braking and simulation of electric motor braking control during descent on sloped surfaces. Next, the recommendations are documented based on the potential of this study to be improved in future work such as the dynamic motion and stability of the EPW.

5.2 Conclusions

In the first phase, the project focused to analyse the braking performance of electrical braking during descent on sloped surfaces. From the regenerative braking analysis, the back EMF that is produced by an electric motor is lower than the terminal voltage. The experimental result shows that the duration of regenerative regime is only 0.73s. Based on the result, it can be concluded that regenerative braking is unsuitable to be applied as the primary braking system in EPW. Then, the braking performance by using dynamic braking is analyzed during descent on slopes at different initial braking speed. From the analysis, it can be understood that dynamic braking is only suitable to be used as a backup braking mechanism and not for primary braking mechanism. It can be observed from the overall analysis that the EPW will still descent on the slope slowly although the dynamic braking is applied. Lastly, in this phase, the braking performance by using plugging or reverse voltage was analysed during descent on the slope at different initial braking speed. Plugging braking is a versatile braking type because it can give different braking torque when the reverse voltage is changed. A higher reverse voltage

will produce higher braking torque. Moreover, various voltage from plugging give the advantage in control work to control the speed of EPW during descent on sloped surfaces. In conclusion, this type of braking is suitable to be used as the braking system in the EPW.

In the second phase, the project is to investigate active braking controller in experimental work. The experimental result of control showed that the speed can be maintained at the desired speed of 0.6m/s. However, when the speed reaches the desired speed, a small fluctuation happens. This is caused by several factors such as mechanical constraints. The experiment of control is only conducted at 0m/s because of the limitation of the motor driver. When the motor braking controller is investigated at the initial speed of 2.5m/s, due to the large back EMF produced during descent on the slope it causes the motor driver to be overheated and broken down.

In the third phase, the objective of the project is to encounter the limitation in phase two by modelling and validating the Electric Powered Wheelchair's (EPW) mathematical model. In this phase, the work scope is divided into three. In the first work scope, the mathematical model of electric motor and EPW dynamic are completely established according to the related dynamic equations in MATLAB Simulink environment. The second work scope, all the parameters are estimated by using the fitting curve technique and Root Square Mean (RMS) method. From the results, the data are distributed well in which the R^2 results exceed 0.9. Overall, it can be concluded that the estimated parameters are valid to be used in the mathematical model of EPW to simulate the braking dynamic of EPW on a dry mosaic surface during descent on slopes. In the third work scope, the simulation method was used to investigate the motor braking during descent on sloped surfaces at the initial speed of 2.5m/s. When the EPW is on a sloped surface, the electric motor braking is activated and reduces the speed of tire and then maintains at the desired speed of 0.6m/s. It is proven that the active braking control integrated with plugging braking can control the speed during descent on sloped surfaces at a high initial speed.

5.3 Recommendations

There are several problems that need to be addressed such as when the motor driver became hot and damaged some components, Thus, these are some recommendations that can be implemented in this project to achieve the idea of

controlling the speed by using a plugging control system at a high braking speed. First, the motor driver needs to be implemented with a cooling system such as fans and fins. This recommendation will lower the overheating of the motor driver during braking at a high speed. Secondly, the motor driver needs to be designed with a high current peak system to prevent the current from suppressing and may cause damage to the motor drive. The usual technique that is used to prevent high current peak is by installing the capacitor at the motor driver. The capacitor acts as the storage, which stores the voltage energy and stabilises it before releasing it into other motor driver electronic components.

Lastly, for this recommendation, the success in developing this HDC system has proven that this system is very important to be used as an active system in the EPW. To make this system more achievable and convenient for EPW users, the gyro or inclino meter is proposed to be added in this system in which it can detect sloped surfaces and activate the HDC system automatically in real time as shown in Figure 5.1. This integrated system can improve the safety of EPW users. Hopefully this system will be able to be implemented in current EPWs and can be commercialised.

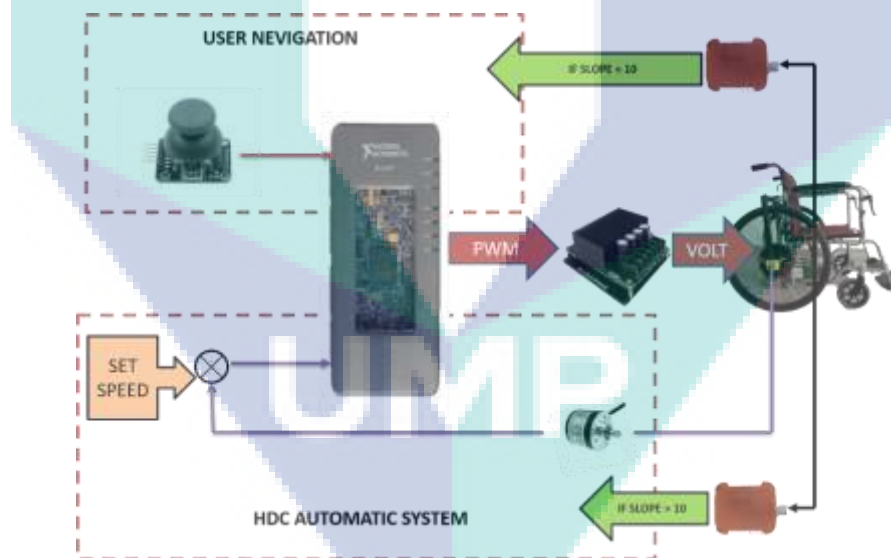


Figure 5.1 Hill descent control intergrated with gyro sensor

REFERENCES

- Abiyev, R. H., Akkaya, N., Aytac, E., Günsel, I., & Çağman, A. (2016). Brain-Computer Interface for Control of Wheelchair Using Fuzzy Neural Networks. *BioMed Research International*, 2016.
- Affanni, A., Bellini, A., Franceschini, G., Guglielmi, P., & Tassoni, C. (2005). Battery choice and management for new-generation electric vehicles. *IEEE Transactions on Industrial Electronics*, 52(5), 1343–1349.
- Aksjonov, A., Vodovozov, V., Augsburg, K., & Petlenkov, E. (2018). *Design of Regenerative Anti-Lock Braking System Controller for 4 In-Wheel-Motor Drive Electric Vehicle with Road Surface Estimation*. 19(4), 727–742.
- Al-sharif, L. (2016). *Overview and Comparison of Electrical and Mechanical Braking in Drive Systems Overview and Comparison of Electrical and Mechanical Braking in Drive Systems*. (December), 1–4.
- Algood, S. D., Cooper, R. A., Fitzgerald, S. G., Cooper, R., & Boninger, M. L. (2004). Impact of a pushrim-activated power-assisted wheelchair on the metabolic demands, stroke frequency, and range of motion among subjects with tetraplegia. *Archives of Physical Medicine and Rehabilitation*, 85(11), 1865–1871.
- Alleyne, A. (1997). Improved vehicle performance using combined suspension and braking forces. *Vehicle System Dynamics*, 27(4), 235–265.
- Alsibai, M. H., Hamran, N. N. N., Nasir, A., & Abdullah, A. A. (2018). A Monitoring System for EPW Safe Use. *Journal of Telecommunication Electronic and Computer Engineering*, 10(1), 131–135.
- Alturbeh, H., Lewis, R., Six, K., Trummer, G., & Stow, J. (2018). Implementation of the water induced low adhesion creep force model (WILAC) into the low adhesion braking dynamic optimisation for rolling stock model (LABRADOR). *International Conference on Contact Mechanics and Wear of Rail/Wheel System*.
- Antony, M. S., & Praveen, Raj, R. . (2015). Four Quadrant Operation of Vector Control of PMSM with Dynamic Braking. *2015 International Conference on Control Communication & Computing India (ICCC)*, (November), 161–164.
- Aqmar, N., Rusly, M., Kamaruzzaman, S. N., Architecture, T., & Lumpur, K. (2018). *Post Occupancy Evaluation Towards Facilities Improvement for Students With Disabilities In University of Malaya*. 9(2), 1–10.
- Asakura, J., & Akagi, H. (2009). State-of-Charge (SOC)-Balancing Control of a Battery Energy Storage System Based on a Cascade PWM Converter. *IEEE Transactions on Power Electronics*, 24(6), 1628–1636.

- Asyraf, S. M., Heerwan, P. M., Izahar, I. M., Zulhilmi, I. M., Zikri, J. M., & Hern, S. C. (2019). Parameters estimation and calibration of BLDC motor for electric powered wheelchair. *AIP Conference Proceedings*, 2059(January).
- Atmur, S. D., & Thomas, S. E. (1996). Brake Rotors/Drums and Brake Pads Particularly Adapted for Aircraft/Truck/Train and other Heavy Duty Application.
- Atsmon, D., Akiva, & Hougui. (2017). *Enhanced Advanced Driver Assistance System (ADAS) System on Chip*.
- Ba, B. W., Watson, N., & Watson, N. (2016). *A Short History of Powered Wheelchairs A Short History of Powered Wheelchairs*. 0435(March).
- Beever, P., & Reynolds, T. (2017). *Brake Control*.
- Benavidez, P., & Jamshidi, M. (2011). Mobile Robot Navigation and Target Tracking System. *6th International Conference on System of Systems Engineering, Albuquerque, New Mexico, USA*, 299–304.
- Bera, T. K., Bhattacharya, K., & Samantaray, A. K. (2011). Evaluation of antilock braking system with an integrated model of full vehicle system dynamics. *Simulation Modelling Practice and Theory*, 19(10), 2131–2150.
- Berger, M., Côté, O., & Chebak, A. (2015). Development of a DC-link protection system for regenerative braking of electric vehicle using a pseudo-cascade controlled IGBT chopper. *2015 IEEE Transportation Electrification Conference and Expo, ITEC 2015*, 1.
- Bertocci, G., Frost, K., & Smalley, C. (2014). Public transit bus ramp slopes measured in situ. *Journal of Disabil Rehabil Assist Technology*, (May 2014), 1–6.
- Bridge, T. (2015). *Tokyo Motor Show 2015 indicates game changes for automotive sector*. 2. Retrieved from <http://thebridge.jp/en/2015/11/tms-2015-game-changes>
- Brown, K. E., Iñigo, R. M., & Johnson, B. W. (1990). Design, Implementation, and Testing of an Adaptable Optimal Controller for an Electric Wheelchair. *IEEE Transactions on Industry Applications*, 26(6), 1144–1157.
- Carrington, P., Hurst, A., & Kane, S. K. (2014). Wearables and chairables. *Proceedings of the 32nd Annual ACM Conference on Human Factors in Computing Systems - CHI '14*, (Figure 1), 3103–3112.
- Chen, J., Yu, J., Zhang, K., & Ma, Y. (2018). Mechatronics Control of regenerative braking systems for four-wheel-independently-actuated electric vehicles R , RR. *Mechatronics*, 50, 394–401.
- Chen, W., Jang, Y., Wang, J., Huang, W., Chang, C.-C., Mao, H.-F., & Wang, Y.-H. (2011). Wheelchair-Related Accidents: Relationship With Wheelchair-Using Behavior in Active Community. *YAPMR*, 92(6), 892–898.

- Chung, M., & Kim, Y. (2014). Design of Roof Type Dynamic Braking Resistor for Railway Carriage by using Thermal Analysis Requirement of Roof Type Dynamic Braking Resistor. *Journal of YAdvanced Science and Technology*, 47, 379–382.
- Claussen, H., & Eickhoff, J. (1999). *Procees for Controlling the Speed of a Vehicle Travelling on a Slope*.
- Cockrell, S., Lee, G., & Newman, W. (2013). Determining navigability of terrain using point cloud data. *IEEE ... International Conference on Rehabilitation Robotics : [Proceedings]*, 2013, 6650496.
- Cooper, R. A. (1993). Stability of a Wheelchair Controlled by a Human Pilot. *IEEE Transactions on Rehabilitation Engineering*, 1(4), 193–206.
- Cooper, R. A., Boninger, M. L., Cooper, R., Dobson, A. R., Kessler, J., Schmeler, M., & Fitzgerald, S. G. (2003). Use Of The Independence 3000 Ibot Transporter At Home And In The Community. *The Journal of Spinal Cord Medicine*, 26(1), 79–85.
- Cooper, R. A., Dvorznak, M. J., O'Connor, T. J., Boninger, M. L., & Jones, D. K. (1998). Braking Electric-Powered Wheelchairs: Effect of Braking Method, Seatbelt, and Legrests. *Archives of Physical Medicine and Rehabilitation*, 79(10), 1244–1249.
- Cooper, R. A., Wolf, E., Fitzgerald, S. G., Boninger, M. L., Ulerich, R., & Ammer, W. A. (2003). Seat and Footrest Shocks and Vibrations in Manual Wheelchairs with and without Suspension. *Archives of Physical Medicine and Rehabilitation*, 84(1), 96–102.
- Cooper, R. A., Wolf, E., Fitzgerald, S. G., Kellerher, A., Ammer, W., Boninger, M. L., & Cooper, R. (2004). Evaluation of selected sidewalk pavement surfaces for vibration experienced by users of manual and powered wheelchairs. *The Journal of Spinal Cord Medicine*, 27(5), 468–475.
- Corfman, T. A., Cooper, R. A., Fitzgerald, S. G., & Cooper, R. (2003). Tips and falls during electric-powered wheelchair driving: effects of seatbelt use, legrests, and driving speed | No commercial party having a direct financial interest in the results of the research supporting this article has or will confer a benefit on . *Archives of Physical Medicine and Rehabilitation*, 84(12), 1797–1802.
- De La Torre, S., Sánchez-Racero, A. J., Aguado, J. A., Reyes, M., & Martínez, O. (2015). Optimal Sizing of Energy Storage for Regenerative Braking in Electric Railway Systems. *IEEE Transactions on Power Systems*, 30(3), 1492–1500.
- Desmond, R., Dickerman, M., Fleming, J., Sinyukov, D., Schaufeld, J., & Padir, T. (2013). Development of Modular Sensors for Semi- Autonomous Wheelchairs. *Ieee*, 6.
- DiGiovine, M. M., Cooper, R. A., Boninger, M. L., Lawrence, B. M., VanSickle, D. P., & Rentschler, A. J. (2000). User assessment of manual wheelchair ride comfort and ergonomics. *Archives of Physical Medicine and Rehabilitation*, 81(4), 490–494.

- Ding, D., & Cooper, R. A. (2005). Electric-Powered Wheelchairs. *IEEE Control Systems*, 25(2), 22–34.
- Ehsani, M. (2010). Design and Control Methodology of Plug-in Hybrid Electric Vehicles. *IEEE Transactions on Industrial Electronics*, 57(2), 633–640.
- El-Sherbiny, Y. M., Hasouna, A. T., & Ali, W. Y. (2012). Friction coefficient of rubber sliding against flooring materials. *ARNP Journal of Engineering and Applied Sciences*, 7(1), 121–126.
- Elkholy, M. M., & Elhameed, M. A. (2015). Braking of Three Phase Induction Motors by Controlling Applied Voltage and Frequency Based on Particle Swarm Optimization Technique. *International Journal of Power Electronic and Drive System*, 5(4), 520–528.
- Evans, A. (1976). Automatic Adjusting Mechanism For A Disc Brake Assembly Having A Mechanically Actuated Parking Brake.
- F, Dunn, P. (2005). *Measurement and Data Analysis for Engineering and Science*.
- Fallon, C., Johannsson, H., Leonard, J. J., & Fallon, M. F. (2012). *Efficient scene simulation for robust monte carlo localization using an RGB-D camera " Efficient scene simulation for robust monte carlo localization using an RGB-D camera Terms of Use Efficient Scene Simulation for Robust Monte Carlo Localization using a.* 1663–1670.
- Farnsworth, J. M. (2011). *Methods and Systems for Regulating Hill Descent Speed of an Electric Vehicle*.
- Fattouh, A., Horn, O., & Bourhis, G. (2013). *Emotional BCI Control of a Smart Wheelchair*. 10(3), 32–36.
- Fišer, R., & Nedeljkovi, D. (2019). Induction Motor Broken Rotor Bar Detection Based on Rotor Flux Angle Monitoring. *Energy Conversion and Management*, 12(february 2019), 794.
- Fritsch, K. (2013). The Neoliberal Circulation of Affects: Happiness, accessibility and the capacitation of disability as wheelchair. *Health, Culture and Society*, 5(1), 135–149.
- Furukawa, Y., & Abe, M. (1997). Vehicle System Dynamics Advanced Chassis Control Systems for Vehicle Handling and Active Safety. *Vehicle System Dynamics*, 28(28), 2–3.
- Gadewar, S., & Jain, A. . (2017). Review of Braking System in Motor. *Proceeding of SARC International Conference*, 81–86. Retrieved from <http://www.mrkulik.ca/science-7/forces--structures>
- Ge, X., Wang, K., Guo, L., Yang, M., Lv, K., & Zhai, W. (2018). *Investigation on Derailment of Empty Wagons of Long Freight Train during Dynamic Braking*. 2018.

- Gökçe, C., Üstün, Ö., & Yeksan, A. Y. (2015). Dynamics and Limits of Electrical Braking. *Journal of Science and Technology*, 2, 268–272.
- Gökçe, C., Üstün, Ö., & Yeksan, A. Y. (2016). *Dynamics and limits of electrical braking*. (November 2013).
- González-gil, A., Palacin, R., & Batty, P. (2013). *Sustainable urban rail systems : Strategies and technologies for optimal management of regenerative braking energy*. 75, 374–388.
- Guo-Zhu, Z., Xiang, H., & Xing, P. (2016). Adaptive Model Predictive Control Research on Regenerative Braking for Electric Bus Cruising Downhill. *Journal of Advanced Manufacturing Systems*, 15(03), 133–150.
- Halim, A., & Almarshoud, A. F. (2008). Electronic Control of Single-phase Induction Motors Using AC Chopper. *Journal of Engineering Computer Science*, 1(2), 83–94.
- Han, J. F., Tao, J., Lu, H. J., & Xin, D. H. (2014). Development and Prospect of Regenerative Braking Technology of Electric Vehicles. *Renewable Energy and Environmental Technology*, 448, 3164–3171.
- Heerwan, M., Peeie, B., Ogino, H., & Oshinoya, Y. (2016). *Skid control of a small electric vehicle with two in-wheel motors : simulation model of ABS and regenerative brake control*. 8265(June).
- Heerwan, P. M., Ashraf, S. M., & Ishak, M. I. (2017). Combination of Skid Control and Direct Yaw Moment Control to Improve the Safety and Stability of the Small Electric Vehicle with Two In-Wheel Motors. *MATEC Web of Conferences*, 135, 00022.
- Henderson, M., Kelly, S., Horne, R., Gillham, M., & Pepper, M. (2014). Powered wheelchair platform for assistive technology development. *2014 Fifth International Conference on Emerging Security Technologies (EST)*.
- Hong, E. K., Dicianno, B. E., Pearlman, J., Cooper, R., & Cooper, R. A. (2016). Comfort and stability of wheelchair backrests according to the TAWC (tool for assessing wheelchair discomfort). *Disability and Rehabilitation: Assistive Technology*, 11(3), 223–227.
- Howley, C. (2001). *Document resume*.
- Jain, S., & Argall, B. (2014). Automated perception of safe docking locations with alignment information for assistive wheelchairs. *IEEE International Conference on Intelligent Robots and Systems*, (Iros), 4997–5002.
- Jordan, S. N. (2012). *A Smart Wheelchair System using a Combination of Stereoscopic and Spherical Vision Cameras*.

- Joseph Godfrey, A., & Sankaranarayanan, V. (2018). A new electric braking system with energy regeneration for a BLDC motor driven electric vehicle. *Engineering Science and Technology, an International Journal*, 21(4), 704–713.
- Kamen, D. L., Ambrogi, R. R., Heinzmann, J. D., Heinzmann, R. K., Herr, D., & Morrell, B. J. (2004). Control of a balancing personal vehicle.
- Kim, J., Yim, E., Jeon, C., Jung, C., & Han, B. (2012). Cold performance of various biodiesel fuel blends at low temperature. *International Journal of ...*, 13(2), 293–300.
- Kirby, R. L., & Macleod, D. A. (2001). Wheelchair-related injuries reported to the National Electronic Injury Surveillance System: An update. *Proc. RESNA 2001 Annu. Conf.*, 385–387.
- Kirby, R. L., Sampson, M. T., Thoren, F. A., & MacLeod, D. A. (1995). Wheelchair stability: effect of body position. *J Rehabil Res Dev*, 32(4), 367–372.
- Kirtley, J. L. (2003). Permanent Magnet “Brushless DC” Motors. *Introduction to Power Systems - Class Notes Chapter 12*.
- Kulp, W. R., Kulp, W. R., & Cavusoglu, M. C. (2012). *Robotic person-following in cluttered environment*.
- Kwarciaak, A. M. (2009). Curb descent testing of suspension manual wheelchairs. *The Journal of Rehabilitation Research and Development*, 45(1), 73–84.
- Leaman, J., & La, H. M. (2015). iChair: Intelligent Powerchair for Severely Disabled People. *The ISSAT International Conference on Modeling of Complex Systems and Environments*.
- Lendal Pty. Ltd. (2001). Rehabilitation Products: GLIDE Series 8. Retrieved from 25 Ledger Rd Balcatta, Western Australia 6021 Australia website: http://www.glide.com.au/wp-content/uploads/2016/12/S8_Owners_Manual_062006.pdf
- Li, L., Zhang, Y., Yang, C., Yan, B., & Martinez, C. M. (2016). Model predictive control-based efficient energy recovery control strategy for regenerative braking system of hybrid electric bus. *Energy Conversion and Management*, 111, 299–314.
- Li, W., Du, H., & Li, W. (2018). *Driver intention based coordinate control of regenerative and plugging braking for electric vehicles with in-wheel PMSMs*.
- Lin, C. H., Liu, H. W., & Wang, C. M. (2010). Design and implementation of a bi-directional power converter for electric bike with charging feature. *Proceedings of the 2010 5th IEEE Conference on Industrial Electronics and Applications, ICIEA 2010*, 538–543.

- Lin, H., & Song, C. (2011). Design of a fuzzy logic controller for ABS of Electric Vehicle based on AMESim and Simulink. *Proceedings 2011 International Conference on Transportation, Mechanical, and Electrical Engineering (TMEE)*, 779–782.
- Lin, W., Lin, C., Member, S., Hsu, P., & Wu, M. (2014). Realization of Anti-Lock Braking Strategy for Electric Scooters. *IEEE Transactions on Industrial Electronics*, 61(6), 2826–2833.
- Linda, Fehr; Edwin, Langbein; Steven, B. S. (2000). Adequacy of power wheelchair control interface for persons with severe disabilities: A clinical survey. *Journal of Rehabilitation Research and Development*, 37(may/june), 353–360.
- Lu, J., & DePoyster, M. (2002). Multiobjective optimal suspension control to achieve integrated ride and handling performance. *IEEE Transactions on Control Systems Technology*, 10(6), 807–821.
- Lu, J., Johnson, K., & Meyers, Joseph, C. (2016). *Vehicle Stability Control System and Method*.
- Luo, R. C., Tse Min Chen, & Meng Hsien Lin. (1999). Automatic guided intelligent wheelchair system using hierarchical grey-fuzzy motion decision-making algorithms. *Proceedings 1999 IEEE/RSJ International Conference on Intelligent Robots and Systems. Human and Environment Friendly Robots with High Intelligence and Emotional Quotients (Cat. No.99CH36289)*, 2, 900–905.
- Luo, Y., Han, Y., Chen, L., & Li, K. (2015). *Downhill safety assistance control for hybrid electric vehicles based on the downhill driver 's intention model*.
- Maeda, A., Teranishi, T., Sato, S., Itoh, M., Hokimoto, N., Fujimura, K., ... Saitoh, E. (2018). *Analysis of accidents during rehabilitation training at an acute-care hospital*. 4(4), 97–102.
- Makki, A., & Siy, P. (2001). A Robust Traction Controller Design Using The Theory of Variable Structure System. *Journal Electric and Electronic Engineering*, 2, 356–359.
- Massy-westropp, N. M., Gill, T. K., Taylor, A. W., Bohannon, R. W., & Hill, C. L. (2011). Hand Grip Strength: age and gender stratified normative data in a population-based study. *BMC Research Notes*, 4(1), 127.
- Mayer, R. E., & Gallini, J. K. (1990). When Is an Illustration Worth Ten Thousand Words? *Journal of Educational Psychology*, 82(4), 715–726.
- Mazumder, O., Kundu, A. S., Chattaraj, R., & Bhaumik, S. (2014). Holonomic wheelchair control using EMG signal and joystick interface. *2014 Recent Advances in Engineering and Computational Sciences, RA ECS 2014*, 6–8.
- Mehta, S., & Hemamalini, S. (2017). A Dual Control Regenerative Braking Strategy for Two-Wheeler Application. *Energy Procedia*, 117, 299–305.

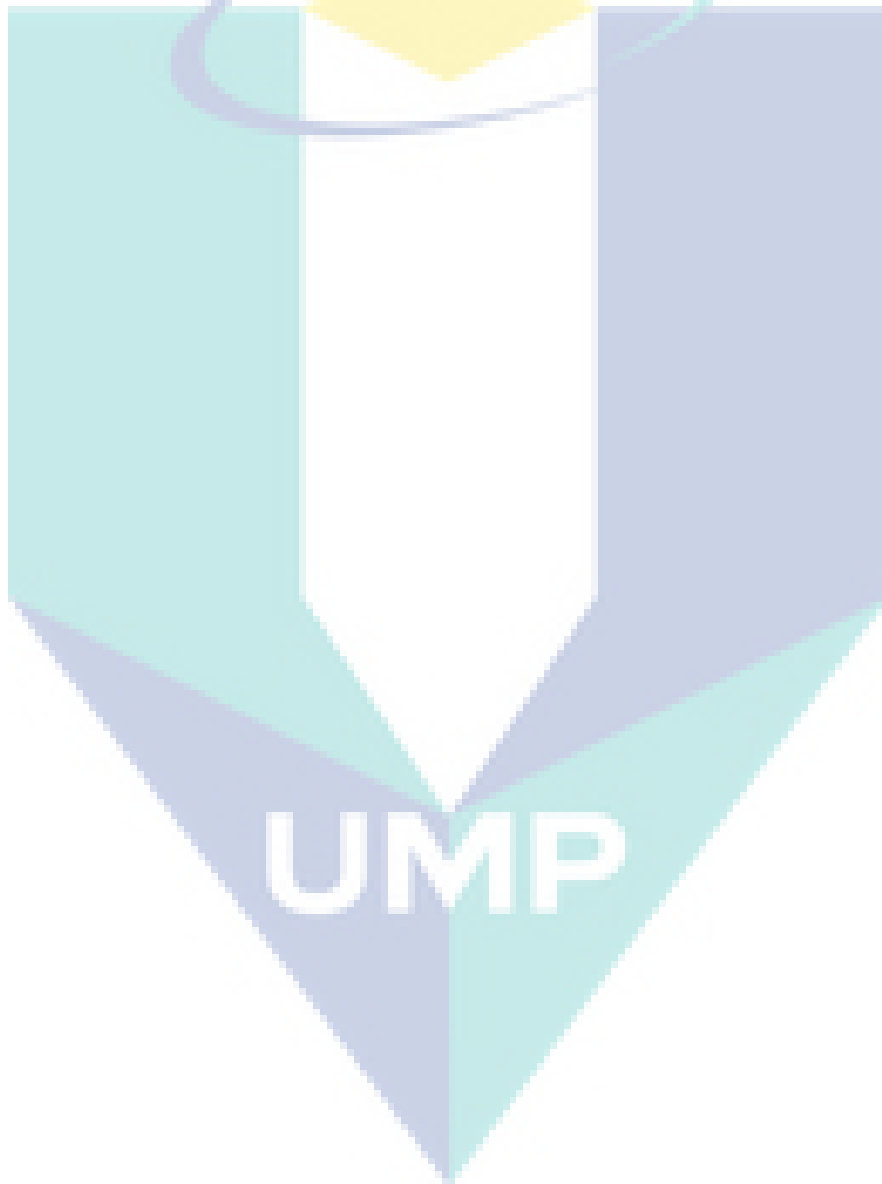
- Millán, J. R. (2013). BCI: Lessons from tests with impaired users. *Annals of Physical and Rehabilitation Medicine*, 56, e373. Retrieved from <http://ovidsp.ovid.com/ovidweb.cgi?T=JS&PAGE=reference&D=emed11&NEWS=N&AN=71225019>
- Model, C. Y. (2017). *Lightweight & Foldable KD Smart Chair*. 1–5.
- Nasari, F., Farjah, E., & Ghanbari, T. (2017). An efficient regenerative braking system based on battery/supercapacitor for electric, hybrid, and plug-in hybrid electric vehicles with BLDC motor. *IEEE Transactions on Vehicular Technology*, 66(5), 3724–3738.
- Nazri, N. A., Yasar, M., Razip, M. H. M., Jelani, K. M., & Sani, M. S. M. (2019). Dynamics Investigation on Motorcycle Chassis Based on Finite Element Modelling and Updating. *IOP Conference Series: Materials Science and Engineering*, 469, 012103.
- Obed, A. A., Abdulabbas, A. K., & Chasib, A. J. (2016). Plugging Braking of Two-PMSM Drive in Subway Applications with Fault -Tolerant Operation Plugging Braking of Two-PMSM Drive in Subway Applications with Fault -Tolerant Operation. *Journal Electric and Electronic Engineering*, 12(August), 1–11.
- Ohnabe, H., & Mizuguchi, F. (2001). Turning characteristics and stability of Manual Wheelchair. *Proceedings of the 23rd Annual EMBS International Conference*, 1408–1411.
- Okajima, H., Yonaha, S., Matsunaga, N., & Kawaji, S. (2010). Direct Yaw-moment Control method for electric vehicles to follow the desired path by driver. *SICE Annual Conference 2010, Proceedings Of*, 642–647.
- Pan, F., Wang, Y. I., & Han, R. (2002). *MOTOR*. (November), 24–27.
- Pasteau, F., Krupa, A., & Babel, M. (2014). Vision-based assistance for wheelchair navigation along corridors. *Proceedings - IEEE International Conference on Robotics and Automation*, 4430–4435.
- Pavasson, J., Ljung, A. L., Karlberg, M., Larsson, I. A. S., Johansson, S., & Lundström, T. S. (2014). Challenges and opportunities within simulation-driven functional product development and operation. *Procedia CIRP*, 22(1), 169–174.
- Pavec, D., Aubin, C.-É., Aissaoui, R., Parent, F., & Dansereau, J. (2001). Kinematic modeling for the assessment of wheelchair user's stability. *IEEE Transactions on Neural Systems and Rehabilitation Engineering*, 9(4), 362–368.
- Peeie, M. H. Bin, Ogino, H., & Oshinoya, Y. (2016). Skid control of a small electric vehicle with two in-wheel motors: simulation model of ABS and regenerative brake control. *International Journal of Crashworthiness*, 21(5), 396–406.

- Peeie, M. H., Ogino, H., & Oshinoya, Y. (2013). Skid control of small electric vehicle (Effect of the regenerative braking force to the hysteresis of friction brake force). *Proceedings - 2013 IEEE Conference on Systems, Process and Control, ICSPC 2013*, (December), 46–51.
- Peeie, M. H., Ogino, H., & Oshinoya, Y. (2014). *Skid control of small electric vehicle with hydraulic-mechanical hybrid brake system (Effect of ABS and regenerative brake control on an icy road). 1(5)*, 1–15.
- Peng, D., Zhang, Y., Yin, C., & Zhang, J. (2008). Combined Control of a Regenerative Braking and Antilock Braking System for Hybrid Electric Vehicles. *International Journal of Automotive Technology*.
- Rakesh, M., & Narasimham, P. V. R. L. (2012). Different Braking Techniques Employed to a Brushless DC Motor Drive used in Locomotives. *International Electrical Engineering Journal (IEEJ)*, 3(2), 784–790.
- Rao, R. S., Conn, K., Jung, S. H., Katupitiya, J., Kientz, T., Kumar, V., ... Taylor, C. J. (2002). *Human robot interaction: Application to smart wheelchairs. 4(Icra)*, 3583–3588.
- Ren, B., Chen, H., Zhao, H., & Yuan, L. (2016). MPC-based yaw stability control in in-wheel-motored EV via active front steering and motor torque distribution. *Mechatronics*, 38, 103–114.
- Rouhani, A., Kord, H., & Mehrabi, M. (2013). A comprehensive method for optimum sizing of hybrid energy systems using intelligence evolutionary algorithms. *Indian Journal of Science and Technology*, 6(6), 4702–4712.
- Sakamoto, Y., Kashiwagi, T., Tanaka, M., Hasegawa, H., Sasakawa, T., & Fujii, N. (2012). *Rail Brake System Using a Linear Induction Motor for Dynamic Braking. 178(2)*, 342–349.
- Sankardoss, V., & Geethanjali, P. (2017). Parameter estimation and speed control of a PMDC motor used in wheelchair. *Energy Procedia*, 117, 345–352.
- Sarkar, D., & Mukherjee, P. . (1992). Temperature Rise of an Induction Motor during Plugging. *IEEE Transaction on Energy Conversion*, 7(1).
- Savary, W., & Soennecken, H. (1975). Lining For Brake Shoes.
- Seidel, H., & Heide, R. (1986). Long-term effects of whole-body vibration: a critical survey of the literature. *Int Arch Occup Environ Health*, 58(1), 1–26. Retrieved from <http://www.ncbi.nlm.nih.gov/pubmed/3522434>
- Seki, H. (2010). Capacitor Regenerative Braking Control of Power-Assisted Wheelchair for Safety Downhill Road Driving. *International Workshop on Advanced Motion Control, AMC*, 56(5), 1393–1400.

- Seki, H., Ishihara, K., & Tadakuma, S. (2008). Novel regenerative braking control of electric power assisted wheelchair for optimal velocity driving on downhill road. *International Workshop on Advanced Motion Control, AMC, 1*, 510–515.
- Seki, H., Ishihara, K., & Tadakuma, S. (2009). Novel Regenerative Braking Control of Electric Power -Assisted Wheelchair for Safety Downhill Road Driving. *2009 2nd IEEE RAS and EMBS International Conference on Biomedical Robotics and Biomechatronics, BioRob 2010*, 56(5), 143–148.
- Shehan, Mark, A., Crombez, S., & Xu, Jack, H. (2000). *Vehicle Speed Control with Continuously Variable Braking Torque*.
- Shuyang, Z., & Chun, J. I. N. (2013). *Research on Engine Cranking Process in Downhill Braking Condition for an Electric Drive Underground Dump Truck*. 364, 92–96.
- Simpson, R. C. (2005). Smart wheelchairs: A literature review. *The Journal of Rehabilitation Research and Development*, 42(4), 423.
- Sinyukov, D., Desmond, R., Dickerman, M., Fleming, J., Schaufeld, J., & Padir, T. (2014). Multi-modal control framework for a semi-autonomous wheelchair using modular sensor designs. *Intelligent Service Robotics*, 7(3), 145–155.
- Smith, D., & Leggat, P. (2005). Whole-body vibration: Health effects, measurement and minimization. *Professional Safety*, (July), 35–40.
- Soleimani, Y., Cruz, S. M. A., Member, S., & Haghjoo, F. (2018). *Broken Rotor Bar Detection in Induction Motors Based on Air-Gap Rotational Magnetic Field Measurement*. 1–10.
- Somrajan, N. R., & Sreekanth, P. K. (2016). Plugging Braking for Electric Vehicles Powered by DC Motor. *International Journal of Modern Trends in Engineering and Research*, 3(1), 352–356.
- Sun, L., & Xu, B. (2018). *An Improved Method for Discerning Broken Rotor Bar Fault and Load Oscillation in Induction Motors*.
- Tadano, S., & Tsukada-, A. (2000). Some Mechanical Problems to Use Electric Wheelchairs in a Snowy Region. *Journal of Human Biomechanic and Injury*, 199–200.
- Tan, H. S., & Tomizuka, M. (1990). Discrete Time Controller Design for Robust Vehicle Traction. *IEEE Control Systems Magazine*, 10(3), 107–113.
- Thomas, F. E., & James, F. A. (1988). Suspension System for Powered Wheelchair.
- Torres, H. G. (2000). Self-Levelling Seat for A Wheelchair.
- Tsai, M.-T., Chun, S., & Chen, S.-L. (1999). Disk Brake Device for use With a Bicycle.

- Ummat, S., & Kirby, R. L. (1994). Nonfatal wheelchair-related accidents reported to the National Electronic Injury Surveillance System. *American Journal of Physical Medicine & Rehabilitation / Association of Academic Physiatrists*, Vol. 73, pp. 163–167.
- Urbano, M., Fonseca, J., Nunes, U., & Zeilinger, H. (2011). Extending a smart wheelchair navigation by stress sensors. *IEEE International Conference on Emerging Technologies and Factory Automation, ETFA*, 2–5.
- Wang, B., Huang, X., Wang, J., & Guo, X. (2015). A robust wheel slip ratio control design combining hydraulic and regenerative braking systems for in-wheel-motors-driven electric Vehicles. *Journal of the Franklin Institute*, 352(2), 577–602.
- William, W., & Payandeh, S. (1999). A study of active shifting of human driver for improving wheelchair tipping stability. *Experimental Robotics Lab., Simon Fraser Univ., Burnaby, BC Canada*, 1–7. Retrieved from <http://www.ensc.sfu.ca/research/erl/med/med4.pdf>
- Xiang, H., Chany, A.-M., & Smith, G. A. (2006). Wheelchair related injuries treated in US emergency department. *Journal of Injury Prevention*, (JUNE 2015), 8–12.
- Xu, G., Member, S., Xu, K., & Member, S. (2016). Fully Electrified Regenerative Braking Control for Deep Energy Recovery and Maintaining Safety of Electric Vehicles. *IEEE Transactions on Vehicular Technology*, 65(3), 1186–1198.
- Xu, Y., Mei, B., Xiao, L., Xia, W., & Tan, G. (2017). Combined Hill Descent Braking Strategy for Heavy Truck in the Featured-Slope. *SAE International in United States*, 1.
- Yang, J., Member, S., Fletcher, J. E., Reilly, J. O., & Member, S. (2010). A Series-Dynamic-Resistor-Based Converter Protection Scheme for Doubly-Fed Induction Generator During Various Fault Conditions. 25(2), 422–432.
- Yang, S., & Chen, J. (2011). Investigation of a dynamic braking scheme for switched reluctance motor drives. *IECON 2011 - 37th Annual Conference of the IEEE Industrial Electronics Society*, 1909–1914.
- Yang, Z., Xia, H., Wang, B., & Lin, F. (2014). An overview on braking energy regeneration technologies in Chinese urban railway transportation. *2014 International Power Electronics Conference, IPEC-Hiroshima - ECCE Asia 2014*, 2133–2139.
- Yokota, S., Hashimoto, H., Chugo, D., Ohyama, Y., & She, J. (2011). Absorption of ambiguous human motion on Human Body Motion Interface. *Proceedings - ISIE 2011: 2011 IEEE International Symposium on Industrial Electronics*, 853–858.
- Yoong, M. K., Gan, Y. H., Gan, G. D., Leong, C. K., Phuan, Z. Y., Cheah, B. K., & Chew, K. W. (2010). Studies of regenerative braking in electric vehicle. *IEEE Conference on Sustainable Utilization and Development in Engineering and Technology 2010, STUDENT 2010 - Conference Booklet*, (November), 40–45.

- Yoshida, K., & Hamano, H. (2002). Motion dynamics of a rover with slip-based traction model. *Proceedings 2002 IEEE International Conference on Robotics and Automation (Cat. No.02CH37292)*, 3(May), 3155–3160.
- Zhu, C. K., & Dan, S. H. (2014). Study on Optimal Dynamic Braking Resistor of Induction Motor. *Advanced Materials Research*, 1070–1072, 1222–1227.
- Zijian Zhang, G. X. (2010). Regenerative Braking for Electric Vehicle based on Fuzzy Logic Control Strategy. *2nd International Conference on Mechanical and Electronics Engineering (ICMEE 2010)*, 1(Icmee), 319–323.



**APPENDIX A
GANTT CHART**

Activities	Year 1												year 2				
	1	2	3	4	5	6	7	8	9	10	11	12	1	2	3	4	5
Literature Review	█	█	█	█	█	█	█										
Experiment on braking performance between mechanical and electrical						█	█	█									
Design motor braking controller in Myrio								█									
Analyze braking performance by using motor braking controller at slope									█	█	█						
Parameters estimation from actual EPW							█	█			█	█					
Modelling EPW in MATLAB Simulink and validation								█	█	█	█	█	█	█			
Design motor braking controller in MATLAB Simulink											█	█					
Simulate braking performance by using motor braking controller at slope condition													█				
Analyze data						█	█		█	█	█	█	█	█			
Writing Journal/Paper					█			█						█			
Writing Thesis			█	█	█	█	█	█	█	█	█	█	█	█	█		

APPENDIX B
SAMPLE APPENDIX 2

Parts	Pages
Raw material, shape and dimension	2
Common parts for purchasing	2
1. Full assembly (both sides)	
1.1 Isometric view	3
1.2 Front and side view	4
2. Clamp	
2.1 Clamp	5
2.2 Assembly of both clamp	6
3. Part 2	7
4. Part 3	8
5. Part 4	9
6. Part 5	10
7. Part 6	11
8. Part 7	12
9. Part 8	13
10. Assembly part by part	
10.1 Assembly of clamp and part 2	14
10.2 Assembly of clamp and part 3	15
10.3 Assembly of part 4, 5 and 6	16
10.4 Assembly of part 6 and 7	17
10.5 Assembly of part 3, 4 and 8	18
10.6 Assembly of part 2 and 4	19

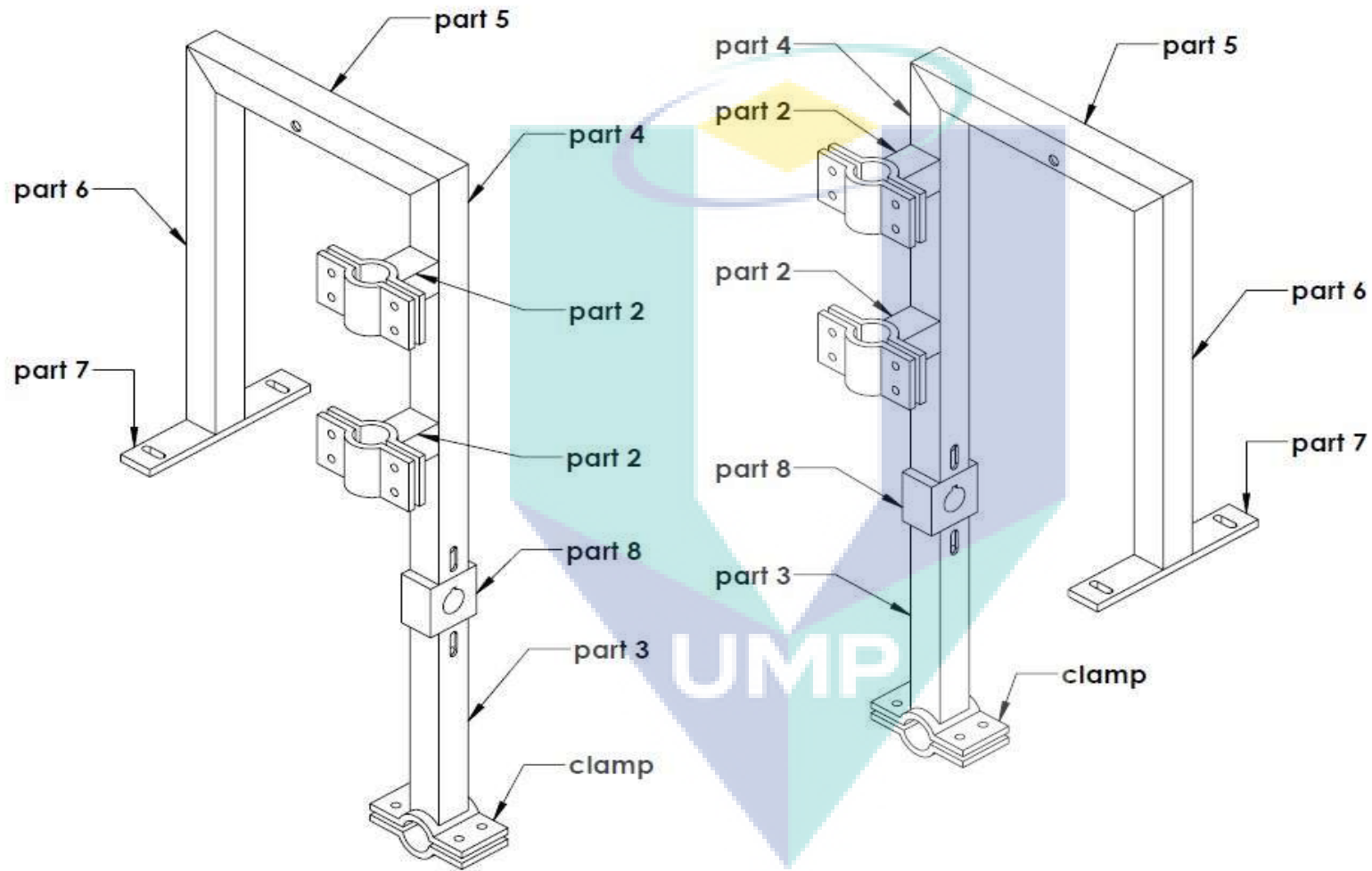
Raw material, shape and dimension

Part	Raw Material shape	Dimension (mm)			Quantity
		Length	Width	Height	
Clamp	Solid mild steel	190	40	83.5	2
2	Hollow square (thick 2mm)	25.4	25.4	40	4
3	Hollow square (thick 2mm)	25.4	25.4	165	2
4	Hollow square (thick 2mm)	25.4	25.4	335	2
5	Hollow square (thick 2mm)	25.4	25.4	225	2
6	Hollow square (thick 2mm)	25.4	25.4	310	2
7	Solid mild steel	25.4	140	6	2
8	Solid mild steel	100	40	40	2

Common parts for purchasing

Material	Specifications	Quantity
M6 bolt	L = 25mm	24
M6 bolt	L = 35mm	4
M6 nut		28
M6 washer		56

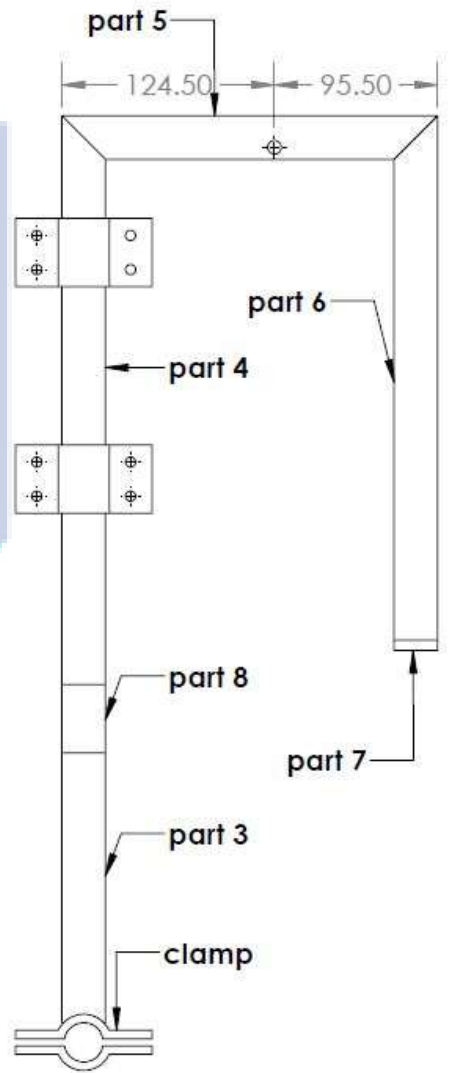
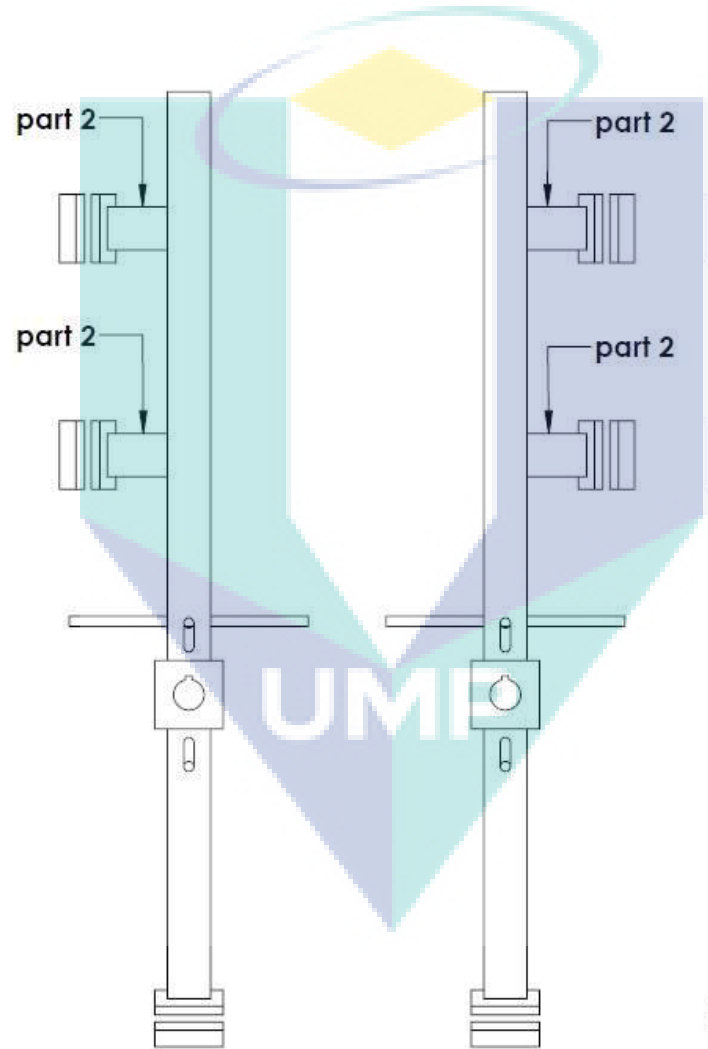
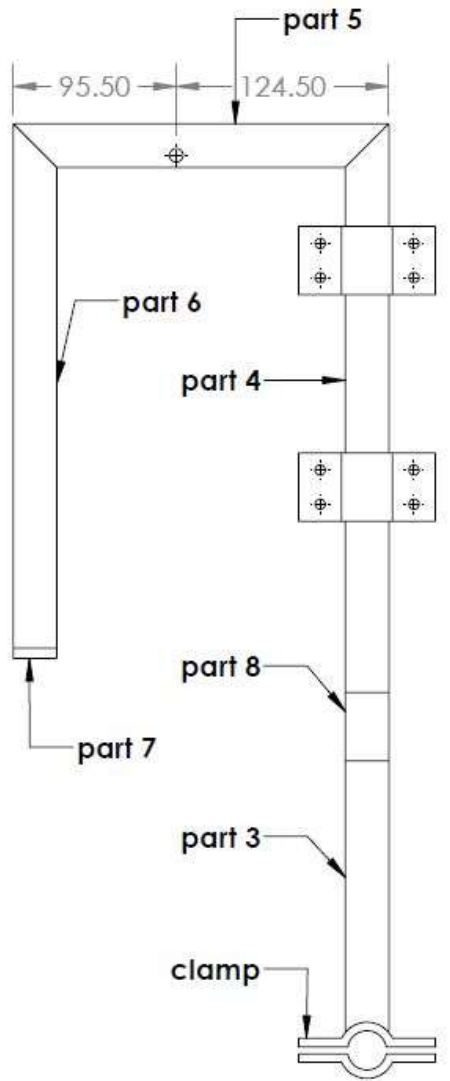
Full assembly



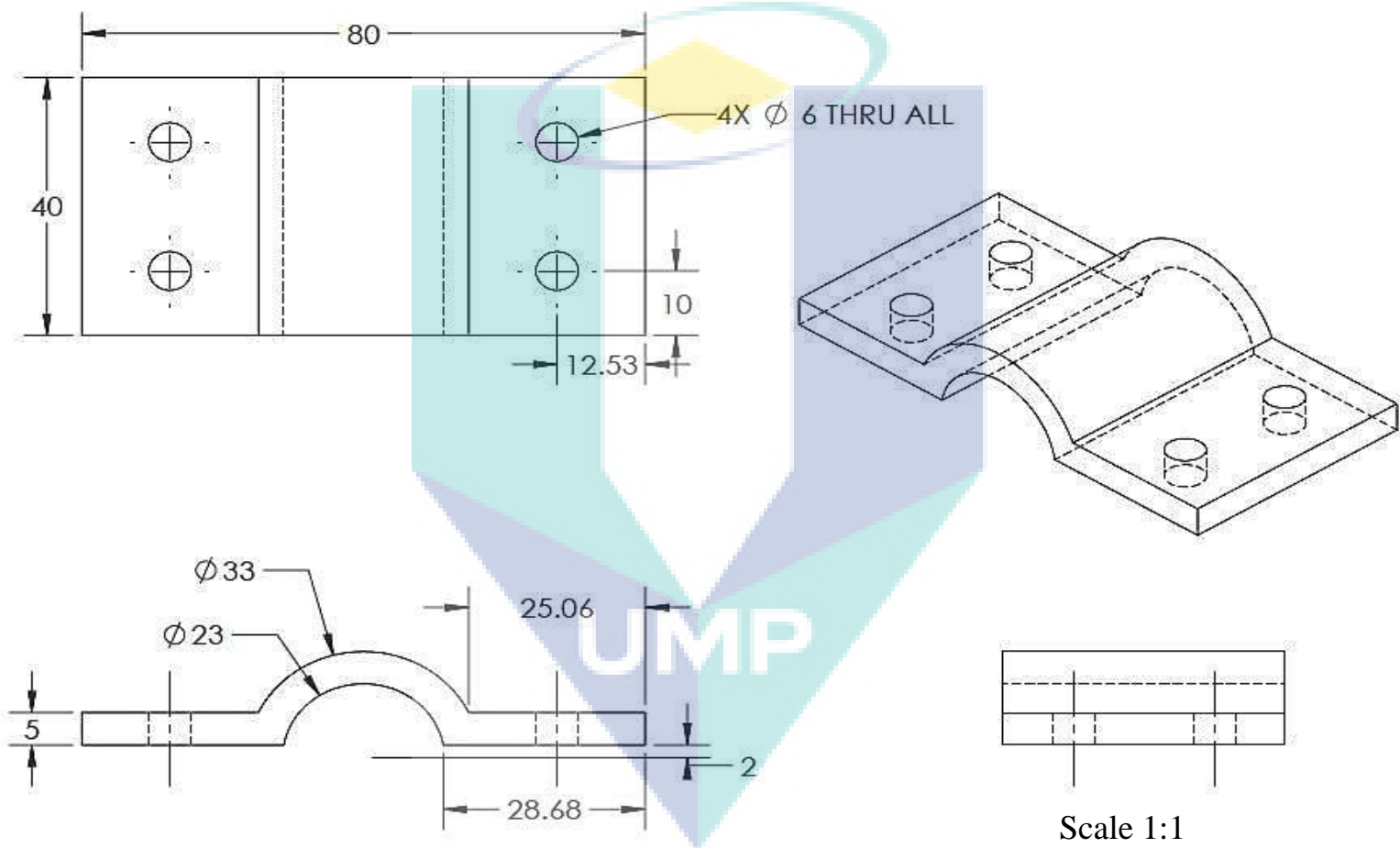
Right assembly

Left assembly

Scale 1:4.4



Clamp

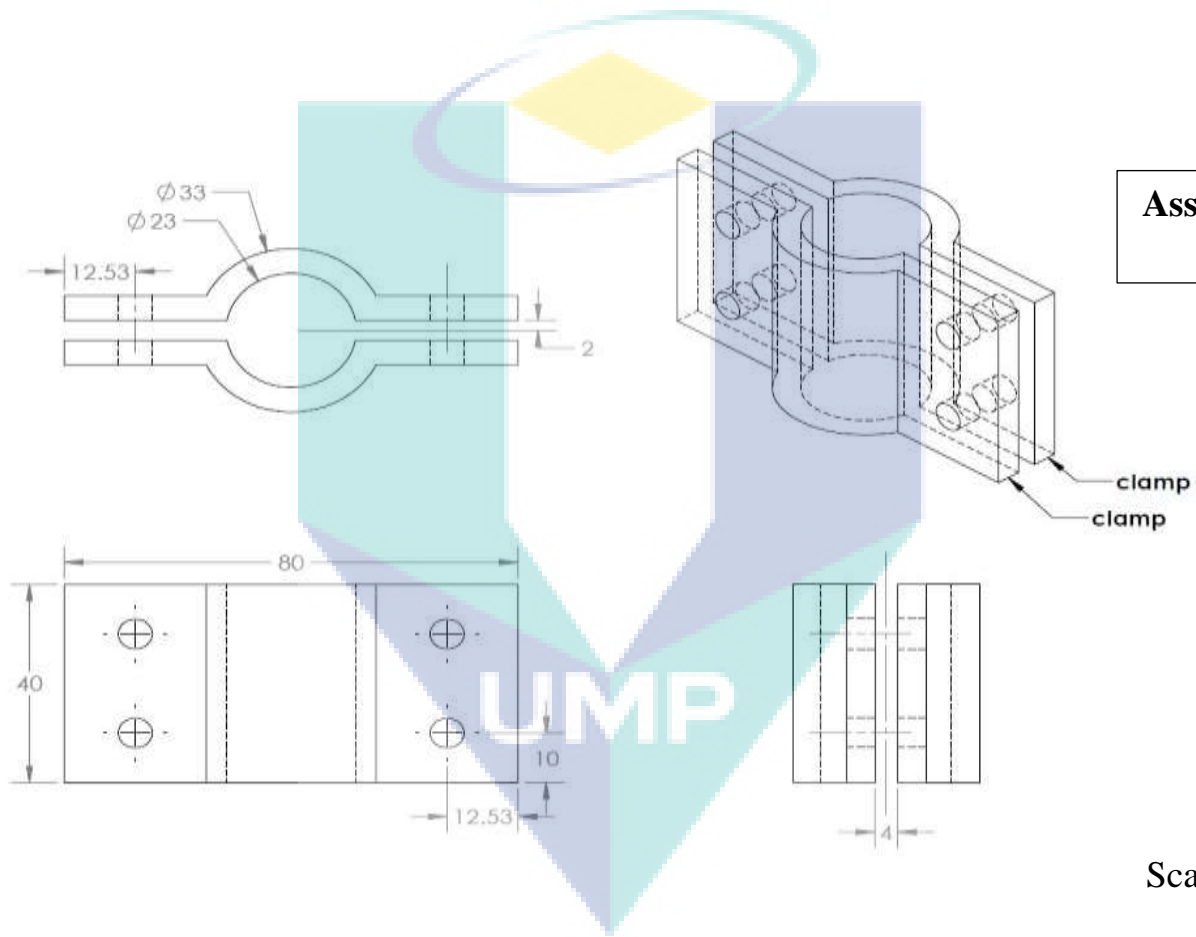


Material	Dimension (length x width x height)	Quantity
----------	-------------------------------------	----------

Solid mild steel

190 x 40 x 83.5 mm

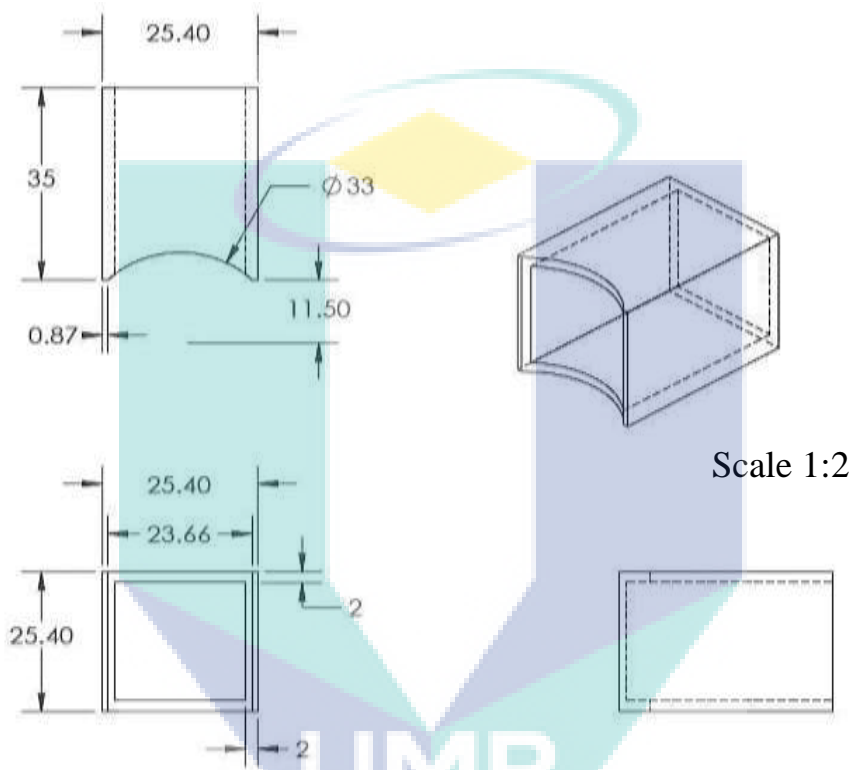
2



**Assemble both
clamp**

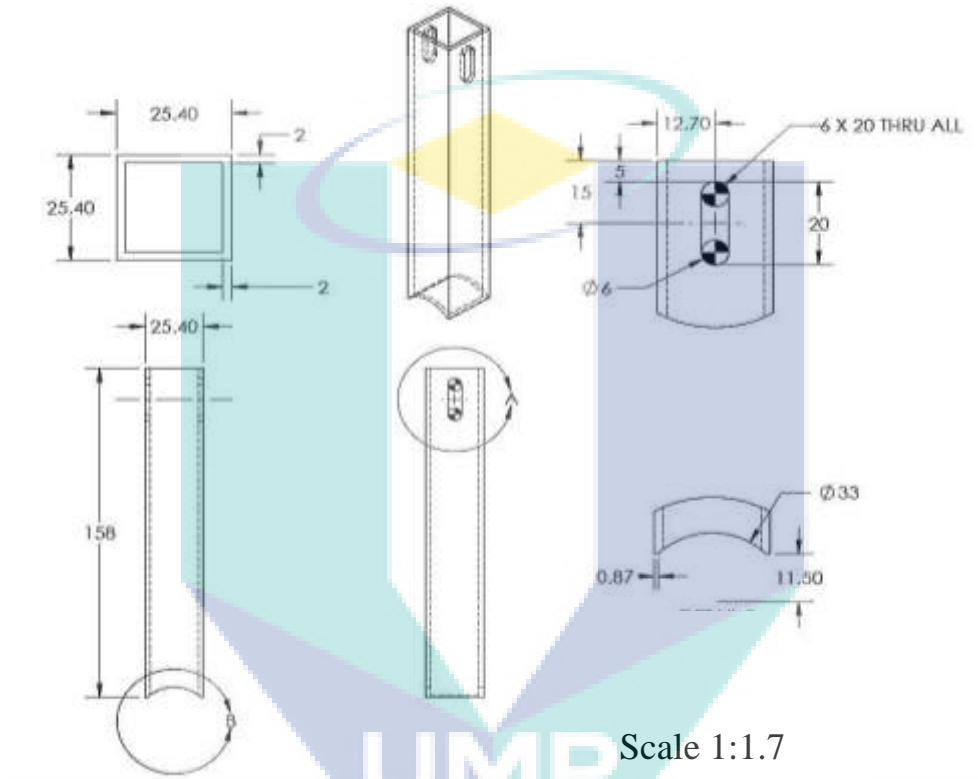
Scale 1:1.3

Part 2



Material	Dimension (length x width x height)	Quantity
Hollow square (thick 2mm)	25.4 x 25.4 x 40 mm	4

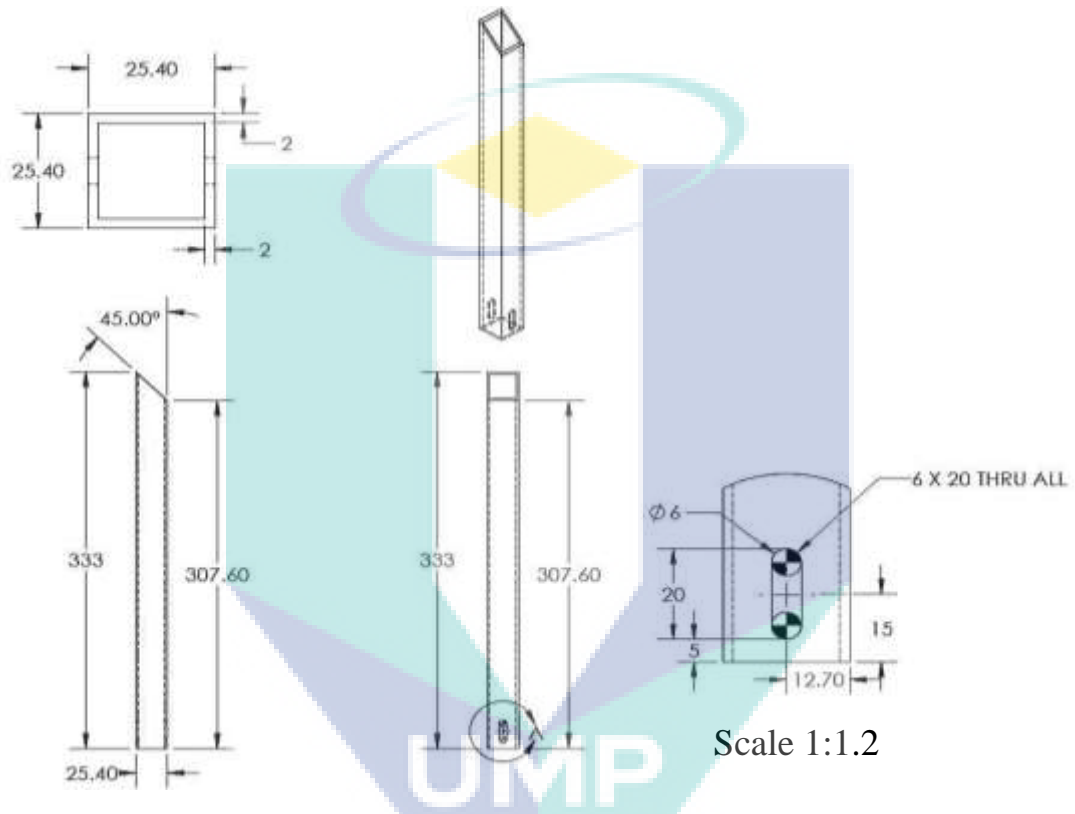
Part 3



Scale 1:1.7

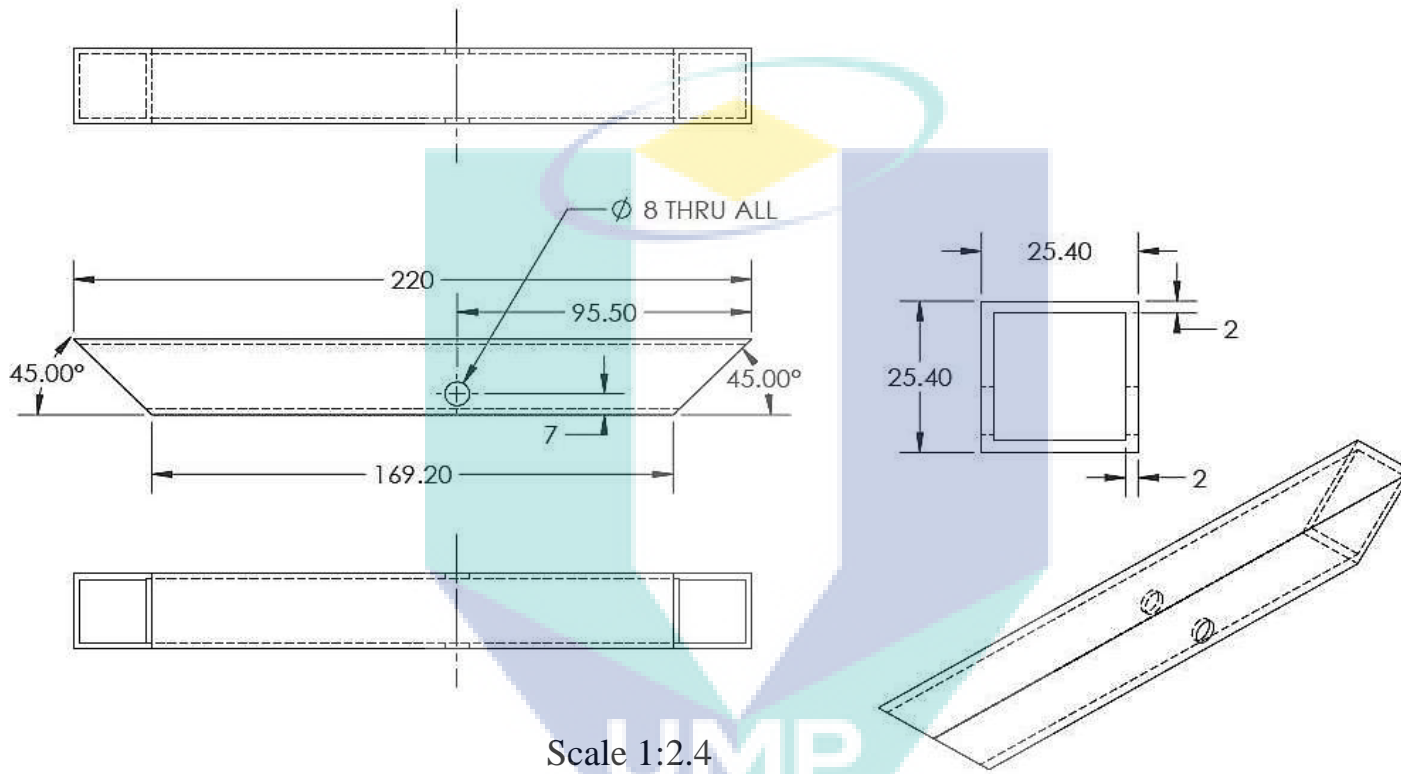
Material	Dimension (length x width x height)	Quantity
Hollow square (thick 2mm)	25.4 x 25.4 x 165 mm	2

Part 4



Material	Dimension (length x width x height)	Quantity
Hollow square (thick 2mm)	25.4 x 25.4 x 335 mm	2

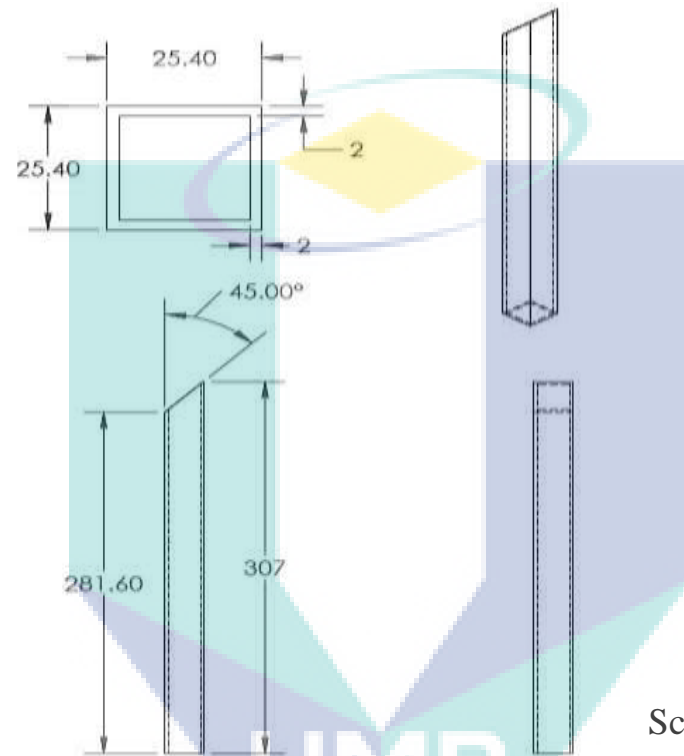
Part 5



Scale 1:2.4

Material	Dimension (length x width x height)	Quantity
Hollow square (thick 2mm)	25.4 x 25.4 x 225 mm	2

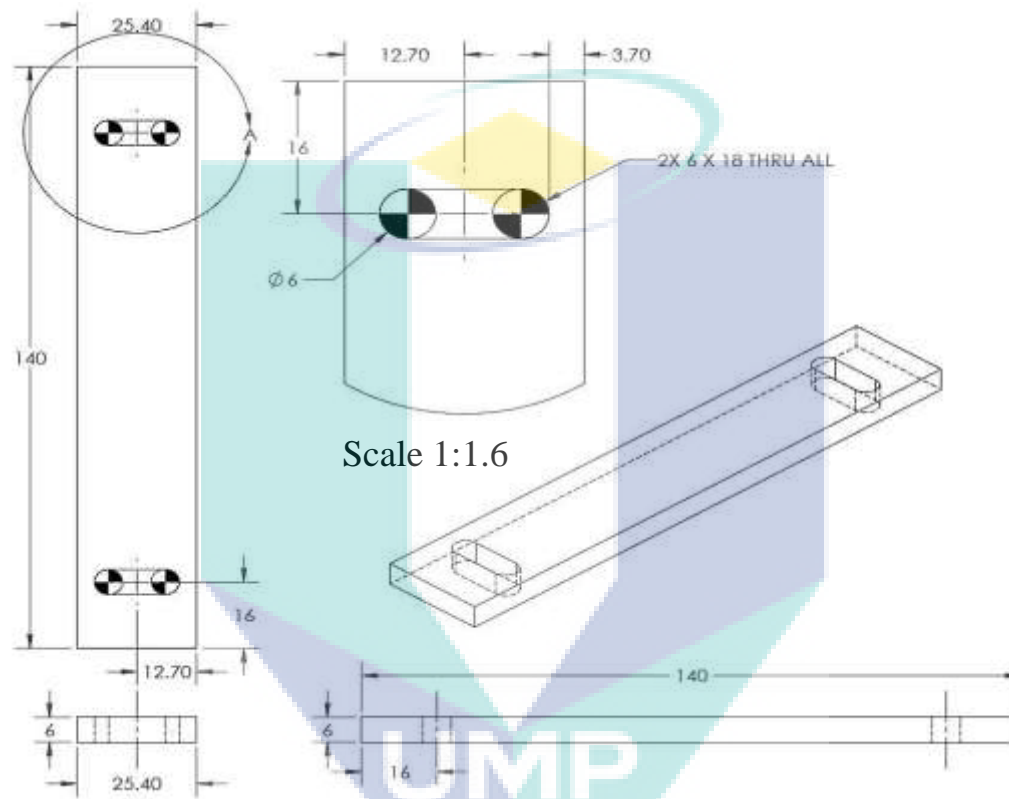
Part 6



Scale 1:2.1

Material	Dimension (length x width x height)	Quantity
Hollow square (thick 2mm)	25.4 x 25.4 x 310 mm	2

Part 7

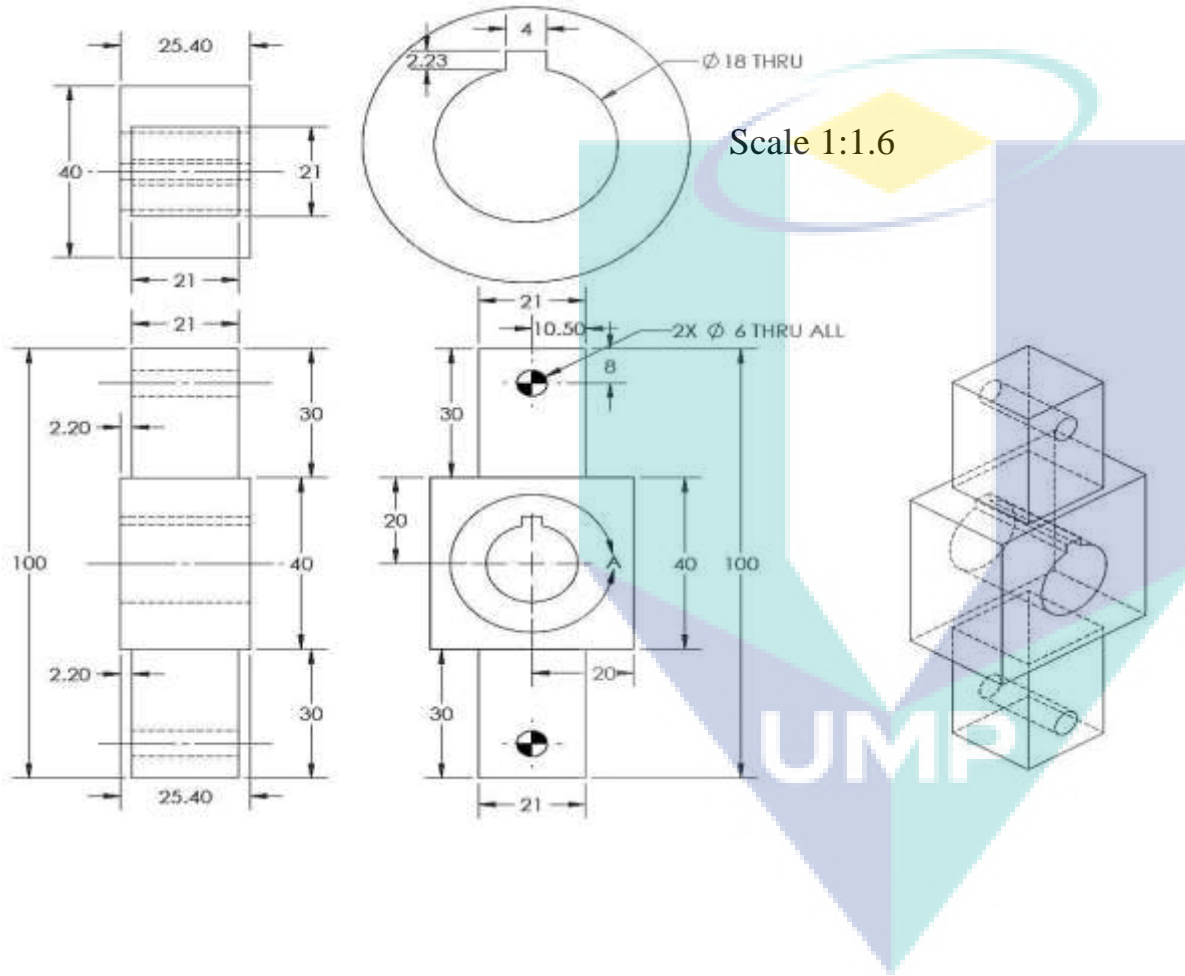


Material
Solid mild steel

Dimension (length x width x height)
25.4 x 140 x 6 mm

Quantity
2

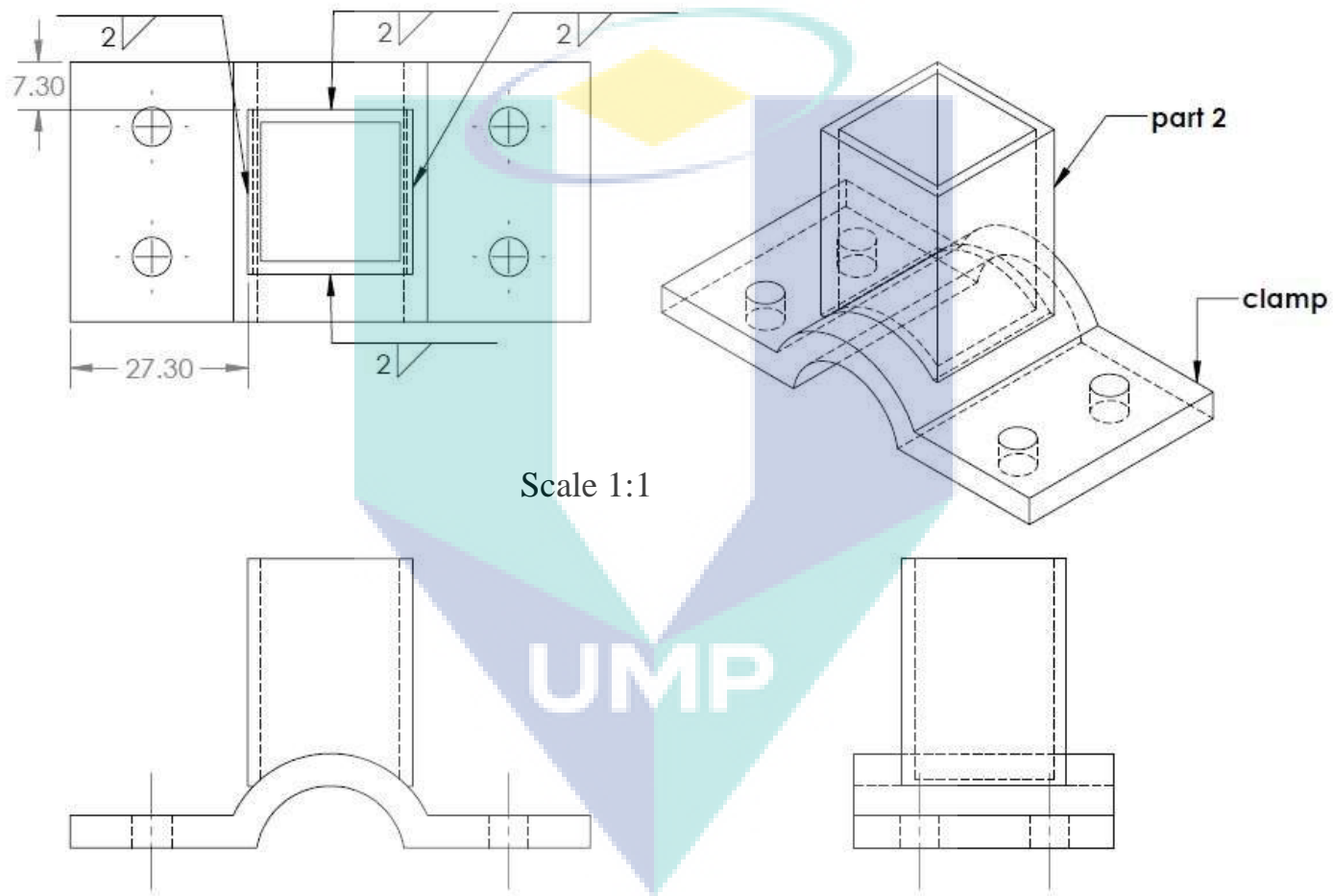
Part 8



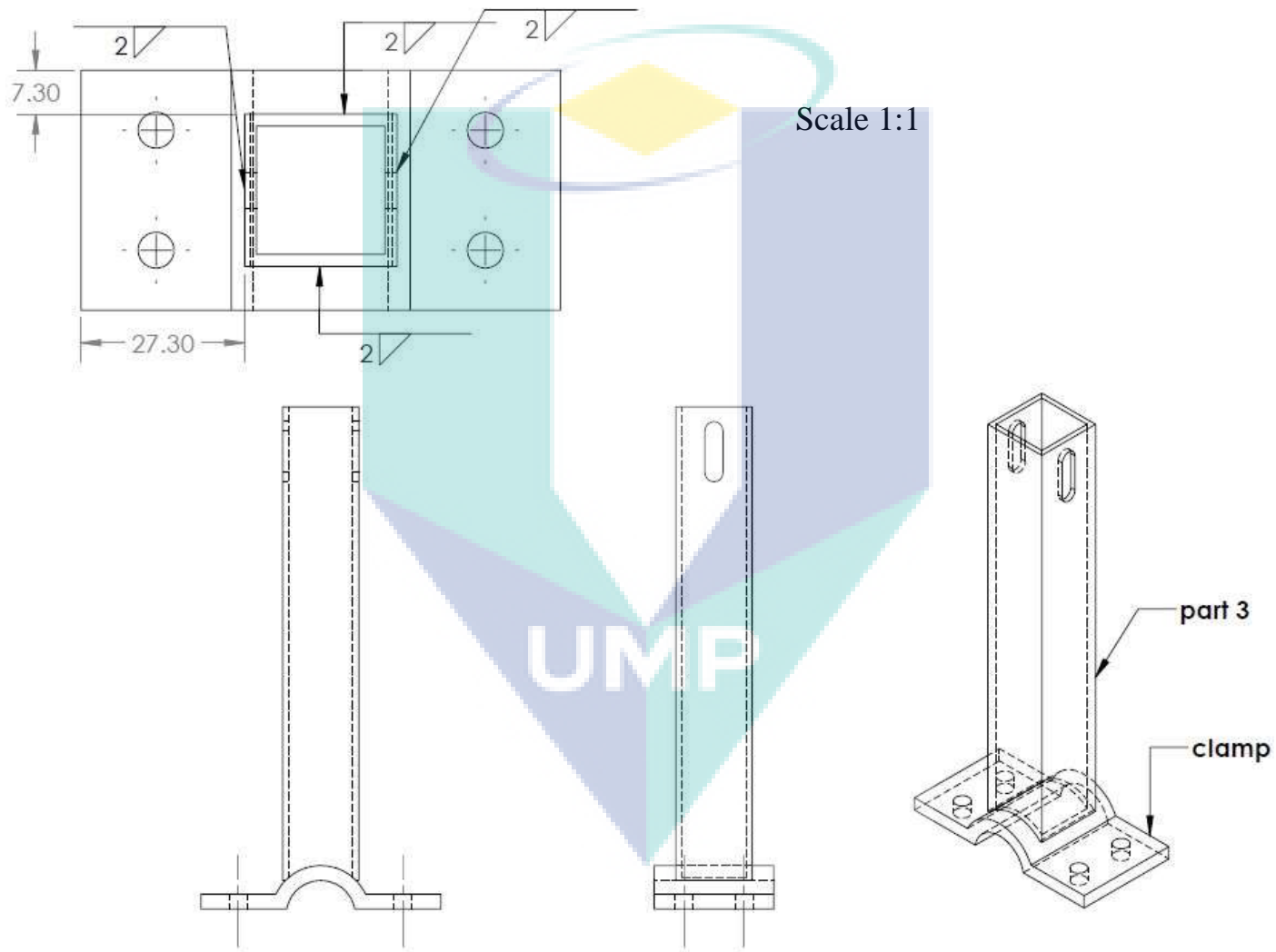
Scale 1:1.6

Material	Dimension (length x width x height)	Quantity
Solid mild steel	100 x 40 x 40 mm	2

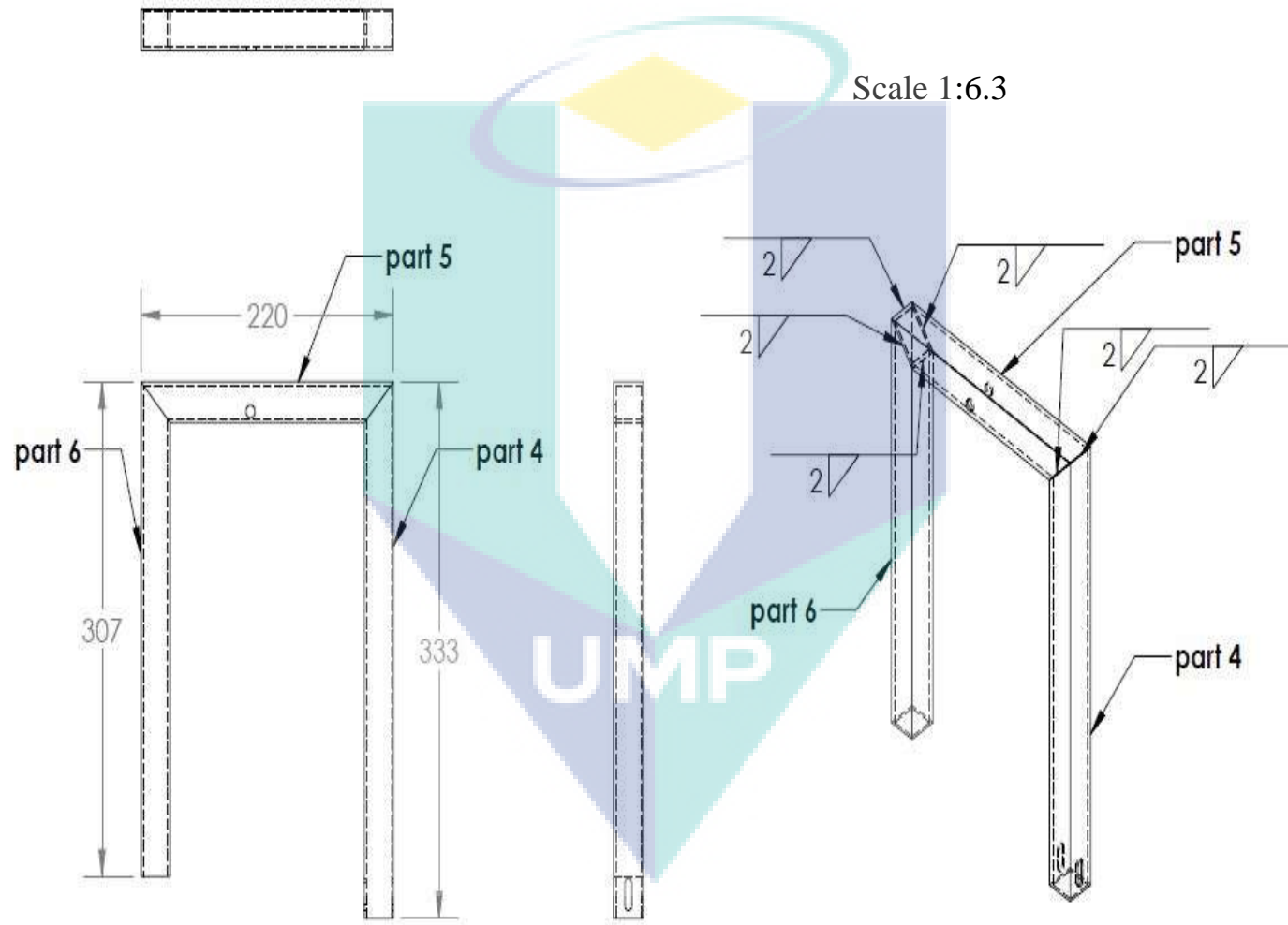
**Assembly of
clamp and part 2**



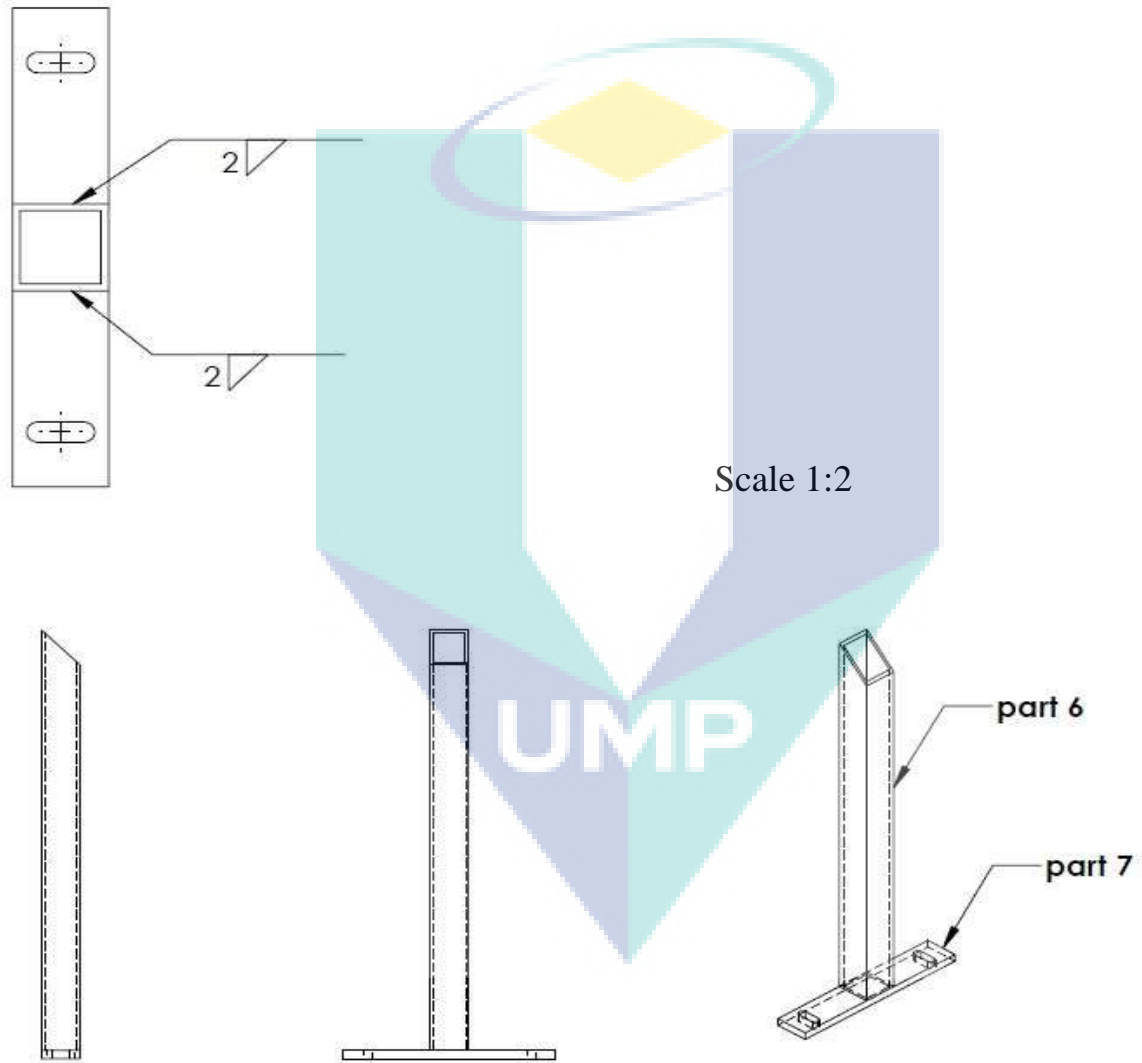
**Assembly of
clamp and part 3**



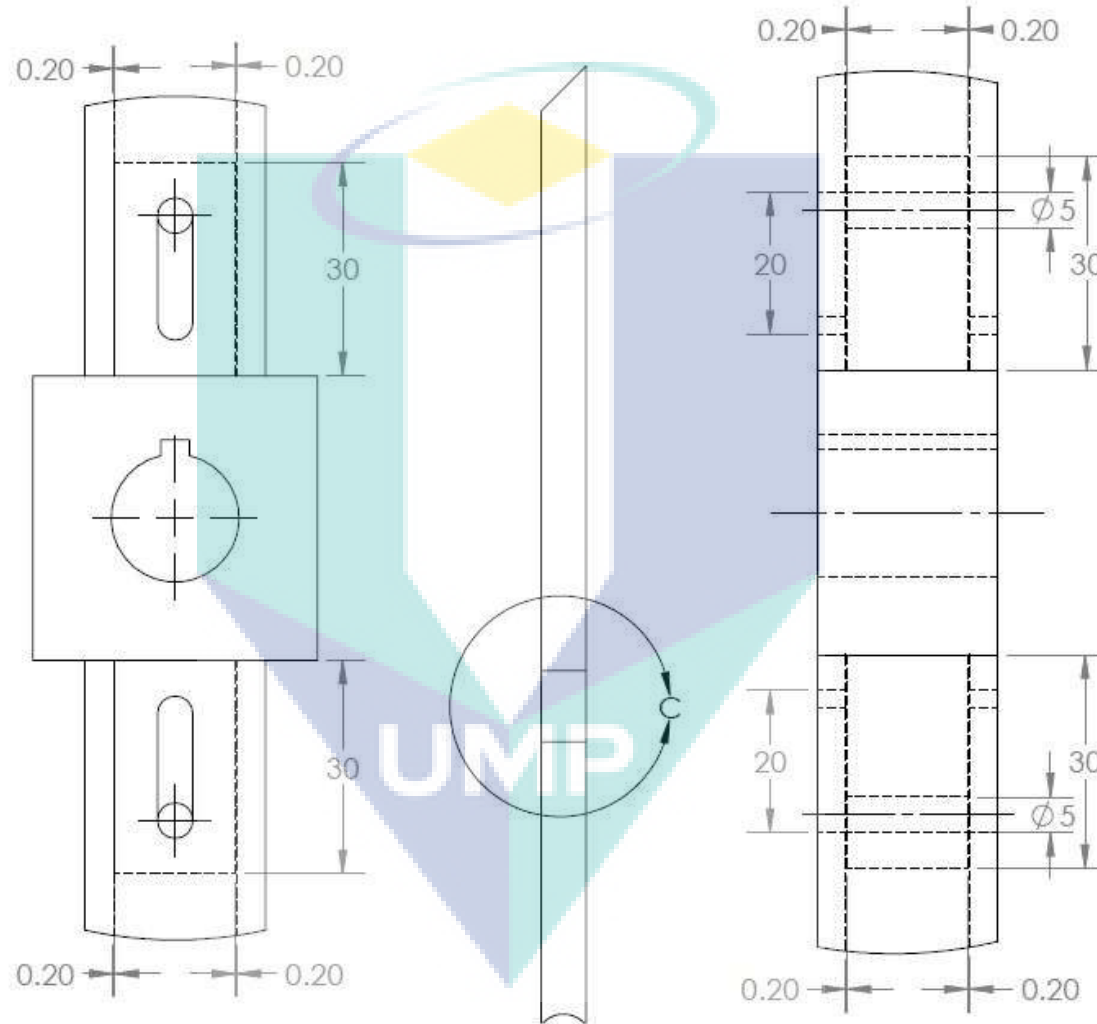
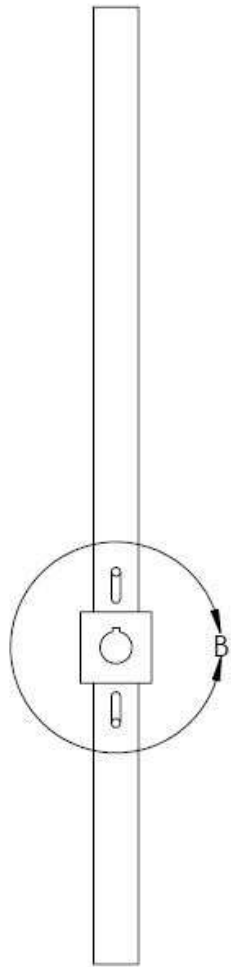
**Assembly part
4, 5 and 6**



**Assembly part
6 and 7**



**Assembly part
3, 4 and 8**



DETAIL B

Scale 1:1

DETAIL C

**Assembly part
2 and 4**

